PYRITE OXIDATION *and* ITS CONTROL

V. P. (Bill) Evangelou

PYRITE OXIDATION *and* ITS CONTROL

Solution Chemistry, Surface Chemistry,
Acid Mine Drainage (AMD),
Molecular Oxidation Mechanisms, Microbial Role,
Kinetics, Control, Ameliorates and Limitations,
Microencapsulation

V. P. (Bill) Evangelou, Ph.D.
Professor of Soil/Water Physical Chemistry
University of Kentucky, Lexington

CRC Press
Taylor & Francis Group
Boca Raton London New York

CRC Press is an imprint of the
Taylor & Francis Group, an informa business

Library of Congress Cataloging-in-Publication Data

Evangelou, V. P.
Pyrite oxidation and its control : solution chemistry, surface chemistry, acid mine drainage (AMD), molecular oxidation mechanisms, microbial role, kinetics, control, ameliorates and limitations, microencapsulation / V.P. (Bill) Evangelou.
p. cm.
Includes bibliographical references and index.
ISBN 0-8493-4732-7 (permanent paper)
1. Acid mine drainage. 2. Pyrites--Oxidation.
3. Microencapsulation. I. Title.
TD899.M5E94 1995
622--dc20
DNLM/DLC

95-7044

International Standard Book Number 0-8493-4732-7
Library of Congress Card Number 95-7044
Printed in the United States of America 3 4 5 6 7 8 9 0
Printed on acid-free paper

PREFACE

After fourteen years of attendance and participation in numerous conferences on acid mine drainage, two things have become apparent to the author of this book. First, much of the basic knowledge on pyrite and its oxidation mechanisms is not being used for the purpose of improving and/or generating new knowledge on controlling pyrite oxidation, and second, not much progress is being made in developing new technologies for controlling pyrite oxidation. Thus, the need for a book on the basic knowledge of pyrite and the use of this knowledge for generating new ideas, concepts and technologies on oxidation and control became apparent.

The focus of this book is on pyrite oxidation theory, experimental findings on oxidation mechanisms as well as application/limitations of amelioration technologies. A discussion on the theory and potential application of novel pyrite microencapsulation technologies for controlling pyrite oxidation currently under investigation in the author's laboratory is also included.

The book is designed to serve research faculty and graduate students in mining/environmental engineering, geology, soil science and environmental professionals dealing with amelioration of acid drainage produced by pyritic waste. The book is not designed to be everything to everybody. However, it is an attempt to gather the scientific knowledge on pyrite and acid mine drainage, evaluate it and use it as a springboard to new and improved control technologies.

I would like to thank all those who have contributed to my education on pyrite and acid mine drainage. Special appreciation goes to Mr. R. W. Hammack, and Dr. R. Kleinmann of the U.S. Department of the Interior, Bureau of Mines Pittsburgh, PA, Ms. Patricia M. Erickson of the U.S. EPA, Cincinnati, OH, and Dr. F. Caruccio of the University of South Carolina, Columbia, SC, for the numerous enlightening discussions on pyrite oxidation in the field.

Special thanks and appreciation go to Elisabeth Portig, laboratory technician, Y. L. Zhang, Post-doctoral Fellow, Louis McDonald, Ph.D. candidate, and Amy Bacon, undergraduate student, for their help in completing this book.

THE AUTHOR

V. P. (Bill) EVANGELOU obtained his B.S. in 1972 and M.S. in 1974 in Agriculture and Plant Science, respectively from California State University, Chico. In 1980, he received his Ph.D in Soil Science specializing in mineralogy and soil/water chemistry from the University of California at Davis.

Dr. Evangelou is currently Professor of Soil/Water Physical Chemistry at the University of Kentucky. He has served as Major Professor to numerous graduate students and supervisor of a number of Postdoctoral Fellows. He teaches courses in soil chemistry, soil physical chemistry and chemistry of sulfate rich geologic environments.

Dr. Evangelou's research is focused on cation exchange equilibria and kinetics of soils and clay minerals, the surface chemistry of soils, physical behavior of soil colloids, plant root cell wall-metal ion interactions and acquisition by plants, kinetics of pyrite oxidation and surface processes controlling rates of oxidation reactions, and recently, organometallic complexes and herbicide colloid suspension interactions and behavior. He has published more than 100 scientific papers on these subjects and has conducted more than 30 short courses on the subject of pyrite chemistry and acid mine drainage (AMD) for federal/state and private industry professionals from the U.S.A., Canada, Europe and South Africa. More than 2000 professionals have attended Dr. Evangelou's short courses on pyrite oxidation and acid mine drainage. He has been recognized for his scientific contributions by a number of awards,

-*Marion L. & Chrystie M. Jackson Soil Science Award*, 1992, Soil Science Society of America, outstanding contributions in the areas of soil chemistry and mineralogy, and graduate student education.

-*Fellow*, American Society of Agronomy, 1993.

-*Fellow*, Soil Science Society of America, 1993.

-*U.S. Patent* (No. 5,286,522) on "Peroxide Induced Oxidation Proof Phosphate Surface Coating on Iron Sulfides", 1994.

-*Fulbright Scholar Award*, 1994-1995.

-*Thomas Poe Cooper Award*, University of Kentucky, College of Agriculture, 1994, distinguished achievement in research.

TABLE OF CONTENTS

This is dedicated to my wife, Shelly, with love for her neverending support as well as gratitude for her help in proofreading the endless documents; and to my daughter Julia and son Peter with love and appreciation for their patience with my absent-minded preoccupation with the writing of this book. Immense respect and gratitude go to my late parents Peter and Glykeria Evangelou who, though they never had the opportunity to attend formal school, gave me support and encouragement to leave Greece at the age of eighteen to come to the United States and pursue my dream of becoming a scientist. To the many people in the United States who have given me support and encouragement to fulfill my dream, I am grateful.

Taylor & Francis
Taylor & Francis Group
http://taylorandfrancis.com

INTRODUCTION

Acid drainage (AD) is a severe environmental pollution problem and results from the oxidation of pyrite and/or other iron sulfides in coal or other mining waste, ore tailings, and overburden. Acid drainage is extremely acidic (pH as low as 2) and enriched with iron, aluminum, sulfate, and heavy metals such as lead (Pb), mercury (Hg), cadmium (Cd), and in some cases thorium (Th) and uranium (U) nuclides. Discharge of AD on land and into rivers and lakes poses an instant threat to the biota and ecological balance. Need to prevent AD formation has thus triggered numerous investigations into the mechanisms of pyrite oxidation and its prevention (Singer and Stumm, 1970; McKibben and Barnes, 1986; McKibben, 1984; Moses et al., 1987 and references therein; Silverman, 1967; Nordstrom, 1982a and references therein; Lowson, 1982 and references therein; Hiskey and Schlitt, 1982 and references therein; Kleinmann, 1980; Luther, 1990 and references therein).

Throughout the world large sums of money are spent yearly for preventing acid drainage formation at its source or treating acid drainage already formed. Conversely, microbiological and chemical oxidation of pyrite and other metal disulfides and/or metal sulfides are beneficial in depyritizing/desulfurizing coal and in commercial recovery of metals from low-grade ores and wastes. Pyrite oxidation is also important in geochemistry, marine chemistry, and soil science with respect to natural mineral weathering, sulfur cycling and sulfur detoxification, and soil development/quality, respectively.

Pyrite oxidation takes place when the mineral is exposed to air and water. The process is complex because it involves chemical, biological, and electrochemical reactions, and varies with environmental conditions. Factors, such as pH, pO_2, specific surface and morphology of pyrite, presence or absence of bacteria and/or clay minerals, as well as hydrological factors, determine the rate of oxidation. There is, therefore, no single rate law available to describe the overall kinetics of pyrite oxidation for all cases.

It has been reported that pyrite in mining waste or coal overburden is initially oxidized by the atmospheric O_2, producing H^+, SO_4^{2-}, and Fe(II). The Fe(II) can be further oxidized by O_2 into Fe(III), which in turn hydrolyzes and precipitates as amorphous iron hydroxide releasing additional amounts of acid (Nordstrom, 1982a and references therein). During this initial stage, pyrite oxidation is a relatively slow process (Ivanov, 1962). However, as acid production continues and the pH in the vicinity of the pyrite surfaces drops below 3.5, formation of ferric hydroxide is hindered and activity of Fe^{III} in solution increases. Under these conditions, oxidation of pyrite by Fe^{III} becomes the main mechanism for acid production in mining waste (Singer and Stumm, 1970; Moses et al., 1987 and references therein).

At low pH, an acidophilic, chemoautotrophic, iron oxidizing bacterium--*Thiobacillus ferrooxidans* catalyzes and accelerates the oxidation

of Fe(II) into Fe(III) by a factor larger than 10^6 (Singer and Stumm, 1970). Thus, due to the participation of bacteria, the processes of reduction of Fe(III) to Fe(II) by pyrite and oxidation of Fe(II) to Fe(III) by atmospheric O_2 constitute an effective continuous pyrite oxidation cycle. Through this cycle, electrons are readily transferred from FeS_2 to the atmospheric oxygen, causing the rapid oxidation of pyrite at low pH (Kleinmann and Crerar, 1979 and references therein; Nordstrom, 1982a and references therein).

Based on the above, approaches in preventing pyrite oxidation are mainly depended on eliminating dissolved Fe(III) from coal waste pore waters. Most such approaches share a common weakness: short span of effectiveness. In order to prevent pyrite oxidation on a long-term basis, it appears essential to block access of the atmospheric O_2 to pyrite surfaces. This could be accomplished through microencapsulating pyrite. Nicholson et al. (1988, 1990) in controlled laboratory studies of oxidizing pyrite in reactors through which a carbonate-buffered solution and air (20% O_2) flowed continuously, were able to demonstrate diminishing rates of pyrite oxidation through formation of iron oxide coatings. However, in such systems, the rate formation of iron oxide coating was extremely slow (it took approximately 100 days to form). Recently, in the author's laboratory, under well controlled conditions, it was demonstrated that pyrite coating, an oxidation inhibitor, could take place through formation of iron phosphate ($FePO_4 \cdot nH_2O$) (Huang and Evangelou, 1994). Thus, potential application of this technology in the field could, in some cases, bring under control production of certain type of acid drainages.

This book is organized into five parts. **Part I** is a review on solution and surface chemistry of minerals, including acid drainage production and control. The latter involves congruent/incongruent dissolution of minerals present in geologic strata coupled to reductive/oxidative dissolution precipitation processes in the presence of pyrite. All of the above processes, solubilization, precipitation, reductive/oxidative dissolution and/or precipitation are subject to classical physical-chemical processes (e.g mineral solubility and surface sorption equilibria, ion activities, kinetics, etc.) and the readers of this book should have some understanding of these processes for the purpose of following the book, and furthermore, for applying the knowledge in predicting and/or controlling acid drainage production.

Part II deals with the molecular and surface properties of pyrite and how such properties influence kinetics of pyrite oxidation. The purpose of this section is twofold. One, is to introduce the reader to the complexity of pyrite oxidation, and two, to allow the reader to understand that elucidating the complexity of pyrite oxidation chemistry could lead to the development of more effective pyrite oxidation control technologies.

Part III involves the role of microorganisms on pyrite oxidation. Even though the book's main focus is the physical chemistry of pyrite, the microbiological component is strongly involved in the physical chemistry of

pyrite oxidation. The purpose of this part is therefore to keep the physical chemistry of pyrite oxidation into proper perspective.

Part IV introduces the reader to some new pyrite microencapsulation technologies (discovered in the author's laboratory) for the purpose of controlling pyrite oxidation. These pyrite microencapsulation technologies are still in the experimental stage, and have not been tested in the natural environment. Nevertheless, they represent a new idea on pyrite oxidation control and in some cases future improvements on the technology and its application may prove to be most effective in controlling long-term pyrite oxidation.

Part V summarizes some of the most important points discussed throughout the book. The author hopes that this material will serve as a useful tool in understanding and controlling pyrite oxidation for the purpose of allowing us to continue using our natural resources and to safeguarding our environment.

Taylor & Francis
Taylor & Francis Group
http://taylorandfrancis.com

PART I

REVIEW OF BASIC CONCEPTS OF SURFACE CHEMISTRY AND CHEMISTRY AND CONTROL OF ACID DRAINAGE

Taylor & Francis
Taylor & Francis Group
http://taylorandfrancis.com

Chapter 1
A REVIEW ON SOLUTION/MINERAL CHEMISTRY

1.1 Ion Activity versus Concentration

It is generally agreed that chemical reactions in nature (e.g., mineral dissolution/precipitation) take place because of electrical and chemical gradients. With regard to the former, there is disagreement as to how one may measure these gradients since they are not directly related to concentration (Amacher, 1984; Sposito, 1984; Sposito and Mattigod, 1979). Aided by computer technology, approaches have been introduced that allow estimation of single-ion activity (a direct reflection of the chemical potential of ionic species) in mixed electrolyte systems (Davies, 1962; Adams, 1971; Sposito, 1984). Experimental data (Pavan and Bingham, 1982; Sposito, 1984) support the argument that single-ion activity best describes/predicts chemical reactions.

Single-ion activity in solution is estimated by employing the equation of effective ionic strength (I)

$$I = 1/2 \sum_{j=1}^{n} Z_j^2 m_j \qquad (1.1)$$

where Z_j and m_j are the charge and effective molar concentration of ionic species (Sposito, 1984). Based on I, activity coefficients of ionic species can be calculated using the Davies equation (Davies, 1962):

$$\log \gamma_j = -AZ_j^2 [I^{1/2} / (1 + I^{1/2}) - 0.3I] \qquad (1.2)$$

where γ is the activity coefficient of ionic species j, and A is a constant equal to 0.512. Single ion activity (α_j) can then be estimated by:

$$\alpha_j = \gamma_j m_j \qquad (1.3)$$

The above calculations necessitate the use of ion association models to make estimates of concentration of ionic species (m_j) using as inputs elemental concentrations (see section *1.1.3, Ion pairing*) (Adams, 1971; Sposito and Mattigod, 1979; Sposito, 1984; Evangelou, 1986). However, direct measurement of single-ion activity in mixed electrolyte systems for the purpose of verifying ion association models cannot be made (Amacher, 1984; Sposito, 1984); validity of ion-association models can only be demonstrated indirectly.

In order to gain an appreciation of the importance of single-ion activity in describing/predicting chemical reactions as opposed to elemental concentration, one needs to look into the effect of ionic strength and ion valence on single-ion activity coefficients (γ) (Equation 1.2). This is demonstrated in Figure 1.1. It shows that at an ionic strength of 0.04 *M*, the γ

value for say Ca^{2+}, is approximately 0.5, while that of a monovalent ion is approximately 0.8.

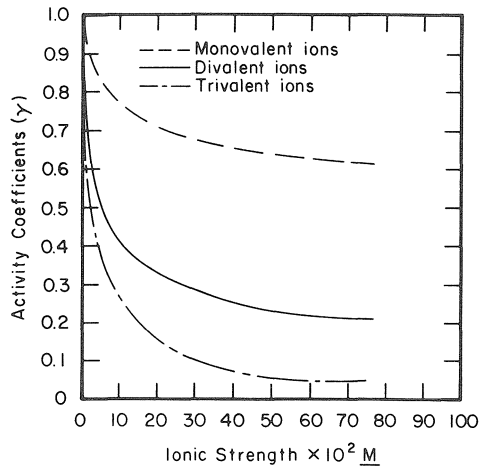

Figure 1.1. Relationship between solution ionic strength and activity coefficients of ions of different valencies. Calculated utilizing the Davies equation (Davies, 1962). (From Evangelou and Sobek, 1988. With permission.)

Examples of practical implications of single-ion activity with respect to pH and mineral solubility are given in sections *1.1.1 and 1.1.2.*

1.1.1 Solution pH

Most reactions in soil/geologic systems are pH driven because of the hydrogen's (H^+) great potential to react with solution chemical species and/or mineral surfaces due to its small size and high electron accepting potential.

Technically, pH is the negative logarithm of the hydrogen ion activity (Equations 1.4)

$$pH = -\log (H^+) \tag{1.4}$$

The pH scale ranges from 0 to 14, with 7 being the neutral point. Values greater than 7 are basic or alkaline, while values less than 7 are acidic. For example, if the hydrogen ion activity of a water sample is 10^{-7} mol L^{-1}, its pH is 7, since 7 is the negative logarithm of 10^{-7}.

Water emanating from surface mine sites for example can vary in ionic strength (I) anywhere from 0.001 to 0.1. Values greater than 0.1 can be observed in acid mine drainages (Lekhakul, 1981). For a solution with an I of 0.008 *M*, the γ value for H^+ will be 0.9. On the other hand, a solution with an I value of 0.04 *M* will exhibit a γ value for H^+ of 0.8. Since pH represents H^+

activity, the same pH in the above systems would represent a different H^+ concentration. For example, at pH of 3 and at an I value of 0.008 *M*:

$$[H^+] = 1.11 \times 10^{-3} \text{ mol } L^{-1} \quad (1.5)$$

while at an I of 0.04 *M*

$$[H^+] = 1.25 \times 10^{-3} \text{ mol } L^{-1} \quad (1.6)$$

Therefore, at an ionic strength of 0.008 *M* the H^+ activity represents 90% of its concentration, while at an ionic strength of 0.04 *M*, the H^+ activity represents 80% of its concentration.

The above example demonstrates that even in the case of a monovalent ion such as H^+, the difference between concentration and activity becomes significant at increasing ionic strength.

1.1.2 Mineral solubility

Gypsum ($CaSO_4 \cdot 2H_2O$) is a mineral commonly produced in limestone ($CaCO_3$) treated pyritic waste. For this reason, $CaSO_4 \cdot 2H_2O$ will be used as an example to demonstrate the influence of ion activity on mineral solubility. The solubility of $CaSO_4 \cdot 2H_2O$ in water is expressed as,

$$CaSO_4 \cdot 2H_2O \underset{k_b}{\overset{k_f}{=}} Ca^{2+} + SO_4^{2+} + 2H_2O \quad (1.7)$$

The components k_f and k_b denote rate constants for the forward and backward reactions, respectively. Reaction 1.7 at equilibrium can be described by:

$$dCa^{2+} / dt = k_f(CaSO_4 \cdot 2H_2O) - k_b(Ca^{2+})(SO_4^{2-})(H_2O)^2 = 0 \quad (1.8)$$

$$\text{and } K_{eq} = k_f / k_b = (Ca^{2+})\,(SO_4^{2-})(H_2O)^2 / (CaSO_4 \cdot 2H_2O) \quad (1.9)$$

where, K_{eq} denotes equilibrium product constant and parentheses denote single-ion activity.

Equations 1.9 can also be derived utilizing Gibb's free energy of formation (ΔG_f) of ionic species in water. From classical thermodynamics,

$$\Delta G_f = \Delta G_f^{\rho} + RT \ln \alpha_x \quad (1.10)$$

where ΔG_f^{ρ} = Gibbs free energy of formation at the standard state in H_2O, R = universal gas constant, T = temperature in degrees Kelvin, and α_x=molar activity of ion X. At equilibrium $\Delta G_f = 0$ and $\Delta G_{f(products)} = \Delta G_{f(reactants)}$. Under equilibrium conditions, the thermodynamic constant (K_{eq}) is defined by the relationship

$$K_{eq} = \exp - (\Delta G_f^{\rho} / RT) \quad (1.11)$$

By substituting each of the terms describing reactants and products in Equations 1.7 by Equations 1.10, and introducing the resulting equation into Equation 1.11 it is shown that

$$K_{eq} = (Ca^{2+})(SO_4^{2-})(H_2O)^2 / (CaSO_4{\cdot}2H_2O) = \quad (1.12)$$

$$\exp - (\Delta G_f(Ca^{2+})^o + \Delta G_f(SO_4^{2-})^o + 2\Delta G_f(H_2O)^o - \Delta G_f(CaSO_4{\cdot}2H_2O)^o/RT$$

Note that at equilibrium, Equation 1.9 implies that the rate of the forward reaction ($CaSO_4{\cdot}2H_2O$ dissolution) is equal to the rate of the backward reaction ($CaSO_4{\cdot}2H_2O$ precipitation). However, according to Equation 1.12 these reaction rates are molar activity dependent.

Based on the above, the activity of an ion in solution is dependent on the ionic strength of the solution; for this reason mineral solubility is ionic strength dependent. Starting from the $CaSO_4{\cdot}2H_2O$ solubility:

$$CaSO_4{\cdot}2H_2O = Ca^{2+} + SO_4^{2-} + 2H_2O \quad (1.13)$$

assuming that ${}^{\alpha}H_2O$ and ${}^{\alpha}CaSO_4.2H_2O$ equal 1

$$K_{sp} = [Ca^{2+}]\gamma_{Ca^{2+}}[SO_4^{2-}]\gamma_{SO4^{2-}} = 2.45 \times 10^{-5} \quad (1.14)$$

where brackets denote ionic or dissociated concentration

$$[Ca^{2+}]\gamma_{Ca^{2+}} = [SO_4^{2-}]\gamma_{SO4^{2-}} = (2.45 \times 10^{-5})^{1/2} = 4.95 \times 10^{-3} \text{ mol L}^{-1} \quad (1.15)$$

The activity coefficient (γ) for Ca^{2+} or SO_4^{2-} for a system in equilibrium with gypsum is approximately equal 0.5 (Evangelou and Sobek, 1988; see also Figure 1.1). Therefore, dissociated $[Ca^{2+}]$ or $[SO_4^{2-}]$ concentration is equal to:

$$4.95 \times 10^{-3} \text{ mol L}^{-1} / 0.5 = 9.9 \times 10^{-3} \text{ mol L}^{-1} \quad (1.16)$$

which is double that of Ca^{2+} or SO_4^{2-} activity.

1.1.3 Ion pairing

When distilled water is added to $CaSO_4{\cdot}2H_2O$, ions in solution tend to associate with each other and form charged and/or uncharged pairs (Adams, 1971). This ion interaction tends to decrease the electrophoretic potential of a mixed electrolyte solution (Tanji, 1969). The ability of ions in solution to associate with each other is shown in Table 1.1. The importance of this ion association can be demonstrated by considering its magnitude and contribution to $CaSO_4{\cdot}2H_2O$ solubility. From Table 1.1,

Table 1.1
Ion pair equilibrium constants in sulfate waters

Reaction	K*
$NaSO^-_4 = Na^+ + SO_2^{2-}$	2.3×10^{-1}
$HSO^-_4 = H^+ + SO_4^{2-}$	1.2×10^{-2}
$CuSO_4^o = Cu^{2+} + SO_4^{2-}$	4.36×10^{-3}
$ZnSO_4^o = Zn^{2+} + SO_4^{2-}$	5.0×10^{-3}
$FeSO_4^o = Fe^{2+} + SO_4^{2-}$	5.0×10^{-3}
$CaSO_4^o = Ca^{2+} + SO_4^{2-}$	5.25×10^{-3}
$MnSO_4^o = Mn^{2+} + SO_4^{2-}$	5.25×10^{-3}
$MgSO_4^o = Mg^{2+} + SO_4^{2+}$	5.88×10^{-3}
$AlSO_4^+ = A1^{3+} + SO_4^{2+}$	6.30×10^{-4}
$FeSO_4^+ = Fe^{3+} + SO_4^{2-}$	7.1×10^{-5}
$MgCl^+ = Mg^{2+} + Cl^-$	3.2×10^{-1}
$KSO_4^- = K^+ + SO_4^{2-}$	1.1×10^{-1}
$KCl^o = K^+ + Cl^-$	Extremely high

* These values were selected from Adams (1971).

$$Ca^{2+} + SO_4^{2-} = CaSO_4^o \quad (1.17)$$

$$(Ca^{2+})\,(SO_4^{2-}) / (5.25 \times 10^{-3}) = CaSO_4^o \quad (1.18)$$

where parentheses denote activity. Substituting values into Equation 1.18 from Equation 1.15,

$$CaSO_4^o = (4.95\times10^{-3})\,(4.95\times10^{-3})/(5.25\times10^{-3}) = 4.67 \times 10^{-3} \text{ mol } L^{-1} \quad (1.19)$$

Therefore, the total calcium molarity (Ca_T) can be expressed as the sum of the concentration of all the calcium ionic species of significant concentration,

$$Ca_T = [(Ca^{2+}) / \gamma_{Ca^{2+}}] + [(CaSO_4^o) / \gamma_{CaSO4^o}] \quad (1.20)$$

Similarly, the total sulfate molarity (SO_{4T}) can be expressed as

$$SO_{4T} = [(SO_4^{2-}) / \gamma_{SO4^{2-}}] + [(CaSO_4^o) / \gamma_{CaSO4^o}] \quad (1.21)$$

where parentheses denote molar activity for the species shown, and γ denotes single ion activity coefficient. Therefore, components that clearly appear to

have an influence on the solubility of $CaSO_4 \cdot 2H_2O$ are the magnitude of the single-ion activity coefficient (γ) and the thermodynamic stability constant of the ion pair ($CaSO_4^o$). The magnitude of γ is dependent on the magnitude of effective ionic strength and valence of the ionic species (see Equations 1.1, 1.2, 1.3).

In order to demonstrate that the magnitude of γ and degree of ion pairing controls Ca_T, Evangelou et al. (1987) compared experimental values of Ca_T (obtained by equilibrating $CaSO_4 \cdot 2H_2O$ in the presence of different concentrations of various electrolytes (Tanji, 1969b) with computer-generated data representing the same conditions. The latter step involves the solution of equations describing I, γ, K_{eq} of $CaSO_4 \cdot 2H_2O$ and thermodynamic stability of pairs (Table 1.1) by a mass balance-iteration procedure described by Adams (1971). Comparison of the experimental data versus the mass balance-iteration method data is shown in Figure 1.2.

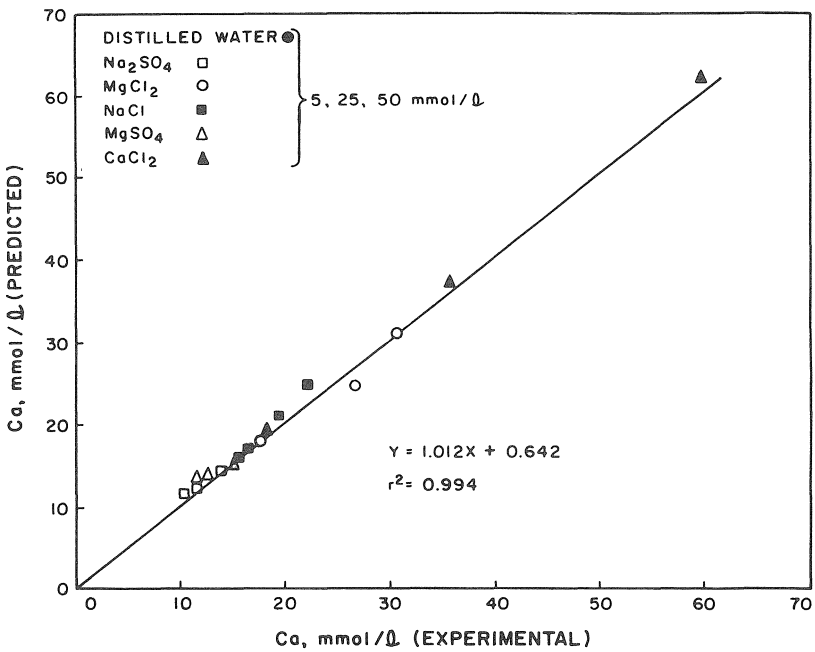

Figure 1.2. Relationship between experimental and computer-simulated $CaSO_4 \cdot 2H_2O$ solubility at different concentrations of various salt solutions employing an ion association model. (From Evangelou et al., 1987. With permission.)

It shows excellent agreement between experimental and predicted values. These data also show that, as expected, the solubility of $CaSO_4 \cdot 2H_2O$ depends on concentration and composition of background electrolyte.

When pure water is added to $CaSO_4 \cdot 2H_2O$, the latter dissolves until its rate of dissolution is equal to its rate of precipitation. This is the chemical equilibrium point. If at the chemical equilibrium point a certain amount of $MgCl_2$ is introduced to the system, the $MgCl_2$ ionizes and interacts with Ca^{2+} and SO_4^{2-}, forming magnesium sulfate ($MgSO_4^o$) and calcium chloride ($CaCl^+$) pairs (Adams, 1971). When this occurs, the rate of $CaSO_4 \cdot 2H_2O$ dissolution will exceed the rate of its precipitation because the number per unit time of successful collisions of Ca^{2+} with SO_4^{2-} would decline. Because of this a new equilibrium point will be established by dissolving more $CaSO_4 \cdot 2H_2O$. Experimental data by Tanji (1969) (Figure 1.3) showed that $CaSO_4 \cdot 2H_2O$ solubility in the presence of 50 mmol L^{-1} $MgCl_2$ increased by 69% in relationship to its solubility in distilled water, while in the presence of an equivalent concentration of NaCl the increase was only 46%. This difference in solubility was due to the difference in pairing abilities of Mg^{2+} and Na^+ with SO_4^{2-} versus Ca^{2+} with Cl^-.

1.1.4 Quantifying the influence of ionic strength and ion pairing on ion activity

Evangelou and Wagner (1987) demonstrated the influence of ionic strength and ion pairing on ion activity through computer simulations. For these computer simulations four different situations were considered: (1) KCl, (2) K_2SO_4, (3) $MgCl_2$ and (4) $MgSO_4$. For these situations a constant concentration of the cation in question under variable ionic strength was assumed. Variability in ionic strength was attained by increasing concentration of NaCl or Na_2SO_4. Ion pairs considered for these systems along with their stability constants are shown in Table 1.1. Ionic strength and single-ion activities were determined by the mass balance-iteration procedure (Adams, 1971; Amacher, 1984).

Results of the above computer simulations are shown in Figure 1.4. In this figure the concentration component for ions with valence greater than 1 is given on an equivalent basis ($mol_c\ L^{-1}$ = mol × ion valence) for the purpose of direct comparison with ions of valence 1. Figure 1.4a shows that K^+ activity for constant K dissolved decreases with increasing ionic strength. This decrease is greater in the SO_4^{2-} system than in the Cl^- system. The difference is due to the greater stability of the KSO_4^- (Table 1.1; Figure 1.4c) as opposed to KCl^o (Adams, 1971). Additionally, the decrease in K^+ activity with respect to ionic strength for all practical purposes can be considered linear.

Data in Figure 1.4a show that there is a significant decrease in Mg^{2+} activity as a function of ionic strength. Furthermore, this decrease is biphasic. The data show that the decrease in Mg^{2+} activity is much greater for the SO_4^{2-} system than for the Cl^- system. The data in Figure 1.4b demonstrate that at 20 $mmol_c\ L^{-1}$ background electrolyte (NaCl or Na_2SO_4) nearly 30% of total dissolved Mg is in the $MgSO_4^o$ form as opposed to about only 3% in the

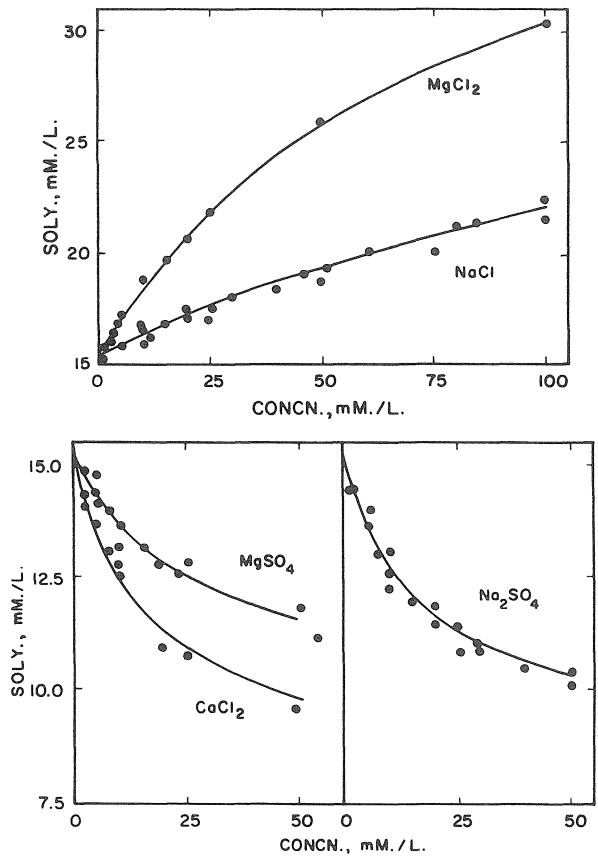

Figure 1.3. Influence of different electrolytes on the solubility of $CaSO_4 \cdot 2H_2O$. (From Tanji, 1969b. With permission.)

$MgCl^+$ form. With respect to Mg^{2+} activity, the data in Figure 1.4a show that at a background electrolyte (NaCl or Na_2SO_4) concentration of 20 $mmol_c\ L^{-1}$ the Mg^{2+} activity represents 52% of total dissolved Mg in the Cl^- system as opposed to only 34% for the SO_4^{2-} system. The above relationships between activity and concentration are in agreement with the experimental results reported by Tanji (1969). Note also that these relationships between activity and concentration, demonstrated above, apply to all ions. Quantification, however, requires the use of ion association models (Sposito and Mattigod, 1979).

1.1.5 Specific conductance

Solution-specific conductance is a function of total dissolved ions, type of ions and their potential to form charged and/or noncharged pairs and/or complexes. The equation that predicts specific conductance (EC), in

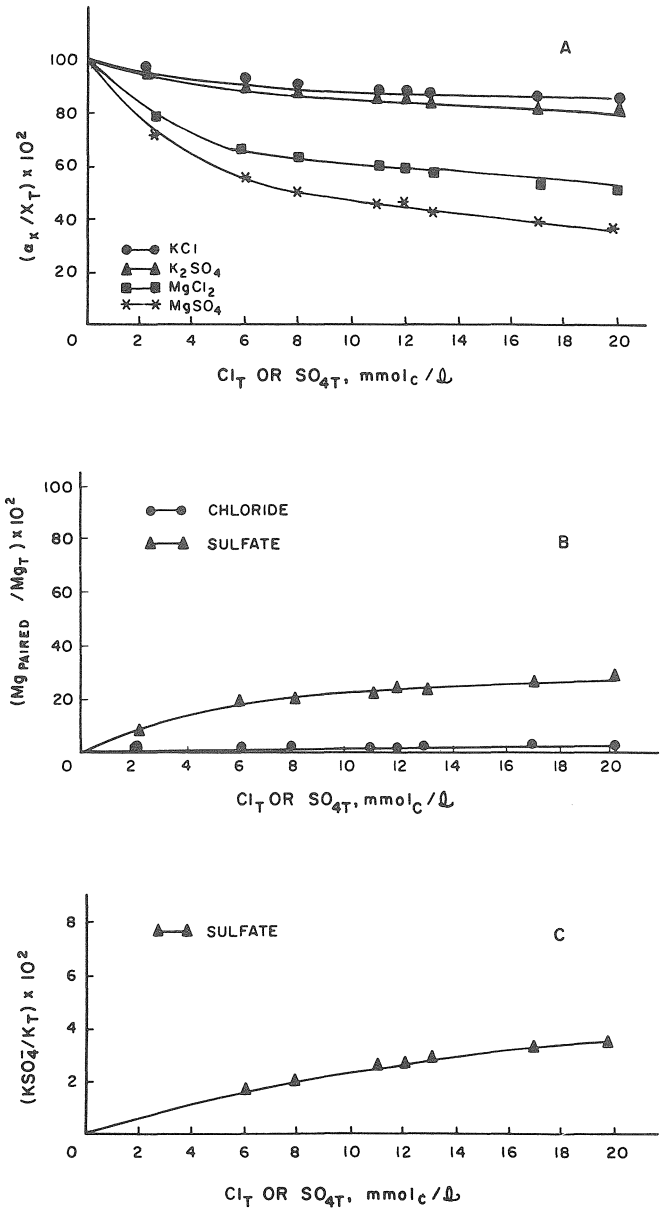

Figure 1.4. Influence of Cl^- and SO_4^{2-} concentration on (a) K^+ and Mg^{2+} activity, (b) Mg^{2+} pairing, and (c) K^+ pairing. (From Evangelou and Wagner, 1987. With permission.)

mhos cm^{-1}, of a solution of a known electrolyte concentration is (Tanji, 1969a)

$$EC = AC/1000 \quad (1.22)$$

where A denotes limiting ionic conductance, in units of cm^2 (Equivalent-ohm)$^{-1}$, and C is concentration in Equivalents L^{-1}. Limiting ionic conductance values (A) for different ions are shown in Table 1.2.

Table 1.2
Equivalent ionic conductance of different ions found in natural water systems

Ion	A (cm^2 (Equivalent-ohm)$^{-1}$)
H^+	349.8
K^+	73.6
Ca^{2+}	59.5
Mg^{2+}	53.1
OH^-	198.0
Cl^-	76.3
SO_4^{2-}	79.8
HCO_3^-	44.5
NO_3^-	71.4

The data shown in Table 1.2 when incorporated into Equation 1.22 demonstrate that any two solutions with the same concentration, in equivalence units, of two ions with different A values will produce different specific conductance values.

Table 1.2 reveals that the most commonly found ions in natural bodies of water with the exception of H^+ and OH^-, exhibit A values in the range of approximately 50 to 80 cm^2 (Equivalent-ohm)$^{-1}$. Hydrogen and OH^- exhibit A values of 349.8 and 198.0, respectively. Equation 1.22 when plotted as C versus EC should produce a straight line with slope 1000/A. The slope of the line should be the same for all salt solutions of any concentration and composition. However, because H^+ and OH^- exhibit A values much greater than the average A value of all other metallic ions found in natural waters and because ions in solution have a tendency to interact physically, pair and/or form strong complexes, the slope of Equation 1.22 is expected to be pH- and salt concentration dependent. At low pH values (<3.5), the contribution of H^+ to specific conductance is significant and mine drainages for example, often have pH values below 3.5 (Lekhakul, 1981). The

influence of ionic interactions on specific conductance is demonstrated in Figure 1.5.

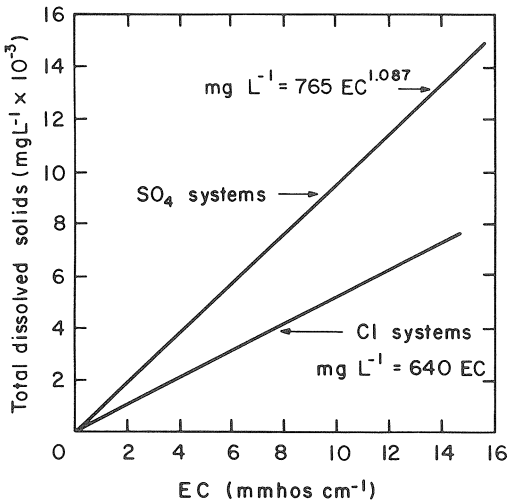

Figure 1.5. Relationship between EC and dissolved solids for Cl dominated and SO_4^{2-} dominated water systems. (From Evangelou and Sobek, 1988. With permission.)

Note that the same EC value of two solutions represented by different anions (Cl^- versus SO_4^{2-}) differ greatly in total dissolved solids. These differences can not be accounted by differences between the two salts in equivalent weights alone. Below a theoretical analysis on specific conductance is carried out to demonstrate the importance of ion activity in predicting electrical conductance of solutions.

Consider a strong electrolyte (completely dissociated) $C\Phi_+M\Phi_-$ where C and M represent cation and anion respectively and Φ_+ and Φ_- represent stoichiometric coefficients, in a tube of cross-sectional area "A" in square meters (m^2) (Figure 1.6).

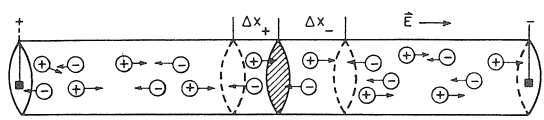

Figure 1.6. Schematic of ionic conductance ($\vec{E}$ = electric field, ΔX_+ = distance travelled by the cation Φ_+; ΔX_- = distance travelled by the anion Φ_-). (From Evangelou and Wagner, 1987. With permission.)

The number of cations (n_+) and anions (n_-) present in the tube can be expressed as n_+ per cubic meter (n_+ m^{-3}) and n_- per cubic meter (n_- m^{-3}). If an electric field E is applied, the cations move with a net speed V_+ toward the

anode, and the anions with a net speed V_- toward the cathode. The average cation will move in a certain time (Δt) some distance X such that $\Delta X_+ = V_+ \Delta t$. Likewise, for the average anion $\Delta X_- = V_- \Delta t$ in the opposite direction. Figure 1.6 also implies that any cation within ΔX_+ will pass through the striped cross-section in Δt. The total electrical current in amperes (I_t) that will pass through the cross section in Δt can be given by

$$I_t = I_+ + I_- \tag{1.23}$$

where I_+ = electrical current due to the cation, and I_- = electrical current due to the anion. The current due to the cation is given by the equation:

$$I_+ = (n_+ A \Delta X_+ Z_+ e) / \Delta t = \text{amperes} \tag{1.24}$$

and for the anion

$$I_- = (n_- A \Delta X_- Z_- e) / \Delta t = \text{amperes} \tag{1.25}$$

where Z_+ = charge of cation, Z_- = charge of anion, e = electron charge, and A cross-sectional area of the tube.

In order to obtain a measurement independent of the cross-sectional area of the tube and the electric field (E) applied, the term specific conductance (K) can be defined by:

$$K = I_t / A \overrightarrow{E} \tag{1.26}$$

Substituting the following terms in Equations 1.24 and 1.25

$$\Delta X_+/\Delta t = V_+ = U_+ \overrightarrow{E} \tag{1.27}$$

$$\Delta X_-/\Delta t = V_- = U_- \overrightarrow{E} \tag{1.28}$$

$$n_+ e = \Phi_+ \alpha F \tag{1.29}$$

$$n_- e = \Phi_- \alpha F \tag{1.30}$$

where U_+ = electric mobility of the cation, U_- = electric mobility of the anion, α = activity in mol L^{-1}, and F = Faraday's constant and introducing these modified expressions of Equations 1.24 and 1.25 into Equation 1.26

$$K = [\Phi_+ \mid Z_+ \mid FU_+ + \Phi_- \mid Z_- \mid FU_-]\alpha \tag{1.31}$$

$$\Lambda = [\Phi_+ \mid Z_+ \mid FU_+ + \Phi_- \mid Z_- \mid FU_-] \tag{1.32}$$

then

$$K = \Lambda\alpha \tag{1.33}$$

Prutton and Maron (1956) pointed out that for a strong electrolyte (highly dissociable) at concentrations less than 2.0 mmol L^{-1} the term Λ is described by the equation

$$\Lambda = \Lambda_o - R\ \alpha^{1/2} \tag{1.34}$$

where Λ_o = equivalent conductance at infinite dilution, and R = constant.

The term R (Equation 1.34) has been expanded (Robinson and Stokes, 1968) to include ionic relaxation and retardation effects (Prutton and Maron, 1956) in order for Equation 1.34 to be applicable for concentrations greater than 2.0 mmol L^{-1}. The expanded form of Equation (1.34) is:

$$\Lambda=\Lambda_o - [0.7816\,|Z^+|\,|Z^-|\,q/(1+q^{1/2})\Lambda_o+30.16(|Z^+|+|Z^-|)]I^{1/2}/1+I^{1/2} \tag{1.35}$$

$$\text{where } q=(|Z^+|\,|Z^-|)(\lambda_{o+}+\lambda_{o-})/(|Z^+|+|Z^-|)(|Z^+|\,\lambda_{o-}+\,|Z^-|\,\lambda_{o+}) \tag{1.36}$$

$$\Lambda_o = \lambda_{o+} + \lambda_{o-} \tag{1.37}$$

and I = effective ionic strength, λ_{o+} = limiting ionic conductance for the cation, and λ_{o-} = limiting conductance for the anion.

Tanji (1969a) employed Equations 1.35 and 1.33 to predict specific conductance of solutions of known composition and concentration. The data in Figure 1.7 demonstrate comparisons between specific conductance values of NaCl solutions obtained from the International Critical Tables (1929) and those calculated from Equation 1.33 by estimating the Λ value with Equation 1.35. For Figure 1.7a parameter α in Equation 1.33 is taken to represent total dissolved concentration of NaCl or single-ion activity of Na^+ or Cl^-. The data in Figure 1.7a demonstrate that when term α is represented by ion activity rather than concentration, a close agreement between experimental (International Critical Tables, 1929) and calculated values occurs. Similar results shown in Figure 1.7b were obtained for $MgSO_4$, a weaker electrolyte than NaCl. For Figure 1.7b the calculated specific conductance values are based on total dissolved concentrations (Equation 1.33) or an effective ionic strength and single-ion activity estimated by ion association modelling due to strong pairing properties of Mg^{2+} and SO_4^{2-}. The comparisons demonstrate that there was excellent agreement between experimental and predicted specific conductance values only when effective ionic strength and single ion activities were considered.

These results in Figure 1.7 demonstrate that specific conductance values of water-salt solutions are directly related to single-ion activities. However, calculated single-ion activities as described in section 1.1 assume that the activity of water is that of pure water. However, the activity of water which is representative of its purity may change in the natural world due to its contamination with solvents, salts, organics etc. When this happens the

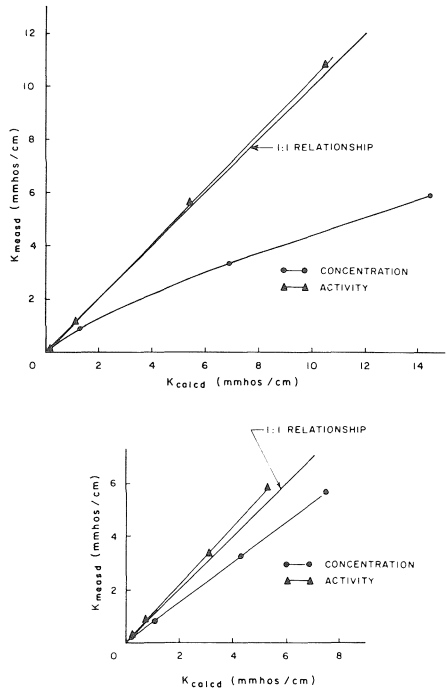

Figure 1.7. Relationship between calculated, based on ion concentration or single ion activity, and measured specific conductance of NaCl or $MgSO_4$ solutions. Raw data taken from Tanji (1969) and the International critical tables, (1929). (From Evangelou and Wagner, 1987. With permission.)

relationship between salt concentration and EC or specific conductance also changes. This is demonstrated in Figures 1.8a and b. These data demonstrate that when the osmotic pressure of the solution changes due to sorbitol, the specific conductance decreases relative to that of pure water. Furthermore, this decrease is greater for ions of higher valence than of those of lower valence.

1.2 Acidity/Alkalinity

Acidity and alkalinity are two important components that are very important to acid drainage production and control and are often misunderstood by field practitioners. By the definition commonly employed by commercial analytical laboratories, acidity refers to the amount of base added to a 1 L solution sample to bring pH to 7 or 8.2. On the other hand, alkalinity refers to the amount of acid added to 1 L of a solution sample to bring pH to 4.2. The above definition of acidity and alkalinity has large limitations because it says nothing of the pH range at which the water sample is represented by maximum pH-buffering capacity.

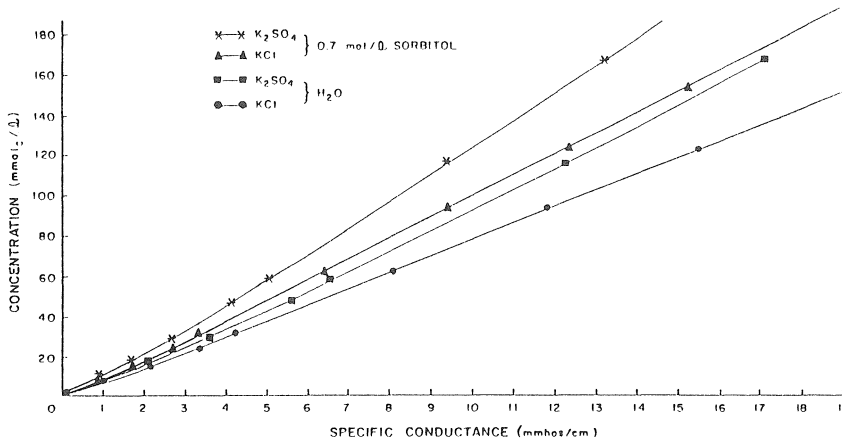

Figure 1.8a. Relationship between specific conductance and concentration of KCl or K_2SO_4 in H_2O or 0.7 mol L^{-1} sorbitol. (From Evangelou and Wagner, 1987. With permission.)

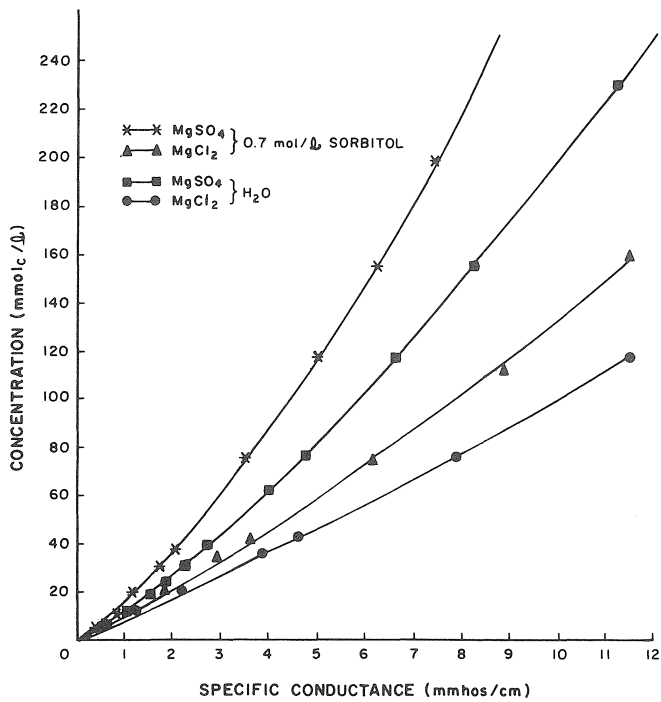

Figure 1.8b. Relationship between specific conductance and concentration of $MgCl_2$ or $MgSO_4$ in H_2O or 0.7 mol L^{-1} sorbitol. (From Evangelou and Wagner, 1987. With permission.)

1.2.1 Alkalinity speciation

There are two potential buffers in natural water systems void of clay sediments; one is the phosphate ($H_2PO_4^-$) and the other is the bicarbonate (HCO_3^-). The role of the $H_2PO_4^-$ buffer is minimal simply because its concentration in natural water systems is normally negligible. Bicarbonate plays a very important role in buffering large natural bodies of water. Below are two examples showing the role of CO_2–H_2CO_3–HCO_3^-–CO_3^{2-} controlling pH of rain and natural bodies of water void of suspended solids (clay colloids). In the case of rain water, the following reactions have effect.

$$pCO_2 + H_2O \overset{K_a}{=} H_2CO_3 \tag{1.38}$$

where pCO_2 denotes partial pressure of CO_2,

$$H_2CO_3 \overset{K_1}{=} H^+ + HCO_3^- \tag{1.39}$$

Summing Reactions 1.38 and 1.39

$$pCO_2 + H_2O \overset{K_aK_1}{=} H^+ + HCO_3^- \tag{1.40}$$

and

$$K_aK_1 = (H^+)\,(HCO_3^-) \,/\, pCO_2 \tag{1.41}$$

Since

$$H^+ = HCO_3^- \tag{1.42}$$

then

$$H^+ = [K_aK_1pCO_2]^{1/2} \tag{1.43}$$

Substituting values into Equation 1.43,

$$H^+ = [(10^{-1.47})\,(10^{-6.4})\,(10^{-3.52})]^{1/2} \tag{1.44}$$

$$H^+ = 2.04 \times 10^{-6} \text{ mol } L^{-1} \tag{1.45}$$

$$pH = 5.69 \tag{1.46}$$

The actual measured pH of rain water in equilibrium with atmospheric pCO_2 is somewhere around 5.6. Values of pH below 5.6 can either be due to an increased pCO_2 or due to industrial emissions causing what is known as "acid rain".

As shown by the calculations, the dissolution of CO_2 in water is the cause of acid water. However, considering that soils and/or geologic systems are sources of HCO_3^- and CO_3^{2-} upon contact of water with the soil or geologic environment, the water picks up additional HCO_3^- and CO_3^{2-} and this shifts pH to higher values.

Maximum buffering capacity of the H_2CO_3–HCO_3–CO_3^{2-} systems occurs at pH 6.4 and 10.3 because at pH 6.4 the H_2CO_3 is equal to HCO_3^- concentration and at pH 10.3 the HCO_3^- is equal to CO_3^{2-} concentration. These pH buffer relationships are shown in Figure 1.9.

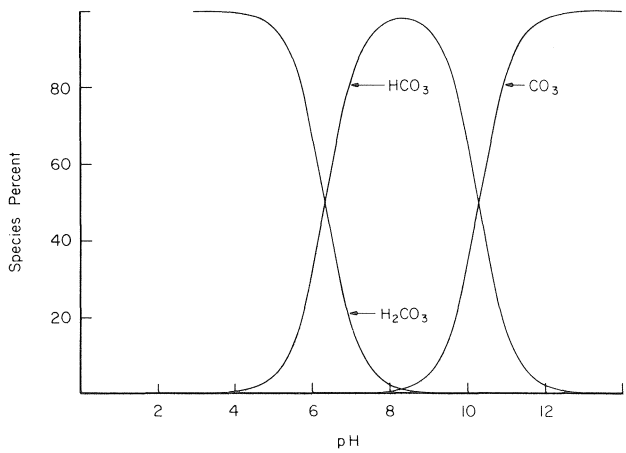

Figure 1.9. Speciation diagram of the carbonate system.

The Y intercepts at 50% of the species shown, when extrapolated to the X-axis, are indicative of the pH values at which maximum buffering capacity occurs. In order to understand Figure 1.9 clearly, the following mathematical relationships should be understood. The total dissolved carbonate (C_t) is described by:

$$C_t = H_2CO_3 + HCO_3^- + CO_3^{2-} \quad (1.47)$$

Percent of any of the carbonate species in relationship to the total carbonate dissolved (C_t) can be expressed as:

$$\text{Percent } H_2CO_3 = (H_2CO_3 / C_t) \times 100 \quad (1.48)$$

$$\text{Percent } HCO_3^- = (HCO_3^- / C_t) \times 100 \quad (1.49)$$

$$\text{Percent } CO_3^{2-} = (CO_3^{2-} / C_t) \times 100 \quad (1.50)$$

Considering the equations,

$$HCO_3^- = (H_2CO_3)\,(K_1) / (H^+) \quad (1.51)$$

and

$$CO_3^{2-} = (K_2)\,(HCO_3) / (H^+) \quad (1.52)$$

by substituting Equations 1.51 and 1.52 into Equation 1.47 and rearranging, the following equations are derived:

$$\text{Percent } H_2CO_3 = [(H^+)^2 \,/\, (H^+)^2 + K_1(H^+) + (K_1K_2)] \times 100 \qquad (1.53)$$

$$\text{Percent } HCO_3^- = [(H^+)\,(K_1) \,/\, (H^+)^2 + K_1(H^+) + (K_1K_2)] \times 100 \qquad (1.54)$$

and

$$\text{Percent } CO_3^{2-} = [(K_1K_2) \,/\, (H^+)^2 + K_1(H^+) + (K_1K_2)] \times 100 \qquad (1.55)$$

where K_1 and K_2 are $10^{-6.4}$ and $10^{-10.3}$, respectively. Knowing the pH of a given water sample and the total concentration of the carbonate dissolved (C_t) (obtained by titration) percent H_2CO_3, HCO_3^-, CO_3^{2-} can be calculated as a function of pH by Equations 1.53, 1.54 and 1.55 as shown in Figure 1.9.

1.2.2 Neutralization potential

Starting from the concept of electroneutrality,

$$\Sigma Z_iC_i - \Sigma Z_j A_j = 0 \qquad (1.56)$$

where Σ denotes sum, Z_i and Z_j valency of cations and anions, respectively, and C_i and A_j denote concentrations of anions and cations, respectively. For any water sample, the electroneutrality equation would appear as follows:

$$[2(Ca^{2+}) + 2(Mg^{2+}) + (Na^+) + (K^+) + (H^+)] - [2(SO_4^{2-}) + (Cl^-)$$

$$+ (NO_3^-) + (OH^-) + 2(CO_3^{2-}) + (HCO_3^-)] = 0 \qquad (1.57)$$

Equation 1.57 can be used to calculate alkalinity by considering:

Alkalinity (Stumm and Morgan, 1970) =

$$2(CO_3^{2-}) + (HCO_3^-) + (OH^-) - (H^+) \qquad (1.58)$$

However, Equation 1.58 does not include the H_2CO_3 component, which is part of the total carbonate dissolved (C_t) (Equation 1.47), and reveals nothing about the pH where maximum buffering capacity is observed.

A more appropriate way of expressing alkalinity and/or acidity of acid waters emanating from disturbed natural environments, e.g., mining, is by defining the term commonly known as "neutralization potential".

Neutralization potential =

$$2(CO_3^{2-}) + (HCO_3^-) + (OH^-) - (HSO_4^-) - (H^+) - 2(Mn^{2+}) -$$

$$2(Fe^{2+}) - 2(Cu^{2+}) - 3(Al^{3+}) \quad (1.59)$$

If the solution to Equation 1.59 gives a negative number, this value is considered to be *acidity*; on the other hand, if the solution to Equation 1.59 gives a positive number, this value is considered to be *alkalinity*.

1.2.3 Alkalinity contribution by $CaCO_3$

Alkalinity of effluents is controlled mostly by carbonate minerals. The most common carbonate mineral in coal mining environments is limestone ($CaCO_3$). The factors that affect $CaCO_3$ solubility are pH and pCO_2. The equations that one needs to consider in estimating solubility and alkalinity are:

$$CaCO_3 \overset{K_1}{=} Ca^{2+} + CO_3^{2-} \quad (1.60)$$

$$H_2CO_3 = pCO_2 \quad (1.61)$$

$$H_2CO_3 \overset{K_2}{=} H^+ + HCO_3^- \quad (1.62)$$

$$HCO_3^- \overset{K_3}{=} H^+ + CO_3^{2-} \quad (1.63)$$

where

$$C = \text{Henry's constant} = 0.0344 \quad (1.64)$$

$$pCO_2 = 3.1 \times 10^{-1} \quad (1.65)$$

$$K_1 = 3.98 \times 10^{-9} \quad (1.66)$$

$$K_2 = 4.28 \times 10^{-7} \quad (1.67)$$

$$K_3 = 4.68 \times 10^{-11} \quad (1.68)$$

Utilizing Equations 1.60 to 1.63 with the appropriate constants (Equations 1.64 to 1.68) and rearranging yields:

$$\log Ca^{2+} = 9.76 - 2pH + \log 1/pCO_2 \quad (1.69)$$

As shown from Equation 1.69, the solubility of $CaCO_3$ in water depends on two interdependent variables and its solution can only be carried out through succesive approximations (Garrels and Christ, 1965). These two interdependent variables are pCO_2 and pH. When pCO_2 changes, pH and Ca

also change. The concentration of Ca reflects the level of alkalinity in water since mass-balance reveals that any Ca quantity (moles) released from $CaCO_3$ must be accompanied by a similar quantity (moles) of CO_3. The solution of Equation 1.69 is given by Figure 1.10.

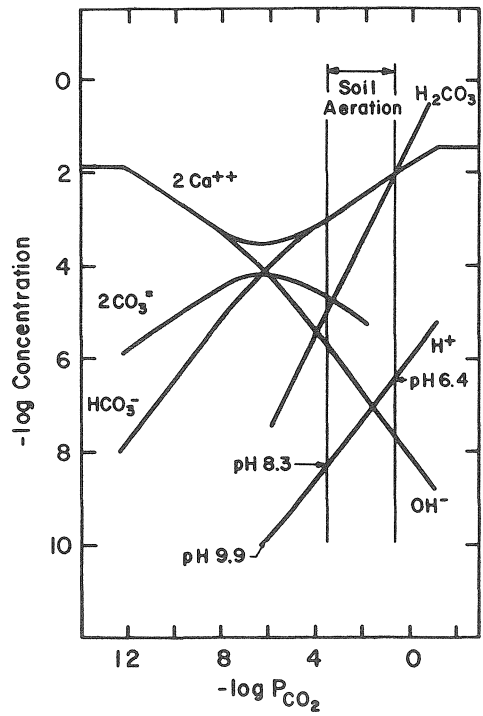

Figure 1.10. Stability diagram of $CaCO_3$ in natural water systems and soil or geologic solutions.

Figure 1.10 indicates that as pCO_2 increases, HCO_3^- concentration also increases and parallels the increase in Ca^{2+} concentration. On the other hand, pH decreases, consequently OH^- and CO_3 decrease. However, the magnitude of the decreases of the latter two components is small in comparison to the increases in the HCO_3^- concentration.

Based on the above, alkalinity increases as pCO_2 increases, but pH decreases. This behavior has brought some confusion with respect to treating acid drainages with $CaCO_3$. Most reactions in the natural environment are driven by OH^-, not alkalinity. The latter ensures a large OH^- supply but it does not mean OH^- concentration in solution would be high enough to drive a given reaction. For example, in order to remove Mn^{2+} (an undesirable ion) from solution, either directly as a hydroxide precipitate or indirectly as an oxide precipitate through oxidation to Mn^{3+} and/or Mn^{4+}, solution pH has to

be raised to higher than 9. However, in order to obtain a solution pH higher than 9 by $CaCO_3$, pCO_2 must be less than that of the atmosphere's. Recall that any increase in the pCO_2 brings an increase in alkalinity but a decrease in OH^- (Figure 1.10). Note that most natural systems exhibit pCO_2 significantly greater than that of the atmosphere.

1.3 Practical Implications

This Chapter focussed on three most important aspects in treating acid waters, e.g., mine effluents. One aspect involved the factors that affect mineral solubility, the second aspect involved factors controlling pH and alkalinity and the third aspect involved utility of specific conductance measurements. When treating acid metallic drainages, metals are removed from solution either as mineral precipitates of given solubility or through mineral surface sorption of given strength. The potential of either of these two mechanisms to effectively remove metals from solution depends on type of ions, and salt quantity remaining in solution. Both factors have tendency to increase undesirable metal ion concentration either through suppressing metal-ion activity and/or increasing solution pairing/complexation. The practical suggestion that comes out from this information is that dilution of heavy-metal contaminated waters should enhance effectiveness of neutralization treatments.

The second practical aspect of this Chapter is to inform the reader of the limitations of limestone as an alkalinity source. The important thing one needs to remember when employing $CaCO_3$ is that its alkalinity release potential increases as pCO_2 increases due to lowering pH. The low pH may not allow heavy metal precipitation even though alkalinity is high. In such situations stronger bases should be used, e.g., NaOH, $Ca(OH)_2$, etc.

The third practical aspect dealt with the limitations of specific conductance measurements. One should be aware that specific conductance measurements of metallic drainages are hard to interpret since such solutions exhibit extremely low pH, and EC reflects mostly H^+, or such solutions have high tendency to form solution pairs/complexes and/or even large -hydroxy polymers which are poor conductors due to their extremely low mobility.

Taylor & Francis
Taylor & Francis Group
http://taylorandfrancis.com

Chapter 2
ELECTROCHEMICAL AND PHYSICAL PROPERTIES OF GEOLOGIC MATERIAL

2.1 Introduction

Acid drainage production in mining environments, popularly known as AMD, is attributed to pyrite oxidation. However, the natural geologic environment is made of many other minerals which may contribute to AMD production or may inhibit AMD production. Commonly, the minerals that are part of the natural geologic system, e.g., mine waste, and could be involved in AMD production/control include *1) aluminosilicates, 2) metal oxides,* and *3) organic matter.* The manner in which these minerals could be involved in the production/control of AMD is mainly through their surface electrochemical properties.

2.2 Aluminosilicate minerals

The silicate minerals constitute the majority of the crystalline natural minerals. They consist of Si-O tetrahedrons in which one silicon atom is centered between four oxygen atoms. These simple structures form chains, rings and sheets by sharing oxygen atoms. As should be expected from the non-homogeneity of nature, minerals of this form are not perfect crystals and have impurities in their structures. The substitution of an aluminum atom for silicon in the tetrahedron is very common. A subgroup of the silicate minerals, the layer silicates or phyllosilicates are of particular importance when considering geologic material because they make up a large part of the < 0.2 μm "clay sized" particles. These minerals are also referred to as clay minerals. For additional information on silicate minerals present in natural geologic environments the reader is referred to *Minerals in Soil Environments* (Dixon and Weed, 1977).

Clay minerals have one or more sheets of Si-O tetrahedrons and one or more sheets of aluminum hydroxide, or gibbsite (Figure 2.1).

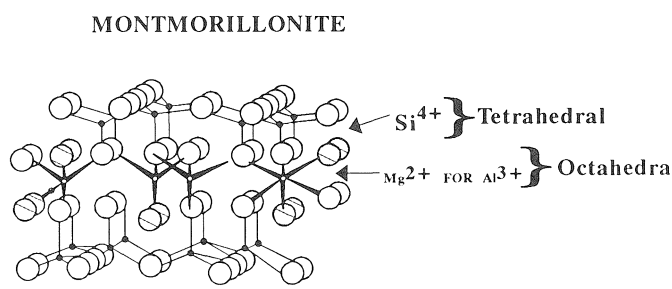

Figure 2.1. Diagram showing the composition and stereochemistry of montmorillonite. (From Dixon and Weed, Eds., 1977. With permission.)

In this latter mineral, the Al atom is in six-fold coordination with the OH molecule. For this reason, it is called the octahedral sheet. In clay minerals each octahedron shares two oxygens, or an edge with its adjacent neighbor. Substitutions can also occur in the octahedral sheet as well as in the octahedral sheet. Magnesium substituting for Al in the octahedral sheet and Al substituting for Si in the tetrahedral sheet are common occurrences. The amount of substitution in the tetrahedral and octahedral sheets and the ratio of octahedral to tetrahedral sheets are the primary differentiating characteristics between the many clay minerals. For example, clays that have two tetrahedral sheets and one octahedral sheet are known as 2:1 clay minerals, while clays that have one tetrahedral sheet and one octahedral sheet are known as 1:1 clay minerals. Table 2.1 gives a brief description of some of the common clay minerals encountered in natural environments.

Table 2.1
Layer silicates with some of their surface properties

Mineral	CEC $cmol_c\ kg^{-1}$	Surface area $m^2\ g^{-1}$	Layer type
Kaolinite	3 - 15	10- 20	1:1
Montmorillonite	60 - 100	600-800	2:1
Vermiculite	110 - 160	600-800	2:1
Illite	20 - 40	40-180	1:1
Chlorite	10 - 30	70-150	2:2
Mica	20 - 40	70-120	2:1

CEC = Cation exchange capacity

2.3 Metal-Oxides

The oxides of iron and manganese are considered here due to their common occurrence, frequently in high concentrations, in natural geologic systems and their role on pyrite oxidation. Iron commonly occurs in the 2^+ and 3^+ oxidation states and manganese in the 2^+, 3^+ and 4^+ oxidation states. The solubilities of these oxides are very low in the pH ranges typically encountered in terrestrial waters, soils and geologic strata. Any of these metals in the reduced state released by weathering or from being brought to the surface through large scale land disturbances (surface mining) may form an oxide or oxyhydroxide in a sequence of events as follows: The first step may be, for example, iron weathering from a silicate rock through the process of water dissolution or iron release through the oxidation of the $-S_2$ present in

pyrite. The second step involves the actual oxidation of iron by giving electrons to an available sink such as atmospheric oxygen (O_2).

Structurally, the Fe and Mn oxides that are commonly formed by the series of events given above are similar to the gibbsite structure previously mentioned. The manganese oxides as a group are almost exclusively in octahedral arrangement. They differ from gibbsite though by having oxygens at the corners of the octahedron instead of hydroxyls. The most common Fe oxides, hematite (Fe_2O_3) and goethite (FeOOH) also have the gibbsite octahedral arrangement. For more information on metal oxides see *Minerals in Soil Environments* by Dixon and Weed (1977).

2.4 Organic Matter

Seventy to eighty percent, by weight, of the organic matter found in most natural geologic material, e.g., soils, and waters consists of humic substances (Schnitzer, 1986). Humic substances are generally defined as condense polymers of aromatic and aliphatic compounds produced during decomposition of plant and animal residues and by microbial synthesis (Martin and Haider, 1986). They are amorphous, dark-colored, hydrophilic, with a wide range in molecular weight from a few hundreds to several thousands (Schnitzer and Kodama, 1977; Schnitzer, 1991). Furthermore, humic substances contain a very large number of sites possessing reproducible properties and non-identical functional groups with different range of pK_a values (Ephraim et al., 1989).

Conventionally, humic substances can be further partioned into three main fractions based upon their solubility in acid-base solutions. The first group is *humic* acid. This compound is soluble in dilute alkali but precipitates on acid solution. The second group is *fulvic acid*. Fulvic acid is soluble both on alkali and acid solutions. The third group is *humin* fraction. This fraction is insoluble both in alkali and acid solutions.

2.4.1 Chemistry of humic substances

As mentioned above, humic substances are complex compounds with various amounts and type of building units, functional groups, and structural units. Based on wet chemistry analyses, many researchers reported that humic substances exhibited similar elemental and functional-group composition in spite of the origin and environmental conditions of their formation (Lowe, 1969; Khan, 1971). However, Skjemstad et al. (1983), Saiz-Jiminez et al. (1986), Novak and Smeck (1991) found out that humic substances formed in different climatic regimes and natural soils contain different range of aromaticity and functional group contents. Furthermore, the aromatic component of soil humic substances ranges from 35 to 92 percent (Hatcher et al., 1981).

Even though a great deal of research has been done on humic substances, their structure is still far from being understood. According to a

current concept, the basic structure of humic substances consists of aromatic rings of the di- or trihydroxy-phenol type bridged by -O-, -CH_2-, -NH-, -N=, -S-, and other groups and contains both free OH groups and the double linkage of quinones (Stevenson, 1982). Some researchers have proposed structural formulae of humic and fulvic acids, however, none of them has proved entirely satisfactory.

Understanding the structural formulae of humic substances will help in understanding the chemical properties and reactivity of humic substances in the natural soil/geologic environment. Generally, humic and fulvic acids have similar structure, but they differ in molecular weights, elemental and functional group contents. Fulvic acid is lower in molecular weight and contains more oxygen-containing functional groups and elemental oxygen, but less nitrogen and carbon per unit weight than humic acid (Schnitzer and Khan, 1972; Sposito et al., 1976; Schnitzer, 1991). Furthermore, practically almost all oxygen in fulvic acid can be accounted by functional groups (COOH, OH, C=O), whereas a high portion of oxygen in humic acid occurs as a structural component of the nucleus (e.g., in ether or ester linkage) (Stevenson, 1985). Functional groups of humic substances are fractioned into three clusters of different dissociation constants. Commonly, the lower the dissociation constant (higher pK_a) the weaker the metal-organic complex. The *very weak cluster* was presumed to include phenolic-hydroxyl residues, carboxyl residues and nitrogenous bases of very high pK_a's. The *weak cluster* was presumed to include various aliphatic and aromatic-carboxyl residues and nitrogenous bases of medium pK_a's. Finally, the *strong cluster* was presumed to include the carboxyl residues of low pK_a, of salicylate or phthalate (Arai and Kumada, 1977).

Buffle (1984) stated that the principal structural characteristics of humic substances that influence their chemical reactivity are: **a**. polyfunctionality; humic substances represent heteropolymer molecules and contain various types of functional groups and therefore, they have a broad range of functional group reactivity; **b**. macromolecular charge; humic substances carry negative charges due to proton dissociation from various functional groups; **c**. hydrophilicity; humic substances tend to form strong hydrogen bonds with water molecules solvating polar functional groups; and **d**. structural lability; humic substances are capable of associating intermolecularly and of changing molecular conformation in response to changes in pH, redox potential (Eh), electrolyte concentration, and functional-group binding.

2.5 Clay Mineral Surface Charge

The dynamic physical behavior of natural geologic particles in solution is due to two characteristics. 1) Large surface area, which to an extent is a result of smaller diameter, i.e , a rock broken into many pieces has more surface per unit mass than when the rock was whole, and 2) The

existence of an electrical charge at the particle's surface. There are two types of charges at the surface of mineral particles: a) permanent charge and b) variable charge.

2.5.1 Permanent structural charge

As previously mentioned, the tetrahedral and octahedral sheets of clays are coordinated by the Si^{4+} and Al^{3+} cations respectively. Minerals in their natural environment of crystallization, however, undergo metal substitutions. A substitution involves the replacement of one coordinating metal cation by another coordinating cation in the structure. The substituting cations are commonly of lower valence. This substitution, known as isomorphous, leaves the mineral within its crystal lattice in a state of non-electrical neutrality. In other words, the number of positive charges due to cations in the mineral structure differ from the number of negative charges due to the negatively charged ions present in the structure.

Since cations of higher valence are replaced by cations of lower valence, a deficit of internal positive charge results, or conversely a net negative charge on the mineral surface is generated. Correspondingly, a negative potential is created at the crystal surface. To maintain electrical neutrality in the system (a law that must always be obeyed), cations from solution are absorbed onto the negatively charged mineral surface (Figure 2.2).

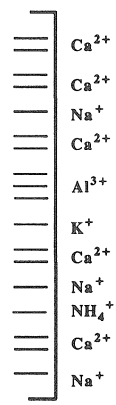

Figure 2.2. Schematic showing a number of cations absorbed to a negatively charged clay surface.

Note that Figure 2.2 is only a representation of exchangeable cations and surface negative charge since the latter is of a delocalized nature and the internal charge deficit is averaged over the whole surface. The surface charge associated with aluminosilicates is not strictly due to isomorphous substitutions. In general, this type of charge dominates this class of minerals.

However, kaolinite, also an aluminosilicate, can have as much as 50% of its charge generated by means of other than isomorphous substitution (Bohn et. al, 1983) (see also section *2.5.2*).

From ion desorption-adsorption data, it is known that regardless of the surface charge, both cations and anions can be found near the surface, and the distribution of ions at the solid:solution boundary is a diffuse one with a high concentration of counterions near the charged surface. As the distance increases from the particle surface into the bulk solution, the concentration of counterions decreases at some exponential rate. This theory of ion adsorption and distribution was first described by Gouy and by Chapman, independently, in 1910 and is now known as the Gouy-Chapman Diffuse Double Layer Theory. The complete derivation of the Gouy-Chapman model has been outline by several authors (Singh and Uehara, 1986; Stumm and Morgan, 1981; Van Olphen, 1977; Gast, 1977; Babcock, 1963).

As previously mentioned, not all absorbed ions are in direct contact with the charged surface. A large portion of the adsorbed cations are at some distance from the mineral surface with water molecules between them and the surface. The electrical potential acting on these cations is pulling them towards the particle surface. Simultaneously, however, these cations are being affected by diffusion. The latter is pulling them towards the bulk solution. Therefore, the absorbed ions extend outward to a point where the force exerted by the surface electric potential equals that of diffusion. The decrease in the electrical potential as distance increases from the charged surface is the basis for the "Diffuse Double Layer Theory". This relationship is quantitatively described by the Poisson-Boltzmann equation

$$d^2S / dx^2 = K^2 \mathrm{Sinh} (zF\psi / RT) / (zF / RT) \qquad (2.1)$$

where, S = local potential (volts),
x = distance from surface (cm),
z = Valence of absorbed ion,
F = Faraday's constant (96,490 coulombs eq^{-1}),
ψ = Surface electrical potential (volts),
R = Universal gas constant (8.314 J mol^{-1} K^{-1}),
T = Absolute temperature (K).

The component K is the inverse of the thickness of the double layer which extends from the solid surface to the point where the local potential is that of the bulk solution. It is given by,

$$K = (e^2 \sum_i n_i z_i^2 / \varepsilon\varepsilon_o kT)^{1/2} \qquad (2.2)$$

where, e = electron charge (1.6×10^{-19} coulombs),
$1/2\sum_i n_i z_i^2$ = ionic strength of the solution (mol L^{-1}),

ε_o = permittivity in vacuum (8.854×10^{-14} coul V^{-1} cm^{-1},
ε = relative dielectric permittivity (dimensionless, $\varepsilon = 80$ for water),
k = Boltzmann constant (1.38×10^{-23} J K^{-1}).

For all practical purposes, the only terms in Equation 2.2 that are variable are the valence and concentration of the ions in the bulk solution. In further dissecting the equation (Equation 2.2), one finds that under constant temperature $e^2/\varepsilon\varepsilon_o kT$ is a constant and can be defined as λ, therefore,

$$K \simeq \lambda^{1/2} (I)^{1/2} \tag{2.3}$$

where, I = ionic strength of the solution (mol L^{-1}). Also for a small ψ the total surface charge (σ_o) is (Stumm and Morgan, 1970)

$$\sigma_o = (\varepsilon K/4\pi)\psi \tag{2.4}$$

Equations 2.3 and 2.4 reveal that when I, e.g., salt concentration, increases, K increases, but ψ decreases leading to a constant σ_o. Note that by definition σ_o is directly related to the experimental cation exchange capacity (CEC) of soil/geologic material.

Since, concentration and valence of the charged solution constituents dictate distance that the diffuse layer extends into the bulk solution, when I increases, either by an increase in ion concentration or by an increase in ion valence, the drop in potential to that of the bulk solution occurs in a short distance from the solid surface, thereby creating a thin diffuse layer. It is the thickness of the diffuse layer that determines how close particles can approach each other (Figure 2.3).

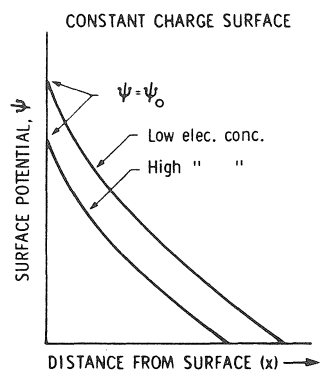

Figure 2.3. Schematic of electric potential distribution for two electrolyte concentrations as a function of distance for a constant charged surface. (From Dixon and Weed, Eds., 1977. With permission.)

Based on the above, the magnitude of the cation exchange capacity (CEC) of a constant charge mineral is independent of pH, salt concentration or type of metal cation. But, according to the double layer theory, even though the CEC is independent of pH, salt concentration, or type of metal cation, most minerals with a charged surface respond to the valence of ions according to the Schulze-Hardy rule. It states, in short, that ions of higher valence will adsorb/flocculate colloids more efficiently than ions of lower valence. This information has practical utility with respect to managing water quality in sediment ponds used for the treatment of acid water in mining operations. For example, sediment ponds with low concentrations of salt will have a tendency to carry high suspended solids of the constant charge type. On the other hand, waters with a higher proportion of divalent cations relative to monovalent cations will have a tendency to carry low suspended solids of the constant charge type even at low salt concentrations. For more information on the concept of suspended solids in sediment ponds and surface charge of minerals see Evangelou (1989) and Evangelou and Karathanasis (1991). The above behavior of charged particles in natural waters is graphically demonstrated in Figure 2.4.

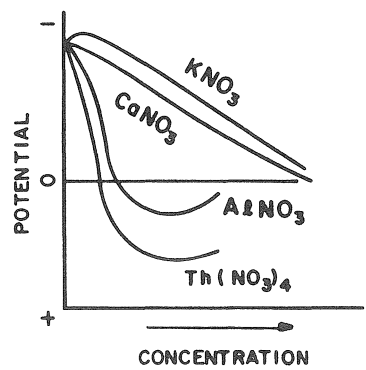

Figure 2.4. Influence of salt concentration and type of salt on surface electric potential. (From Taylor, 1972. With permission.)

The figure shows that cations with higher valence are more effective in suppressing the surface electrical potential, hence, better flocculants. However, note that large concentrations of cations with high valence have a tendency to induce charge reversal, a phenomenon which reverses the process of mineral particle (colloid) flocculation, e.g., increases suspended solids.

2.5.2 Variable charge

Unlike clay minerals, metal oxides and other nonsilicate minerals maintain electrical neutrality within their crystal lattice and their charge does

not arise from isomorphic substitution. These minerals have variable, or pH-dependant charge.

Variable charge arises from the protonation and deprotonation of functional groups at particle surfaces. Figure 2.5 is a representation of the terminal edge of an iron oxide crystal under three pH conditions. In the acid condition, there is an excess absorption of H^+ ions resulting in a net positive charge at the oxygen and hydroxyl functional groups. At the other end of the scale, high pH conditions leave the exposed oxygens deprotonated and the surface has a net negative charge. At a pH value near neutral, the degree of protonation is such that the positive and negative charges at the adsorption sites are equal. The pH value is commonly referred to as the "point of zero charge" (PZC_{pH}). For variable charge minerals, the PZC_{pH} represents the pH at which maximum particle agglomeration occurs. Generally speaking, it also represents the pH value of lowest solubility for the mineral (Parks and DeBruyn, 1962). Metal oxides are by no means the only minerals having variable charge characteristics. Kaolinite is an aluminosilicate that may attain as much as 50% of its negative charge by deprotonation of terminal oxygens and hydroxyls at high pH (pH~7) (Figure 2.6).

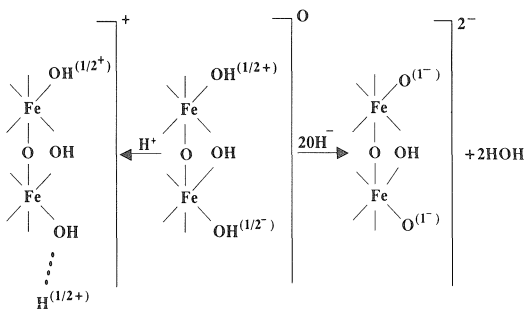

Figure 2.5. Schematic showing the zero point of charge of an iron oxide surface and the charge generated as a function of added Hydrogen (H^+) or Hydroxyls (OH^-). (From Sparks, Ed., 1986. With permisssion.)

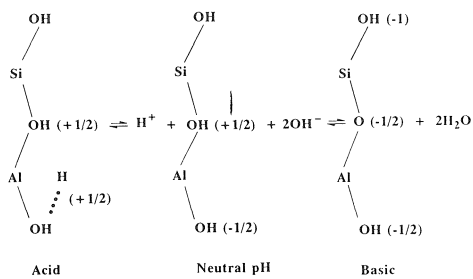

Figure 2.6. Schematic of pH-dependent charge at kaolinite edges. (From Schofield and Samson, 1953. With permission.)

It is important to note that for variable charge minerals, the potential at the surface remains constant and is not affected by the concentration of ions in solution (Figure 2.7). In the case of permanent charge minerals on the other hand, for which adsorption capacity remains unaffected by pH, the surface potential varies with the concentration of salt in solution (Figure 2.3). This difference in the behavior of the potential of the two types of minerals with respect to the electrolyte concentration influences the physicochemical stability of charged mineral particles. Oster et al. (1980) reported that montmorillonitic particles (constant charge, variable surface potential) have a tendency to form tactoids (surface to surface aggregation) while illitic particles which have a large fraction of their charge at the edges (variable charge, constant surface potential) have a tendency to aggregate in an edge to surface mode.

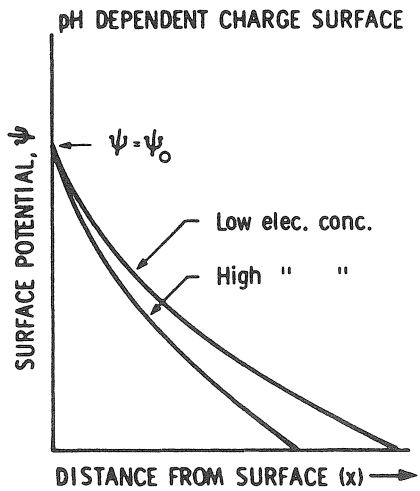

Figure 2.7. Schematic of electric potential distribution for two electrolyte concentrations as a function of distance for a pH-dependant charged surface. (From Dixon and Weed, Eds., 1977. With permission.)

Variable charge minerals exhibit amphoteric characteristics with respect to the nature of this charge. At some pH value, depending on the mineral type, the net charge of the mineral is zero. This point, as was indicated earlier, is known as PZC_{pH}. At pH values above the PZC_{pH}, the mineral exhibits a net negative charge, while at pH values below the PZC_{pH}, the mineral exhibits a net positive charge. The pH value that is identified as the PZC_{pH} is also known as the point of coflocculation or agglomeration.

The relationship between surface electric potential and charge is given by the Gouy-Chapman model,

$$\sigma_o = [(2c\varepsilon kT)^{1/2}/(\pi)] \sinh (zeS_o/2kT) \quad (2.5)$$

where, σ_o = total surface charge (esu cm^{-2}),
c = electrolyte concentration (ions cm^{-3}) and all other terms are as previously defined,
ε = dielectric constant of solution,
S_o = surface electric potential,
kT = Boltzman's constant times absolute temperature,
z = valence, and
e = electron charge.

Equation 2.5 reveals that as surface electrical potential (S_o) increases, the charge on the surface increases. For constant electrical potential surfaces (variable charge minerals), S_o can be described by the Nernst equation,

$$S_o = (RT/F)\ln C/C_o \quad (2.6)$$

where, C = concentration of potential determining ion in solution,
C_o = concentration of potential determining ion at $S_o = 0$,
and F = Faraday's constant.

Since H^+ and OH^- are considered to be potential determining ions (PDI's), Equation 2.6 can be written as:

$$S_o = (RT/F) \ln H^+/H_o^+ \quad (2.7)$$

or

$$S_o = 59(-pH + pH_o) \text{ at } 25^\circ \text{ C}, \quad (2.8)$$

where pH_o is the pH at which σ_o and S_o are equal zero, also defined as the PZC_{pH}. The above reveal that the CEC of soil/geologic material composed of a mixture of constant and variable charge minerals is dependent on pH, salt concentration, and ion valence. Note, for example, that based on Equation 2.8, as pH increases above the PZC_{pH}, S_o decreases. Equation 2.5 reveals that as S_o increases, σ_o or CEC also increases. Equation 2.5 also points out that as salt concentration and/or ion valence increases, σ_o also increases. The above are demonstrated in Figure 2.8 which considers that geologic systems are mixtures of variable and constant charge minerals. This figure demonstrates that as pH rises above 3, the positive charge or anion exchange capacity (AEC) of the minerals decrease, but the CEC remains unaffected up to pH 5 but begins to increase dramatically above pH 5. The practical meaning of these data is that above pH 5 the potential of this geologic/soil material to adsorb cations, e.g., Ca^{2+} Mg^{2+} Mn^{2+}, Fe^{2+}, increases dramatically. On the other hand, the potential of this soil/geologic material to adsorb anions, e.g., SO_4^{2-}, decreases. This mineral surface charge behavior

due to pH changes has important ramifications in the chemical quality of water emanating from disturbed sites, e.g., mining operations.

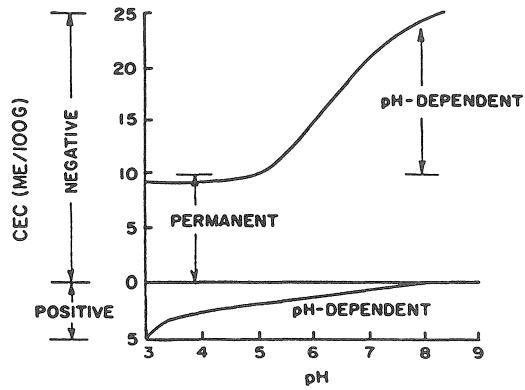

Figure 2.8. Mineral cation exchange capacity (CEC) behavior as a function of pH. (From Bohn et al., 1979. With permission.)

The relationship between pH and surface charge is not easy to predict in natural soil/geologic systems. This is especially true in natural systems where the clay minerals are a mixture of constant and variable charge. Processes that control the apparent PZC_{pH} of such systems are specific absorption and/or chemisorption of cations and/or anions and exchange reactions which some of the potential determining ions also undergo. However, it is specific adsorption and/or chemisorption only that dictates nature and magnitude of the variable surface charge.

Surface charge generation and behavior on variable charge colloid surfaces takes place due to the specific adsorption or inner-sphere complex formation (see section *2.6.1*) of H^+ and OH^-. However, specific adsorption is not limited to H^+ and OH^-. Other ions such as HPO_4^{2-}, Fe^{3+}, Al^{3+}, etc., are also specifically adsorbed and thus have influence on the surface charge of soils (Wann and Uehara, 1978; Singh and Uehara, 1986; Uehara and Gillman, 1981; Sposito, 1981, 1984). Wann and Uehara (1978) and Singh and Uehara (1986) also presented evidence of weak specific adsorption having influence on variable charge surfaces. Ions forming outer-sphere complexes differ with respect to their potential to influence the surface charge of variable charge minerals, e.g., metal-oxides, when compared to ions forming inner-sphere complexes, e.g., HPO_3^{2-}, $FeOH^{2+}$. Generally, cations forming outer-sphere complexes, e.g., Ca^{2+}, shift the PZC_{pH} to lower pH values while cations forming inner-sphere complexes, e.g., Al^{3+}, shift the ZPC_{pH} to higher pH values (Singh and Uehara, 1986). On the other hand, anions forming outer-sphere complexes, e.g., SO_4^{2-}, shift the PZC_{pH} to higher pH values, while

anions forming inner-sphere complexes, e.g., HPO_3^{2-}, shift the ZPC_{pH} to lower pH values (Sposito, 1981; Singh and Uehara, 1986).

Wann and Uehara (1978) reported that in an iron rich soil the use of $CaCl_2$ as background electrolyte shifted the PZC_{pH} to lower pH values than when the background electrolyte was NaCl. They attributed this shift to the ability of Ca^{2+} to undergo low affinity specific adsorption or form outer-sphere complexes, thus increasing the negative charge of the mineral surface by displacing protons. Wann and Uehara (1978) also reported a drop in the PZC_{pH} of an Oxisol (an extensively weathered soil) from pH 4.7 to pH 3.5 in the presence of 1500 ppm P as PO_4^{3-} with $CaCl_2$ as the background electrolyte (Figure 2.9). At the practical level, the data in Figure 2.9 reveal that the potential of the mineral material to adsorb cations increases as a function of pH, phosphate added and valence of the cation.

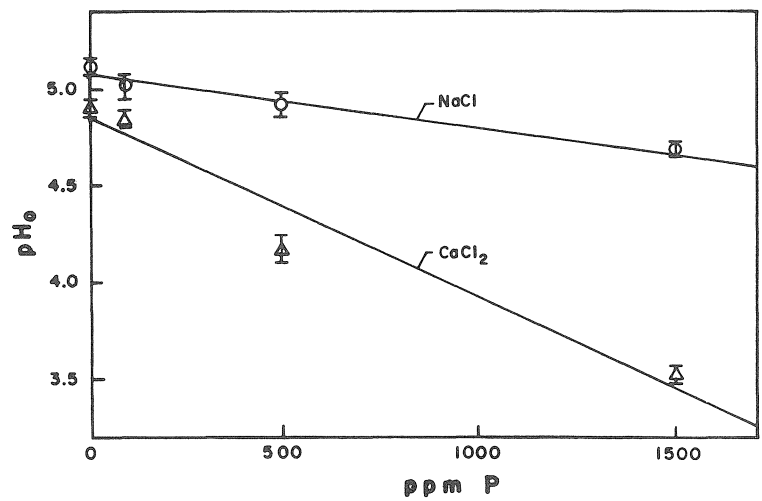

Figure 2.9. Relationship between PZC_{pH} (pH_o) and phosphorus (P) levels. (From Wann and Uehara, 1978. With permission.)

The higher the valence the higher the potential of the charged mineral surface to adsorb cations. The role of pH on metal adsorption by soils/geologic material is also demonstrated in Figure 2.10. These data clearly show that as pH increases, lead (Pb) adsorption increases. This increase in Pb adsorption as a function of pH appears to take place in both soil horizons. However, Pb adsorption appears to be greater for A soil horizon than B soil horizon suggesting that since A soil horizon contains a greater amount of organic matter this increase in metal adsorption is due mostly to organic matter. This is most likely due to the organic matter's high charge density and nature of functional groups (see sections 2.6 and *2.6.1*). For the above reasons, addition of limestone, phosphate and/or organic matter to pyritic geologic

material is recommended because of the increase in the potential of such mineral material to adsorb heavy metals, including Fe^{2+}, Fe^{3+} and Mn^{2+}. Adsorption of Fe^{3+} would inhibit pyrite oxidation (see also Chapters 5 and 6).

There are mainly three forms of chemical constituents in pyritic geologic/soil material, 1) *pore-solution constituents*, 2) *surface adsorbed constituents*, and 3) *potentially decomposeable/soluble solids*. *Pore-solution constituents* represent those dissolved in the pore water. *Surface adsorbed constituents* are those composed of minerals or nutrients, e.g., Ca, Mg, K,. Na, etc., and heavy metals, e.g., Al, Fe, Mn, Cu, Pb, etc., and/or H^+. *Potentially decomposeable/soluble solids* include pyrite, carbonates, metal oxides, and primary minerals such as feldspars. Additional information on

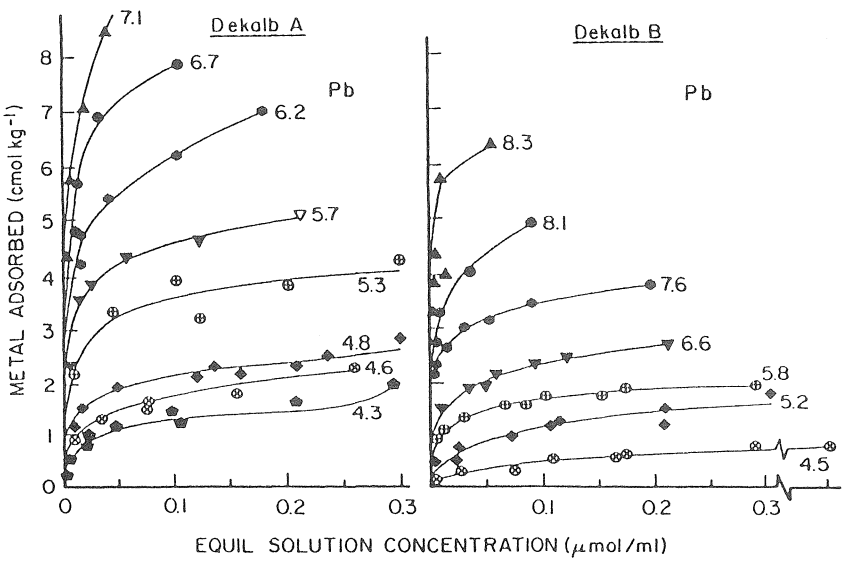

Figure 2.10. Adsorption isotherms for lead (Pb) by a soil's A and B horizons adjusted at various pH levels by $Ca(OH)_2$. (From Harter, 1983. With permission.)

the above is given in chapters 4 and 5. Commonly, field reclamation practitioners are interested in the quantities of pyrite and alkalinity ($CaCO_3$ equivalents) present in a sample but give little attention to the actual dissolved constituents (see Chapter 5) or surface adsorbed constituents. It is assumed that these components play an insignificant role in the reclamation

process. However, this is not always the case. A second reason for ignoring adsorbed constituents is lack of information on the meaning of such data.

The CEC of a soil/geologic material is composed of two types of constituents, 1) weak acid metals or commonly referred to as "bases", e.g., Ca^{2+}, Mg^{2+}, K^{+}, and Na^{+}, and 2) relatively "strong" acid metals which includes heavy metals as well as H^{+}, depending on the nature of the sample, e.g., industrial geologic waste or natural soil (Al^{3+}, H^{+}, Fe^{2+}, Fe^{3+}, and Mn^{2+} describe mining spoils or "waste"). The term percent (%) base saturation is commonly used to describe the percent exchangeable "bases" relative to the CEC near pH 7 or at pH 7 (CEC_7). The equation for % base saturation is given as

$$\%\text{base saturation} = (\text{Exchangeable bases}/CEC_7) \times 100 \qquad (2.9)$$

An empirical relationship between pH and % base saturation is shown in Figure 2.11.

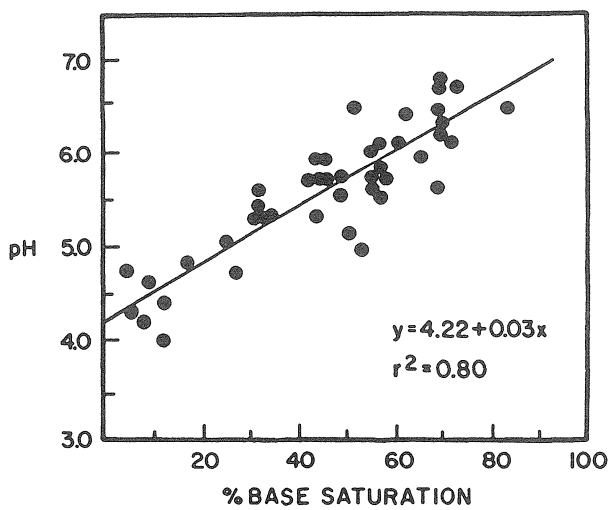

Figure 2.11. The relationship between soil suspension pH and % base saturation. (From Magdoff and Bartlett, 1985. With permission.)

Note that this relationship appears to be linear. However, this linearity does not imply any mechanistic/molecular meaning because soils/clay minerals contain many different functional sites. The general behavior of these data however, is of practical value. For example, a sample with base saturation of approximately 20% will exhibit a pH of approximately 5, while a pH of approximately 7 suggests a % base saturation of 100%. Field practitioners tend to apply to the field enough limestone, as an alkalinity reservoir, to take

care of the acid produced by the oxidation of pyrite. However, if the quantity of limestone applied is solely based on pyritic sulfur there will not be enough limestone to raise % base saturation above 65% in order to attain an approximate pH of 6. Percent base saturation can be converted to limestone requirement by taking into consideration a) the CEC of the material, b) the % base saturation prior to limestone addition, c) the % base saturation desired, and c) 1 $cmol_c\ kg^{-1}$ mineral surface acidity requires one ton of limestone, assuming a 50% limestone neutralization efficiency.

2.6 Reaction Among Humic Substances, Clays, and Metals

The interaction between heavy metals and soil colloids (clay, organic matter, or combination) has been described as ion exchange, surface adsorption, and chelation reactions (Mortensen, 1963; Nand Ram and Raman, 1983). The capability of humic substances to form complexes with heavy metals is attributed to their high content of oxygen-containing functional groups such as carboxyl (COOH), hydroxyl (OH), and carbonyl (C=O) (Piccolo and Stevenson, 1982).

Many studies have been carried out to evaluate the ability of clay minerals, organic matter (humic substances) or clay-humic-substances mixtures to adsorb heavy metals or to form complexes with heavy metals. Most of these studies dealt with desorption-adsorption reactions (Schnitzer and Skinner, 1965; Khan, 1969; Tiller et al., 1984; Di Toro et al., 1986). The results of these studies suggested that the extent of heavy metal retention by mixtures of geologic or soil colloids has been found to vary with ionic strength, pH, type of clay minerals, organic functional groups and type of competing cations.

Hatton and Pickering (1980) studied the effect of pH on the retention of Cu^{2+}, Pb^{2+}, Zn^{2+}, and Cd^{2+} by clay-humic acid mixture. They reported that the amount of metal ion adsorbed by the solid surface increased with increasing pH from 3 to 6 for illite-humic acid mixture, but decreased for the kaolinite-humic acid and montmorillonite-humic acid mixture. The same result was reported by Beveridge and Pickering (1980). They observed that the metal ions adsorbed in acid media increased with pH until the threshold value required for partial dissolution of solid and formation of soluble metal-humate complexes was exceeded. Moreover, the increase in metal binding capacity of colloid surface suggested that protons (H^+) competed with cations for specific binding sites (Inskeep and Baham, 1983a; Iwasaki et al., 1990; Saar and Weber, 1982). However, hydroxyl ion (OH^-) competes with humic substances for the cationic metal-ion. As pH is raised, humic substances become more available for complexation, but the metal-ions become less available. An intermediate pH most favors complexation between humic substances and metal-ions (Saar and Weber, 1982).

2.6.1 Mechanisms of complex formation

The retention of metal ions by clay, organic, or clay-organic complex surfaces has been a focus of much research in recent years (Sposito, 1985). Various mathematical models have been developed to predict the speciation of metals in natural water and soil systems. Furthermore, mechanistic models have been formulated to quantify the complexation of metals by both mineral and organic soil constituents (Gamble et al., 1983; Dzombak et al., 1986; Dudley and McNeal, 1987).

The adsorption reaction that occurs between metallic ions and the charged surfaces of clay mineral particles may involve either formation of relatively *weak outer-sphere* complexes or formation of *strong inner-sphere* complexes. An *outer-sphere* complex is a relatively weak electrostatic association between a hydrated cation and a charged surface. This weakly surface-associated cation is easily exchanged by other cations that form only *outer-sphere* complexes. On the other hand, an *inner-sphere* complex is a strong covalent association between an unhydrated cation and a charged surface. This strongly surface associated cation can not be readily exchanged by other cations that form only *outer-sphere* complexes (Sposito, 1984; Evans, 1989).

A number of studies have been carried out to evaluate the metal-organic complexes. For example, Sposito, Holtzclaw, and LeVesque-Madore (1978, 1979) studied Ca^{2+} and Cu^{2+} ion complexation by fulvic acid extracted from sewage sludge-soil mixture. They found out that fulvic acid extracted from sewage sludge exhibited two distinct classes of functional groups. The *first class* of functional groups, identified as the most strongly acidic functional group, appears to form a stronger complex with cations (Cu^{2+}, Ca^{2+}). The *second class* forming a weaker metal complexes appears to comprise several kinds of weakly acidic functional groups.

Humic substances which are characterized by having a complex structure and more than one functional group can interact with metal ions in several ways. The schematic presentation of humic substances-metal complexes can be seen in Figure 2.12. The interaction labeled **1** represents the electrostatic interaction between humic substances (negatively charged) and metal ions (positively charged). This interaction (outer-sphere complex) is relatively weak and can easily be exchanged by non-specifically bound cations. The interaction labeled **2** shows complex formation or chelation or inner-sphere complexation. For chelation to occur, the ligand must contain at least two donor atoms capable of bonding the same metal ion and positioned within the ligand so that formation of a ring is sterically possible. This type of interaction can occur in two modes: the first and the most important mode is metal bound in both phenolic OH and COOH groups (**2a**), whereas the second mode involves only COOH groups (**2b**) (Schnitzer, 1969; Gamble et al., 1970). The interaction labeled **3** demonstrates the metal-humic

substances complex through water bridging. This interaction is weak and involves metals with high hydration energy.

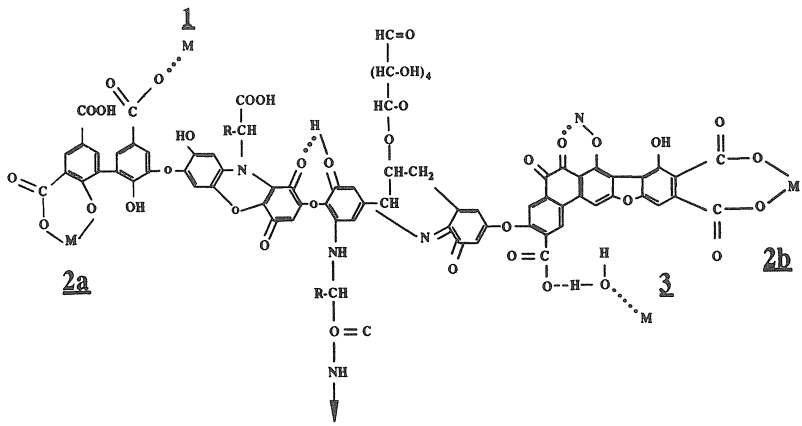

Figure 2.12. Schematic presentation of metal-humic substances complexation 1 Electrostatic interaction, 2 Inner-sphere complexation, 3 Weak water-bridging. (After Stevenson, 1982. With permission.)

Van Dijk (1971) illustrated the reaction between Cu^{2+} and humic acid as affected by pH as follows: At low pH, a proton is displaced from an acidic OH group of humic acid, whereas at high pH a proton dissociates from water molecules covalently bound to Cu^{2+}, therefore a hydroxo-complex is formed (Figure 2.13).

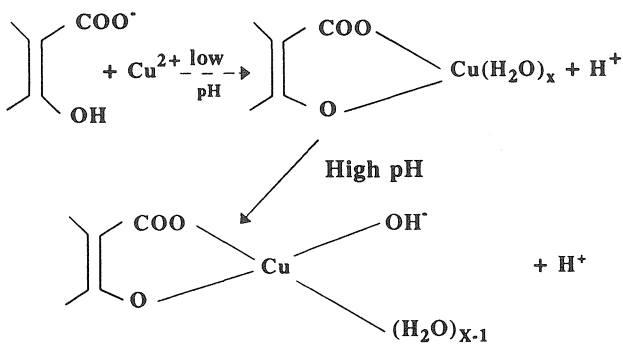

Figure 2.13. Schematic presentation of strong Cu^{2+}-humic complexation.

Another possible mechanism of Cu-humic substances complex formation is one Cu^{2+} molecule bound into two molecules of organic substances. This mechanism is described by Schnitzer (1969) as shown in Figure 2.14.

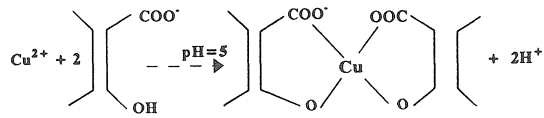

Figure 2.14. Schematic presentation of inner-sphere Cu^{2+}-humic complexation.

The same mechanisms are involved in Cd^{2+} complexes, however, Cu^{2+} forms stronger complexes with organics than Cd^{2+} (Stevenson, 1976; Guy and Chakrabarti, 1976; Abd-Elfattah and Wada, 1981).

In general, humic substances carry negative charges. These charges of humic substances are due to proton dissociation of the functional groups, e.g., carboxylic OH, phenolic OH, alcoholic OH, and serve as reactive sites involving ion adsorption and/or chelation reactions.

There is evidence that in natural soils or geologic systems humic substances form a strong complex with clay and cannot be readily broken except with drastic treatment. The most probable mechanisms of clay-humic substances complexes as summarized by Greenland (1971) are: **1** by anion and ligand exchange to clay edges, **2** by cation or water bridges to basal clay surfaces, **3** by H-bonding to the siloxane or gibbsite sheet, **4** by Van der Waals forces, **5** by trapping in the crystal pores, and **6** by adsorption in interlayer spaces. However, the relative contribution of various mechanisms to forming clay-humic complexes are different for different clay minerals. For example, due to the non-expandable properties of illite, the interlayer adsorption of humic substances is negligible (Varadachari et al., 1991; Jardine et al., 1989). Maintaining soil moisture is important for this mode of interaction to take place. An interaction commonly referred to as "specific adsorption" the anion penetrates the coordination shell of an aluminum atom at the edge of an octahedral sheet. The anion cannot be displaced from the complex simply by leaching with a non-specifically adsorbed anion such as chloride. Clay-humic complexes may also be induced by anion exchange and referred to as "non-specific" adsorption. This interaction is probably due to the fact that at low pH Al at the edges of Al-octahedral sheet carries positive charge. Therefore, coulombic forces operate in this interaction.

It is very hard to distinguish the potential of organic material to form *inner-sphere* complexes with heavy metals but it is commonly known that such complexes represent a significant fraction of the total charge of the organic material. The total charge of decomposed organic material, e.g., humic acids, appears to be related to the average pK_a as shown in Figure 2.8. These data show that the greater the pK_a the lower the charge (CEC). The fact that the CEC of organic material is pK_a dependent also demonstrate that

the CEC is also pH dependent. Thomas and Hargrove (1984) and references therein reported that the CEC of organic material varied from 36 $cmol_c\ kg^{-1}$ at pH 2.5 to 213 $cmol_c\ kg^{-1}$ at pH 8. Furthermore, Thomas and Hargrove (1984) showed that the apparent pK_a of organic matter increased from 4 to 6 when trivalent metals (e.g., Al^{3+}) were complexed. This suggested that when Al^{3+} and organics formed a complex the CEC of organic matter was expected to decrease by more than half (Figure 2.15). An alternate explanation for this observed CEC decrease was formation of Al-hydroxy *inner-sphere* complexes which blocked off exchange sites as demonstrated in Figure 2.13.

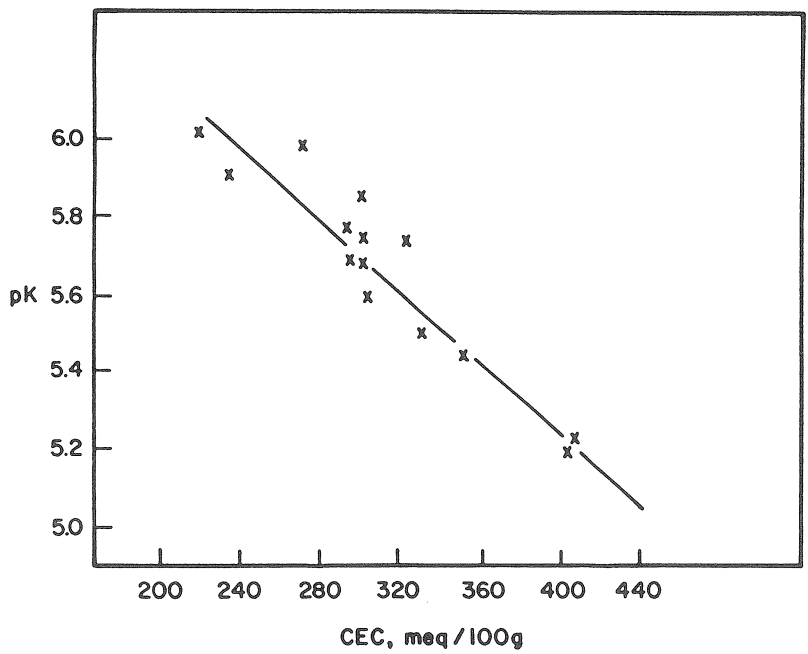

Figure 2.15. The relationship between cation exchange capacity (CEC) and pK_a values. (From Posner, 1966. With permission.)

The above imply that organic matter because of its great potential to complex metals such as Fe^{3+}, may have the potential to suppress pyrite oxidation. Under certain conditions, ferric iron (Fe^{3+}) is known to be an effective pyrite oxidant (see Chapter 6).

2.7 PZC_{pH} and Potential Pyrite Oxidation Implications

The PZC_{pH} of a solid phase is most often determined by potentiometric titration of a mineral sample suspension in several concentrations of NaCl. The latter is an indifferent electrolyte. An

indifferent electrolyte is one in which neither the anion or the cation specifically absorbs to the solid surface. If the pH of a suspension is above the PZC_{pH} of the solid and NaCl is added, sodium will go onto the solid's surface displacing H^+, and thus suspension pH will decrease. On the other hand, if suspension pH is below the PZC_{pH} of the solid's surface and NaCl is added, Cl^- will go onto the solid's surface displacing OH^-, and suspension pH will increase. When the suspension pH is at the PZC_{pH} of the solid's surface then the addition of an indifferent electrolyte would have no influence on the pH of the suspension. This is demonstrated in Figure 2.16 which clearly shows the cross-over point of the potentiometric titrations of an iron oxide.

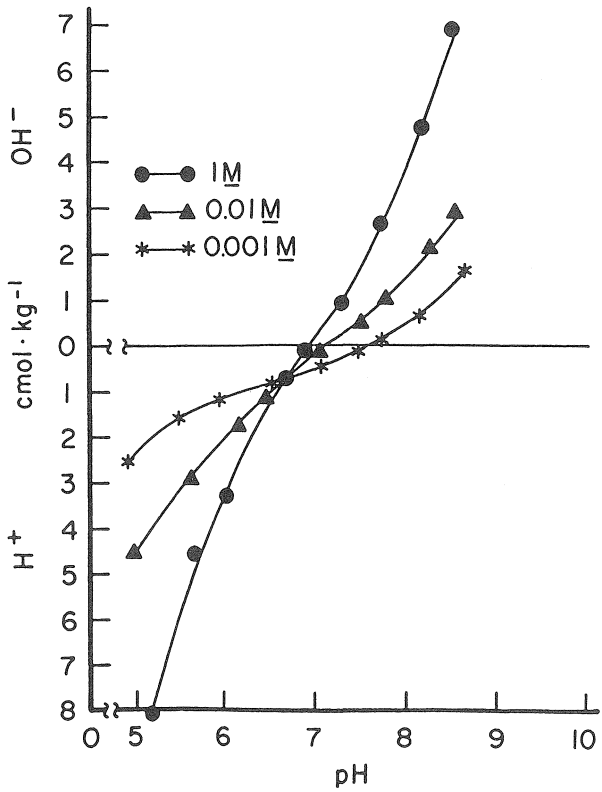

Figure 2.16. Potentiometric titrations of an iron oxide (hematite) formed under laboratory conditions (The point at which all three lines converge is representative of the PZC_{pH}).

This cross-over point is important because it represents the pH at which the iron oxide coagulates and stabilizes chemically, e.g., forms an iron oxide coating. This is shown in Figure 2.17, which reveals that maximum iron oxide particle settling took place around PZC_{pH}.

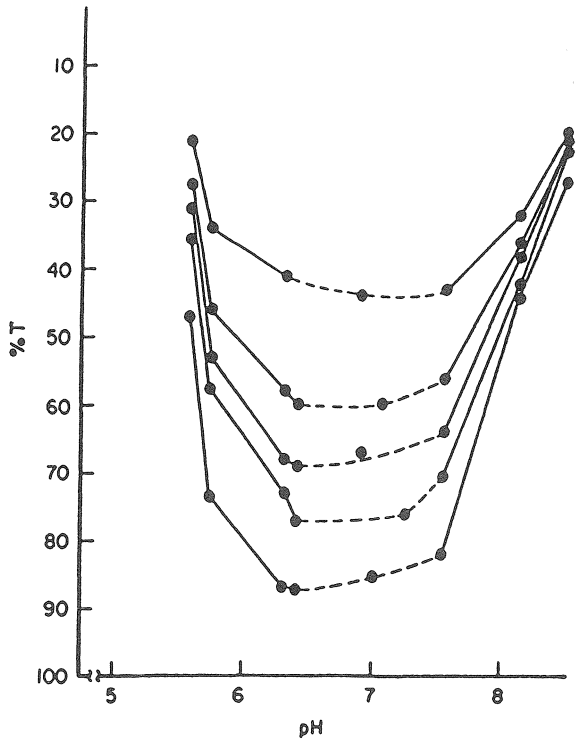

Figure 2.17. Settling characteristics of an iron oxide (hematite) formed under laboratory conditions, as a function of pH.

The above potentiometric technique has been deemed questionable for hybridized systems. The technique was originally designed to measure the PZC_{pH} (also referred to as the isoelectric point (IEP)) of purely variable charged systems. For these systems it can be assumed that functional groups are the only consumers of acid or base. This, however, may not be valid since the hydronium ion (H_3O^+) is also involved in exchange reactions and mineral dissolution (Parker et. al., 1979). This is demonstrated in Figure 2.18. These data point out that this particular coal spoil sample does not exhibit a titration cross-over point perhaps because its PZC_{pH} is near pH 4 where clay mineral dissolution may also be taking place.

Several electrokinetic methods, such as electrophoresis and streaming potentials have been utilized to locate PZC_{pH} values. In general, they measure the rate at which particles move through a solution when an electric current is imposed on them. If the particles are positively charged

they move toward the anode, and if they are negatively charged they move toward the cathode.

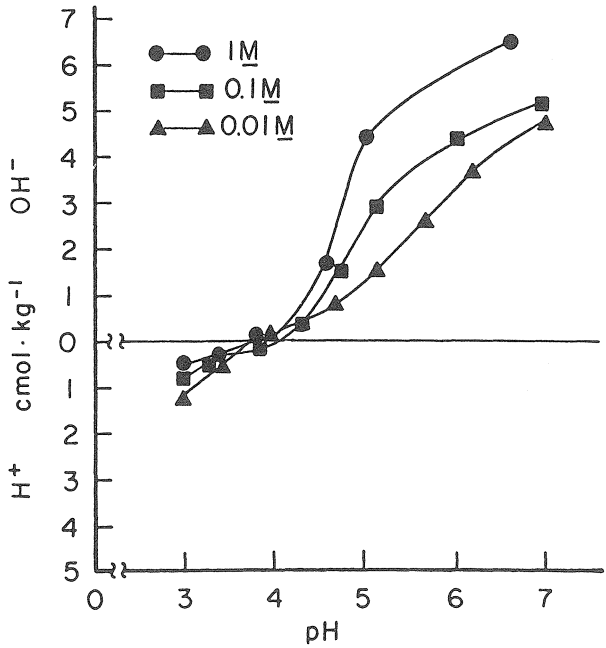

Figure 2.18. Potentiometric titrations of a coalmine waste sample (The point at which all three lines converge is representative of the PZC_{pH}).

The pH at which such charged particles do not move is the PZC_{pH} or IEP. Data are shown in Figure 2.19a,b. They represent electrophoretic mobility data in terms of the Zeta potential which is the electrical potential manifesting itself at the outer side of the Helmholtz Layer (Figure 2.20). The data in Figure 2.19 clearly suggest that when pyrite ages in the presence of O_2 the PZC_{pH} shifts to higher pH values or close to those of an iron oxide. This suggests that it is possible to microencapsulate pyrite in a coating of iron oxide (Nicholson et al., 1988, 1990). This topic is discussed in some detail in Chapter 9.

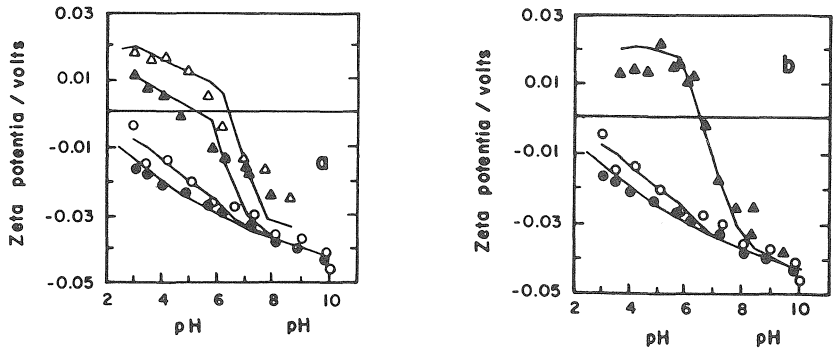

Figure 2.19a. Zeta potential of pyrite as a function of pH and for conditioning time of: 0.5 hr in argon; 0.5 hr in air; 2 hr in air; 19 hr in air. (From Fornasiero et al., 1992. With permission.)

Figure 2.19b. Zeta potential of pyrite as a function of pH and for conditioning time of: 0.5 hr in argon; air; oxygen. (From Fornasiero et al., 1992. With permission.)

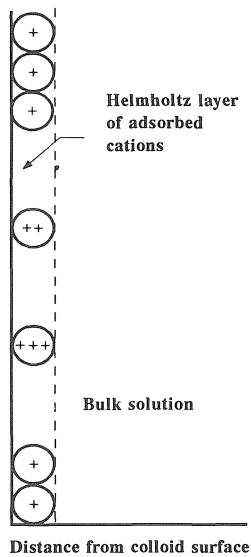

Figure 2.20. Distribution of cations near the surface of montmorillonite according to the Helmholtz model.

Chapter 3
CHEMICAL AND PHYSICAL PROPERTIES OF GEOLOGIC MATERIAL (MINE WASTE)

3.1 Mine 'Waste'/Spoil

Mine 'waste' or spoil refers to the heterogeneous mass of geologic material left on the surface of deep mined sites or surface mined sites. Such geologic 'waste' can also be produced on land disturbed by highway construction, industrial/housing development, airport construction, etc. This heterogeneous geologic material may be composed of decomposing sandstones, siltstones, limestones, gray or black shale of marine or deltaic origin, and clays. In many cases it may also contain mixtures of 'A,' 'B' or 'C' soil horizons.

In the case of surface mining, this last situation occurs less often in the U.S. since the passage of 'The Surface Mining Control and Reclamation Act of 1977'. The act specifies that when any land is to be surface mined, its soil should be removed in the sequence of its horizons and each horizon should then be separately stockpiled. After completion of the mining process the soil should be spread back in its proper sequence. However, often undisturbed land has a relatively thin layer of 'top soil' or 'A' horizon so its segregation is economically unfeasible. Also, in many instances, the subsoil is of very low quality as a medium for plant growth. Under these conditions, the mine operator may rely on chemical tests of the geologic substrata to determine if the resulting mine 'waste' may be material suitable for plant growth and if so, use it as 'topsoil'. On occasion, the mine operator may stockpile the so-called 'top soil' or 'A' horizon that may account for a depth of at least 15 cm. Below 15 cm depth, the newly generated 'soil profile' would be dominated by mine 'waste'.

Based on the above, reconstructed surface mined lands are of three types: a) mined lands, the surface of which is composed of redistributed 'A,' 'B' and 'C' horizons, b) mined lands, the surface of which is composed mainly of mine 'waste' and c) mined lands, the surface of which is composed of 'A' horizon underlaid by mine 'waste' or on occasions 'B horizon' if such material was available.

Shale and sandstone are two of the most common geologic material found in the coal mine fields of the U.S. These fields are separated into two distinct groups, depending on geographic location, 1) the western U.S. coal fields, and 2) the eastern U.S. coal fields. In general, the western coal fields yield low sulfur coal, and the clay mineral fraction maybe mostly smectite, kaolin, mica, chlorite and interstratified mica and collapsible vermiculite (Evangelou, 1981; Dollhopf and DePuit, 1981). On the other hand, the eastern coal fields are generally known to produce high sulfur coal and the clay mineralogy of the resultant mine 'waste' is mostly dominated by kaolinite, mica, quartz and chlorite (Barnhisel and Massey, 1969; Barnhisel et

al., 1982). Barnhisel and Massey (1969) pointed out that based on the various mine 'waste' samples they analyzed for texture determination, nearly 30% of any particular sample was represented by particles of clay size fraction. It has been the personal experience of this author that, in general, mine 'waste' may vary in texture from sand, to more than 50% clay, to fine silt (Table 3.1).

Table 3.1
Textural classification of various mine 'waste' samples

Sample Number	Location	Textural classification
1	Pleasant Run Watershed, KY.	SICL
2	Ohio County, KY.	SIL
3	West Virginia coal fields	SL
4	Hopkins County, KY.	SL
5	Pleasant Run Watershed, KY.	SIL
6	Hopkins County, KY.	SIL
7	White City-Drakes Creek, KY.	SIL
8	Pleasant Run Watershed, KY.	SIL
9	Hopkins County, KY.	SIL
10	Hopkins County, KY.	SIL
11	Pleasant Run Watershed, KY.	SIL
12	Hopkins County KY.	SIL
13	Johnson County KY.	SIL

SL = Sandy Loam; L = Loam; SIL = Silty Loam; SICL = Silky Clay Loam

In some cases, the clay mineralogy of mine 'waste' is similar to the clay mineralogy of the surrounding soils, an observation which suggests that soils and spoils of the particular area have derived from similar geologic strata. However, even though the clay mineralogy of soils and spoils of a given area may be similar, the overall chemistry of soils when compared to that of spoils may not be the same. Long-term exposure of soils to the elements of nature (temperature fluctuations, organic matter accumulation, salt leaching, agricultural utilization) have brought about changes.

Commonly, mine 'waste' of certain geographic location are chemically treated similarly to soils of the same location. This is an ill-advised practice since the overall chemistry of mine 'waste' will be dictated by the environmental and the depositional conditions existing at the time of formation of a particular stratum. For example, was the area tropical subtropical or temperate? Also, was the environment an ocean basin, a lake

basin, or a delta? Knowing these conditions helps determine what one might expect from exposing a certain geologic stratum to the elements of nature.

The above depositional conditions generally produce five types of mine 'waste' in terms of overall chemistry (Table 3.2)

Table 3.2
Chemical composition of water from coalmine spoils at saturation

Sample Identification	Classification	Ca^{2+}	Mg^{2+}	K^{+}	Na^{+}	pH	EC
		$mmol_c\ L^{-1}$					$mmhos\ cm^{-1}$
Kentucky	Acid	18.9	13.6	0.2	1.2	3.6	2.6
"	Neutral	19.1	8.1	0.4	0.5	7.1	2.1
Montana	Sodic calcareous	2.6	19.5	1.5	77.7	9.0	3.4
North Dakota*	Sodic calcareous	2.2	1.8	-	34.7	8.0	3.0
Kentucky	Calcareous	4.0	2.1	0.3	0.4	7.0	0.7
Illinois**	Coal refuse saline-acid	186.6	29.5	7.0	166.5	5.1	15.4
Kentucky	Saline gypsiferous acid	24.4	93.7	<0.1	<0.1	4.0	7.0
"	Saline gypsiferous neutral	19.3	94.7	0.1	0.4	7.5	7.9
"	Gypsiferous acid	20.2	22.9	0.1	0.2	4.6	3.3

* Jurinak et al., 1981.
** Hiller, 1981.
Note : Spoils are highly variable. It is not unusual for all samples listed from Kentucky to be found within an area of one acre.

1) mine 'waste' that are *rainwater-leached*, 2) mine 'waste' that are *sodic-calcareous/gypsiferous* or strictly *calcareous*, 3) mine 'waste' that are *saline acid/gypsiferous*, 4) mine 'waste' that are *acid-nonsaline nongypsiferous pyritic* and may or may not contain calcareous material and 5) mine 'waste' that are extremely *acid-saline gypsiferous*.

Rainwater-leached mine 'waste' may be either slightly acidic since much of the cation exchange capacity is occupied by H^{+} and/or Al^{3+}, or near neutral because much of their cation exchange capacity is base saturated, i.e.,

mostly occupied by Ca^{2+} and Mg^{2+}. Mine 'waste' that are *sodic-calcareous* or strictly *calcareous* are mainly products of strata of marine or deltaic origin; thus, the environment was conducive to carbonate precipitation. Presence or absence of sodium suggested an environment in which rain-water percolation was relatively restricted, or relatively free, respectively (Evangelou, 1981). The sodium present may not be always associated with chloride or sulfate as one might expect but it may be held on the exchange phase of clay-shales (Evangelou, 1981; Jurinak et al., 1981; Miller and Moor, 1981).

Mine 'waste' that are *saline* in nature are primarily products of geologic strata deposited in marine basins where water was entrapped. These type of strata are limited in coal fields, occasionally however, they are encountered in U.S. mines (Hiller, 1981) and in some mines of the former Eastern European countries. Some mine 'waste', that are pyritic in nature may be base (mainly Ca^{2+} and/or Mg^{2+}) saturated. However, during acidification due to pyrite oxidation these bases may be replaced by Al^{3+}, Fe^{3+}, Fe^{2+}, Mn^{2+} and H^{+}. Thus, depending on the type of cations dominating the exchange phase of the clays, the overall make-up of the chemistry of such spoils may vary from slight to very acid with low salinity (mainly gypsum saturated) or from slight to very acid but with high salinity. Thus, salinity is composed mostly of soluble metal sulfates, e.g. magnesium sulfate, aluminum sulfate, iron sulfate, manganese sulfate, copper sulfate, zinc sulfate, etc. (Barnhisel and Massey, 1969) (Tables 3.3 and 3.4).

The saturation extract data shown in Table 3.4 reveal that 'waste' samples in general can be classified according to pH (which is the traditional approach). However, the most obvious characteristic of these 'waste' samples is that besides having a wide pH range (1.68 to 8.0) they also have a wide range of acid-salinity levels. It can be seen that most samples have a Ca^{2+} concentration greater than 20 $mmol_c\ L^{-1}$, which suggests that they contain free gypsum. The next component that is relatively high in some samples is magnesium which varies in concentration from approximately 0.5 $mmol_c\ L^{-1}$ to 19 $mmol_c\ L^{-1}$. The most obvious difference between some of these 'waste' samples is the iron and aluminum content, shown to vary from near zero to 500 $mmol_c\ L^{-1}$. Such solution acidity levels may have dramatic influence on the effectiveness of limestone (see Chapter 5).

Commonly, results from pyritic-spoil leaching studies are employed to determine a 'waste's' AMD production potential and/or to evaluate acid drainage control treatments. Examples of such studies include those of Hood and Oertel (1984), Infanger and Hood (1980) and Stiller et al. (1985). However, most often, in such studies no attempt is made to quantify the readily available acid components prior to leaching. Chemical measurements made in saturation paste extracts reveal the immediate potential of spoils to produce acid drainage.

Table 3.3
Average chemical composition of spoil leachate after an 8-month reaction period (Lekhakul, 1981)

Type of Spoil	Lime* treatment	pH		Ca^{2+}	Mg^{2+}	Na^{+}	K^{+}	Al^{3+}	Mn^{2+}	Fe^{2+}	SO_4^{2-}
		After a 4-month period	After a 8-month period								
	mt/ha			$mmol_c\ L^{-1}$							
Black Shale	0	1.8	1.8	29.66	337.76	5.41	0.21	301.91	42.66	1166.18	2304.02
	125	4.0	2.2	26.05	508.88	6.28	0.98	41.54	16.40	80.39	734.31
	250	7.0	4.2	24.19	350.50	7.18	1.77	0.47	4.30	0.09	398.85
Siltstone	0	3.8	3.0	23.12	148.86	6.72	0.57	10.40	6.88	1.42	201.54
	67.5	6.8	4.2	23.45	116.07	7.27	0.74	0.72	0.72	0.06	140.27
	135	7.1	4.5	23.31	106.07	7.26	0.76	0.45	0.45	0.05	128.14
Black Shale: Siltstone (1:1)	0	1.8	1.9	28.68	382.25	4.84	0.22	168.36	41.49	589.81	1332.97
	10	4.3	2.2	24.78	354.95	6.13	0.80	20.13	9.20	24.96	458.07
	20	7.7	5.3	23.35	222.79	6.83	1.21	0.16	0.88	0.0	260.64

* Lime rate represents the total measured acidity in the sample.

Table 3.4

Values of pH, electrical conductivity (EC), various cations of the spoil saturation extracts, and redox (Eh) values of the spoil water saturated paste

Sample I.D.*	pH	EC	Eh	Ca	Mg	K	Na	Fe	Mn	Al	SO_4
		mmhos cm^{-1}	mV	$mmol_c\ L^{-1}$							
1	2.4	8.01	−42.70	25.08	15.96	0.34	0.21	3.19	3.90	89.75	138.43
2	7.9	2.15	189.30	17.32	11.66	0.30	0.70	0.09	0.05	0.39	30.51
3	8.0	2.79	299.80	33.82	5.16	0.14	0.89	0.11	0.03	0.16	40.31
4	1.7	19.50	−22.20	24.63	6.00	0.02	0.22	464.66	0.55	470.52	966.60
5	2.7	4.60	−43.20	22.24	12.46	0.06	0.32	0.38	2.15	42.88	80.49
6	3.1	3.83	53.30	24.18	9.60	0.03	0.22	0.66	0.70	35.87	71.26
7	2.1	16.60	−23.20	21.80	17.66	0.03	0.18	587.32	8.94	260.23	896.16
8	7.6	5.79	40.80	23.88	2.26	0.13	0.32	0.14	7.28	13.51	65.52
9	1.9	19.37	1.70	24.70	14.11	0.01	0.15	53.36	1.12	59.71	153.16
10	2.6	8.90	−8.70	21.16	19.11	0.02	0.22	6.50	6.57	134.54	188.12
11	3.1	5.08	−7.20	22.33	11.50	0.15	0.31	0.20	4.50	64.73	103.57
12	3.8	3.83	43.80	25.20	11.96	0.19	0.31	0.48	2.77	9.76	50.67
13	2.9	0.84	37.30	0.62	0.27	0.12	0.16	0.22	0.03	45.53	46.95

*See Table 3.1

Currently, classification of spoils is based on pH, potential acidity, and traditional soil fertility tests. Although these tests reveal what is in storage in terms of acidity and metals, they reveal little about the readily available acidity and dissolved components, i.e., metals, sulfate, alkalinity. Often, these latter parameters (e.g., readily available acidity and dissolved components) dictate water quality emanating from such spoils during the initial phases of a leaching event.

3.2 Chemical and Physical Properties

A number of soil extraction techniques have been developed and tested mainly on agricultural soils for the purpose of determining fertility status or particular farming suitability (Jackson, 1958; Chapman, 1965; Polemio and Rhodes, 1977; Thomas, 1982). The use of these procedures in mine 'waste' are considered adequate for relating available metals to pore water and/or plant roots (Sobek et al., 1978; Severson and Gough, 1985). These techniques mainly involve water extractions (e.g., saturation extract) for salt determination and various pH buffered and pH unbuffered salt solution extractions for determining extractable cations/anions.

Cation exchange capacity (CEC) of mine 'waste' refers to cation adsorption potential, while anion exchange capacity (AEC) refers to anion adsorption potential. Thus, magnitude of CEC and AEC describes the potential of geologic material to store cations and anions, respectively. The data in Table 3.5 show magnitude of CEC and AEC for various mine 'waste' samples (described in Table 3.1) employing various techniques (pH buffered/unbuffered). These data reveal variability in CEC depending on technique used. In general, CEC varies from approximately 1 $cmol_c\ kg^{-1}$ to 11 $cmol_c\ kg^{-1}$ which is considered relatively low (see Chapter 2, Table 2.1). Anion exchange capacity varies from approximately 1.5 $cmol_c\ kg^{-1}$ to 3.8 $cmol_c\ kg^{-1}$ which is also considered low but significant. It is of interest to note also that the NH_4Cl determined CEC is in general higher than the $BaCl_2$+triethanolamine (TEA) pH 8 or the ammonium acetate (NH_4AC) pH 7 determined CEC. The results indicate that these mine 'waste' do not exhibit apparent pH-dependent charge. If this is true, such spoil materials would be prime candidates to be treated with sewage sludge, or organic mulch, or phosphate. All of these materials are known to add significantly to the CEC of geologic materials.

The acid components of pyritic mine 'waste' are the potentially available Al^{3+}, iron (Fe^{2+}, Fe^{3+}), Mn^{2+}, and H^+. These acid components may also be referred to as exchangeable acidity. Commonly, these particular acid components have been mostly ignored with respect to their potential role in AMD abatement. However, the most important factor in bringing AMD production under control is to identify and classify these potentially readily available acid components.

Table 3.5
Cation exchange capacity (CEC) and anion exchange capacity (AEC) values determined by various techniques

Sample I.D.*	Cation exchange capacity			Anion exchange capacity
	NH_4AC	NH_4Cl	$BaCl_2$+TEA	NH_4Cl
	$cmol_c\ kg^{-1}$			$cmol_c\ kg^{-1}$
1	9.07	11.61	10.93	2.39
2	4.81	8.69	6.14	1.65
3	4.31	5.04	4.73	1.46
4	7.05	8.57	8.23	2.18
5	6.29	10.06	9.61	2.91
6	7.54	9.01	7.58	2.60
7	5.67	6.17	5.85	3.82
8	5.85	6.96	5.95	3.50
9	5.65	7.13	6.90	2.98
10	7.58	9.25	9.01	3.68
11	7.14	9.29	8.93	3.08
12	7.66	10.14	9.96	3.16
13	1.04	3.98	1.33	2.43

*See Table 3.1

Table 3.6 reveals the quantities of extractable or exchangeable "bases", Ca^{2+}, Mg^{2+}, K^+, Na^+, and the quantities of extractable or exchangeable adsorbed acids, Fe^{2+}, Fe^{3+}, Mn^{2+}, Al^{3+}, using 1 *M* NH_4Cl. Extractable or exchangeable "bases" determined by $BaCl_2$ + TEA pH 8.2 are shown in Table 3.7. These data reveal that the $BaCl_2$ + TEA pH 8.2 extracted fewer metal "bases" than the NH_4Cl (Table 3.6). This suggested that in the case of some of these mine 'waste' samples, increase in pH may increase surface adsorption of acid metals. Based on this, one may conclude that the neutralization potential of such mine 'waste' samples may increase significantly after liming. On the other hand, a number of 'waste' samples in Tables 3.6 and 3.7 do not appear to exhibit such behavior.

The data in Table 3.6 reveal % base saturation, an index of acidity/toxicity, for a number of spoil samples. It is of interest to note in these data that correlation between % base saturation and pH is not as apparent as demonstrated in Chapter 2, Figure 2.11. The reason for this is that coal spoil

Table 3.6
Extractable cations by the NH_4Cl procedure

Sample #	Ca	Mg	K	Na	Fe	Mn	Al	NH_4Cl^*	NH_4Cl^{**}	pH	
	$cmol_c\ kg^{-1}$							% Base Saturation			
1	1.02	0.35	0.09	0.20	0.10	0.04	4.93	18.2	14.2	2.4	
2	5.59	2.51	0.13	0.21	0.02	0.01	0.28	175	96.9	7.9	$CaCO_3$ present
3	13.02	0.26	0.08	0.21	0.03	0.00	0.26	314	268	8.0	$CaCO_3$ present
4	7.78	0.04	0.07	0.21	1.00	0.00	0.74	114	93.8	1.7	$CaSO_4$ present
5	2.77	0.12	0.07	0.21	0.06	0.02	1.39	50.6	31.6	2.7	
6	15.48	0.11	0.06	0.20	0.04	0.01	1.37	210	175	3.1	$CaSO_4$ present
7	0.38	0.20	0.06	0.20	0.47	0.02	0.60	14.8	13.6	2.1	
8	4.61	0.55	0.08	0.20	0.03	0.07	2.26	92.8	78.07	7.6	
9	22.99	0.07	0.06	0.21	2.01	0.01	0.60	406	333	1.9	$CaSO_4$ present
10	4.92	0.28	0.07	0.21	0.39	0.04	1.20	72.2	59.0	2.6	$CaSO_4$ present
11	1.37	0.13	0.08	0.21	0.05	0.05	1.65	25.0	19.2	3.1	
12	18.38	0.30	0.09	0.21	0.04	0.04	2.02	247	186	3.8	$CaSO_4$ present
13	0.11	0.02	0.07	0.21	0.05	0.00	0.10	39.0	10.3	2.9	

#See Table 3.1 * NH_4-acetate CEC ** NH_4-chloride CEC

materials are not well weathered/leached, and presence of minerals such as $CaSO_4 \cdot 2H_2O$ or $CaCO_3$ may contribute excess Ca, thus increasing their apparent % base saturation.

Table 3.7
Extractable cations by the $BaCl_2$ + Triethanolamine (TEA), pH 8.2 procedure

Sample* #	Ca	Mg	Na	K	Total
	$cmol_c\ kg^{-1}$				
1	0.79	0.12	0.05	0.03	0.99
2	4.51	2.03	0.14	0.03	6.70
3	12.13	0.23	0.04	0.02	12.42
4	2.18	0.02	0.03	0.01	2.23
5	2.03	0.04	0.02	0.01	2.10
6	4.47	0.04	0.02	0.01	4.54
7	0.06	0.08	0.02	0.02	0.18
8	2.03	0.29	0.06	0.02	2.40
9	1.72	0.02	0.02	0.01	1.77
10	2.73	0.19	0.04	0.01	2.97
11	0.06	0.06	0.03	0.02	0.17
12	4.42	0.13	0.05	0.02	4.61
13	1.10	0.02	0.02	0.01	1.15

*See Table 3.1

Commonly, a suspension pH of less than 4 implies that % base saturation approaches zero. Based on this observation, one would conclude that the amount of limestone needed to increase base saturation to nearly 100% would be directly related to CEC. Considering a 50% limestone efficiency, for each $cmol_c\ kg^{-1}$ acidity approximately one ton of limestone per 1 million tons of spoil would be required, or for a spoil sample with 10 $cmol_c\ kg^{-1}$ CEC and zero % base saturation, 10 tons of limestone per one million tons of spoil would be required. This limestone requirement is in addition to that needed to neutralize solution acidity (Table 3.4) and/or potential pyritic acidity.

3.2.1 Mine 'waste' surface chemistry

One of the important mine 'waste' parameters is the so-called point of zero charge (PZC_{pH}). It is defined as the pH at which the net charge of all charge sources (oxides and clays) is zero (Gast, 1977). Therefore, below the PZC_{pH} the mine 'waste' gains positive charge, while above the PZC_{pH} the mine 'waste' gains negative charge. Mine 'waste', due to their certain clay mineral content, also contain permanent charge arising from charge imbalances in the clay mineral structures (see Chapter 2).

In essence, mine 'waste' may possess two types of charges: a) The so called *pH-dependent* charge arising from pure oxides (iron, manganese, aluminum) and oxides associated with edges of clay minerals, and b) *permanent* surface charge arising from the clay lattice. Oxides can be considered as amphoteric compounds that exhibit certain dissociation constants. When the dissociation constants are high, the PZC_{pH} is low. On the other hand, when the dissociation constants are low, the ZPC_{pH} is high. Note that the ZPC_{pH} of a mineral surface is determined by the average value of the two pKa's associated with the particular surface. For example, organic material, a relatively strong acid, is expected to have a low PZC_{pH}. The same can be said for SiO_2, MnO_2, α-$Al(OH)_3$, and kaolinitic edges ($PZC_{pH}<5$) (Stumm and Morgan, 1970). On the other hand, MgO, '$Fe(OH)_3$' amorphous, CuO, α-Al_2O_3 are considered weak acids and have a PZC_{pH} greater than 8.5 (Stumm and Morgan, 1970).

The ability of oxides to adsorb cations appears to be related to the PZC_{pH}. An oxide in the pH range of 6 to 7 with a relatively low PZC_{pH} (e.g. $PZC_{pH} = 4$) will have a larger heavy metal adsorption capacity than an oxide with higher PZC_{pH} (e.g., $PZC_{pH} = 8$), assuming the same charge sites per unit weight, and the same cation affinity constant. However, oxides vary greatly in charge sites per unit weight. Benjamin and Leckie (1980) reported that γ-Al_2O_3, an oxide of PZC_{pH} 8.3, exhibits a charge density per unit weight that is approximately 67 times greater than that of a-SiO_2 with a PZC_{pH} of 2.5. Furthermore, within an oxide surface, charge sites exhibit different electrostatic bonding strengths for a particular metal-cation surface (Benjamin and Leckie, 1980); the bonding strengths of two different oxides with a particular metal-cation may also differ and may be independent of the PZC_{pH}. This latter statement explains the fact that strong metal-cation adsorption (specific adsorption) by an oxide surface can take place below its PZC_{pH} (Kuo and Baker, 1980).

Based on the above, as a general rule, for a given chemical solution composition as pH increases above the PZC_{pH}, ability of spoil to adsorb cations increases (Kuo and Baker, 1980). On the other hand, as pH decreases, the ability of spoil to adsorb cations decreases (Mehlich, 1981), and below the PZC_{pH}, anion adsorption capacity exceeds cation adsorption capacity.

Oxides, besides exhibiting an electrostatic force, interact chemically with cations as well as anions that further modify the nature of the surface charge. The following are examples of such interactions.

$$\begin{array}{l} \quad | \qquad\qquad\qquad\quad | \\ \text{--S-OH} + SO_4^{2-} \;=\; \text{--S-}OSO_3^{2-} + OH^- \\ \quad | \qquad\qquad\qquad\quad | \\ \quad \text{Metal or} \\ \text{clay surface} \end{array} \qquad (3.1)$$

Similarly,

$$\begin{array}{l} \quad | \qquad\qquad\qquad\quad | \\ \text{--S-OH} + HPO_4^{2-} \;=\; \text{--S-}OPO_3H^- + OH^- \\ \quad | \qquad\qquad\qquad\quad | \end{array} \qquad (3.2)$$

For metals,

$$\begin{array}{l} \quad | \qquad\qquad\qquad\quad | \\ \text{--S-OH} + Zn^{2+} \;=\; \text{--S-}OZn^+ + H^+ \\ \quad | \qquad\qquad\qquad\quad | \end{array} \qquad (3.3)$$

Equations 3.1 and 3.2 reveal that when SO_4^{2-} or HPO_4^{2-} specifically react through-OH^- displacement with an apparently neutral surface, the newly produced surface possesses negative charge which could adsorb metal-cations. This process could also be viewed as metal-sulfate or metal-phosphate surface precipitation and it may take place at concentrations below those predicted by the mineral solubility product (K_{sp}) . On the other hand, Equation 3.3 reveals that metal specific adsorption by a mineral surface may also take place through H^+ displacement, leading to a positively charged surface which maybe compensated by anion adsorption, e.g., SO_4^{2-}. Specific criteria for these reactions to occur include the chemical nature (i.e., pK_a, pK_b, PZC_{pH}, etc) of a) mineral surface, and b) cations and anions.

The above reactions (3.1 through 3.3) become apparent during oxidative-liming of 'waste' materials containing large quantities of soluble salts (i.e., $FeSO_4$, $MnSO_4$, $CaSO_4$, $MgSO_4$, $Al_2(SO_4)_3$). Upon oxidative-liming, cations of Fe^{III}, Mn^{III}, Mn^{IV} and Al^{3+} form new variable charge surfaces, and soluble salts of $CaSO_4$ and $MgSO_4$ adsorb onto these newly formed charged surfaces. The end result of such surface reactions is that soluble salt concentration falls below the level(s) expected from classical thermodynamic mineral solubility considerations.

3.2.2 Technique comparisons

Quantities of extractable or exchangeable metal cations and/or anions from mine 'waste' material are technique dependent. The data in Figures 3.1, 3.2, and 3.3 demonstrate that the HCl + H_2SO_4 single 1:5 solid to solution extraction technique, as expected due to its strong acidity, extracts the most cations and it correlates best with the NH_4AC extraction.

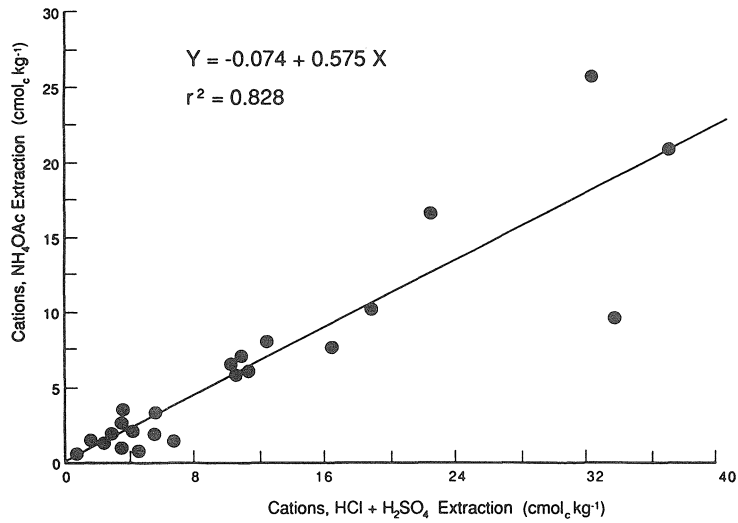

Figure 3.1. Relationship between NH_4Cl and the rapid HCl + H_2SO_4 extraction techniques.

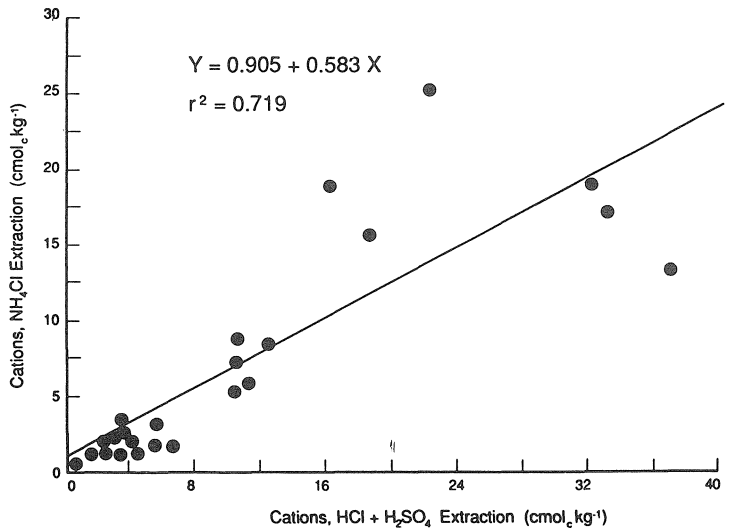

Figure 3.2. Relationship between $BaCl_2$+triethanolamine (TEA) and the rapid HCl + H_2SO_4 extraction techniques.

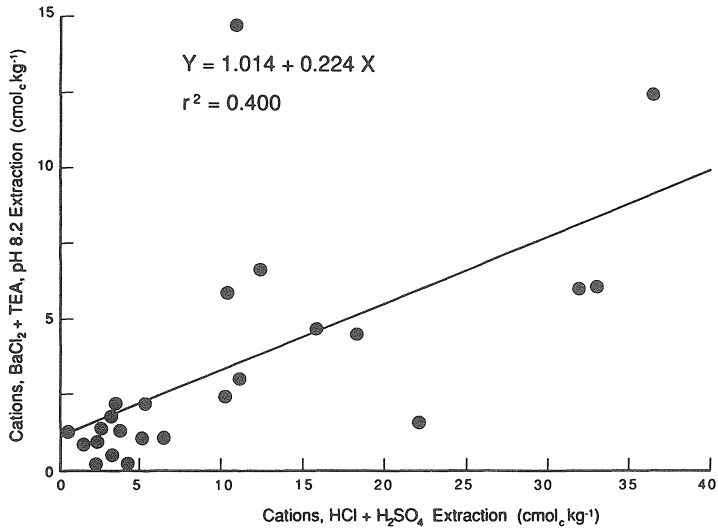

Figure 3.3. Relationship between NH_4AC and the rapid HCl + H_2SO_4 extraction technique.

The difference in magnitude between the HCl + H_2SO_4 rapid extraction and the $BaCl_2$ + TEA pH 8.2 extraction or the NH_4AC extraction reveals the potential of a given mine 'waste' to build pH-dependent charge upon liming. In general, the greater the difference between the sum of the extractable cations by a buffered solution ($BaCl_2$·TEA pH 8.2) and an unbuffered solution (HCl + H_2SO_4 or NH_4Cl), the greater is the neutralization and/or desalinization potential of the particular spoil due to liming. This conclusion is supported by the data in Figures 3.4 and 3.5 which demonstrate that a linear relationship between CEC, obtained by the various techniques employed, exists only between the $BaCl_2$+TEA and NH_4Cl determined CEC (Figure 3.4). The $BaCl_2$+TEA pH buffered technique appeared to underestimate CEC relative to NH_4Cl. This suggested that at high pH many of the exchange sites were blocked off by specifically adsorbed cations.

The data in Table 3.5 show that the AEC of these 'waste' material is significant. It varies from approximately 1.5 $cmol_c\ kg^{-1}$ to approximately 3.8 $cmol_c\ kg^{-1}$. In practical terms, these AEC values may represent a range of approximately 800 to 1800 mg L^{-1} dissolved sulfate assuming a 50% spoil water content..

The data in Table 3.8 show aluminum content extracted by NH_4Cl or HCl + H_2SO_4. These data reveal that aluminum content varies significantly among the different spoil samples, and furthermore, many of these 'waste'

materials contain a significant quantity of absorbed aluminum. These aluminum values vary from near zero to approximately 5 $cmol_c\ kg^{-1}$. The

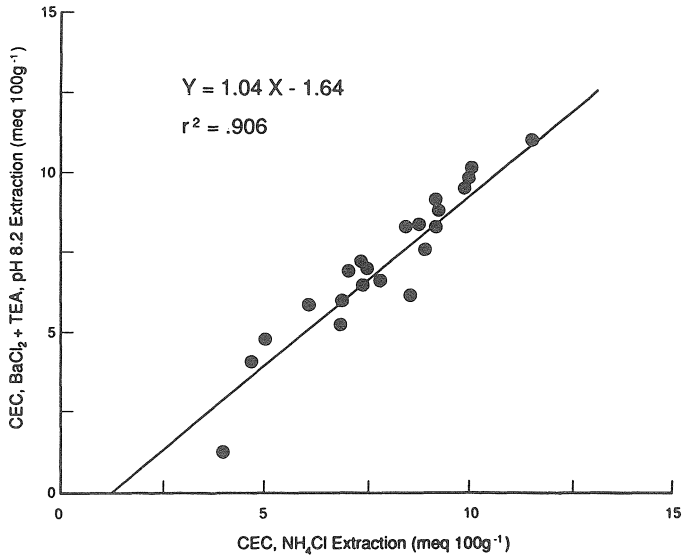

Figure 3.4. Relationship between cation exchange capacity (CEC) values determined by NH_4AC and CEC values determined by NH_4Cl.

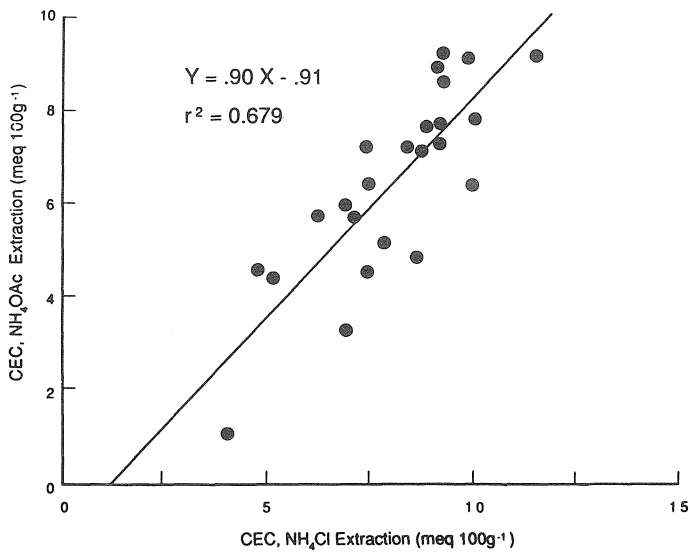

Figure 3.5. Relationship between cation exchange capacity (CEC) values determined by $BaCl_2$+triethanolamine (TEA) pH 8.2 and CEC values determined by NH_4Cl.

Table 3.8
Aluminum content in $cmol_c\ kg^{-1}$ of various mine spoils determined by two different extracting techniques

Sample* ID	$HCl + H_2SO_4$ Extraction	NH_4Cl Extraction
1	4.42	4.93
2	0.64	0.28
3	0.56	0.26
4	1.75	0.74
5	4.24	1.39
6	2.92	1.37
7	1.84	0.60
8	4.72	2.26
9	1.45	0.61
10	3.46	1.20
11	3.76	1.65
12	5.10	2.02
13	0.26	0.11

*See Table 3.1

latter value represents approximately 500 mg L^{-1} dissolved aluminum assuming a 50% spoil water content. Considering that aluminum can be toxic to plants at 2 to 3 mg L^{-1}, a quantity of 5 $cmol_c\ kg^{-1}$ extractable aluminum would be considered highly troublesome. The relationship between Al content obtained by the two extraction methods (NH_4Cl or $HCl+H_2SO_4$) show excellent agreement (Figure 3.6) even though $HCl+H_2SO_4$ extracted significantly greater quantities. Knowing this, it can be said that either of these two extractants could be employed to determine potential Al release.

The above data represent only a small fraction of mine 'waste' material. For this reason, great generalizations could not be drawn about techniques and behavior of solution acidity, exchangeable acidity and % base

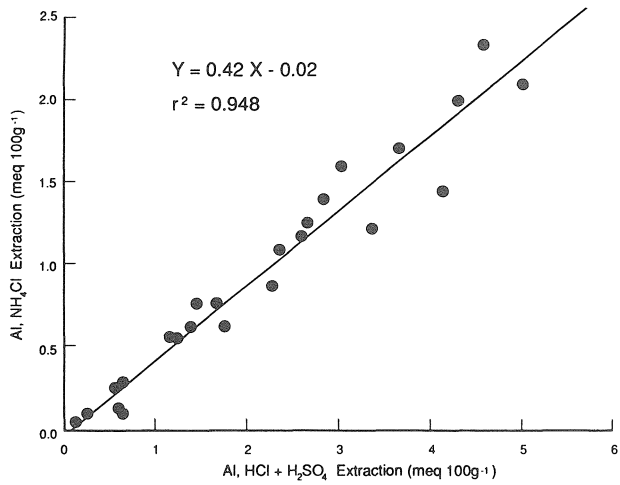

Figure 3.6. Relationship between aluminum (Al) extracted with NH_4Cl and Al extracted with the Hajek et al. (1972) procedure.

saturation. These data, however, do point out the need for each spoil sample material to be carefully analyzed and carefully evaluated prior to deciding on AMD abatement approaches.

3.2.3 Mine 'waste' solution chemistry

Factors that need a great deal of consideration in predicting mine 'waste' solution chemistry are a) thermodynamic solubility of minerals and b) ionic interactions of constituents in solution. The dominant anion in mine 'waste' solutions is sulfate and its total concentration is mostly a function of parameters such as total amounts and types of cations, oxidation state of transition metal ions, pH, and presence of metal chelating agents. The latter is demonstrated in Figure 3.7. Theoretically, the relationship between electrical conductivity (EC) of solutions and dissolved solids should be linear but in Figure 3.7 such linearity is not apparent. A possible reason for this is the presence of dissolved organics which possess metal-cation chelating potential (see also Chapter 1).

As pointed out in Chapter 1, in order to predict metal-cation and/or anion release to the percolating solution in spoils it is necessary to understand the difference between the absolute solubility of minerals and their thermodynamic solubility product constants (K_{sp}). For example, the best way to demonstrate this difference is through predicting the absolute solubility behavior of gypsum ($CaSO_4 \cdot 2H_20$), the most prevalent evaporite mineral in mine 'waste', using its K_{sp}. The thermodynamic solubility product expression for $CaSO_4 \cdot 2H_2O$ is as follows:

$$(Ca^{2+})(SO_4^{2-})(H_2O)^2/CaSO_4 \cdot 2H_2O = 2.45 \times 10^{-5} \qquad (3.4)$$

setting by convention activity of H_2O and solid phase gypsum to one, calcium and sulfate activity in solution would be 4.95 x 10^{-3} moles per liter (see Chapter 1).

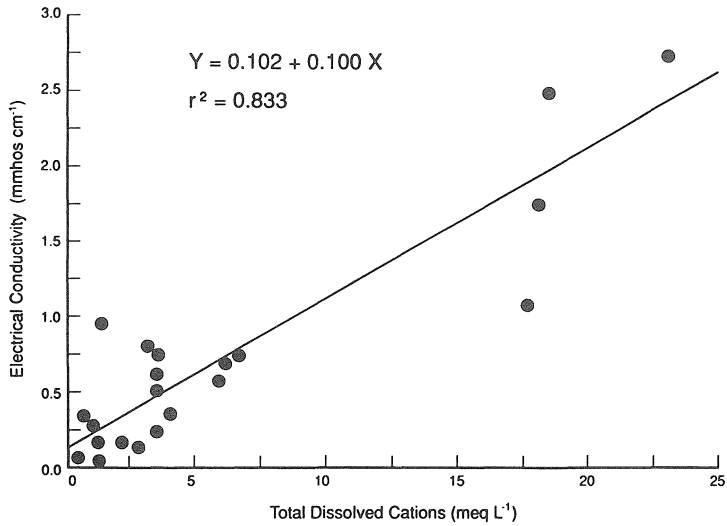

Figure 3.7. Relationship between electrical conductivity (EC) and total dissolved solids of 1:25 spoil:water extracts.

If one calculates single-ion activity coefficients (γ) by the Debye-Huckel equation, the γ values for Ca^{2+} or SO_4^{2-} would range from 0.45 to 0.55. Converting single-ion activity to dissociated concentration gives Ca^{2+} = SO_4^{2-} = 9.9 mmol L^{-1}. The total dissolved concentration includes the dissociated ion concentration plus the $CaSO_4^o$ pair which amounts to 5 mmol L^{-1} (see Chapter 1 for details). Therefore, the thermodynamic solubility of gypsum is 4.95 mmol L^{-1}, while its absolute solubility is 14.9 mmol L^{-1}. The above values are in agreement with the experimental values reported by Tanji (1969). Therefore, it should be apparent that the absolute solubility of any mineral is a function of the magnitude of a) thermodynamic solubility product constant, b) solution ionic strength, and c) ion-pair stability constants.

Based on the above, as solution ionic strength increases, single-ion activity coefficients (γ) decrease and mineral solubility increases. Furthermore, mineral solubility is enhanced by ion-pair formation and polymerization, (e.g., hydroxy-Al). Also of interest with respect to mineral solubility is the fact that ions with higher valence suppress single-ion activity coefficients (γ) more than ions with lower valence. For example, for a solution of ionic strength 0.042, the corresponding single-ion activity coefficient (γ) values for monovalent, divalent and trivalent ions would be

0.85, 0.58 and 0.17, respectively. Therefore, when solution ions of certain valence are replaced by ions of different valence (e.g., cation exchange reactions) a 'cascade' effect sets in that affects the behavior of all ions in solution.

The 'cascade' effect could be observed when an acid mine 'waste'-sulfate solution system is in equilibrium with gypsum. As hydrogen reacts with and solubilizes aluminosilicates, formation of solution aluminum sulfate pairs takes place, thus, decreasing sulfate activity. The end result is dissolution of additional gypsum, effectively increasing total solution concentration of calcium and sulfate. Similarly the 'cascade' phenomenon could work in reverse; as aluminum is removed from solution, calcium and sulfate are also removed in the form of gypsum precipitate. This effect should also be observed with iron, manganese, copper, zinc, etc. An example or iron removal by oxidation and hydrolysis and its effect on the solubility of gypsum is shown below:

$$Fe^{2+} + H^{+} + 3/2SO_4^{2-} + 1/4O_2 = Fe^{3+} + 3/2SO_4^{2-} + 1/2H_2O \qquad (3.5)$$

and

$$Fe^{3+} + 2H_2O + 3/2SO_4^{2-} = FeOOH(s) + 3H^{+} + 3/2SO_4^{2-} \qquad (3.6)$$

Reactions 3.5 and 3.6 reveal that upon removal of Fe from solution as FeOOH(s), solution SO_4^{2-} activity would increase considerably due to the breakdown of $FeSO_4^{o}$ pairs. Since Reactions 3.5 and 3.6 require limestone (e.g., $CaCO_3$ or $Ca(OH)_2$) to continuously form FeOOH(s), the free SO_4^{2-} reacts with the limestone liberated Ca^{2+} to precipitate gypsum as follows:

$$xCa^{2+} + xSO_4^{2-} + 2H_2O = x(CaSO_4 \cdot 2H_2O) \qquad (3.7)$$

Interactions between ions in solution and mineral surfaces are demonstrated in Table 3.3 (Lekhakul, 1981). These data show that when a mine 'waste' solution reacts with calcium carbonate, the concentration of Al, Mn^{2+} and Fe^{2+} decreases by precipitating as hydroxides and/or oxyhydroxides. Additionally, the calcium liberated by acid dissolution of calcium carbonate precipitates a major portion of the dissolved sulfate in the form of gypsum. The data in Table 3.3 show that indeed calcium and sulfate concentration decreased as limestone application rate was increased. Since sulfate concentration decreased at the higher limestone application rates, one would expect that calcium concentration should increase to satisfy the solubility product (K_{sp}) of gypsum. However, when Al^{3+}, Mn^{2+} and Fe^{2+} precipitated as hydroxides and/or oxyhydroxides, sulfate pairs decreased, solution ionic strength decreased, and sulfate activity increased which suppressed the solubility of gypsum and therefore solution calcium was expected to decrease somewhat (Table 3.3).

The data in Table 3.3 show that liming had a significant suppressing effect on the concentration of aluminum and magnesium (Table 3.3), and it appeared that at the higher liming rates aluminum precipitated as aluminum hydroxy-sulfate or hydroxide, thus, effectively removing itself from the clay exchange sites, producing an apparent clay pHdependent charge (Coleman and Thomas, 1967) and leading to surface adsorption of magnesium. In the case of a Ca-SO_4 - Ma-SO_4 exchange system the mass-action law predicts that at near neutral pH (low solution concentration of heavy metals) the exchange phase will be dominated by magnesium if its solution concentration is greater than that of calcium. The data in Table 3.3 indicates that for the black shale at the 125 mt/ha liming rate magnesium concentration increased by approximately 170 $mmol_c\ L^{-1}$. This increase could be related to the hydroxy-Al species, formed at the higher pH values, which have a higher affinity for the clay exchange sites, thus, effectively displacing magnesium from such sites (Bloom et al., 1977).

Thus, the data in Table 3.3, clearly show that in a system when one ion is affected by a specific chemical event all ions present undergo adjustments (cascade effect) to satisfy the system's newly established thermodynamic state. In treating acid sulfate containing waters such interactions should be well understood in order to predict the outcome of water chemical treatments.

Aluminum is one of the cations most difficult to predict with respect to its behavior in solution. This is because of its ability to form complex ions, such as sulfate pairs and hydroxy-Al aluminum monomers and polymers. Nordstrom (1982b) reported that the presence of sulfate in water can alter the solubilities of gibbsite and kaolinite considered to control the concentration of aluminum in natural waters. Thus, minerals of lesser solubilities control the aluminum concentration in acid sulfate waters. These minerals most likely are: alunogen ($Al_2(SO_4)_3 \cdot 17H_20$) with a K_{sp} of 10^{-7}, alunite ($KAl_3(SO_4)_2(OH)_6$) with a K_{sp} of $10^{-85.4}$, jurbanite ($Al(SO_4)(OH) \cdot 5H_20$) with a K_{sp} of $10^{-17.8}$, and basaluminite ($Al_4(SO_4)(OH)_{10} \cdot 5H_2O$) with a K_{sp} of $10^{-117.7}$. Nordstrom (1982b) also calculated the pH stability range for these species at SO_4^{2-} activity of 10^{-4} or 10^{-2} *M*. He found that between pH 0 and 3.3, jurbanite controlled aluminum concentration, while between pH 3.33 and 4.47 alunite controlled aluminum concentration. Beyond pH 4.47 gibbsite ($Al(OH)_3$) controlled aluminum concentration. Nordstrom (1982b) supported his conclusions by the fact that certain acid drainages contained a lesser concentration of aluminum than expected when in equilibrium with gibbsite. This is demonstrated in Figure 3.8a. On the other hand, when SO_4^{2-} activity was increased from 10^{-4} *M* to 10^{-2} *M*, Nordstrom (1982b) reported that between pH 0 and 4, jurbanite controlled aluminum concentration, whereas between pH 4 and 5.7, alunite controlled aluminum concentration. Beyond pH 5.7 gibbsite ($Al(OH)_3$) controlled aluminum concentration (Figure 3.8b).

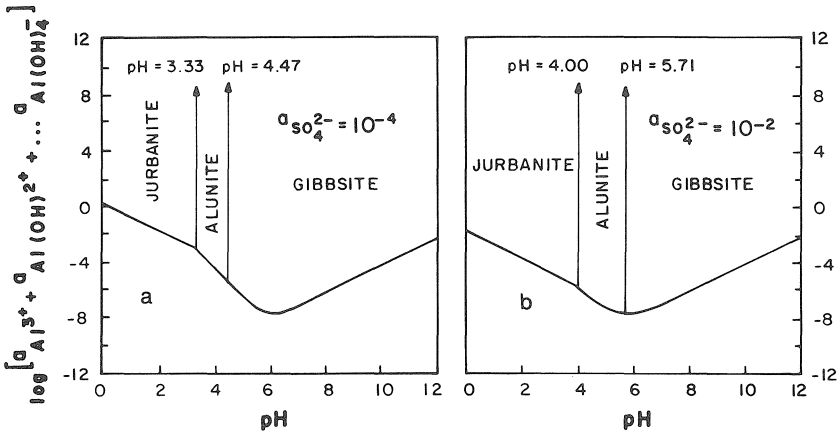

Figure 3.8. Solubility diagrams showing the pH range for the most stable Ai-OH–SO_4 minerals for a potassium activity of 10^{-4} *M* and a sulfate activity of a) 10^{-4} *M* and b) 10^{-2} *M*. (From Nordstrom 1982b. With permission.)

However, these observations may not always be valid. Data from Lekhakul (1981) show aluminum concentrations up to 0.1 moles per liter (Table 3.3). If such a system was truly in equilibrium with jurbanite (K_{sp} $10^{-17.8}$) only a fraction of this aluminum would be in solution (Figure 3.9a,b).

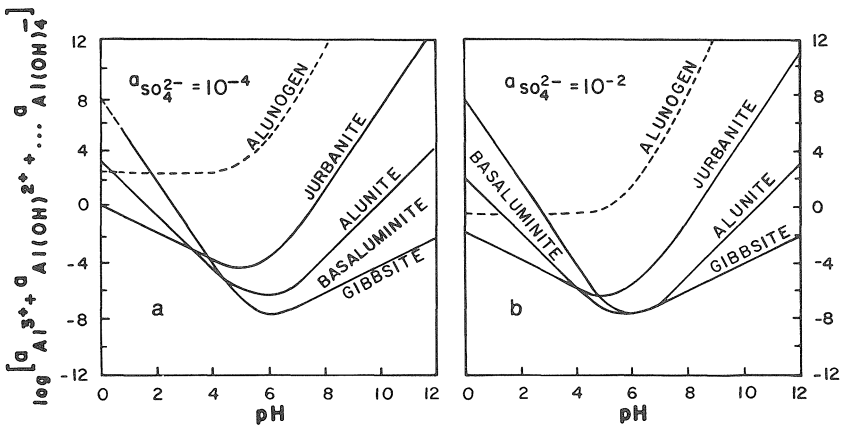

Figure 3.9. Solubility curves for various Al–OH–SO_4 minerals for a potassium activity of 10^{-4} *M* and a sulfate activity of a) 10^{-4} *M* and b) 10^{-2} *M*. (From Nordstrom 1982b. With permission.)

Kinetics, perhaps, may play a major role in the formation of such aluminum sulfate salt species. In other words, metastable aluminum-hydroxy-sulfate species in solution (as postulated by Nordstrom, 1982b), may take a long time (days and months) to form stable precipitates. Therefore, such metastable ionic species, as well as aluminum sulfate pairs, may play a major role in maintaining high aluminum concentrations in acid mine drainages.

An example of sulfate pair influence on maintaining relatively high aluminum concentrations can be demonstrated as follows: Assuming an acid sulfate water sample with SO_4^{2-} activity at 5 x 10^{-3} *M*, pH 3, and ionic strength somewhere around 0.04 *M*, is in equilibrium with jurbanite. Under such conditions, considering the solubility of jurbanite

$$Al(SO_4)(OH)\cdot 5H_2O = Al^{3+} + SO_4^{2-} + OH^- + 5H_2O \quad (3.8)$$

the equilibrium expression is

$$(Al^{3+})(SO_4^{2-})(OH^-)(H_2O)^5/Al(SO_4)(OH)\cdot 5H_2O = 10^{-17.8} \quad (3.9)$$

Substituting values into Equation 3.9 and considering solid phase jurbanite and water activities of one

$$(Al^{3+}) = [10^{-17.8}/(5 \times 10^{-3})\ (10^{-11})] = 3.17 \times 10^{-5}\ M \quad (3.10)$$

From Table 1.3 in Chapter 1,

$$AlSO_4^+ = (Al^{3+})(SO_4^{2-})/K \quad (3.11)$$

and by substituting values in Equation 3.11

$$AlSO_4^+ = (3.17 \times 10^{-5})(5 \times 10^{-3})/6.30 \times 10^{-4} = 2.51 \times 10^{-4}\ M \quad (3.12)$$

Based on 0.04 *M* ionic strength, the activity coefficient (γ) for Al^{3+} would be around 0.2, and its concentration would be

$$(3.17 \times 10^{-5})/0.20 = 1.58 \times 10^{-4}\ M \quad (3.13)$$

By adding dissociated and paired aluminum, the total aluminum concentration in solution would be 4.09 x 10^{-4} *M*. The important observation to be made from the above example is that of the total aluminum in solution, sixty-one percent (61%) would be paired with sulfate.

Sulfate is commonly used as means of quantifying pyrite oxidation rates. However, the data discussed above suggested that using SO_4 determinations to quantify pyrite oxidation rate may be misleading. For example, in the pH range 4 to 5.7, SO_4 may control aluminum solubility by forming Al-hydroxy-sulfate minerals. However, above pH 5.7 such minerals would undergo incongruent-like dissolution by precipitating Al as $Al(OH)_3$ and releasing SO_4 to the solution (Figure 3.8a,b). This implies that SO_4 release from a spoil could not be directly associated with pyrite oxidation, nor absence of SO_4 from solution could imply absence of pyrite oxidation. Under such conditions, pyrite oxidation could be quantified by extracting the SO_4

from the solid phase employing extractants such as strong acids or Al complexation agents. Release of SO_4 to solution would also depend on the nature of OH^- introduced to the geologic material. If OH^- was introduced as $Ca(OH)_2$ or $CaCO_3$, SO_4 would precipitate as $CaSO_4 \cdot 2H_2O$ (see also Chapter 1). On the other hand, if OH^- was introduced as $Mg(OH)_2$, SO_4 release to solution would increase dramatically since magnesium sulfate is highly water soluble.

Taylor & Francis
Taylor & Francis Group
http://taylorandfrancis.com

Chapter 4
ACID DRAINAGE PRODUCTION, CHEMISTRY, AND PREDICTION

4.1 Pyrite Occurrence, Formation, Morphology and Chemistry

The two major forms of iron-disulfide (FeS_2) in geologic strata are pyrite and marcasite. Both minerals have the same chemical composition, but differ crystallographically. The structure of marcasite is orthorhombic while that of pyrite is isometric (Stumm and Morgan, 1970). Because of its particular structure, marcasite is less stable than pyrite. Based on crystallographic examinations, pyrite is the most prevalent form present in coals (Greer, 1977; Lorenz and Tarpley, 1963; Grady, 1977).

Pyrite is generally associated with coal fields in the United States and elsewhere in the world. Pyrite is also associated with many ores including zinc, copper, uranium, gold, silver, etc. In the eastern coal fields of the United States pyrite is most commonly found associated with the geologic strata adjacent to, immediately above, or below the coal seam (Evangelou, 1985 and references therein). A pyrite-rich layer in Pennsylvania-age shales in Missouri was found capped with limestone (Ainsworth et al. 1982). Caruccio and Geidel (1978, 1980) reported that pyrite is not uniformly distributed throughout a geologic stratum as one observes with blanket deposits of calcium carbonate, but rather in clusters or scattered pockets of accumulation. It has been found that horizontal variation of pyritic content to be up to 4% within centimeters from one sampling to another, whereas vertical variation of pyritic content of geologic strata appeared to be of a lesser magnitude.

Pyrite is formed in a reducing environment with a continuous supply of sulfates and iron in the presence of easily decomposable organic matter. Barriga and Fyfe (1988) proposed that iron sulfide precipitation may have taken place under a thin veneer of siliceous sediments. Carbon-to-sulfur ratio, availability of iron, and oxidation potential are the major factors that determine the rate of pyrite formation. For typical anoxic marine sediments overlain by oxic water, the major processes involved in the formation of sedimentary iron sulfide were summarized by Berner (1970) by the following three steps: 1) reduction of sulfate to sulfide by bacteria, 2) reaction of the hydrogen sulfide with iron minerals to form iron monosulfides, and 3) reaction of the iron monosulfides with elemental sulfur to form pyrite.

It is generally accepted that limited supply of organic carbon in marine sediments results in lower rate of sulfate reduction. Pyrite formation in such environments is considered a slow process giving rise to framboidal pyrite (strawberry-like) (Goldhaber and Kalan, 1974; Berner, 1984; Giblin, 1988). On the other hand, in salt marshes where organic matter content is high and sulfate reduction is rapid, pyrite is believed to form rapidly, hours to days, via precipitation of iron with polysulfides. This direct precipitation normally gives rise to small single pyrite crystals (Richard, 1975; Howarth

and Teal, 1979; Giblin, 1988). The difference in the mechanisms of pyrite formation between marine and marsh sediments can be partially explained by the low pH of marsh sediments that keep the solution undersaturated with respect to monosulfides but supersaturated with respect to pyrite (Howarth and Teal, 1979; Luther, 1982). Finally, the rate of pyrite formation in freshwater sediments is much lower than that in marine sediments due to the fact that in freshwater sulfate concentrations are two to three orders of magnitude lower than in seawater.

Pyrite can vary significantly in grain size and morphology, depending on the environment of formation. Arora et al. (1978) reported that pyrite occurred as acicular forms, coarse-grained masses, euhedral forms, framboidal and polyframboidal forms, and octahedral and pyritohedral crystals (Figure 4.1). They also reported that pyrite isolated from lignite coal was composed of porous and nonporous irregular grains. Ainsworth et al. (1982) studied the morphology of pyrite isolated from Pennsylvanian-age shale in Missouri and reported his findings in terms of three pyrite groups: 1) pyrite with smooth crystal surfaces which included octahedral, cubic and pyritohedral; 2) conglomerates with irregular surfaces composed of many cemented particles; and 3) framboids in which the cemented crystals formed a smooth sphere. They also reported that the conglomerates were the predominant form. Zhang et al. (1993) characterized the chemical and morphological properties of pyrite separated from scrubber sludge, gob and slurry of coal residue. Their results indicated that scrubber sludge contained trace amount of pyrite in the form of smooth-rounded, conglomerates, and framboidal forms. Both gob and slurry contained 2-5% pyrite with the predominant forms of conglomerates and framboids or polyframboids. Numerous octahedral, cubic, pyritohedral and twinned crystals were also found. Chemical and physical analyses of the above pyrite samples by Zhang et. al. (1993) also indicated that these pyrite coal residues had crystal structures, forms, and compositions similar to those commonly described for pyrite.

Caruccio and Geidel (1978) pointed out that pyritic grains have been found to vary in size from greater than 400 μm to 5 μm. However, reactivity of pyrite crystals that usually form large or massive agglomerations is usually limited. The most reactive forms of pyrite have been determined to be the so-called framboid and/or polyframboid pyrites due to their high specific surface, and high porosity (Caruccio et al., 1977). It has been well documented that pyrite oxidation is a surface controlled reaction (Hoffmann et al., 1981; Singer and Stumm, 1970; Moses et al., 1987; Moses and Herman, 1991). Framboid/polyframboid pyrite is an agglomeration of various sizes crystals and has been found to comprise more than 50% of the total pyrite found in coal mining environments (Caruccio and Geidel, 1978). The large surface area exposed to environmental and microbial degradation is conducive to faster rates of reactivity in comparison to the so-called massive

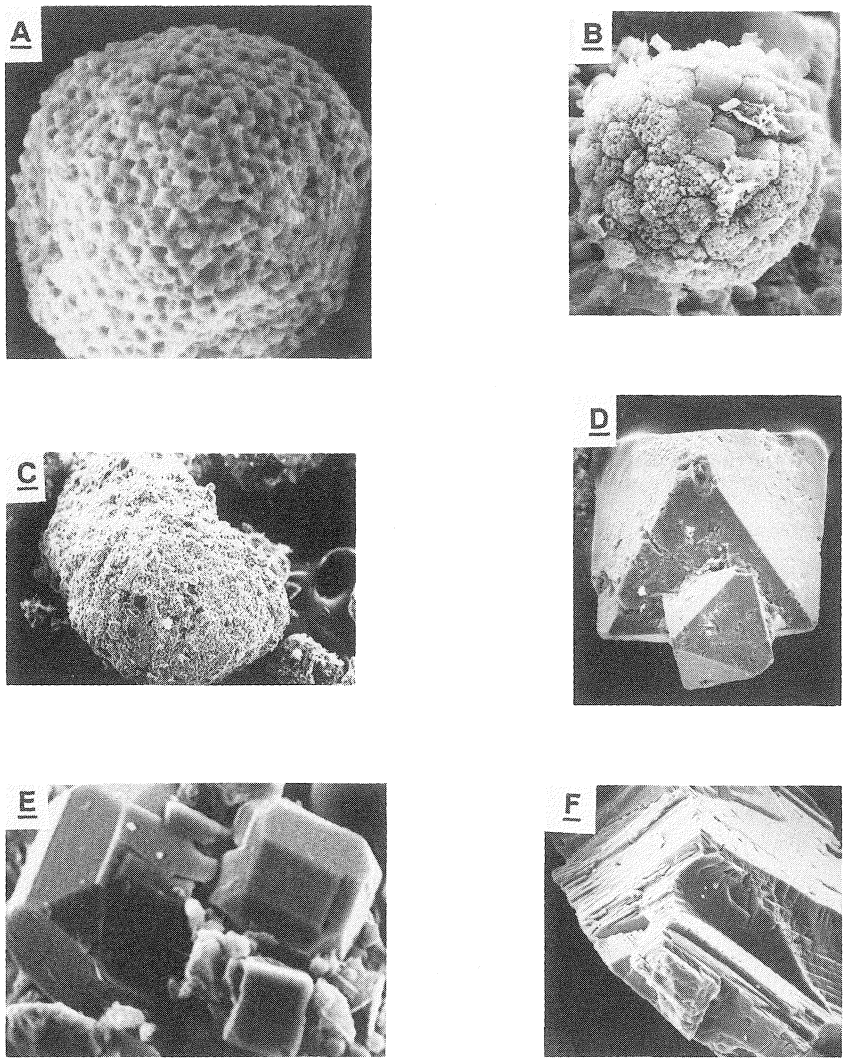

Figure 4.1. Various forms of pyrite, A) framboid with high surface area and high porosity; B) polyframboid, a cluster of framboids; C) conglomerate with irregular surface; D and E) octahedron and pyritohedron with smooth surface; F) massive Missouri museum pyrite with little or no surface porosity. (From Zhang et al., 1993. With permission.)

pyrite. Thus, it is the belief of most geochemists that framboidal pyrite is the major contributor to the degradation of water quality and, in general, the cause of environmental pollution during the process of mining.

The reactions of pyrite upon exposure to air and water are as follows:

$$FeS_2 + 7/2O_2 + H_2O \rightarrow Fe^{II} + 2SO_4^{2-} + 2H^+ \quad (4.1)$$

$$Fe^{II} + 1/4\ O_2 + H^+ \rightarrow Fe^{III} + 1/2\ H_2O \quad (4.2)$$

$$Fe^{III} + 3H_2O \rightarrow Fe(OH)_3 + 3H^+ \quad (4.3)$$

$$FeS_2 + 14Fe^{III} + 8H_2O \rightarrow 15Fe^{II} + 2SO_4^{2-} + 16H^+ \quad (4.4)$$

The above reactions even though they are mass and charge balanced they do not have any molecular/mechanistic meaning, nor do they have any rate reaction meaning. Pyrite oxidation involves many other chemically metastable species and more detail on this is given in Chapter 6. Reaction 4.1 shows oxidation of the disulfide, thus releasing ferrous iron (Fe^{II}) and two protons. In Reaction 4.2 the ferrous iron is oxidized to ferric (Fe^{III}) which hydrolyzes to form ferric hydroxide (an insoluble compound at pH greater than 3.5) and in the process, as shown in Reaction 4.3, three more protons are released. Thus, for every mole of pyrite (FeS_2) five protons are released. However, since one proton is consumed for the oxidation of ferrous to ferric, only four protons are actually produced.

Upon initiation of pyrite oxidation, the ferric iron can be reduced by the pyrite itself as shown in Reaction 4.4 (Singer and Stumm, 1970; Stumm and Morgan, 1970). Therefore, pyrite continues to oxidize as long as ferric iron is regenerated. Stumm and Morgan, (1970) pointed out that the conversion of ferrous to ferric is also the rate limiting step in the oxidation of pyrite. However, since oxidation of ferrous to ferric in the pH range of 3 is extremely slow (half-life in the order of 100 days), it appears that pyrite oxidation in this pH range would be extremely slow, unless oxidation of ferrous at low pH is catalyzed by microorganisms. It turns out that in the pH range of 2.5-3.5 (Jaynes et al., 1984), *T. ferrooxidans* rapidly oxidize ferrous iron to ferric iron. Also, sulfur-oxidizing bacteria such as *T. thiooxidans* and *T. ferrooxidans* can eliminate the need for ferric iron when in the presence of oxygen and some organic substrate.

The information shown by Reactions 4.1 through 4.4 has been summarized also by Nordstrom (1982a) and demonstrated in Figure 4.2. At low pH (< 4.5) pyrite is oxidized by Fe^{III} much more rapidly than by O_2, and more rapidly than dissolved Fe^{II} is oxidized by O_2 to Fe^{III}. For this reason, Reaction 4.2 is known to be the rate-limiting step in abiotic pyrite oxidation (Singer and Stumm, 1970). However, iron-oxidizing bacteria, especially *T.*

ferrooxidans, can accelerate the rate of Fe^{II} oxidation by a factor of 10^6 (Singer and Stumm, 1970; Dugan, 1975).

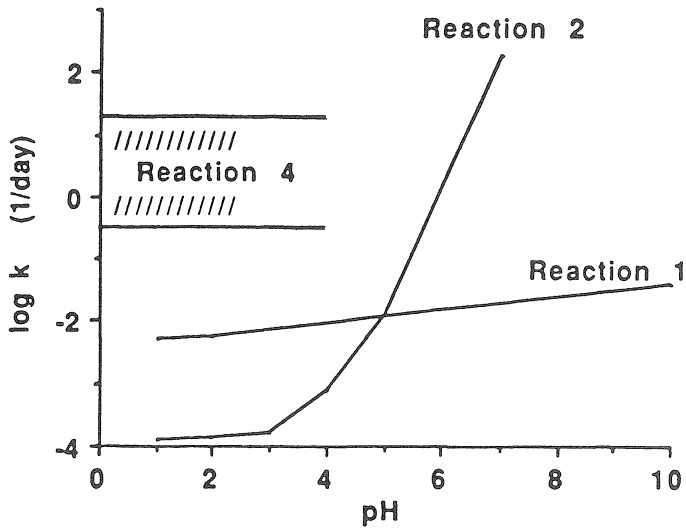

Figure 4.2. Comparison of rate constants as a function of pH for Reaction 4.4, oxidation of pyrite by Fe^{3+}; Reaction 4.2, oxidation of Fe^{2+} by O_2; and Reaction 4.1, oxidation of pyrite by O_2. Reactions 4.1, 4.2, and 4.4 are given in the text. (From Nordstrom, 1982a. With permission.)

T. ferrooxidans is an acidophilic chemolithotrophic organism that is ubiquitous in geologic environments containing pyrite (Nordstrom, 1982). Thus, in the presence of *T. ferrooxidans* and under low pH conditions pyrite oxidation can be described by Reactions 4.2 and 4.4.

At neutral to alkaline pH, the abiotic rate of Fe^{II} oxidation rises rapidly (Figure 4.2) but Fe^{III} concentration also decreases greatly due to precipitation of ferric hydroxide as described by Reaction 4.3. Because there is probably very little bacterial participation in pyrite oxidation at neutral to alkaline pH, some researchers suggested that in such environments O_2 is a more important pyrite oxidant than Fe^{III} (Goldhaber, 1983; Hood, 1991). This suggestion, however, is contradicted by recent findings which pointed out that Fe^{III} is the preferred pyrite oxidant at circumneutral pH and the major role played by O_2 is to oxidize Fe^{II} and thereby sustain the pyrite oxidation cycle (Moses et al., 1987; Moses and Herman, 1991; Luther, 1987 and 1990). Finally, Reaction 4.3, taking place at pH values as low as 3, is a readily reversible dissolution/precipitation reaction that serves as a source as well as a sink of solution Fe^{3+}, and is a major step in the release of acid to the environment.

4.2 Transitional Metal-Pyrite Oxidation

Asghar and Kanehiro (1981) observed that ferrous iron can be oxidized to ferric iron (Reaction 4.5) in the presence of manganese oxides at pH less than or equal to 5.5.

$$MnO_2 + 4H^+ + 2Fe^{2+} = Mn^{2+} + 2H_2O + 2Fe^{3+} \qquad (4.5)$$

In fact, the rate of Reaction 4.5 is approximately equal to the biological oxidation of iron in the same pH range (Stumm and Morgan, 1970; 1981). Asghar and Kanehiro (1981) reported that 95% of 100 ppm of ferrous sulfate was oxidized to ferric within a day when added to a soil sample of pH 4.4 and manganese oxide content of 3.04%. Some mine 'waste' are known to contain large quantities of manganese oxides (Barnhisel and Massey, 1969; Lekhakul, 1981). Aller and Rude (1988) studied metal sulfide oxidation in anoxic marine sediments in the presence and absence of manganese oxides or iron oxides, specifically goethite (a relatively high specific surface metal oxide). Results from this study are shown in Figure 4.3.

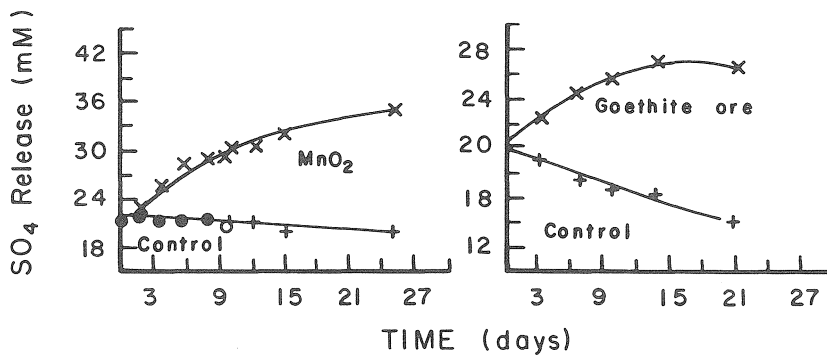

Figure 4.3. Release of SO_4 from marine sediments containing solid phase sulfides under anoxic conditions in the presence and absence of MnO_2 and goethite (FeOOH). (From Aller and Rude, 1988. With permission.)

These data clearly demonstrate that sulfate production takes place when metal oxides are added to anoxic marine sediments containing solid phase metal sulfides. Two possible macroscopic (non-molecular) pathways can be postulated for explaining pyrite oxidation in anoxic environments by transitional metal-oxides. One mechanism involves the reaction of MnO_2 with Fe(II) leading to production of Fe(III) (Equation 4.5) which in turn oxidizes pyrite according to Equation 4.4. The second mechanism involves direct oxidation of pyrite by MnO_2. This mechanism can be represented by the reaction:

$$4MnO_2 + 8H^+ + 0.5FeS_2 = 4Mn^{II} + SO_4 + 0.5Fe^{II} + 4H_2O \qquad (4.6)$$

The experimental results by Aller and Rude (1988) (Figure 4.3) and Equations 4.4, 4.5 and 4.6 strongly suggest that metal oxides could serve as electron acceptors promoting sulfide oxidation. Aller and Rude (1988) and references therein concluded that oxidation of solid phase sulfides in anoxic sediments by transitional metal-oxides was bacteria-catalyzed and Mn(IV) was a far more effective electron sink than Mn(III) or Fe(III) associated with goethite. Evangelou et al. (1994) demonstrated that the kinetics of the chemically induced reductive dissolution of $Mn(IV)O_2$ was approximately 100-fold faster than that of Mn(III)OOH; furthermore, the activation energy for the reductive dissolution of Mn-oxides was greater in the case of Mn(III)OOH than in the case of $Mn(IV)O_2$. These evidence suggested that Mn(IV) would be a more effective solid phase disulfide oxidizer than Mn(III) as observed by Aller and Rude (1988).

Luther et al., (1992) indicated that dissolution of ferric iron minerals, e.g., goethite (FeOOH), permit direct formation of aqueous Fe^{III} as follows:

$$FeOOH + 3H^+ \rightarrow Fe^{3+} + 2H_2O \quad (4.7)$$

$$FeOOH + C_6H_4(OH)_2 \rightarrow \{Fe^{3+}[C_6H_4(OH)_2]\}^+ + H_2O \quad (4.8)$$

or

$$FeOOH + 3H^+ + Ligand \rightarrow Fe(III)\text{-}Ligand + OH^- \quad (4.9)$$

Reaction 4.7 is well-known and is the basis of many analytical methods for some minerals containing Fe(III). Reaction 4.8 represents dissolution of Fe(III) minerals by siderophores (ligand) of which catechol ($C_6H_4(OH)_2$) is a common component (Hider, 1984). The ligands in Reaction 4.9 are weak field organic acids produced by plant and bacteria and generally contain oxygen in the form of hydroxyl or carboxyl functional groups (Hider, 1984). Some mine waste and coal residue are known to contain large quantities of Mn- and Fe-oxides (Barnhisel and Massey, 1969; Lekhakul, 1981). Ferric iron produced through the above reactions may oxidize pyrite. For additional information see Chapter 6.

4.2.1 Effect of ferric hydroxide species on pyrite oxidation

Under most natural conditions (e.g., pH > 3.5) Fe^{III} exists in the natural system as ferric hydroxide or ferric oxyhydroxide solids. However, because of the ferric iron's high affinity for OH^-, ferric hydroxide solution species composed of $Fe(OH)^{2+}$, $Fe(OH)_2^+$, $Fe(OH)_3^o$ and $Fe(OH)_4^-$ are present in concentration high enough perhaps to influence pyrite oxidation. The distribution of the ferric-hydroxy species is dependent on pH (Fornasiero et al., 1992; Hamilton and Woods, 1981). This is demonstrated in Figure 4.4, which was produced employing GEOCHEM-PC, an ion-association computer model (Sposito and Mattigod, 1979). Among the species shown in Figure

4.4, $Fe(OH)^{2+}$ and $Fe(OH)_2^{+}$ are more interesting because these positively charged ions maybe adsorbed, as a result of electrostatic interactions, by the negatively charged pyrite surface at pH values near or higher than the isoelectric point of pyrite which is slightly greater than pH 1 (Fornasiero et al., 1992).

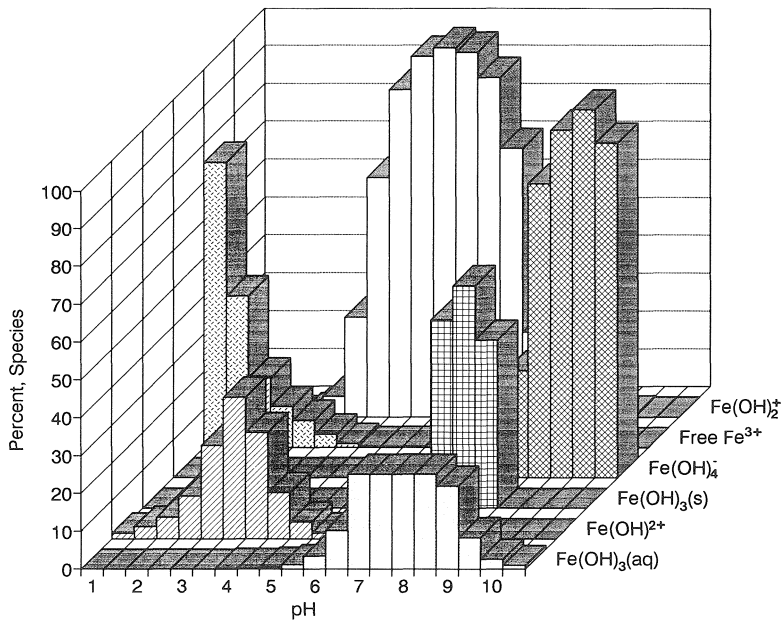

Figure 4.4. Percent of ferric-hydroxy species as a function of pH.

A pyrite/surface-$Fe(OH)_n^{n-3}$ complex could form according to the following reaction

$$\text{-Fe-S-S}^- + Fe(OH)_n^{3-n} \rightarrow \text{-Fe-S-S-}Fe(OH)_n^{3-n} \qquad (4.10)$$

Representative relationships between pH and adsorbed $Fe(OH)^{2+}$ and $Fe(OH)_2^{+}$ are shown in Figure 4.5. These iron species, $Fe(OH)^{2+}$ and $Fe(OH)_2^{+}$, are primarily surface adsorbed at low pH (pH < 3) and circumneutral pH, respectively. But, it is unknown to what degree the rate of pyrite oxidation is related to the concentration of these two iron-hydroxy species on the surface of pyrite. It is important to note that formation of iron-hydroxy species in the solution phase (Figure 4.4) appears to be related to formation of iron-hydroxy species on the pyrite surface (Figure 4.5). The presence of OH^- as $Fe(III)(OH)_n^{n-3}$ on the pyrite surface is most likely

involved in the electron transfer process between the disulfide and Fe(III) (Brown and Jurinak, 1989).

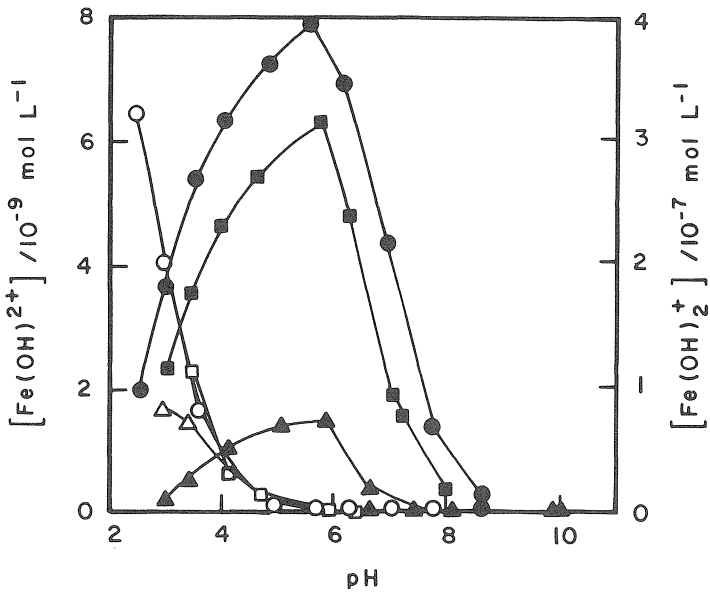

Figure 4.5. Concentration of $Fe(OH)^{2+}$ and $Fe(OH)_2^+$ adsorbed on pyrite as a function of pH (open symbols represent $Fe(OH)^{2+}$; closed symbols represent $Fe(OH)_2^+$; triangles denote 0.5 hr in air; squares denote 2 hr in air; circles denote 19 hr in air. (From Fornasiero et al., 1992., With permission.)

Increase in the abiotic pyrite oxidation rate as a function of pH may in fact be related to the increase in availability of surface OH^-.

4.2.2 Galvanic effect on metal-disulfide oxidation

Physical contact between two different metal-disulfide minerals in an acid/ferric sulfate solution creates a galvanic cell. This galvanic cell results in a selective electrochemical dissolution of the metal-disulfide minerals (Torma et al., 1979; Mehta and Murr, 1983). According to Torma (1988) and Mehta and Murr (1983), in the case of two metal-disulfide minerals with different electrical rest potential, the mineral with lower electrical rest potential, acting as anode, will be dissolved, while the mineral with higher rest potential, acting as cathode, will be galvanically protected (Mehta and Murr, 1983). For example, Torma (1988) pointed out that in the case of chalcopyrite/pyrite galvanic cell ($CuFeS_2/FeS_2$), chalcopyrite, with lower rest potential, will dissolve rapidly while pyrite will remain practically intact. Furthermore, Torma (1988) pointed out that the role of bacteria in the

galvanic cell is to continuously oxidize the elemental sulfur (produced from the anodic oxidation reaction) to sulfate, thus, formation of a sulfur barrier on the surface of chalcopyrite is eliminated.

The galvanic reaction of the $CuFeS_2/FeS_2$ cell can be described by an anodic oxidation reaction on the $CuFeS_2$ surface and a cathodic oxygen reduction on the FeS_2 surface (Torma, 1986 and references therein). The anodic oxidation reaction on the chalcopyrite surface can be expressed by:

$$CuFeS_2 \rightarrow Cu^{2+} + Fe^{2+} + 2S^o + 4e^- \quad (4.11)$$

while the cathodic oxygen reduction taking place on the FeS_2 surface can be given by:

$$O_2 + 4H^+ + 4e^- \rightarrow 2H_2O. \quad (4.12)$$

Thus, the sum of the galvanic reaction can be expressed as:

$$CuFeS_2 + O_2 + 4H^+ \rightarrow Cu^{2+} + Fe^{2+} + 2S^o + H_2O \quad (4.13)$$

Elemental sulfur (S^o) and ferrous iron shown in Reaction 4.13 will be oxidized by bacteria according to Reactions 4.14 and 4.15

$$4FeSO_4 + 2O_2 + 2H_2SO_4 \rightarrow 2Fe_2(SO_4)_3 + 2H_2O \quad (4.14)$$

and

$$2S^o + 3O_2 + 8H_2O \rightarrow 2H_2SO_4 \quad (4.15)$$

Pyrite is the most abundant disulfide mineral and is associated in varying amounts with other sulfide/disulfide minerals, such as those of copper, nickel, and zinc. Quantitative contribution of galvanic reactions in the dissolution of metal disulfides or metal sulfides in these natural environments are unknown. It is most likely that in these systems different mechanisms of oxidative/dissolution operate simultaneously. These mechanisms may include galvanic dissolution, electrochemical oxidation, and oxidation by Fe^{3+}, O_2 and bacteria.

4.2.3 Ferrolysis

In nature, acid drainage is a product of pyrite oxidation or perhaps oxidation of various other unstable metal sulfides. However, acid drainage could also be produced by a process known as *ferrolysis*. In order for *ferrolysis* to take place in disturbed geologic strata the following conditions would need to be met: 1) Possession of some CEC by the 'waste' material, 2) presence of pyrite and limestone, and 3) presence of alternating reducing/oxidizing conditions. The process can proceed as follows: Upon pyrite oxidation and acid neutralization by limestone two products are

formed: 1) $Fe(OH)_3$ and 2) $CaSO_4{\cdot}2H_2O$. Ferric trihydroxide ($Fe(OH)_3$) is water insoluble under natural pH values, e.g., pH greater than 3.5, but $CaSO_4{\cdot}2H_2O$ is quite soluble (Evangelou and Wagner, 1987; Evangelou et al., 1987) and leaches, leaving behind $Fe(OH)_3$. The latter, under reducing conditions transforms to $Fe(OH)_2$ (Stumm and Morgan, 1970, 1981) which is soluble below pH 8 (Lindsay, 1979). Enrichment of pore water with Fe^{II} promotes displacement of Ca^{2+} from the 'waste' exchange sites (Wang et al., 1993; Marsi and Evangelou, 1993). Under strong oxidizing conditions, the surface adsorbed Fe^{II} (due to Fe^{II}-Ca^{2+} exchange) undergoes oxidation and hydrolysis, releasing a large quantity of acid (depending on magnitude of adsorbed Fe^{III}), thus, bringing the pH around 3 (Figure 4.6).

$$S\text{---}Ca^{2+} + Fe(OH)_2 + H^+ \text{--->} S\text{---}Fe(II) + Ca^{2+} \qquad (4.16a)$$

and

$$S\text{---}Fe(II) + O_2 + H_2O \text{--->} S\text{---}Fe(III)(OH)_2 + H^+ \qquad (4.16b)$$

Figure 4.6. Schematic of equations demonstrating *ferrolysis*. S denotes surface.

The process of *ferrolysis* is a well known phenomenon in iron rich soils under high rainfall and alternating reducing/oxidizing conditions. Documentation of *ferrolysis* in mine 'waste' in the temperate regions of the U.S.A have been made by the author in areas with relatively shallow but transient water table.

4.3 Predicting Acid Drainage Potential

An important component in controlling AMD production is being able to predict it. There are several approaches that can be used to predict AMD production. These approaches include: 1) determination of potential acidity, 2) acid-base accounting; 3) simulated weathering, and 4) computer simulation modeling. A brief discussion on each of these approaches is carried out below. Although the factors that control pyrite oxidation in the field are well understood, quantifying some of these factors is difficult. Such factors include rate of oxygen diffusion, rate of water infiltration, pH, temperature, presence of alkaline minerals in the strata ($CaCO_3$, $MgCO_3$, $CaMg(CO_3)_2$), vertical or lateral variability in the strata, and modes of pyrite oxidation (chemical or bacterial).

4.3.1 Determination of potential acidity

It is commonly necessary to quantify the acid producing potential of geologic strata before mining begins. For this reason, a rapid, accurate, and

reproducible potential acidity method is required. Several methods for determining potential acidity have been proposed (Aspiras et al., 1972; Caruccio, 1975; Murthy and Sharada, 1960 Sorenson et al., 1979). Each of these methods measures either sulfur or iron associated with pyrite and therefore provide an indirect estimate of the potential acidity. A direct determination of acid producing potential is the rapid pyrite oxidation technique utilizing 30% H_2O_2. The actual acid produced during pyrite oxidation by H_2O_2 is termed potential acidity (Sobek et al., 1978; O'Shay et al., 1990). The technique determines the amount of acid produced during complete oxidation of Fe^{2+} and S_2^{2-} of pyrite as follows:

$$FeS_2 + 7.5H_2O_2 \rightarrow Fe(OH)_3(s) + 2H_2SO_4 + 4H_2O \qquad (4.17)$$

Reaction (4.17) demonstrates that complete pyrite oxidation liberates two moles of H_2SO_4 for every mole of FeS_2 oxidized.

4.3.2 Acid-base accounting

Acid-base accounting is the most widely used method for characterizing overburden geochemistry because it is simple, relatively inexpensive, and reliable. The three fundamental measurements comprising the acid-base accounting method are: a) pH, b) percent total sulfur or pyritic sulfur, and c) neutralization potential. The purpose of acid-base accounting on a geologic sample is to identify the acid producing potential due to pyrite and the neutralization producing potential due to alkaline material such as rock carbonates and/or clays due to their percent base saturation. The difference between the two potentials (acid producing potential vs. base producing potential) indicates if there is enough base present to neutralize all acid that is to be produced from the oxidation of pyrite (Smith and Sobek, 1978).

Caruccio and Geidel (1981) criticized the technique of acid-base accounting because it did not consider differences between the rate of pyrite oxidation and the rate of carbonate dissolution. Furthermore, the technique considered that all pyrite present in the sample is oxidizable under natural oxidizing conditions. Acid-base accounting has been applied with some success to mine planing in the east, midwest, western coal fields of the United States, and is used in overburden analysis in Canada, Australia, and Russia (Skousen et al. 1987).

4.3.3 Simulated weathering techniques

The basic idea behind simulated weathering is leaching natural overburden in laboratory scale experiments so that the results are applicable to the field. The effluent is collected and analyzed for pH, acidity, sulfate, iron, etc. The results from these analyses are then used to evaluate AMD production potential.

Caruccio and Geidel (1981) developed a simulated weathering technique ('humidified test cells') where a 300-500 g sample of geologic material was allowed to oxidize in the presence of humid air, followed by periodic distilled water washings. The collected solution was then titrated to determine the amount of acid generated from the oxidation of pyrite. Their argument was that such a technique considered rates of oxidation and rates of base released. Furthermore, the technique considered oxide coatings of both the pyrite and the carbonates, something that the acid-base balance approach did not consider.

Other versions of the 'humidified test cells' (Caruccio and Geidel, 1981) have been developed and adapted by researchers and industry which include long-term leaching tests and aggressive pyrite sample weathering approaches employing a Soxhlet (Renton et al., 1988). A major limitation for some of these techniques, especially aggressive ones, is that complete pyrite destruction is induced. However, as discussed in Chapter 6, pyrite oxidation in the natural environment is a surface controlled reaction and for this reason pyrite oxidation under such conditions may never come to completion. Sturey et al. (1982) developed a leaching procedure in where various rock types are mixed, layered, or treated to simulate the potential sequence of materials placement in a backfill. Leaching with acid water (inoculated with *Thiobacillus* bacteria) allows for accelerated pyrite oxidation and provides a small-scale model to predict drainage quality.

One of the advantages of simulated weathering is that it considers relative weathering rates of pyrite and carbonate materials. It is, however, still very difficult to say to what degree the technique resembles a mine 'waste' profile where oxygen diffusion, water infiltration, bacteria effectiveness and salt and clay mineral influences on pyrite oxidation are unknown. Therefore, although the simulated weathering technique does consider some of the factors that the acid-base balance does not, it can hardly be taken for granted that it simulates a mine 'waste' profile.

4.3.4 Computer simulation models

Perhaps the best way to predict AMD production potential is to consider computer simulation models that employ a maximum number of interactive variables. Such computer-generated predictions can first be tested with data from laboratory column-leaching studies and then tested in the field. An approach taken to generate such models is through conceptual understanding of the factors controlling pyrite oxidation, e.g., O_2, temperature, pH, and use of functional approaches in predicting kinetics of pyrite oxidation. Such conceptual model description of pyrite oxidaion is shown in Figure 4.7 adapted from Jaynes et al. (1984) and modified.

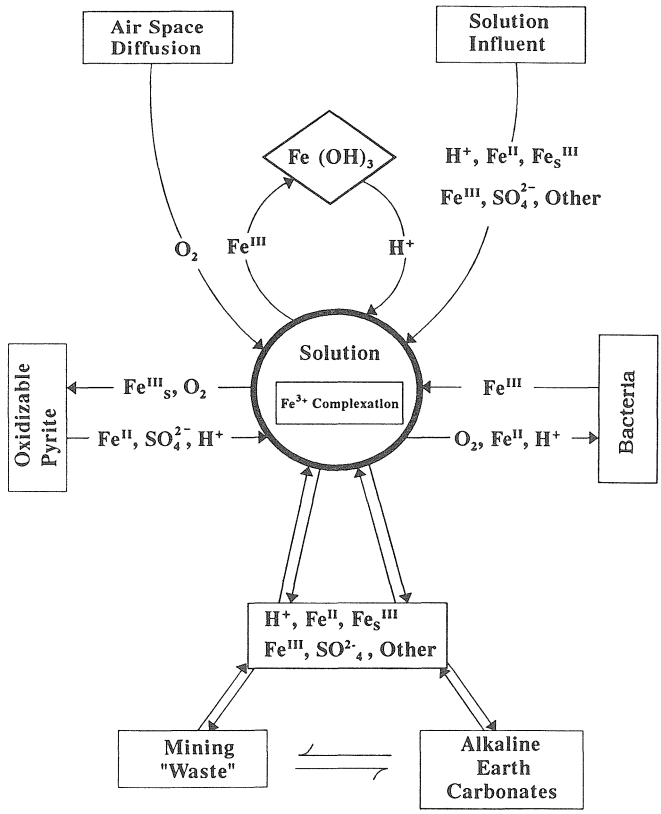

Figure 4.7. Conceptual schematic diagram of pyrite oxidation in pyritic mine "waste". Ferric iron complexes designated as Fe_S include all solution species. (Afterm Jaynes et al., 1984. With permission.)

In this conceptual model representation, pyrite oxidation is carried out by O_2 or Fe^{III} (see left-hand side of Figure 4.7). Regeneration of Fe(III) is considered to take place by bacteria. Reactions between pyrite oxidation products, carbonates, and mine 'waste' surfaces are also included at the lower portion of Figure 4.7. This conceptual model would allow one to predict acid production. However, model accuracy would depend on how one would go about quantifying the above processes.

Pyrite oxidation models can be grouped into two categories depending on approach employed to make predictions: 1) *deterministic functional models*, and b) *mechanistic models*. Deterministic models include functional and mechanistic approaches to make pyrite oxidation predictions. According to Addiscott and Wagenet (1985), in general, *functional* models are "models that employ simplified treatments to make outcome predictions" for a given process, e.g., pyrite oxidation, and "make no claim to

fundamentality", whereas *mechanistic* models employ "the most fundamental mechanisms of the process".

Currently, there are a number of pyrite oxidation models in the literature (Jaynes et al., 1984; Renton et al. 1988; Batarseh et al. 1989; Caruccio and Geidel, 1980, 1981, 1985; Scharer et al. 1991; Bronswijck and Groenenberg, 1993); for the most part these models are considered to be *functional* models. According to this author's opinion, currently, the models by Jaynes et al (1984) and Bronswijck and Groenenberg (1993) represent the best *deterministic functional* models. They use mechanistic and functional approaches to describe pyrite oxidation rates as controlled by inorganic physical and biophysical chemical processes.

In order to obtain a conceptual picture of a pyrite oxidation model, one needs to have an understanding of all the reactions involved in the oxidation of pyrite present in mine 'waste'. These reactions can be classified into four broad categories: 1) Diffusion of oxygen (O_2), 2) chemical reactions, 3) transport of pyrite oxidation products, and 4) fate of pyrite oxidation products and their influence on oxidation. Fate of pyrite oxidation products and influence on oxidation, e.g., kinetics, can be broken down to a number of subcategories. These subcategories include: 4a) precipitation/dissolution of metal hydroxides, metal sulfates, e.g., $CaSO_2 \cdot 2H_2O$, $PbSO_4$, $AlOH\text{-}SO_4$, etc., 4b) acid dissolution of 'waste' material other than pyrite, e.g., clays, oxides, etc., 4c) surface sorption reactions of metallic cations and oxyanions, e.g., Fe^{II}, Mn^{II}, Al^{3+}, SO_4^{2-}, AsO_4^{3-} etc., 4d) ion-exchange reactions with constant charge minerals, e.g., clay minerals, and variable charge minerals, e.g., organics, metal oxides, pyrite (see also chapters 2 and 3), and 4e) acid neutralization by alkaline earth carbonates, e.g., various limestone types (see Chapter 5).

All reaction categories and subcategories listed above are interdependent. For example, pyrite oxidation is known to be indirectly dependent on pH (Smith and Shumate, 1970; Goldhaber, 1983; Moses et al., 1987; Jaynes et al., 1984; Hood, 1991 and references therein), however, pH in oxidizing pyritic 'waste' is controlled by a simultaneous quasi-chemical equilibrium state between solid, liquid and gaseous phases present in the system. Because of this enormous complexity, model predictions are commonly based on simpler systems employing well thought-out assumptions.

Jaynes et al. (1984) considered that pyrite oxidation is carried out directly by oxygen and/or ferric iron. One could describe these oxidation processes at a mechanistic (molecular) level by including the O_2 adsorption process on the surface of pyrite and the actual electron transfer process from the disulfide to the O_2. A similar approach can be taken for iron (III). Therefore, equations would have to be developed to describe the pyrite-surface O_2 and Fe^{III} competitive interactions, electron transfer, reaction

products, and oxidation-products detachment from the pyrite surface. Such a model would have some mechanistic value.

However, Jaynes et al.'s model makes pyrite oxidation predictions based on simple diffusion processes and Fe^{III} concentration estimates. Ferric iron is estimated through the solubility product constant of $Fe(OH)_3$ when the system is saturated with respect to $Fe(OH)_3$, or through a mass balance approach when the system is undersaturated with respect to $Fe(OH)_3$. A quasi-empirical simple redox-Fe(II)/Fe(III) chemistry equation, based on oxygenation and/or microbial action, is used to speciate dissolved iron with respect to Fe-hydroxy species. The pH is also predicted empirically employing an arbitrary pH buffering coefficient by the geologic waste. Additionally, experimental first-order rate constants representing the two pyrite oxidants (O_2 and Fe^{III}) are employed. The biggest weakness of this model is the simplicity with witch it treats solute transport processes relative to the actual complexity of such processes (Addiscott and Wagenet, 1985). The model computes solute transport by the difference between annual precipitation and evaporation plus runoff. It is well known that the leachate transport mode influences concentration of pollutants. For example, two different geologic systems containing the same quantity of water-available pollutants, the one with macropore flow patterns would release the least polluted drainage (Thomas and Phillips, 1979; Quisenberry and Phillips, 1976, 1978).

Based on the above, Jaynes' et al. (1984) model does not take into consideration the complex molecular processes involved in solution and the pyrite surface (see Chapter 1 and 6); nor does it take into consideration processes such as nutrient availability to the iron oxidizing bacteria. However, in such chemically complex environments most of the molecular processes are difficult to model and therefore it maybe necessary to employ functional approaches to make pyrite oxidation predictions.

The pyrite oxidation model by Bronswijck and Groenenberg (1993) is capable of predicting pyrite oxidation in alkaline environments. In this model, it is assumed that O_2 diffusion is the rate limiting step in the pyrite oxidation process. The model does not assign any role to Fe(III) but it does take into consideration cation exchange reactions, disolution/precipitation reactions, and gypsum production reactions (Table 4.1). This model is also classified as a *functional* model.

Models such as those by Renton et al. (1988), Batarseh et al. (1989), Caruccio and Geidel (1980, 1981, 1985) and Scharer et al. (1991) also describe pyrite oxidation but at a more functional level than Jaynes' model. One should keep in mind that just because a model is strictly functional it does not imply that the model is not accurate. It simply implies that under certain environmental conditions, due to the empiricity of the model its sensitivity would be quite low or may lack any sensitivity for any particular pyrite oxidation controlling factor.

Table 4.1
Estimated and simulated quantities of pyrite oxidation in a soil column during the first 70 days of the experiment. After Ritsema and Groenenberg (1993)

Depth	Initial FeS_2 content	Estimated FeS_2 oxidation	Simulated FeS_2 oxidation
cm	g	g	g
0-10	9	3	3
10-35	289	11	11
35-55	437	7	7
55-75	337	3	3
75-90	0	0	0

For example, the model by Renton et al. (1988) and Bataresh et al. (1989) employ empirical rate constants for predicting AMD production. These models however, could not predict Fe(II)/Fe(III) ratios and their effect on pyrite oxidation kinetics, nor they could evaluate bacteria substrate availability and its role on oxidation kinetics. Similar observations apply to Caruccio and Geidel's model which relies heavily on pyrite and alkalinity distribution in the strata to make acid drainage prediction potentials. Such models are also referred to as macroscopic models.

Macroscopic models are excellent tools for understanding extreme situations. For example, in general, the models by Renton et al. (1988), Batarseh et al. (1989), Caruccio and Geidel (1980, 1981, 1985) and Scharer et al. (1991) could predict if a given stratum under oxidative conditions would produce AMD. These models however, could not predict pH and/or heavy metal concentration in the leachate as a function of time simply because they do not consider chemical processes, molecular or otherwise, that would allow such predictions. On the other hand, macroscopic models are excellent tools for providing an overview on the outcome of complex reactions in nature. For a more detailed discussion on this see Chapter 9.

Taylor & Francis
Taylor & Francis Group
http://taylorandfrancis.com

Chapter 5
ACID DRAINAGE CONTROL AND ITS LIMITATIONS

5.1. Prevention Technologies

Federal water quality standards in the United States require that mine-water discharges have a pH between 6 and 9, and total iron and manganese concentrations equal to or less than 3.0 mg L^{-1}, and 2.0 mg L^{-1}, respectively. At many active and inactive mine sites water quality standards are not met by the drainage and needs to be treated before is discharged. In the United States, the mining industry spends over $1 million per day to treat AMD.

The U.S. Bureau of Mines estimated that abandoned coal and metal mines and the associated piles of mine 'waste' adversely affect over 12,000 miles of river and streams, and over 180,000 acres of lakes and reservoirs in the United States (Kleinmann 1989). Wildeman (1991) pointed out that handling the environmental aspects of a coal mining operation can be just as costly as the actual coal extraction, and abatement of present AMD is far more troublesome than planning to avoid the problem.

Conventional and current technologies used to avoid production of AMD at the source and to abate AMD will be reviewed here. These include conventional methods of inundating and neutralizing pyritic material and current methods employing wetlands, limestone, and phosphate.

5.2 Alkaline Earth Carbonates

The most common method of controlling acid water is through the use of carbonates in the form of limestone, e.g., calcite or dolomite (see also Chapter 1). In order to understand the neutralization potential of rock carbonates applied to pyritic mine 'waste' one needs to understand the forms of acidity present in these material (see also Chapters 2 and 3). There are mainly three forms of acidity in pyritic 'waste' material, 1) *pore-solution acidity*, 2) *surface acidity*, and 3) *potential pyritic acidity*.

Pore-solution acidity is the most readily available acidity to the percolating water. It is composed of heavy metals including H^+, Fe^{II}, Fe^{III}, Mn^{II}, Al^{3+}, etc. Generally, the source of these components is pyrite, under oxidation, and aluminosilicates (e.g., clays), under dissolution. In aged pyritic 'waste' this form of acidity represents a large fraction of the total acidity in the system. Note for example the data in Table 5.1 which show that for some of the 'waste' samples water extractable cations exceed CEC, suggesting that *pore-solution* acidity would most likely exceed *surface acidity*. Reactions of *pore-solution* acidity with limestone, e.g., $CaCO_3$ or $CaMg(CO_3)_2$, and products formed are shown in Equations 5.1 and 5.2.

Table 5.1
Values of pH, electrical conductivity (EC), water extractable acid cations (Fe, Mn, Al) and cation exchange capacity (CEC) of various pyritic waste samples

Sample* I.D.	pH	EC mmhos cm^{-1}	Water extractable acid cations $cmol_c\ kg^{-1}$	Cation exchange capacity $cmol_c\ kg^{-1}$
1	2.36	8.01	4.8	11.6
2	7.86	2.15	0.03	8.7
3	8.00	2.79	0.01	5.0
4	1.68	19.50	46.8	8.6
5	2.74	4.60	2.3	10.1
6	3.14	3.83	1.9	9.0
7	2.08	16.60	42.8	6.2
8	7.62	5.79	1.0	6.9
9	1.89	19.37	5.7	7.1

* see Table 3.1

Solution Neutralization with Calcite

$$H_2SO_4 + CaCO_3 = CaSO_4 + H_2O + CO_2 \qquad (5.1)$$

and

Solution Neutralization with Dolomite

$$2H_2SO_4 + CaMg(CO_3)_2 = CaSO_4 + MgSO_4 + 2H_2O + 2CO_2 \qquad (5.2)$$

These reactions, as shown, do not have actual mechanistic meaning, nor do the chemical species shown represent the exact chemical species present in the *pore-solution*. Equation 5.1 shows that upon reacting solution acidity with $CaCO_3$ the main product produced is $CaSO_4$ or gypsum ($CaSO_4{\cdot}2H_2O$), while in the case of dolomite ($CaMg(CO_3)_2$) the products generated are gypsum and $MgSO_4$. Gypsum has a solubility of 2,200 milligrams per liter of water (see also Chapter 1) while $MgSO_4$ exhibits a solubility of around 70,000 mg L^{-1}. According to Reaction 5.1, piston type flow (ideal porous media flow) in geologic 'waste' containing free $CaSO_4{\cdot}2H_2O$ would release leachate containing a maximum of approximately 1,200 mg L^{-1} SO_4. On the other hand, according to Reaction 5.2, piston type flow in geologic 'waste'

containing free $MgSO_4$ would release leachate containing much greater than 1,200 mg L^{-1} SO_4. However, commonly, flows in pyritic 'waste' are described as macropore type than micropore or ideal type due to their karst-like geology. For this reason, in the case of calcite SO_4 concentration in the leachate is expected to be much lower than that predicted by the solubility of gypsum (Reaction 5.1) and in the case of dolomite SO_4 concentration in the leachate is expected to be much lower than the expected maximum (70,000 mg L^{-1}; Reaction 5.2). Based on the above and according to Cathles (1982), such pyritic 'waste' would continue to release SO_4 enriched leachate for many years, depending on the total amount of SO_4 present. Based also on the above, calcite treated 'waste' is expected to produce better quality leachate than dolomite treated 'waste' in terms of SO_4 concentration.

The above, with respect to neutralizing low pH solutions with calcite or dolomite, also apply to neutralizing solutions containing relatively strong acid metals, e.g., Al^{3+}, Fe^{III}, etc., as shown in Equations 5.3 and 5.4,

Heavy Metal Precipitation

$$1/3Al_2(SO_4)_3 + CaCO_3 + H_2O = 2/3Al(OH)_3 + CO_2 + CaSO_4 \quad (5.3)$$

and

$$1/3Al_2(SO_4)_3 + 0.5CaMg(CO_3)_2 + H_20 = 2/3Al(OH)_3 + CO_2 + 0.5CaSO_4 + 0.5MgSO_4 \quad (5.4)$$

Reactions 5.3 and 5.4 reveal that $Al_2(SO_4)_3$, a product of aluminosilicate (clay) dissolution by strong acid, upon reacting with calcite or dolomite produces $Al(OH)_3$ (which is relatively insoluble above pH 5 (Lindsay, 1979)), $CaSO_4 \cdot 2H_2O$, and $CaSO_4 \cdot 2H_2O$ plus $MgSO_4 \cdot nH_2O$, respectively. Therefore, if sufficient alkaline material is added to pyritic 'waste' and the nature of this alkaline material is such that is able to raise the pH up to 9 most of the metals will be hydrolyzed and precipitated. Metals such as iron and manganese must be oxidized before being precipitated as stable compounds, which is why aeration and neutralization are combined in treating AMD in active mine sites. Other materials, such as alkaline fly ash and topsoil or their mixtures with lime have been found to significantly reduce drainage iron concentration as well as manganese and sulfate (Jackson et al., 1993).

Surface acidity represents that adsorbed of the surface of minerals carrying negative charge. This form of acidity is representative of the acidity in solution and its magnitude depends on the fraction of CEC occupied by H^+ Al^{3+}, Fe^{3+}, Fe^{2+} and Mn^{2+}, as well as any other heavy metals. *Surface acidity* maybe equal to, less than, or greater than *pore solution acidity*, depending on the amount of pyrite that has been oxidized. However, before significant accumulation of *pore-solution acidity* takes place, the CEC of the 'waste' has to be dominated by acid metals and H^+. For this reason, at times,

surface acidity maybe significantly greater than *pore-solution acidity*. Note, for example, the data in Table 5.1 show that in some of the pyritic 'waste' samples *pore-solution acidity* represents an insignificant fraction of the CEC, suggesting that most of the acidity in these 'waste' samples would most likely be *surface acidity*. In most agricultural acid soils *surface acidity* exceeds *pore-solution acidity*, suggesting that the presence of oxidizable pyrite is a requirement for *pore-solution acidity* to exceed *surface acidity*. A practical yardstick for understanding *surface acidity* is to consider that for a mineral 'waste' with a CEC of 10 $cmol_c\ kg^{-1}$ saturated with acidic cations, approximately 5 metric tons of pure $CaCO_3$ per 1000 metric tons of 'waste' would be required for acid neutralization. Finally, in general, limestone-*surface acidity* reactions are more complex than limestone-*pore-solution acidity* reactions. This is probably due to variability in surface charge with pH (see Chapters 2 and 3).

Liming agents when applied to mine 'waste' bring drastic changes in chemistry and behavior to 'waste' solution and charged surfaces (see also Chapters 2 and 3). The reaction below demonstrates the interaction between $CaCO_3$ and *surface acidity*.

Surface Neutralization with Calcite

$$\text{(Surface-Al)+(Surface-H)} + H_2O + 2CaCO_3 = 2\text{(Clay-Ca)} + Al(OH)_3 + 2CO_2 \quad (5.5)$$

Equation 5.5 demonstrates neutralization of clay surfaces containing exchangeable\neutralizable H^+ and/or Al^{3+}. The net result of the reaction is displacement of H^+ and Al^{3+} from the clay surface by Ca^{2+} and production of $Al(OH)_3$ as solid, and CO_2 as gas. An alternate view of the neutralization process demonstrated by Reaction 5.5 is that of mineral surface charge increase due to pH increase (Sposito, 1984; Mehlich, 1981; Uehara and Gillman, 1980; Van Raij and Peech, 1972; Lumbanraja and Evangelou, 1991). In this view, hydroxyls (OH^-) produced by CO_3^{2-} and H_2O react chemically with the clay/oxide surface and produce negative surface charge on to which Ca^{2+} (released from $CaCO_3$) adsorbs (see Chapter 2). Such surfaces, also referred to as variable charge surfaces, tend to react with cations as well as anions. Generally, greatest cation/anion simultaneous chemical surface reactivity is observed near the pH of zero point of charge (PZC_{pH}) which is defined as the pH at which the sum of all positive charges equals the sum of all negative charges. Most of the iron-oxides (present in pyritic 'waste) responsible for variable charge exhibit a PZC_{pH} somewhere between pH 6 and 7. In this pH range, most likely, the 'waste' adsorbs both SO_4 and associated metallic cations from the *pore-solution* (see also Chapters 2 and 3).

Based on the above, an increase in pH above the PZC_{pH} is followed by an increase in the CEC but a decrease in the anion exchange capacity

(AEC), leading to increasing cation adsorption and decreasing anion adsorption. The reverse is expected when pH drops below PZC_{pH}. Soil variable charge has been found to vary anywhere from near zero to approximately twenty $cmol_c\ kg^{-1}$ (Mehlich, 1981). Mine 'waste' with high oxide and kaolinite content are considered to have the highest proportion of variable charge in relationship to the permanent charge. The permanent charge is relatively higher in smectite dominated mine "waste". Organic matter (humates/fulvates), a high charge surface (200 to 800 $mmol_c\ kg^{-1}$), is commonly found in extremely small amounts in pyritic mine "waste". For more information on magnitude and behavior of surface charge in geologic matter see Chapters 2 and 3.

Potential pyritic acidity variability is demonstrated by the data in Table 5.2 representing mine 'waste' material from eastern U.S. coal fields.

Table 5.2
The pH, buffer pH, and potential acidity of various mine 'waste' samples

Sample*	pH	Buffer pH	Tons of limestone obtained from buffer	Potential acidity in limestone equivalents
			tons $(acre)^{-1}$	tons $(acre)^{-1}$
1	2.74	4.26	20	17.60
2	7.24	7.43	--	4.30
3	7.05	7.31	--	0.00
4	2.17	2.54	>25	77.00
5	3.14	4.57	15	14.30
6	3.79	5.50	8	61.00
7	2.35	3.60	>25	69.20
8	4.33	6.15	6	7.80
9	2.24	2.21	>25	92.50
10	3.14	4.27	20	65.10
11	3.39	4.60	15	16.40
12	3.90	5.00	11	33.40
13	4.59	7.09	--	3.80

*see Table 3.1

The magnitude of this acidity may vary from a few tons of $CaCO_3$ per 1,000 tons of 'waste' to several hundred tons of $CaCO_3$ per 1,000 tons of 'waste' material. More details on potential pyritic acidity are given in Chapters 3, 4, and 6.

A great deal of attention has been given to the use of rock phosphate for controlling pyrite oxidation (Stiller et al. 1986; Meek, 1984, 1989). There

are *three major mechanisms* by which rock phosphate or semi-refined apatite rock [$Ca_5(F,Cl,OH{\cdot}0.5CO_3)(PO_4)_3$] may control pyrite oxidation. The *first mechanism* is dissolution of rock phosphate and release of phosphate into pore-solution which in turn reacts with solution Fe(III) (a pyrite oxidizer) or Fe(II) and precipitates as strengite ($FePO_4{\cdot}2H_2O$) or vivianite ($Fe_3(PO_4)_2{\cdot}8H_2O$), respectively (Baker, 1983; Hood, 1991; Huang and Evangelou, 1994). The *second mechanism* involves precipitation of $Fe(PO_4){\cdot}nH_2O$ as pyrite surface-coating which in turn limits O_2 diffusion to the pyrite surface, hence stopping oxidation (see also Chapters 9, 10, 11, and 12). The *third mechanism* is simply increase in pH due to the fact that PO_4 in solution acts as a weak base (note that phosphoric acid exhibits three pK_a values, 2.2, 7.2 and 12.2; they represent pH values at which strong buffering is observed). Increase in pH limits availability of Fe(III) in *pore-solution*; therefore, the potential of Fe^{III} to act as a pyrite oxidant can be reduced by the addition of phosphate. Spotts and Dollhopf (1992) evaluated two sources of apatite and two phosphate byproducts applied at a concentration of 30 g kg^{-1} by weight to pyritic mine overburden. Their relatively short-term results indicated that the materials were apparently effective in controlling pyrite oxidation. However, Huang and Evangelou (1992) carried out a series of experiments trying to demonstrate that indeed phosphate limits pyrite oxidation. The results of these studies indicated that this inhibition is only temporary because of iron armoring (Huang and Evangelou, 1992; Evangelou et al., 1992) (see also Chapter 10).

Schematic diagrams of the reactions of rock phosphate in soils/geologic systems in the absence of Fe, or Mn, or Al are shown in Figure 5.1.

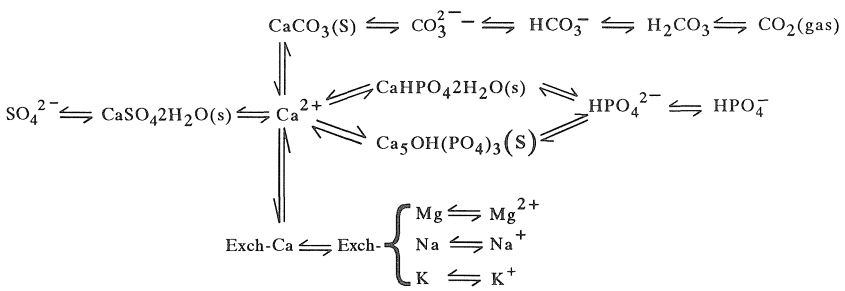

Figure 5.1. Schematic of reactions of rock phosphate in the absence of Fe, or Mn, or Al. s = Solid, Exch- = Exchangeable.

The diagram in Figure 5.1 implies that the concentration of phosphate in solution is regulated by pH and the concentration of Ca^{2+} (in limed pyritic

mine 'waste' Ca^{2+} is controlled by the solubility of gypsum, $CaSO_4 \cdot 2H_2O$; see Chapter 1) and types and quantities of exchangeable cations. In general, as pH increases, availability of phosphate in solution decreases since extremely low solubility phosphate minerals are in control of phosphate, namely fluorapatite ($Ca_{10}(PO_4)_6(F)_2$) or hydroxapatite ($Ca_5(PO_4)_3(OH)$). However, as divalent cations become surface-adsorbed by clays/organics/oxides through monovalent cation surface displacement (e.g., K^+, Na^+) phosphate in solution increases. On the other hand, according to Figure 5.2, as pH decreases, phosphate in solution increases due to the fact that hydroxapatite or fluorapatite dissolve incongruently, thus forming more soluble phosphate minerals, namely octocalcium phosphate ($Ca_4H(PO_4)_3$) or dicalcium phosphate ($CaHPO_4$), depending on pH and single-ion activities (see Chapter 1).

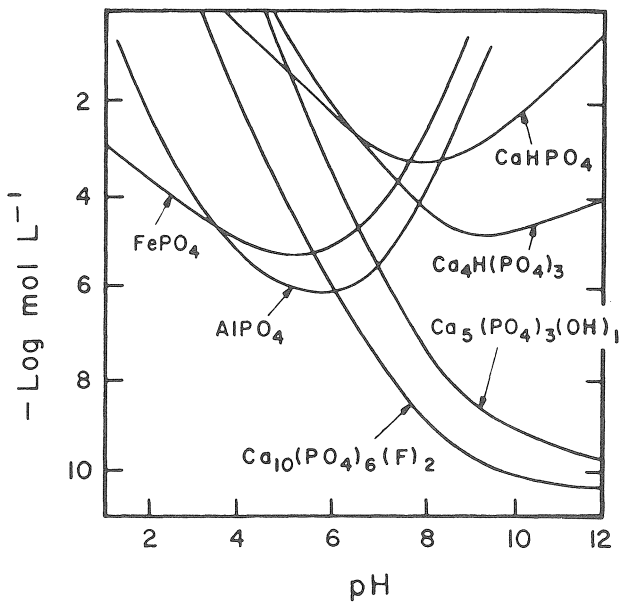

Figure 5.2. Solubility of various metal-phosphates as a function of pH. (From Stumm and Morgan, 1981. With permission.)

Note that, according to Figure 5.2 maximum stability of hydroxyapatite ($Ca_5(OH)(PO_4)_3$) is exhibited at pH values greater than 8 (actually, maximum stability is exhibited at the lowest point on the curve, or at d[Me]/d[pH] = 0; Me = metal cation). In this pH range, $CaCO_3$ may also be present (Figure 5.1) depending on the quantity of available Ca^{2+} present relative to that of phosphate. Thus, since stability of $Ca_5(OH)(PO_4)_3$ maximizes at pH around 10 and since pH in such 'waste' is in the range of 6 to 7, phosphate release to the percolating rock phosphate treated 'waste' solution is expected to be a

continuous process due to the solubilization of hydroxapatite ($Ca_5(OH)(PO_4)_3$) or fluorapatite ($Ca_{10}(PO_4)_6(F)_2$).

In the case of pyritic 'waste' containing water soluble Al and or Fe(III) application of hydroxapatite ($Ca_5(OH)(PO_4)_3$) or fluorapatite ($Ca_{10}(PO_4)_6(F)_2$) would be followed by their incongruent-like dissolution, leading to formation of ferric phosphate compounds (e.g., $Fe(OH)_2H_2PO_4$) or aluminum phosphate compounds (e.g., $Al(OH)_2H_2PO_4$) as shown in Figure 5.3a and Figure 5.3b.

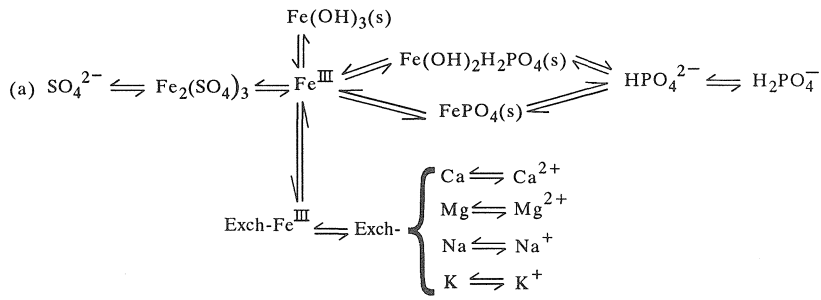

and

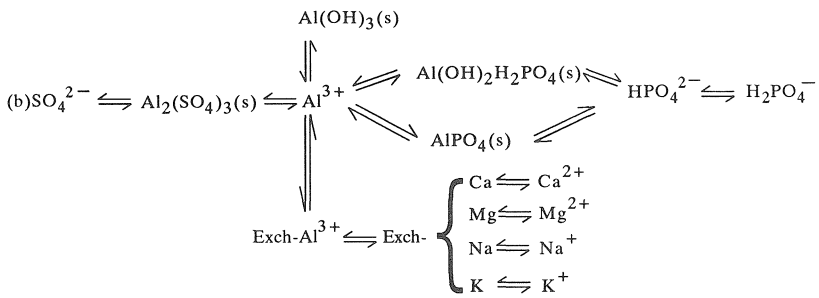

Figure 5.3. Schematic of reactions of rock phosphate in the presence of a) Fe(III) and b) Al (competitive interactions between OH^- and PO_4^{3-} appear to take place above pH 7 (Figure 2) leading to metal phosphate solubilization at high pH. s = Solid, Exch- = Exchangeable.

This is expected, since as shown in Figure 5.2 phosphate compounds of Al and Fe(III) exhibit maximum stability at lower pH values relative to that of calcium phosphate minerals (Stumm and Morgan, 1981). For additional information on Al and SO_4 chemical interactions and their practical importance, see also Chapter 3.

The schematic diagram in Figure 5.4 shows that rock phosphate may also react with Fe(II) thus, forming vivianite ($Fe_3(PO_4)_2 \cdot 8H_2O$) a relatively insoluble compound which in the presence of O_2 converts to water-insoluble $FePO_4$ solid.

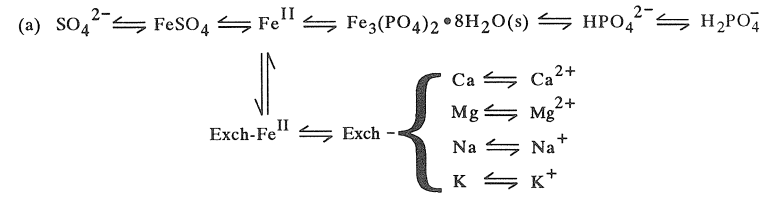

Similarly, when in the presence of Mn(II), formation of $MnHPO_4$ takes effect, which exhibits extremely low water solubility.

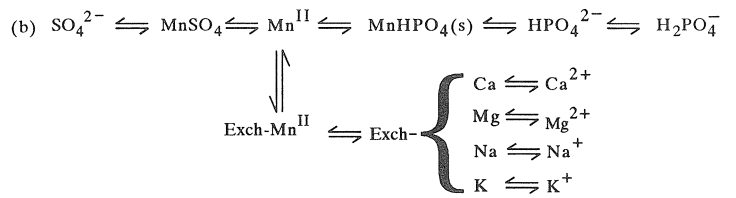

Figure 5.4. Schematic of reactions of rock phosphate in the presence of a) Fe(II) or b) Mn(II). s = Solid, Exch- = Exchangeable.

In addition to the above, phosphate may appear to control pyrite oxidation by its ability to act as a potential determining ion (Wann and Uehara, 1978). Phosphate may chemisorb on the surfaces of clay minerals and oxides, increasing their pH-dependent negative charge. This increase also represents an increase in the size of the cation sink, e.g., Fe^{III} (Van Raij and Peech, 1972; Uehara and Gillman, 1980; Lumbanraja and Evangelou, 1991) (see also Chapters 2 and 3).

5.2.1 Coating limitations

Earth carbonates (crushed limestone rocks) are a cheap source of alkalinity for controlling acid drainages. However, carbonate rock effectiveness in controlling pyrite oxidation is at times controversial. Earth carbonates are known to have a reducing effect on acid production from pyrite oxidation by limiting Fe(III) in solution, but carbonates are not known to be able to limit pyrite oxidation in a chemical way.

There are three mechanisms by which carbonates may control pyrite oxidation. The *first mechanism* involves precipitation of Fe(III) (a pyrite oxidizing agent) as an oxyhydroxide (Lindsay, 1979). The *second mechanism* involves raising the pH high enough (6.1 to 8.4) so that microbiological

oxidation diminishes (Jaynes, 1991), and the *third mechanism* involves formation of iron-oxide coating, inhibiting O_2 diffusion to the pyrite surface (Nicholson et al., 1988; 1990; Huang and Evangelou, 1992, 1994) (see also Chapter 9). However, there are also evidence which suggest that at high pH carbonate may in fact enhance pyrite oxidation (Hood, 1991, Evangelou et al., 1985; Stiller et al., 1985) but carbonate-enhanced pyrite oxidation rates are not expected to approach those commonly observed at low pH (e.g., pH 2.7) (Jaynes et al, 1984, Jaynes, 1991 and references therein) (see also Chapter 6).

Limestone is readily available in most coal mining areas and has considerable cost advantage over other alkaline materials. However, limestone is not as effective in controlling AMD as one might expect because of its limited solubility under equilibrium conditions near neutral pH values and its tendency to armor with ferric hydroxide precipitates through surface adsorption of Fe^{II} followed by oxidation to Fe^{III} (Wentzler and Aphan 1972, US EPA 1983). When mine waters enriched with iron contact limestone in an oxidizing environment, the limestone is coated rapidly with ferric hydroxide precipitates. The rate of dissolution of the coated limestone is inhibited and production of alkalinity is significantly diminished.

Adsorption of transitional metals onto alkaline surfaces such as those of $MgCO_3$ and $CaCO_3$ has been reported in the literature (Boischot et al., 1950; McBride, 1979; Stumm and Morgan, 1970; Garrels and Christ 1965). McBride (1979) employing calcite Mn^{II} adsorption isotherms and electron spin resonance (ESR) spectroscopy showed that at low Mn^{II} levels in solution Mn^{II} chemisorbed onto the surfaces of $CaCO_3$. However, at high levels of Mn^{II} in solution, after saturation of surface sites, nucleation at $CaCO_3$ surfaces was followed by slow precipitation of $MnCO_3$. One expects similar reactions with Fe^{II}, Al^{3+}, etc. In the case of Fe^{II}, due to its instability in high pH environments, e.g., limestone surfaces, it rapidly forms an oxyhydroxide coating (Hood, 1991 and references therein).

Evangelou et al (1992) studied Mn^{II} adsorption on particles of calcite, dolomite and rock phosphate under various sizes. The data shown in Figure 5.5a show that rock phosphate (fluorapatite) exhibits the highest Mn^{II} adsorption capacity followed by calcite and dolomite. The overall data in Figure 5.5 clearly show that adsorption of Mn^{II} by calcite dolomite and rock phosphate in the solution concentrations encountered in their study is followed by desorption of an equivalent quantity of Ca^{2+}. This latter observation is consistent with geochemistry literature (Stumm and Morgan, 1970; Garrels and Christ, 1965).

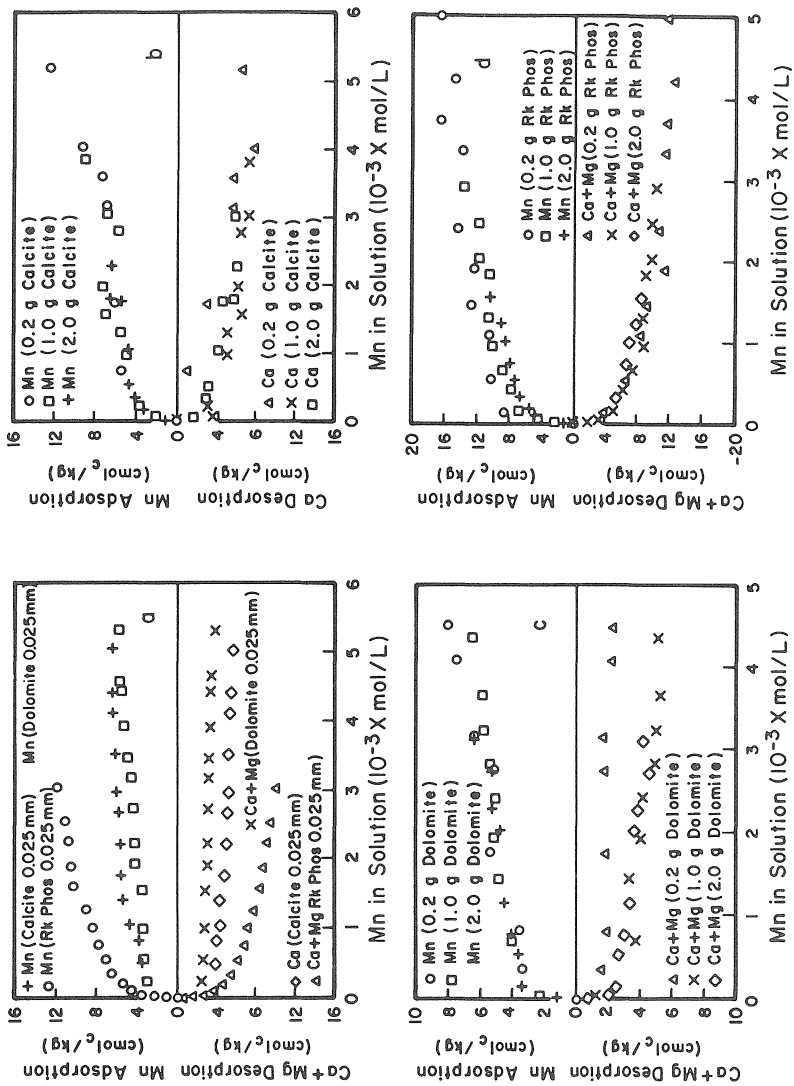

Figure 5.5. (a) Adsorption behavior of Mn^{II} and desorption behavior of Ca^{2+} or Ca^{2+} plus Mg^{2+} by calcite, dolomite and rock phosphate (Rk Phos) of 0.025 mm size particles and 2:25 solid to solution suspension ratio and (b), (c), (d) adsorption behavior of Mn^{II} and desorption behavior of Ca^{2+} or Ca^{2+} plus Mg^{2+} by the same minerals with the same size particles under various solid to solution ratios (From Evangelou et al., 1992. With permission.)

Scanning electron microscope photos in Photo A and Photo B show acid-rinsed dolomite, and dolomite coated with manganese, respectively.

Photo A

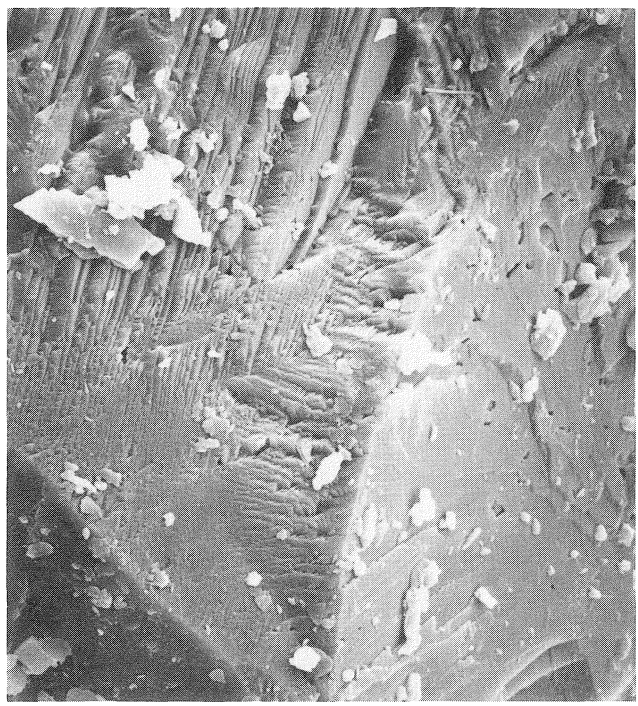

Photo B shows the initial stages of a manganese oxide coating formation on the surface of dolomite.

McBride (1979) postulated that Mn^{II} removal from solution in the presence of calcite can be accomplished via two different mechanisms. One mechanism involves the precipitation of Mn^{II} as $MnCO_3$ by the reaction of solution Mn^{II} with HCO_3^- followed by the liberation of H^+. This hydrogen is consumed by the dissolution of $CaCO_3$. The net effect of this mechanism is an equivalent surface displacement of Ca^{2+} by Mn^{II} with no change in pH. A second mechanism involves the direct surface displacement of Ca^{2+} by Mn^{II} with also no change in pH. The major difference between these two mechanisms is that the first forms a separate $MnCO_3$ phase while the second forms a new phase on the surface of calcite (solid solution) by substituting Ca^{2+} by Mn^{II}.

Photo B

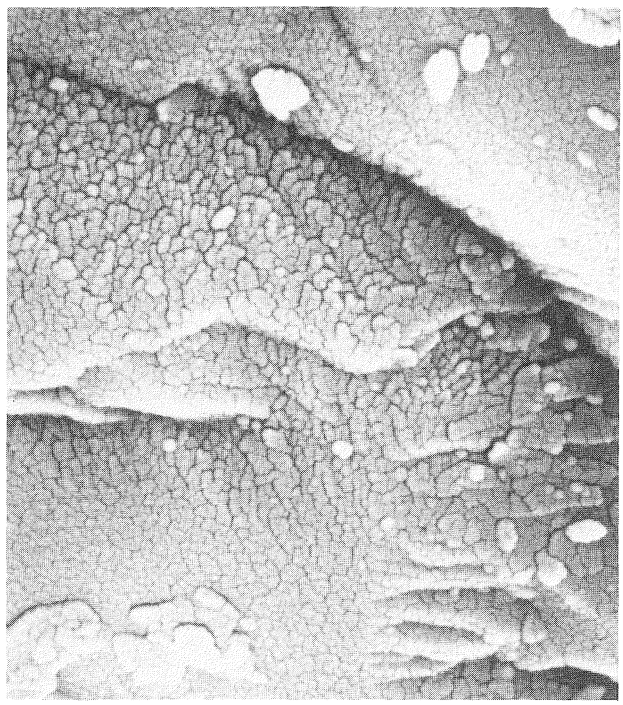

Further solution chemistry evidence on the possible mechanisms of Mn^{II} adsorption by calcite, dolomite and rock phosphate is presented in Figs. 5.5b, 5.5c and 5.5d. These data demonstrate that the adsorption of Mn^{II} by all three solid phases tested was independent of solid to solution ratio. The data in Figure 5.6 also demonstrate that Mn^{II} adsorption was particle size dependent. The smaller the particle size, the greater the quantity of Mn^{II} adsorbed. The above two observations, Mn^{II} adsorption independency of solid to solution ratio and Mn^{II} adsorption dependency on particle size, suggested that Mn^{II} was not removed from solution as a discrete phase, i.e. $MnCO_3$, but rather the process was catalyzed by the mineral's surface.

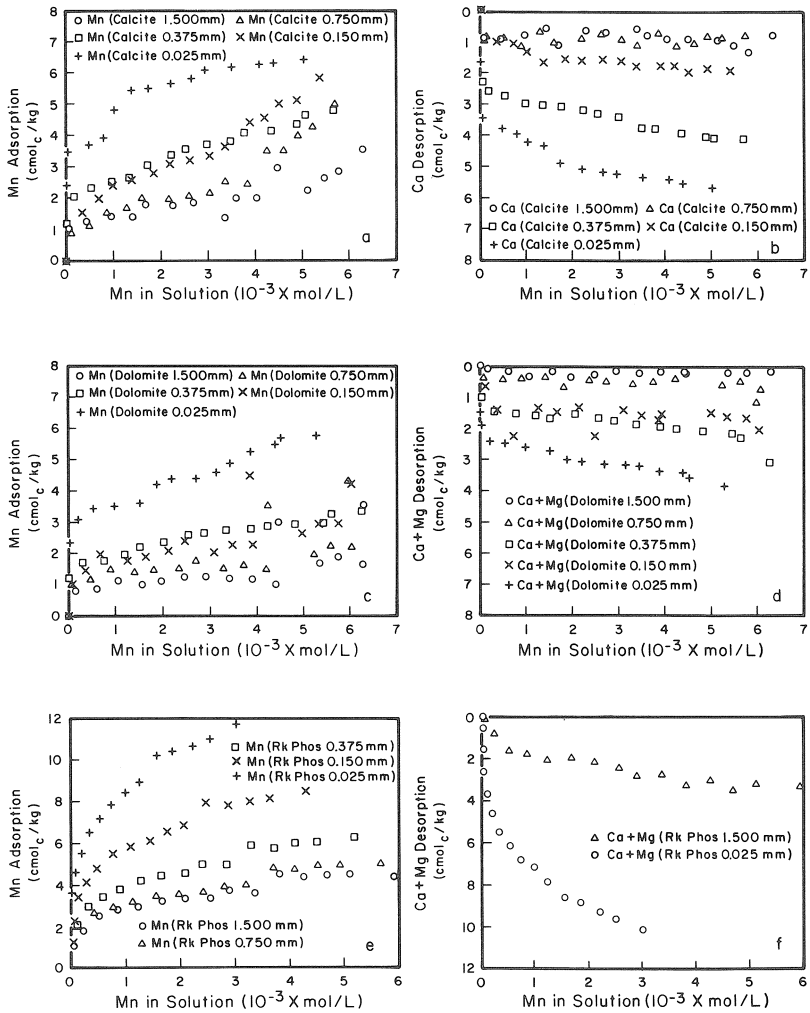

Figure 5.6. Adsorption of Mn^{II} and desorption of Ca^{2+} or Ca^{2+} plus Mg^{2+}, depending on the mineral by (a, b) calcite, (c, d) dolomite, and (e, f) rock phosphate (Rk Phos) of various sizes particles in 2:25 solid to solution suspensions. (From Evangelou et al., 1992. With permission.)

However, it is of interest to note that when Mn^{II} adsorption by dolomite was plotted as a function of specific surface ($m^2\ g^{-1}$) for each of the particle sizes

used, no single relationship was observed (Figure 5.7) suggesting that the reaction was not entirely surface controlled.

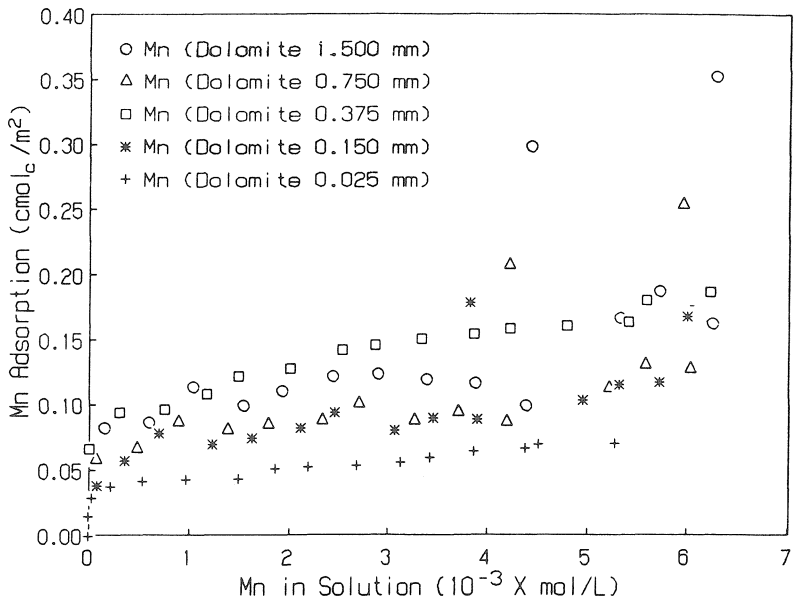

Figure 5.7. Adsorption of Mn^{II} by (a, b) calcite, (c, d) dolomite, and (e, f) rock phosphate (Rk Phos) of various sizes particles in 2:25 solid to solution suspensions as a function of surface area. (From Evangelou et al., 1992. With permission.)

It appears from these data, as postulated also by McBride (1979), that two mechanisms may operate in the removal of Mn^{II} from solution. One mechanism operating at low metal concentrations may involve surface chemisorption, while a second mechanism operating at high metal concentrations may involve quasi-incongruent dissolution of limestone ($CaCO_3$ or $CaMg(CO_3)_2$) when in the presence of solution Mn^{II} since the K_{sp} of $MnCO_3$ is approximately 100 times greater than the K_{sp} of $CaCO_3$ or the K_{sp} of $CaMg(CO_3)_2$ on one mole carbonate basis ($0.5K_{sp(dolomite)}$). Note that the above mechanisms apply also to all other heavy metals that exhibit high affinity for the carbonate species.

Considering that the specific surface of the various size particles tested by Evangelou et al. (1992) varied from 0.01 $m^2\ g^{-1}$ to 0.082 $m^2\ g^{-1}$, according to Jurinak and Bauer (1956) the amount of Mn^{II} that would be adsorbed (on a theoretical basis) on the carbonates could not exceed 0.2 $cmol_c\ kg^{-1}$. However, all samples under the various particle sizes tested by Evangelou et al. (1992) exceeded that value. In order to elucidate the cause of these observations, Evangelou et al (1992) introduced cation activity data into stability diagrams. The data in Figure 5.8a showed that Mn^{II} activity in

solution supported a supersaturated state with respect to $MnCO_3$, however, the solution was undersaturated with respect to $Mn(OH)_2$.

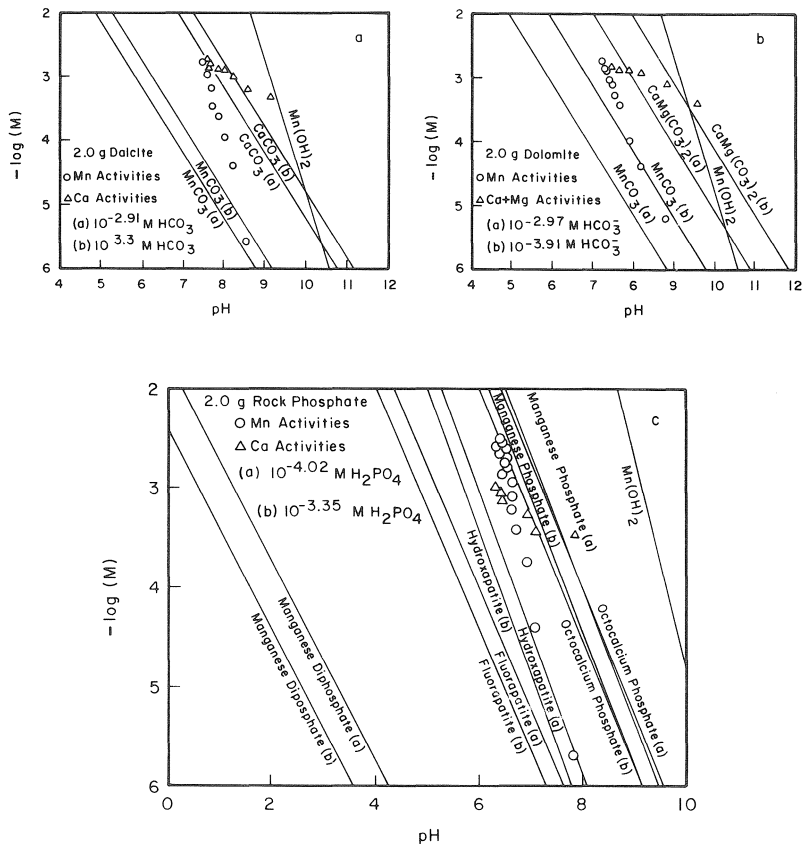

Figure 5.8. Values of pH and log Ca^{2+} or log (Ca^{2+} + Mg^{2+}), depending on the mineral, or log Mn^{2+} for the 0.025 mm size particles in 2:25 solid to solution suspensions in reference to (a) calcite, $Mn(OH)_2$ and $MnCO_3$; (b) dolomite, $Mn(OH)_2$ and $MnCO_3$; (c) $Mn(OH)_2$, octacalcium phosphate, hydroxapatite, fluorapatite, manganese phosphate and manganese diphosphate. (From Evangelou et al., 1992. With permission.)

The latter's solubility is too high to control the equilibrium concentration of Mn^{II}. The data of Ca^{2+} activity in Figure 5.8a showed that the system was

nearly at saturation with respect to $CaCO_3$ at the highest levels of Mn^{II} added (low pH values on the plot) but supersaturated at the lowest levels of Mn^{II} added (high pH values on the plot). In the case of dolomite (Figure 5.8b) the results showed similar trends. The solution was close to equilibrium with $MnCO_3$ but slightly undersaturated with respect to dolomite at high levels of Mn^{II} added (low pH values on the plot) and near supersaturation at low levels of Mn^{II} added (high pH values on the plot). A possible explanation for the above behavior was that surface adsorption of Mn^{II} could have disrupted the stabilities of calcite and dolomite, releasing Ca^{2+} or Ca^{2+} + Mg^{II}, depending on the mineral, and thus the solution was no longer in equilibrium with calcite or dolomite.

Activity data of the H_2PO_4 species in the rock phosphate system at the highest and the lowest levels of Ca^{2+} and Mn^{II} activities followed closely the stability line of octacalcium phosphate ($(Ca_4H(PO)_3 \cdot 2.5H_2O)$; Figure 5.8c)). However, Mn^{II} activity data show undersaturation with respect to $Mn_3(PO_4)_2$ and $Mn(OH)_2$ but supersaturation with respect to $MnHPO_4$ at high/low levels of H_2PO_4 activities. Calcium activity data for the same system showed undersaturation with respect to octacalcium phosphate. The degree of undersaturation increased as Ca^{2+} activity increased (Figure 5.8c). Note that even through rock phosphate was known to be fluorapatite (Occidental Chemical Corporation, 1991, personal communication), the solution appeared to be supersaturated with the mineral. This could be due to the fact that the mineral's surface chemistry, which controls the solution phase, tends to transform itself to the most stable phase which in this study was shown to be octacalcium phosphate (Figure 5.8c).

Based on the above, the surface reactions of alkaline earth carbonates with Me^{II} (Me^{II} = Fe^{II} or Mn^{II}) can be represented by:

$$-Ca_n(CO_3)_n(s) + Me^{II} = -Ca_{n-x}Me_x(CO_3)_n(s) + Ca^{2+} \qquad (5.6)$$

Similarly for rock phosphate,

$$-[(Ca_5)_n((F,Cl,OH \cdot 0.5CO_3)(PO_4)_3)_n](s) + Me^{II} = -[(Ca_5)_{n-x}Me)_x((F,Cl,OH \cdot 0.5CO_3)(PO_4)_3)_n](s) + Ca^{2+} \qquad (5.7)$$

where $0 < x < n$ and s denotes solid and n denotes number of moles of the designated ionic species. The above schematic reactions indicate that application of rock phosphate or limestone to pyritic 'waste' containing dissolved heavy metals leads to surface precipitation of metals through Ca^{2+} displacement. Furthermore, in the case of metals such as Fe(II) and/or Mn(II) rapid oxidation is followed leading to an oxide coating which is clearly visible on limestone particles in the field. This coating renders these minerals inactive with respect to their potential to act as acid drainage ameliorates.

5.2.2 Kinetic limitations

As pointed above, the carbonates most commonly used as liming agents for treating pyritic 'waste' are calcite ($CaCO_3$) and dolomite [$CaMg(CO_3)_2$]. Besides their obvious chemical compositional differences, calcite and dolomite also differ with respect to their ability to react with acids. This latter property has been employed as means to rapidly identify and quantify the two minerals in mixtures. For example, Petersen and Chesters (1966) and Petersen et al. (1966) used selective dissolution of calcite and dolomite in Na-citrate dithionite in order to quantify the two minerals in rock mixtures or in soils. Skinner et al. (1959) and Evangelou et al. (1984) quantified calcite and dolomite in mixtures by employing differences in their rate of dissolution in strong acid (Figure 5.9).

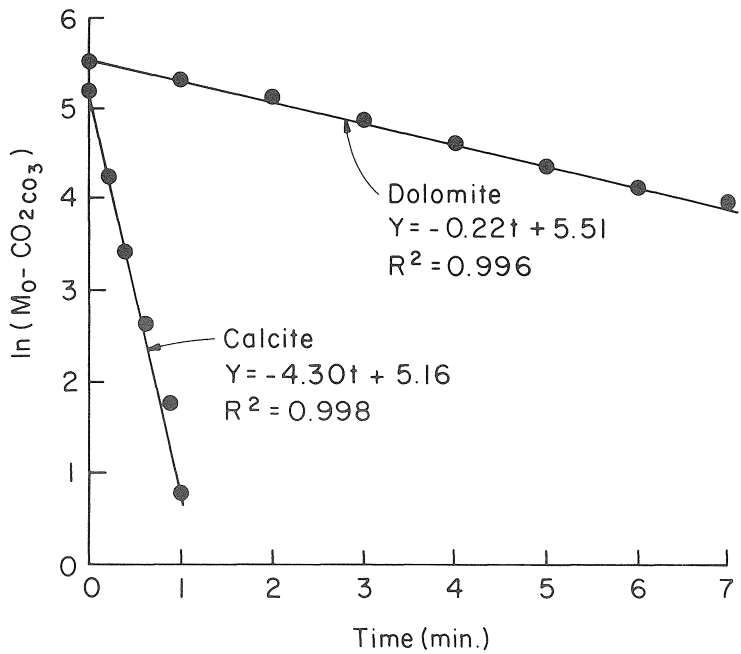

Figure 5.9. Examples of carbonate acid dissolution data obtained automanometrically. (From Evangelou et al., 1984. With permission.)

They showed that the reaction of calcite with excess 4 mol L^{-1} HCl is complete approximately within a minute while the reaction of HCl with dolomite may go on for several hours. Evangelou et al. (1984) and Skinner et al. (1959) employed a pressure transducer and a mercury manometer, respectively, to follow the dissolution rate by continuously recording the

pressure caused by the evolution of CO_2 gas. The pressure data were plotted as a pseudo first-order reaction (ln CO_{2gas} versus time). A single slope was taken to represent calcite or dolomite, depending on its magnitude, while a two-slope plot was taken to represent the presence of both minerals. Extrapolation of the second slope to the y-axis of the pseudo first-order plot allowed them to quantify the two minerals. The slope of the linear regression was taken to represent the first-order rate constant (k) (Figure 5.10).

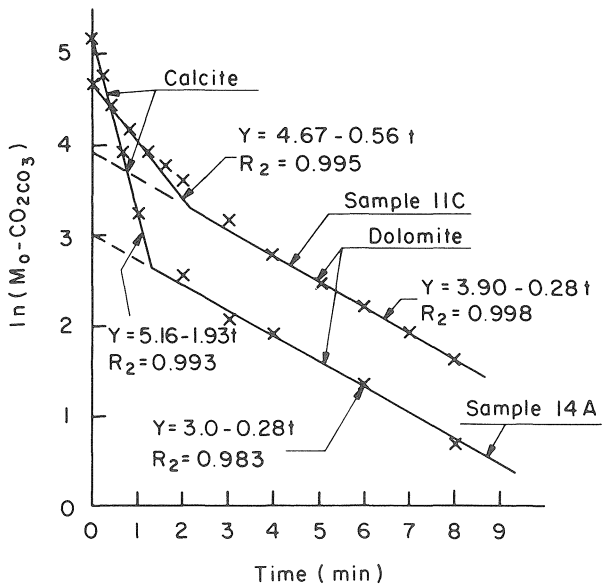

Figure 5.10. Example of a carbonaceous shale acid dissolution data obtained automanometrically. (From Evangelou et al., 1984. With permission.)

Sajwan and Evangelou (1991) estimated activation energies (E_a) of dissolution of calcite and dolomite employing the Arrhenius equation (Daniels and Alberty, 1975)

$$\ln k = (-E_a/1.987)(1/T) + \ln A \qquad (5.8)$$

where A is the pre-exponential factor and T is temperature. Their findings, including specific surface area, and first-order rate constants are reported in Table 5.3. The data in Table 5.3 show that dolomite exhibited E_a values in the range of 44.47 kJ mol^{-1} to 51.13 kJ mol^{-1}.

Table 5.3

Specific surface area and acid-dissolution kinetic parameters of calcite, dolomite and limestone samples

Sample	Sample identification	Regression equations	Specific surface $m^2\ g^{-1}$	Rate constants at temperature 14°C	21°C	30°C	Activation energies (E_a) kJ mol^{-1}	r^2
1	Dolomite	y = −6150X + 19.98	0.35	0.21	0.41	0.72	51.13	0.9973
2	Dolomite	y = −6100X + 19.12	0.18	0.11	0.19	0.37	51.13	0.9967
3	Dolomite	y = −5350X + 17.31	0.19	0.24	0.43	0.70	44.48	0.9965
4	Calcite	y = −1300X + 5.34	0.18	2.24	2.41	2.91	10.81	0.9337
5	Calcite	y = − 900X + 3.66	0.20	1.66	1.80	1.99	7.48	0.9959
6	Calcite	y = −2300X + 7.85	0.17	0.79	1.10	1.26	19.12	0.9407
7	Calcite	y = −3150X + 11.57	0.18	1.80	2.18	3.39	26.19	0.9501
Ward's calcite		y = −1500X + 5.96	0.02	2.12	2.20	2.86	12.47	0.8479
Ward's dolomite		y = −5500X + 16.03	0.02	0.04	0.07	0.12	45.72	0.9999
Reagent grade $CaCO_3$ chips		y = −2250X + 8.41	0.02	1.68	2.18	2.64	18.71	0.9920

The E_a values for all dolomitic samples appeared to be in close agreement with the E_a value (56.48 kJ mol^{-1}) reported by Skinner (1959). An additional point that could be made about the dolomitic samples is that the E_a values were relatively independent of specific surface magnitude. Specific surface of dolomitic samples varied from 0.02 m^2 g^{-1} (Ward's dolomite) to 0.35 m^2 g^{-1} (sample No. 1). This result shows that for a 17.5-fold increase in specific surface, there was only an 11.8% increase in E_a. The finding does not suggest that E_a values are completely independent of specific surface. It appears that E_a magnitude is independent of specific surface for the range encountered in this particular study.

Acid dissolution data for calcite and dolomite and calcitic and dolomite limestone samples as a function of temperature reported in Table 5.3 indicate that the dissolution of calcite was less temperature dependent, for the range of temperature tested, than the dissolution of dolomite. This result is demonstrated by the observation that E_a values for calcite, in general, were much lower than E_a values of dolomite. The E_a values for calcitic samples ranged from 7.48 kJ mol^{-1} to 26.19 kJ mol^{-1}. All calcite samples displayed E_a values below that reported by Turner and Skinner (1959) (39.75 kJ mol^{-1}). The large difference between Turner and Skinner's (1959) E_a value and the E_a values reported in this study could be due to differences in sample crystallinity as well as to errors of the manually-read mercury manometer for the calcite study by Turner and Skinner (1959).

The data in Table 5.3 also show that there was a great deal of variation in E_a for calcite but not for dolomite. This variation may be due to coatings and/or precipitated ions in the calcitic materials. Calcitic limestone samples used in this study contained a significant quantity of impurities and varied significantly between samples. On the other hand, the dolomitic limestone samples displayed approximately the same degree of purity. These observations supported the suggestion that E_a values of carbonate minerals appear to be more dependent on chemical impurities than on specific surface area.

The above clearly demonstrate that the ability of dolomite to release alkalinity is highly dependent on temperature. However, the ability of calcite to release alkalinity is not as dependent on temperature which leads to the suggestion that in cold climates one should use calcite as a source of alkalinity for neutralizing acid drainages.

5.2.3 Placement limitations

A great deal of attention has been given to the identification of pyritic material and its proper burial. A study carried out by Infarger and Hood (1980) involved the proper sequence for burial of three geologic formations found within a coal region of Illinois. The formations were: Black shale (high in pyrite), Gray shale (pH near neutral) and limestone. The materials were crushed and passed through a 2 mm sieve and then stacked in

210 cm columns of 5 cm in diameter. Each formation, in the column, occupied a length of 60 cm. The columns were leached by 1 L water increments, referred to as cycles. Results from one of the cycles are presented in Table 5.4.

Table 5.4
Effect on the chemistry of leachates by different stacking sequence of geologic material. After Infarger and Hood (1980)

Stacking sequence	Leaching cycle	Fe^{2+}	Mn^{2+}	Total dissolved solids
		mg L^{-1}		
GBL*	12	1.09	0.57	800
GLB	12	5.60	2.23	800
BLG	12	1 18	29.80	2100
BGL	12	1.01	8.30	2100
LGB	12	1.01	3.00	400
LBG	12	0.72	0.89	400

* G = gray shale (neutral)
B = black shale (pyritic)
L = limestone
First letter from left indicates that the material was located on top of the column.

The data clearly point out that when the most basic material was placed on top of the most acid material control of acid production was most effective.

There are two important reasons for the results obtained from the above stucking sequences. When alkaline geologic material are placed on top of the acid producing material the former are not subject to coating or armoring as discussed previously. On the other hand, placement of alkaline material deep in the profile limits its neutralization effectiveness because of potential high pCO_2. The latter may increase the solubility of limestone but it has a dramatic suppressing effect on pH which does not allow precipitation of $Fe(OH)_2$ or $FeCO_3$ or iron oxide formation due to lack of O_2. Brown and Jurinak (1989b), however, argued that large soluble forms of alkalinity on top of pyritic waste should be avoided because of its potential in increasing pyrite oxidation through formation of large quantities of soluble sulfoxy anions (thionates) (see Chapter 6).

5.2.4 Chemical equilibria limitations

Finely ground limestone interdispersed in pyritic material is believed to control acid generation. However, finely ground limestone incorporated in pyritic 'waste' may have a very small effect on acid neutralization even in laboratory columns. Iron oxide coatings may not be needed to explain the phenomenon.

During wetting of limestone treated pyritic 'waste', reaction of acid with calcium carbonate leads to formation of CO_2 (Equations 5.1 and 5.2); microbial activity may also contribute additional CO_2. The data in Figure 5.11, representing a pyritic 'waste' profile, show depletion of O_2 with respect to depth, relative to that of the open atmosphere, and dramatic enrichment with CO_2 relative to that of the open atmosphere (0.03%).

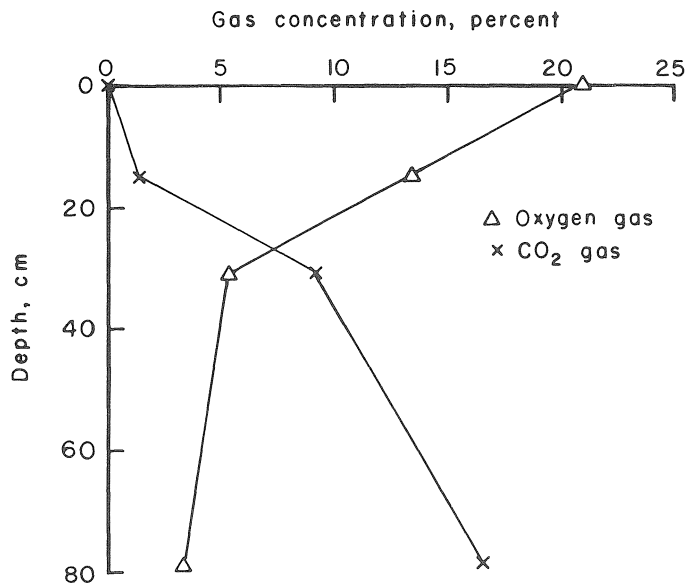

Figure 5.11. Oxygen and carbon dioxide profiles of an unreclaimed site in Morgan county, Ohio. (From Erickson et al., 1985. With permission.)

The data in Figure 5.12a reveal that as pCO_2 increases and approaches the maximum shown in Figure 5.12, pH drops below 7 and alkalinity (HCO_3) approaches 500 mg L^{-1} (Figure 5.12b) If one hypothesizes that this alkaline solution will encounter acid drainage, e.g., solution rich in dissolved iron (Fe(II)) but void of O_2, the result of the reaction is that in such a system Fe^{II} concentration would be controlled by $FeCO_3$ (Stumm and Morgan, 1981).

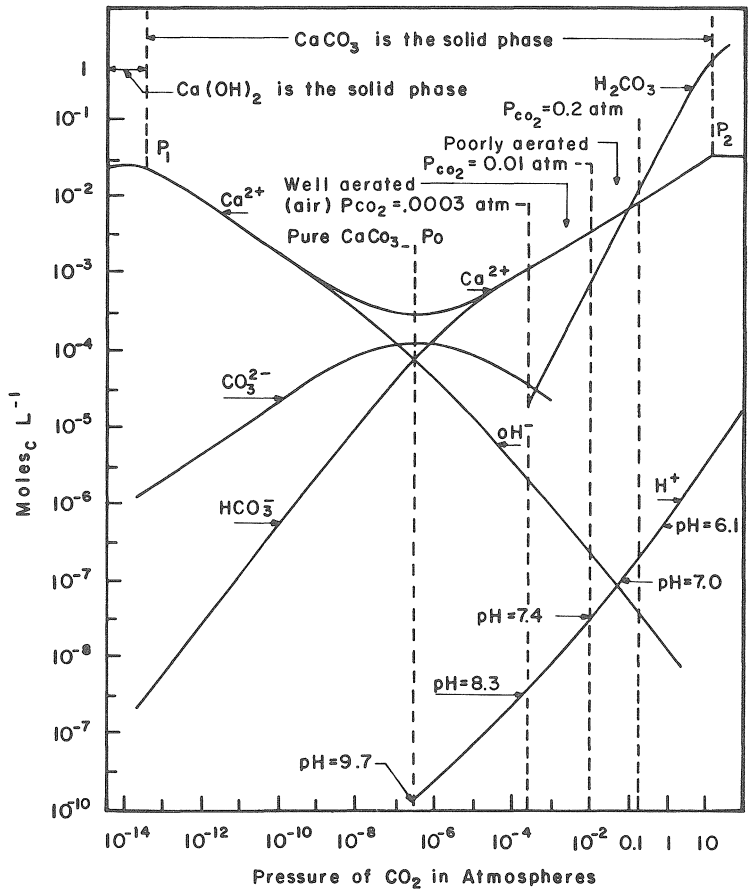

Figure 5.12a. Solubility diagram of the $CaCO_3$-CO_2 system.

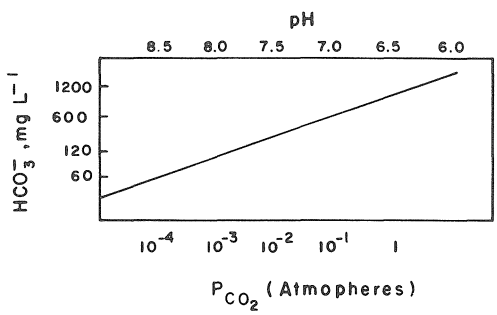

Figure 5.12b. Solubility of $CaCO_3$ in terms of HCO_3^- concentration as a function of pCO_2 or pH.

This is demonstrated in Figure 5.13, e.g., assume a solution pH slightly less than 7 and pCO_2 somewhere between 10^{-2} and 1 atmospheres.

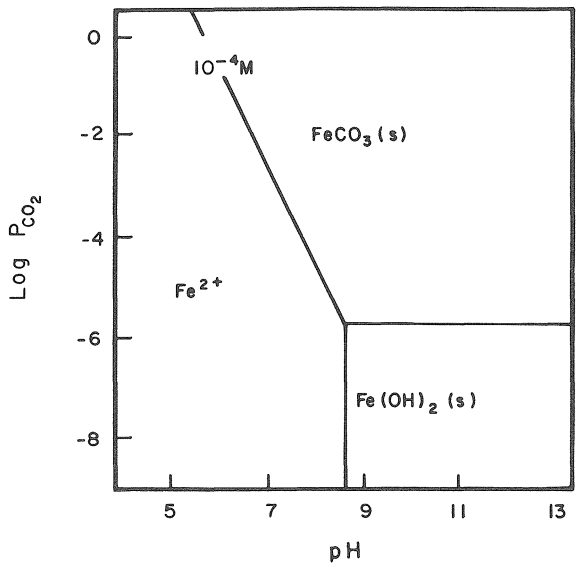

Figure 5.13. Stability diagram of $Fe(OH)_2$ and $FeCO_3$ with total dissolved carbonate of 10^{-3} mol L^{-1} and Fe^{II} activity of 10^{-4} mol L^{-1}. (From Stumm and Morgan, 1981. With permission.)

Based on this example, the data in Figure 5.14 show that for a pH slightly less than 7, concentration of Fe^{II} due to the solubility of $FeCO_3$ would be somewhere around 177 mg L^{-1} ($10^{-2.5}$ mol L^{-1}). Under the same conditions, the concentration of Ca^{2+} due to the solubility of $CaCO_3$ would be greater than 400 mg L^{-1} while the concentration of a metal such as Cd^{2+} due to the solubility of $CdCO_3$ would be somewhere around 3.5 mg L^{-1}. This is also supported by the data of the insert in Figure 5.14 which shows that for a 100-fold increase in the K_{so} or K_{sp} of a metal carbonate an approximately ten-fold increase in the concentration of the metal associated with the particular carbonate is expected. Note that under actual conditions total concentration of dissolved Fe(II) would be significantly higher than that predicted under near zero ionic strength.

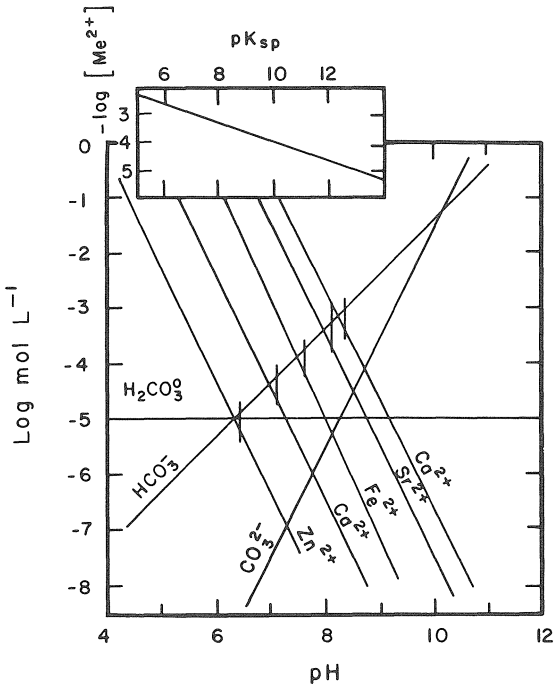

Figure 5.14. Solubility diagrams of metal carbonates as a function of pH and $10^{-3.5}$ pCO_2 (the intercepts of the short vertical lines for each metal line represent the point points at which $2Me^{2+} = HCO_3^-$. (From Stumm and Morgan, 1981. With permission.)

This can be demonstrated as follows:

Considering that

$$CO_2 + H_2O = H_2CO_3 \quad (5.9)$$

$$H_2CO_3 = H^+ + HCO_3^- \quad (5.10)$$

$$HCO_3 = H^+ + CO_3^{2-} \quad (5.11)$$

$$H_2CO_3 = C \cdot pCO_2 \quad (5.12)$$

where

C = Henry's constant = 0.0344

Also,

$$K_1 = (H^+)(CO_3^{2-}) / C \cdot pCO_2 = 4.28 \times 10^{-7} \quad (5.13)$$

$$K_2 = (H^+)(CO_3^{2-}) / (HCO_3^-) = 4.68 \times 10^{-11} \quad (5.14)$$

Assuming that the system is anoxic with high pCO_2, iron in solution will be controlled by the K_{sp} of iron carbonate (Stumm and Morgan, 1970)

$$K_{sp(siderite)} = (Fe^{II})(CO_3^{2-}) = 3.98 \times 10^{-11} \quad (5.15)$$

Combining Equations 5.13, 5.14, and 5.15 and rearranging yields:

$$\log(Fe) = -2pH - \log pCO_2 + 7.76 \quad (5.16)$$

Based on Equation 5.16, for an anoxic system with pH 6 and a pCO_2 of 10^{-1} maximum Fe^{II} activity in solution would be:

$$(Fe^{II}) = 10^{-2(6)+1+7.76} \quad (5.17)$$

or

$$(Fe^{II}) = 10^{-3.24} \text{ mol } L^{-1} \quad (5.18)$$

If one considers formation of $FeSO_4^o$ pairs by assuming a SO_4^{2-} activity of 10^{-2} mol L^{-1} (a SO_4^{2-} activity commonly encountered in pyritic 'waste'), then:

$$FeSO_4^o = (Fe^{II})(SO_4^{2-}) / 5.0 \times 10^{-3} \quad (5.19)$$

where 5.0×10^{-3} is the dissociation constant of the pair; substituting values into Equation 5.19:

$$FeSO_4^o = (10^{-3.24})(10^{-2}) / 5.0 \times 10^{-2.3} = 10^{-2.94} \text{ mol } L^{-1} \quad (5.20)$$

The above example reveals that under the $CaCO_3$-SO_4 equilibria conditions given, iron sulfate pairs ($FeSO_4^o$) alone would contribute a minimum of $10^{-2.94}$ mol L^{-1} Fe(II) (approximately 60 mg L^{-1}) in solution. It is clear from the above that mineral solubility equilibria as affected by CO_2 play a major role in controlling metal concentrations in limestone treated pyritic 'waste'.

5.2.5 Anoxic limitations

When AMD comes in contact with limestone in an anoxic environment is assumed that limestone dissolution and subsequent production of alkalinity can proceed without inhibitory armoring. The idea of generating alkalinity in anoxic limestone drains (ALD) is given close attention for its effectiveness in treating AMD (Turner and McCoy, 1990; Nairn et al., 1991 and 1992; Watzlaf and Hedin, 1993; Brodie et al., 1991). An anoxic limestone drain can be constructed as follows: An excavation is made to intercept the AMD in surface mine 'waste' and the excavation is filled with limestone and then covered by plastic and clay to inhibit oxygen penetration

and loss of carbon dioxide gas. Under these conditions, limestone will then be dissolved at a higher level due to higher pCO_2 (Figure 5.12b). Furthermore, iron armoring of limestone will be eliminated due to inhibition of iron oxidation. The water discharged from ALD would contain a significant concentration of HCO_3^- (Figure 5.12b) and relatively high concentrations of iron and manganese, if present. This water would then be aerated and metal oxidation, hydrolysis, and precipitation would occur in a strongly-buffered alkaline solution of a settling pond or constructed wetland. The scheme of the entire passive ALD treatment system is shown in Figure 5.15.

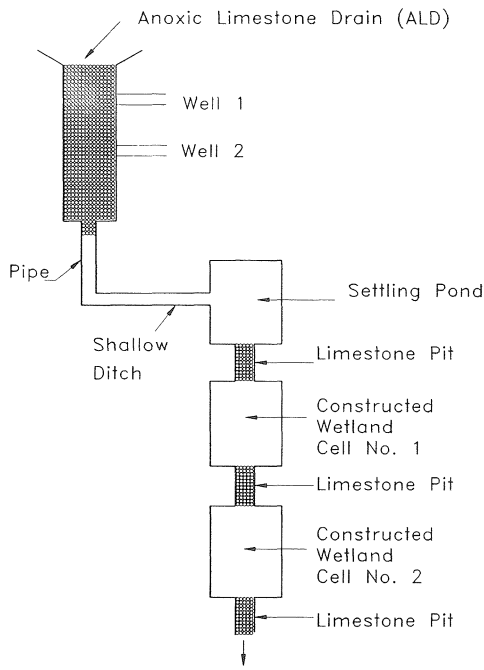

Figure 5.15. Schematic of the entire passive anoxic limestone drain (ALD) treatment system.

Nairn et al. (1992) tested an anoxic limestone drain in a surface mine site and found out that a) the water discharged exhibited circumneutral pH (pH 6 to 8), and b) considerable metal removal occurred in the pond and constructed wetland following the drain. The above, however, is an oversimplification of ALD.

Three hypothetical cases will be examined to demonstrate some of the complexity of employing ALD systems. *1) Low pH solution with extremely low iron concentration (e.g., less than 10 mg L^{-1}), 2) low pH solution with iron concentration in the range of 10 mg L^{-1} to 50 mg L^{-1},* and *3) low pH solution with extremely high iron concentration.* For all three systems it will be assumed that residence of water in the drain will be too short to allow significant SO_4 reduction, and all incoming iron will be in the Fe(II) state. In case *one*, the small Fe(II) quantity is expected to be chemisorbed on the surfaces of $CaCO_3$ without significantly impacting the quality/reactivity of the limestone (McBride, 1979; Evangelou et al. 1992). Under such conditions one may predict alkalinity behavior employing the following process:

$$CO_3^{2-} = Ca^{2+} + Fe^{II} \tag{5.21}$$

since,

$$Ca^{2+} = K_{sp(CaCO3)}/CO_3^{2-} \tag{5.22}$$

$$Fe^{II} = K_{sp(FeCO3)}/CO_3^{2-} \tag{5.23}$$

by substituting Equations 5.22 and 5.23 into Equation 5.21 and introducing K_{sp} values

$$CO_3^{2-} = [(10^{-8.3})/CO_3^{2-}] + [(10^{-10.3})/CO_3^{2-}] \tag{5.24}$$

upon rearranging,

$$(CO_3^{2-})^2 = (10^{-8.3}) + (10^{-10.3}) \tag{5.25}$$

and since $10^{-8.3}$ is 100 times greater than $10^{-10.3}$, Equation 5.25 reduces to

$$(CO_3^{2-})^2 = 10^{-8.3} = K_{sp(CaCO3)} \tag{5.26}$$

Equation (5.26) demonstrates that for a system under simultaneous $CaCO_3$ and $FeCO_3$ equilibria alkalinity concentration would be controlled by $CaCO_3$. Iron carbonate ($FeCO_3$) on the other hand, would have minimum impact on alkalinity release. For this reason also, alkalinity release potential could be predicted employing Figure 5.12a or 5.12b. Upon reacting H^+ with $CaCO_3$ (in the absence of Fe^{II}) significant quantities of CO_2 gas are produced (Reaction 5.1). Assuming that this quantity of CO_2 gas reaches approximately 20% ($pCO_2=10^{-0.70}$), based on equilibria considerations the concentration of HCO_3^- in the percolating water could reach approximately 600 mg L^{-1} (an approximately 10-fold increase from pure atmospheric conditions) (Figure 5.13a,b). The pH of such a system would be somewhere between 6 and 7 (see also Figure 5.13a). However, when the percolating solution exits the drain and equilibrates with the atmosphere pH is expected to reach near 8 (ideally 8.4) and approximately 90% of the dissolved HCO_3^-

would reprecipitate as $CaCO_3$. Thus, potentially dissolved alkalinity at the discharge point would decrease but total potentially available alkalinity in the form of $CaCO_3$ solid would increase. Note that the above apply to equilibrium conditions; in the case where kinetics become a limiting factor, alkalinity release would significantly decrease. Based on laboratory observations, soft limestone ($CaCO_3$) would be most suitable for ALD.

In case *two*, where Fe(II) concentration becomes significantly larger than that of case *one*, upon reacting the $FeSO_4$ solution with limestone, $FeCO_3$ is expected to form because the K_{sp} of $FeCO_3$ is two orders of magnitude smaller than the K_{sp} of $CaCO_3$ ($10^{-10.3}$ vs. $10^{-8.3}$). Thus, $CaCO_3$ in the presence of Fe(II) would undergo incongruent-like dissolution by precipitating as $FeCO_3$ which would control alkalinity release. This can be demonstrated as follows:

$$CaCO_3 = Ca^{2+} + CO_3^{2-} \tag{5.27}$$

and

$$K_{sp} = [(Ca^{2+})(CO_3^{2-})]/(CaCO_3) \tag{5.28}$$

where parenthesis denotes activity. In the case where $CaCO_3$ is pure, its activity is set to 1 by convention

and

$$K_{sp} = (Ca^{2+})(CO_3^{2-}) \tag{5.28}$$

However, activity of the $CaCO_3$ solid is described by the quantity of limestone-surface Ca^{2+} that has been replaced by Fe^{II}. Complete surface coverage of $CaCO_3$ by Fe^{II} will reduce the solid $CaCO_3$ activity to zero,

$$K_{sp} = (Ca^{2+})(CO_3^{2-}) = 0 \tag{5.29}$$

Under these conditions, alkalinity release would be controlled by the solubility of $FeCO_3$ which is smaller than that of $CaCO_3$ by a factor of 10.

Case *three* is identical to case *two* with one important difference. Concentration of $FeSO_4$ in solution is high enough so that a fraction of the total dissolved Fe(II) would precipitate as $FeCO_3$ on the surface of $CaCO_3$ and may act as coating and thus, Equation 5.29 would apply. Under this condition, the concentration of alkalinity in solution might be controlled by $FeCO_3$ (Figure 5.14), and the excess Fe(II) in solution would introduce an apparent common ion effect (see Chapter 1, the common ion effect is discussed with respect to the solubility of gypsum), further suppressing alkalinity release. Based on the K_{sp} of $FeCO_3$ ($10^{-10.3}$), under the above conditions alkalinity release would decrease by 10-fold relative to that released by $CaCO_3$ ($K_{sp} = 10^{-8.3}$) under the same conditions (Figure 5.14 insert). This could suppress pH by approximately 1.5 units relative to that of

$CaCO_3$ in the pH or pCO_2 range at which the condition $2(Me^{II}) = HCO_3^-$ is met (see Figure 5.14). Therefore, in case *three* alkalinity release may diminish, and may render anoxic limestone drains ineffective. However, under such conditions, any abrasive action by the solution moving through the drain could expose $CaCO_3$ surfaces restoring reactivity.

Figure 5.16 demonstrates schematically the processes involved in cases *one, two and three.*

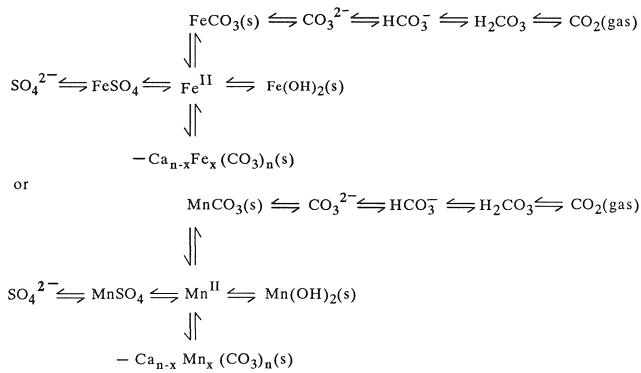

Figure 5.16. Schematic of reactions of anoxic limestone drains with solutions rich in $FeSO_4$ or $MnSO_4$. s = Solid.

Based on Figure 5.16, when equilibrium is displaced upward, alkalinity release would be controlled by $FeCO_3$ or $MnCO_3$ (case *three*). Under these conditions, alkalinity in the water would diminish due to the fact that it is being controlled by $FeCO_3$ or $MnCO_3$, unless physical abrasion keeps the $CaCO_3$ surfaces free of Fe^{II} or Mn^{II}. Note, $FeCO_3$ and $MnCO_3$ are approximately 10-fold less soluble than $CaCO_3$. On the other hand, when the equilibrium is displaced downward alkalinity release would be controlled by degree of $CaCO_3$ surface coverage by either Fe^{II} or Mn^{II}. Partial surface coverage of $CaCO_3$ by either Fe^{II} or Mn^{II} would diminish alkalinity release proportionally. Note, formation of pure $Fe(OH)_2$ or $Mn(OH)_2$ would be highly unlikely in anoxic drains because pH would be suppressed (< 8) by high pCO_2 (> 10^{-3}) (Figure 5.13).

Additional factors that may make anoxic limestone drains ineffective include long residence of sulfate rich water in the anoxic drain which may lead to Fe-sulfide deposition. Influx of aerobic conditions in such system could lead to acid production. Finally, strong rainstorms may flash out of the drain $FeCO_3$ precipitated gels and may overwhelm the aerobic part of the treatment.

The above discussion relative to the three cases presented are also applicable to Mn(II) since $MnCO_3$ exhibits a K_{sp} ($10^{-10.1}$) slightly greater than that of $FeCO_3$. Also, the solubility of $Mn(OH)_2$ is greater than that of

$Fe(OH)_2$ which further limits the former's precipitation potential under the conditions discussed above.

5.3 Hydrologic Influences

Solute movement in spoils (assuming micropore flow) tends to form a pulse and this pulse tends to increase in magnitude with depth (Evangelou et al., 1982a, b; Evangelou, 1983; Evangelou and Phillips, 1984). The data in Figure 5.17 show that any given mine 'waste' material gives different leachate chemistries when subjected to different types of flow, macropore flow vs. micropore flow.

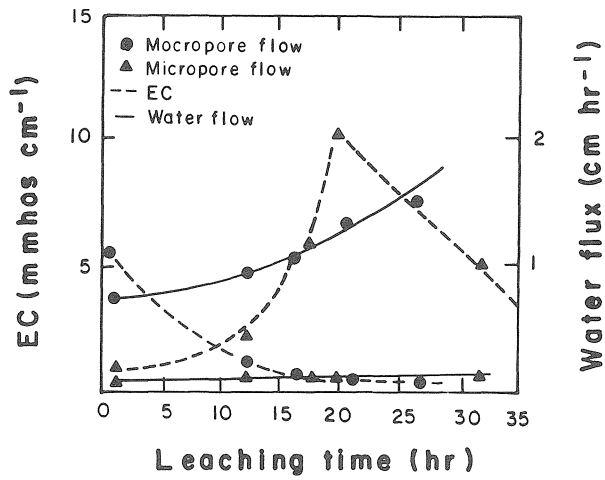

Figure 5.17. Effect of macropore and micropore flow on water quality in laboratory simulated mine 'waste' columns. (From Evangelou et al., 1982a. With permission.)

Note, EC under micropore flow was much greater than that under macropore flow. These data strongly suggest that macropore flow would produce improved quality leachate. In simulated laboratory weathering studies (Caruccio and Geidel, 1980), the introduction of acid sulfate water to pyrite had an enhancement effect on the rate of pyrite oxidation. Based on such results, the suggestion has been made that in order to improve water quality in mine 'waste' one should artificially introduce macropore flow and direct water runoff to the pyritic mine waste. Field data are needed to verify such a hypothesis.

5.4 Bactericides

Anionic surfactants (common cleaning detergents), organic acids and food preservatives have been used as pyrite oxidation inhibitors by controlling bacterial growth (Erickson and Ladwig 1985, Kleinmann, 1981; Dugan, 1987). In the presence of such compounds bacteria allow hydrogen ions in the acidic environment to move freely into or through cell membranes causing their deterioration.

U.S. Bureau of Mines researchers (Kleinmann, 1989) showed that anionic surfactants decrease the activity of bacteria and thereby retard pyrite oxidation (Figure 5.18; Table 5.5).

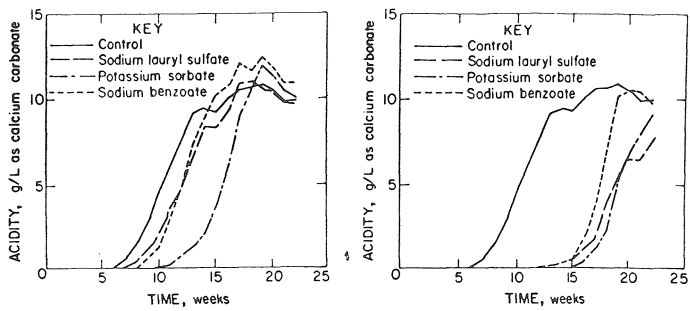

Figure 5.18. Acidity levels in leachate from coal refuse treated with 500 mg L^{-1} (Left figure) or 5000 mg L^{-1} (Right figure) of chemical inhibitor. (From Erickson et al., 1985. With permission.)

Table 5.5
Effect of anionic detergents on acid production by pyritic coal spoils. After Kleinmann (1980)

Anionic Detergent	Rate of application (mg L^{-1})	Acidity to pH 8.3 in units of $CaCO_3$ (mg L^{-1})	Iron (mg L^{-1})
Sodium Lauryl Sulfate	0	6,000	3,000
"	15	3,500	1,600
"	25	1,100	800
Alkyl Benzene Sulfate	0	5,100	2,600
"	15	2,500	900
"	25	2,000	800
α-Olefin Sulfate	0	4,900	2,000
"	15	3,100	1,000
"	25	2,500	900

They also reported that anionic surfactants were most applicable to coal refuse piles and isolated zones of fresh pyrite material reducing acid production by 60% to 95%. The surfactants sprayed or applied on the surface mine are now commercially available. However, wide use of anionic surfactants is limited for two specific reasons: 1) Anionic surfactants are very soluble and move with water, thus repeated treatments are required to prevent bacteria repopulation, and 2) anionic surfactants may also be adsorbed on the surfaces of minerals and may not reach the pyrite-bacteria interface (Erickson and Ladwig, 1985; Shellhorn and Rastogi, 1985).

5.5 Inundation

Inundation of pyritic materials is a conventional method generally used in curtailing AMD. Oxygen diffusion to pyritic 'waste' is greatly reduced upon inundation because the diffusion coefficient of O_2 through the covering water table is only 1/10000 of that through the waste atmosphere. Thus, the rate of O_2 consuming reactions becomes low and rate limiting, and bacterial oxidation of pyrite becomes slow or nil. Kleinmann and Crerar (1979) confirmed that there was no significant growth of *T. ferrooxidans* in water saturated environments. However, complete inhibition of pyrite oxidation by flooding may never be possible because of the availability of Fe^{3+} as an alternate oxidant. A field study by Foreman (1972), a laboratory column leaching study by Watzlaf (1992), and an O_2 free incubation by Pionke et al. (1980) have shown that when pyritic waste was flooded there was usually a significant, albeit incomplete reduction of acidity.

Underwater disposal of pyritic materials has been used by the metal mining industries with some success (Ritcey, 1991). Bell (1987) summarized the opinion of many people concerned with metal mine disposal as follows: "At the current time, the only practical and proven long-term approach to controlling the formation of acid in sulfide tailings is to limit the availability of oxygen as a reactant by maintaining the waste in a saturated or submerged condition." However, concerns with underwater disposal include the potential presence of dissolved O_2 and Fe^{3+}, two pyrite oxidants, as well as being able to maintain complete and continuous water saturation. Biotic oxidation of pyrite is not limited until pore gas oxygen is reduced to less than 1% (Carpenter, 1977; Hammack and Watzlaf, 1990). One may argue that based on current reclamation practices this low level of O_2 will be hard to attain. Water table fluctuations in the pyritic stratum usually cause incomplete inundation and move the active oxidation zone to a higher elevation in the mine, promoting acid formation.

Because of the increasing recognition of the importance of wetland formation and retention, and the large amount of pyritic waste needed to be disposed of, burying pyritic materials beneath wetlands has been suggested. Wetland provides a cover of water that isolates pyritic waste from the atmosphere and prevents oxidation and acid formation. But, data are needed

to evaluate the role of O_2 released from the root of aquatic plants, growing in the wetland, in pyrite oxidation. Zhang et al. (1994) employing microelectrodes measured rhizosphere pH and redox potential (Eh) of a pyrite soil in a wetland with cattail (*Typha latifolia L.*). Based on the observations they made (1) rhizosphere pH was one unit lower than bulk soil pH; 2) oxidation potential and sulfate concentration of rhizosphere were higher than bulk soil, and 3) iron oxides/oxyhydroxides were observed on the root surfaces and on the soil immediately adjacent to root surfaces), they concluded that cattail roots can significantly oxidize pyrite present in the rhizosphere. They also suggested that time scale and root density may be an important consideration for predicting the amount of oxidized pyrite when buried beneath a cattail wetland.

5.6 Alkaline Recharge Trenches

A more recent approach in controlling AMD production is the use of alkaline recharge (e.g., NaOH, $CaCO_3$) (Ladwig et al., 1985; Caruccio and Geidel, 1985). Neutralizers such as sodium hydroxide because of their high solubility can be easily moved with percolating water deep in the strata to sites where acid drainage is produced. Thus, no physical mixing of the strata with the ameliorator is required. However, effectiveness may only last only as long as someone supplies neutralizers. This maybe costly and at times not practical.

5.7 Wetland Systems

Over the last decade, wetlands have been constructed to treat AMD. The wetland processes previously identified as having the potential for removing metals from AMD include: adsorption of metals by ferric oxyhydroxides; plant and algae uptake of metals; complexation of metals by organic materials; precipitation of metals into oxides, oxyhydroxides, and as sulfides. From the above processes, only precipitation as either oxides or sulfides have long-term metal removal potential. The rest of the listed processes are considered to be insignificant or to have finite capacity.

Wetland may be a poor environment for the formation of metal oxides and/or oxyhydroxides because of the typically low redox potential (Eh) associated with wetland and wetland sediments. Studies are now focused on optimizing the activity of sulfate-reducing bacteria that thrive in the anaerobic zone of wetland. These sulfate-reducing bacteria consume acidity and most of the hydrogen sulfide they produce reacts with heavy metals to yield insoluble precipitates. Results from column and reactor studies simulating reducing conditions indicated that trace metals such as Co, Cu, Cd, Ni, Pb, and Zn, can be removed as sulfides (Staub and Cohen, 1992; Eger, 1992; Hammack and Edenborn, 1991).

It must be emphasized that in order for significant SO_4 reduction to occur, the high-sulfate AMD must flow through the anaerobic portion of the

wetland. However, according to Wildeman (1991), the typical natural wetland and most constructed wetlands may not have sufficient permeability to fully take advantage of this process.

5.8 Organic Waste

Organic waste may inhibit pyrite oxidation via various mechanisms including 1) consumption of O_2 because of bacterial growth other than *T. ferrooxidans or T. thiooxidans*, 2) removal of Fe^{III} from solution through complexation, and 3) formation of pyrite-Fe^{II}-humate complexes.

Luther et al. (1992) demonstrated that Fe^{II} complexation by any ligants containing oxygen as the ligating atom promotes Fe^{II} oxidation due to the potential increase in frontier molecular orbital electron density. The latter increases Fe^{II} basicity and consequently, Fe^{II} acts as a stronger reductant. Organic waste, however, may also promote pyrite oxidation by solubilization of $Fe(OH)_3$ through formation of soluble Fe^{III}-carboxylate complexes. Such complexes, especially if positively charged, e.g., Fe^{III}-catechol, $Fe^{III}[C_6H_4O_2]^+$, could adsorb onto the pyrite surface and act as electron acceptors in an outer sphere mode (Luther et al., 1992). These electron transfer reactions could also be favored in cases when Fe^{II}-carboxylate complexes are more stable than Fe^{III}-carboxylate complexes (Luther et al., 1992). To avoid such potential pyrite oxidation problems, well decomposed organic waste (Loomis and Hood, 1984) (composted or heat treated so that simple carboxylic acids are destroyed) should be applied to pyritic waste prior to formation of $Fe(OH)_3$ precipitates so that a) pyrite-Fe^{II}-humate complexes would be the only complexes, b) Fe^{III}-humate complexes formed should be preferably neutral or negatively charged (note, pyrite surface is also negatively charged), and c) any Fe^{III}-humate complexes formed should be preferably water insoluble.

Note, Fe^{III}-organic complexes have a tendency to decompose with time through electron transfer from the organic component to Fe^{III} releasing CO_2 and soluble Fe^{II}. In order to avoid the latter, large quantities of composted organic waste should be added and at times composted organic waste replacement may be needed.

5.9 Macroencapsulation

Liner technologies (e.g., clays, plastic), another form of acid mine drainage control, can be cost prohibitive as well as ineffective over time due to deterioration (Caruccio and Geidel, 1983; Skousen et al., 1987).

5.10 Microencapsulation

Huang and Evangelou (1992, 1994) and Evangelou (1994), using small leaching columns, have developed two new novel microencapsulation (coating) methodologies for preventing pyrite oxidation and acid production in coal pyritic waste. The *first coating methodology* involves leaching coal

'waste' with a solution composed of low but critical concentrations of H_2O_2, KH_2PO_4, and a pH buffer. During the leaching process, H_2O_2 oxidizes pyrite and produces Fe^{3+} so that iron phosphate precipitates as a coating on pyrite surfaces. The purpose of pH buffer in the coating solution is to eliminate the inhibitory effect of the protons, produced during pyrite oxidation, on the precipitation of iron phosphate. The coating process is shown schematically in Figure 5.19.

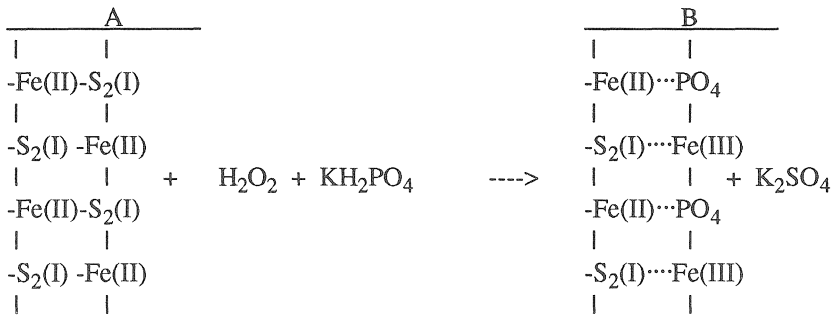

Figure 5.19. Schematic of H_2O_2 induced, oxidation proof phosphate surface coating.

When iron (Fe^{3+}) reacts with PO_4^{3-} it forms a relatively acid-resistant ferric phosphate ($FePO_4$) coating, which prevents any further oxidation of pyrite. The dotted lines in B signify physical bonding between pyrite and $FePO_4$. The physical appearance of this ferric phosphate coating is shown by comparing the scanning electron microscope photos (SEM) in Figure 20B and 20C. Figure 20B shows the physical appearance of framboidal pyrite without any surface coating, whereas Figure 20C shows the physical appearance of ferric phosphate coated pyrite.

A *second coating methodology* involves leaching pyritic 'waste' with a solution composed of low but critical concentrations of H_2O_2 and a pH buffer. During the leaching process, H_2O_2 oxidizes pyrite and produces an iron oxide coating on the surface of pyrite (Figure 20A). The purpose of a pH-buffer in this case is to buffer the solution during coating formation at a pH between 5 and 7 where iron oxide formation is promoted, a stable mineral at low pH.

Successful application of such coating methodologies in the field could mean long term solution to certain types of acid mine drainage problems. These coating methodologies are expected to be highly cost effective since they involve readily available materials and only cover the surface of pyrite particles. Furthermore, the coating solution could be applied to any coal mine waste material that possesses hydraulic properties, thus, little or no physical disturbance of coal mine waste during treatment would be necessary.

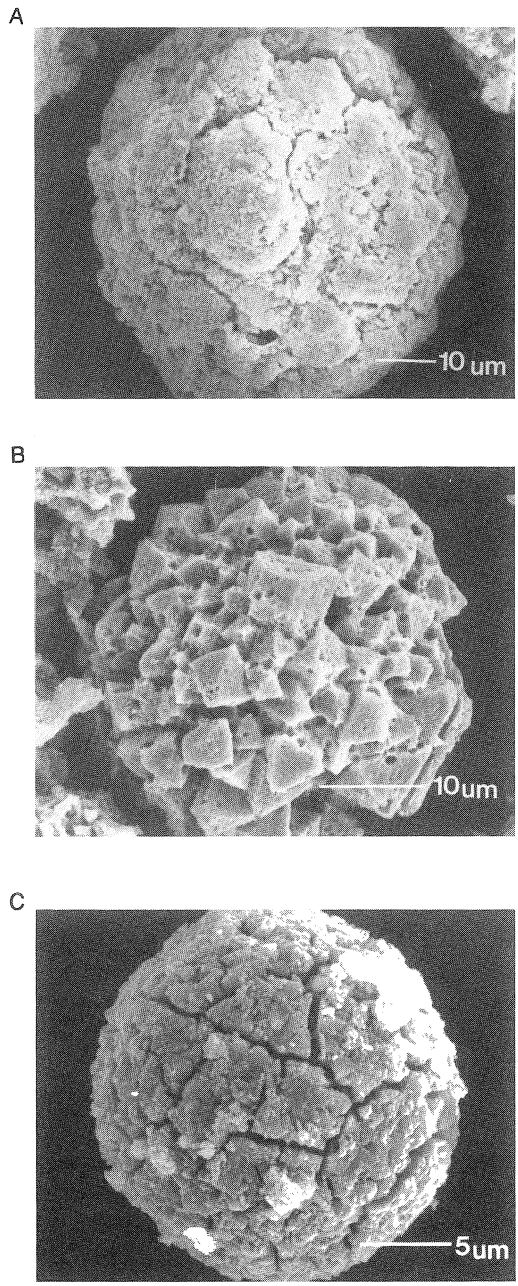

Figure 5.20. Scanning electron microscope photos of residual framboidal pyrite particles after oxidation under the following conditions: A, 0.147 mol L^{-1} H_2O_2; B, 0.147 mol L^{-1} H_2O_2 plus 0.013 mol L^{-1} EDTA; C, 0.147 mol L^{-1} H_2O_2 plus 10^{-3} mol L^{-1} KH_2PO_4.

The role of this coating on pyrite oxidation is shown in Figure 5.21.

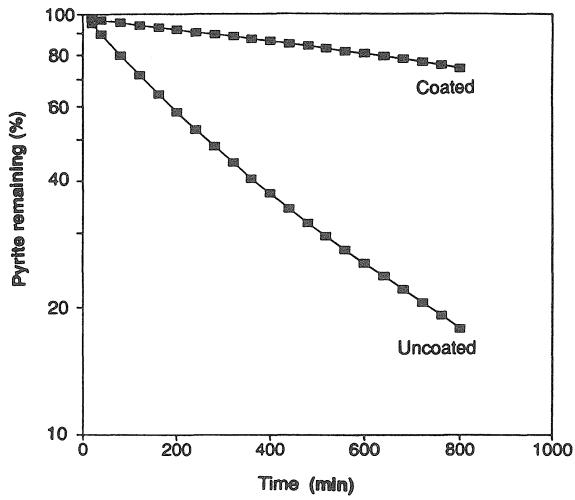

Figure 5.21. Relationship between log(100 x M/Mo) (M = pyrite remaining in the column at any time t; M_o = initial amount of pyrite in the column) and time (t) for uncoated and coated pyritic shale samples oxidized by leaching with 0.088 mol L^{-1} H_2O_2. (The coating was established by leaching the pyritic shale with a solution containing 10^{-4} mol L^{-1} KH_2PO_4, 0.053 mol L^{-1} H_2O_2 and 0.2 mol L^{-1} NaCl. During coating (leaching), 10% of the pyrite in the shale was oxidized.

Note the difference in the release of SO_4 from coated and uncoated pyrite in coal 'waste' material. These data strongly suggest that surface pyrite coating, if it could be applied at the field level successfully, could be effective in controlling oxidation of pyrite.

It is important to note that the technology of coating pyrite as described above, is not to be confused with the field application of rock phosphate (Flynn, 1969). Rock phosphate complexes dissolved iron (Fe(II)) and thus reduces the potential of Fe(III) production, reducing the potential for pyrite oxidation as well (Stumm and Morgan, 1970). Rock phosphate *does not* coat pyrite, rather, it complexes released Fe(II) from the oxidizing pyrite (Evangelou et al., 1992). This rock phosphate surface coating with Fe(II) renders rock phosphate inactive. Therefore, the effectiveness of rock phosphate in controlling pyrite oxidation is short lived. Currently, other environmentally friendly compounds are being tested in our laboratory and appear to be more promising than phosphate in coating pyrite.

Taylor & Francis
Taylor & Francis Group
http://taylorandfrancis.com

PART II

MOLECULAR CHEMISTRY OF PYRITE

OXIDATION KINETICS AND PYRITE REDOX CHEMISTRY

Taylor & Francis
Taylor & Francis Group
http://taylorandfrancis.com

Chapter 6
MECHANISMS AND KINETICS OF PYRITE OXIDATION

6.1 Structural Chemistry

As pointed out in Chapter 4, sulfur-bearing minerals, e.g., pyrite, are associated with coal and many other ores. In the case of coal mines, the pyritic form of iron sulfides is usually associated with geologic strata of sandstone or shale adjacent to, immediately above, or below the coal seam. Pyrite is not uniformly distributed throughout a geologic stratum as one might expect, but rather it may be found in clusters or scattered pockets of accumulation (Caruccio and Geidel, 1978, 1980).

Pyrites or pyritic crystals vary in size from 5 μm to greater than 400 μm (Caruccio and Geidel, 1978). Their shape may also vary from cubical to polyhedral (Ainsworth, 1979) with an octahedral molecular arrangement. Every iron atom in the divalent form, Fe^{2+}, is surrounded by six disulfides, each with a charge of −2. Conversely, each disulfide is surrounded by six iron atoms (Lowson, 1982; Luther, 1987) (see also Chapter 4). The molecular structure of pyrite is shown in Figure 6.1.

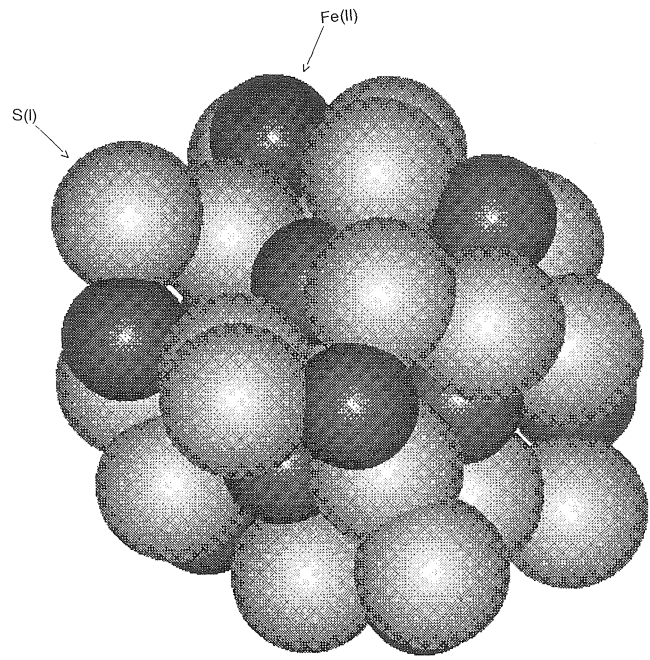

Figure 6.1. Pyrite structural composition simulated by *HyperChem, Autodesk, Inc.* The simulation was carried out by Louis McDonald, Ph.D. candidate at the University of Kentucky.

Pyrites come in various forms that vary in shape and size (see Chapter 4). The most reactive form of pyrite is the framboidal. It is a "grape like" agglomeration of approximately 0.25 μm diameter crystals (Caruccio and Geidel, 1978). The large surface area of framboidal pyrites exposed to environmental and potential microbial degradation are conducive to fast rates of reactivity. Thus, it is the belief of most geochemists that framboidal pyrite is the major contributor to the degradation of water quality.

In order to understand the mechanisms of pyrite oxidation, one needs information on the molecular structure and frontier molecular electron orbital configuration of pyrite. Detailed information on this is given by Luther (1990). Understanding the potential electron sharing/donating behavior of pyrite allows one to understand pyrite's oxidation behavior. Numerous studies have dealt with the pyrite's electron sharing/donating potential in controlling oxidation, as well as rates and mechanisms of oxidation (Singer and Stumm, 1970; McKibben and Barnes, 1986; McKibben, 1984; Moses et al., 1987; Silverman, 1967; Nordstrom, 1982a and references therein; Lowson, 1982 and references therein; Hiskey and Schlitt, 1982; Kleinmann, 1980; Luther, 1987; Luther et al., 1992; Goldhaber, 1983; Nicholson et al., 1988, 1990; Moses and Herman, 1991; Brown and Jurinak, 1989). The results of these studies clearly point out that pyrite oxidation is a surface controlled reaction but specific mechanisms involved may vary, depending on the nature of the oxidant, e.g., O_2, Fe^{3+}, H_2O_2.

6.2 Reaction Progress Variables (RPV)

Several reaction progress variables (RPV) can be chosen to evaluate pyrite oxidation reactions. Each selected RPV has its own inherent strengths and weakness, depending on information sought and oxidation conditions used. Oxidation reactions based on measurement of total iron in solution have been shown to be an accurate indicator of reaction progress in low pH studies (McKibben and Barnes, 1986), but its use in neutral to higher pH is precluded due to the low solubility of $Fe(OH)_3$ under these conditions. Nicholson et al. (1988, 1990) chose sulfate as the rate indicating variable and assumed under their experimental conditions there was complete oxidation of intermediates to sulfate (Moses et al., 1987). On the other hand, Hood (1991) used experimental conditions similar to Nicholson et al. (1990) and found that sulfur-containing species, other than sulfate, constituted a significant proportion of the total sulfur. Furthermore, the proportion of the sulfur present as sulfate was found to vary with certain experimental parameters such as pH, O_2 and Fe^{3+} (Moses et al., 1987).

Measurement of pyrite oxidation based on changes in oxidation potential of iron couple is operative in acidic conditions, especially $pH < 2$, in which ferric iron hydrolysis and oxidation of ferrous iron are negligible and the activity of the free ferric ion is high compared to the activity of ferric complexes (Wiersma and Rimstidt, 1984). Measurement of the change in

total weight or volume of pyrite is considered inappropriate RPV because of very low sensitivity at low percentage of reaction as well as difficulties encountered due to solid oxidation product formation and surface retention, such as iron oxide or ferrous sulfate (Evangelou and Huang, 1994; Nicholson et al., 1990).

Generally speaking, measurements of pyrite oxidation have a degree of uncertainty. The level of uncertainty decreases as the system variables are better understood.

6.3 Reaction Mechanisms

According to Singer and Stumm (1970), Fe^{3+} is the major pyrite oxidant in the acidic pH region, while O_2 is expected to be the direct pyrite oxidant at neutral to alkaline pH. The essential feature of the above reaction mechanisms (low or high pH) is initiation of pyrite oxidation by adsorption of O_2 onto partially protonated pyrite surface (Goldhaber, 1983). However, recent investigations on pyrite oxidation carried out by Moses et al. (1987), Moses and Herman (1991) and Brown and Jurinak (1989a) demonstrated that Fe^{3+} may be a very effective oxidant at circumneutral pH. The conclusion that Fe^{3+} could be the major direct pyrite oxidant at circumneutral pH was supported by theoretical considerations based on magnetic properties and/or on molecular orbital theory of the reactants involved (Moses et al., 1987; Luther, 1987 and 1990; and Luther et al., 1992). Moses et al. (1987) pointed out that there was low probability for a direct reaction between paramagnetic bimolecular O_2 and diamagnetic pyrite. But the transfer of a hydroxyl radical from $Fe(H_2O)_5(OH)^{2+}$ complex to S_2^{2-} overcomes a similar restriction on the reaction between Fe^{3+} and pyrite. The experimental results by Moses et al. (1987) indicated that pyrite oxidation over the pH range 2-9 was favored in the presence of Fe^{3+} as opposed to dissolved O_2, and a low concentration of Fe^{3+} was very effective in oxidizing pyrite.

Luther (1987) explained that the faster rate of pyrite oxidation by Fe^{3+} was due to the fact that Fe^{3+} can bind chemically to the pyrite surface whereas O_2 cannot. Adsorption of O_2 to the surface of pyrite, attributed to a physical process, has been pointed out by Goldhaber (1983) and McKibben and Barnes (1986). The difference in binding between Fe^{3+} and O_2 with the pyrite surface can be explained on the basis of molecular orbital theory. It turns out that because Fe^{3+} has a vacant orbital, it binds to the pyrite surface *via* sulfur to form a persulfido bridge ($Fe\text{-}S\text{-}S\text{-}Fe(H_2O)_5(OH)^{2+}$, a transition state intermediate. Through this bridge an electron can be transferred from the highest occupied molecular orbital of S_2^{2-} to the lowest unoccupied molecular orbital of Fe^{3+}. Unlike Fe^{3+}, O_2 cannot form a transition state intermediate with the pyrite surface. This Fe^{3+} pyrite oxidation mechanism, suggested by Luther (1987), is also consistent with the following well known experimental observations: 1) sulfoxy species ($S_2O_3^{2-}$) are intermediates produced during the process of pyrite oxidation by either Fe^{3+} or O_2; 2) O_2

does not oxidize $S_2O_3^{2-}$ as readily as Fe^{3+} so that when O_2 is the sole pyrite oxidant sulfoxy compounds are more prevalent; 3) water is the source of oxygen for the sulfoxy intermediates and/or sulfate (the latter have been demonstrated experimentally by Taylor et al. (1984 a, b) employing oxygen isotopes).

Considering that electron transfer reactions are limited to only one or two simultaneous electron transfer events, Luther (1987) proposed a molecular orbital (MO) inner sphere transfer pyrite oxidation mechanism assuming that this electron transfer would take place in a symmetrical fashion. This involves transfer of electrons from the highest occupied molecular orbital (HOMO) of the reductant (FeS_2) to the lowest unoccupied molecular orbital (LUMO) of the oxidant (e.g., Fe^{3+}). The process requires that all electron transfers would involve the reduced sulfur of pyrite and the pyrite-surface adsorbed oxidant, thus, no electron transfer would take place between pyrite structural Fe^{2+} and oxidant. The MO mobel proposed by Luther (1987) is consistent with the pyrite oxidation data of Moses et al. (1987), Goldaher (1983), McKibben and Barnes (1986), Wiersma and Rimstid (1984), and the model proposed by Moses et al. (1987) and more recently by Moses and Herman (1991).

The molecular structure of pyrite can be represented as (Luther, 1990):

$$\text{Fe(II)} - \underline{\underline{S_A}} - \underline{\underline{S_B}} \; | \qquad (6.1)$$

Based on the Frontier-Molecular-Orbital theory as described by Luther (1990), the surface exposed S_B in the pyrite structure possesses an unshared pair of electrons. This S_B unshared pair of electrons produces a slightly negatively charged pyrite surface which can attract molecules or cations willing to share the pair of electrons. Clearly, preference would be given to those ions or molecules acting as Lewis acids (willing to accept the unshared pair of electrons of S_B). Compounds or ions that could accept this pair of electrons fall into three broad categories 1) Metallic transitional cations, e.g., Fe^{2+}, Fe^{3+}, Cr^{2+}, etc., 2) bimolecular halogens, e.g., F_2, Cl_2, I_2 and Br_2, and 3) singlet or light activated oxygen ($^1O_2$) and H_2O_2 (Luther, 1990).

The experimental literature clearly points out that the major pyrite oxidant (electron acceptor) in biotic and/or abiotic natural systems is Fe^{3+} (Moses et al., 1987); Goldhaber, 1983); McKibben and Barnes, 1986); Wiersma and Rimstid, 1984; Singer and Stumm, 1970). Luther (1987) described the oxidation of pyrite by Fe^{3+} in three major *steps*. The *first step* involves the removal of a water ligand from $Fe(H_2O)_6^{3+}$ or its hydrolysis product $[Fe(H_2O)_5(OH)]^{2+}$.

$$Fe(H_2O)_6^{3+} \rightarrow Fe(H_2O)_5^{3+} + H_2O \qquad (6.2)$$

In the *second step*, the coordinately unsaturated $Fe(H_2O)_5^{3+}$ species can bind to the surface of pyrite through S_B forming a persulfido bridge. The latter is defined as two metals sharing a common ligand. In this case, the pyrite structural Fe^{2+} and the $Fe(H_2O)_5^{3+}$ share the disulfide ($-S_2^{2-}$).

$$\text{Fe(II)} - \underline{\underline{S_A}} - \underline{\underline{S_B}} - \text{Fe}(H_2O)_5^{3+} \qquad (6.3)$$

In the *third step*, a symmetrical electron transfer or electron transfer within similar molecular bonding orbitals takes place and the following pyrite surface radical is formed

$$\text{Fe(II)} - \underline{\underline{S_A}} - \underline{\underline{S_B}} - \text{Fe}(H_2O)_5^{3+} \rightarrow$$

$$\text{Fe(II)} - \underline{S_A} - \underline{\dot{S}_B} - \text{Fe}(H_2O)_5^{2+} \qquad (6.4)$$

The product of Reaction 6.4 reacts with $Fe(H_2O)_6^{3+}$ and H_2O and transfers a second electron to $Fe(H_2O)_6^{3+}$ and one oxygen atom from H_2O to the pyrite surface (Taylor, et al., 1984a,b). In the process, two H^+ and a S_2O are produced as follows:

$$\text{Fe(II)} - \underline{S_A} - \underline{\dot{S}_B} - \text{Fe}(H_2O)_5^{2+} + \text{Fe}(H_2O)_6^{3+} + H_2O \rightarrow$$

$$\text{Fe(II)} - \underline{\underline{S_A}} - \underline{\underline{S_B}} - \underline{\underline{O}} \; | \; + \; 2\text{Fe}(H_2O)_6^{2+} + 2H^+ \qquad (6.5)$$

Pyrite electron transfer continues until iron thiosulfate (FeS_2O_3) formation and detachment from the pyrite surface is completed. Reaction 6.6 reveals the transfer of two additional electrons, while Reaction 6.7 shows the transfer of the final two electrons leading to $S_2O_3^{2-}$ formation

$$\text{Fe(II)} - \underline{\underline{S_A}} - \underline{\underline{S_B}} - \underline{\underline{O}} \; | \; + \; 2\text{Fe}(H_2O)_6^{3+} + H_2O \rightarrow$$

$$\text{Fe(II)} - \underset{|}{\overset{|}{S_A}} - \underset{|}{\overset{|}{S_B}} - \underset{|}{\overset{|}{O}} + 2Fe(H_2O)_6^{2+} + 2H^+ \qquad (6.6)$$

and

$$\text{Fe(II)} - \underset{|}{\overset{|}{S_A}} - \underset{|}{\overset{|}{S_B}} - \underset{|}{\overset{|}{O}} + 2Fe(H_2O)_6^{3+} + H_2O \rightarrow$$

$$\text{Fe(II)} - \underset{|}{\overset{|}{S_A}} - \underset{|}{\overset{|}{S_B}} - \underset{|}{\overset{|}{O}} + 2Fe(H_2O)_6^{2+} + 2H^+ \qquad (6.7)$$

Finally, surface product detachment produces solution iron thiosulfate ($Fe^{II} + S_2O_3^{2-}$)

Based on the above reactions, two electron transfer mechanisms account for the pyrite-surface oxidation process, 1) formation of surface free radicle (Reaction 6.4), and 2) transfer of an oxygen atom from the water molecule to S_B (Reaction 6.5) (Taylor et al., 1984a,b). Each one of the mechanisms is responsible for the transfer of three electrons for a total of six. Moses et al. (1987) and Brown and Jurinak (1989a) postulated that three of the electrons are transferred through an OH^- bridging ligand between Fe^{3+} and the pyrite surface, while the remaining three electrons are transferred by the removal of H^+ from Fe-S_A-S_B-OH by formation of H_2O. The OH^- bridging ligand between Fe^{3+} and the pyrite surface mechanism appears to account for the large increase in pyrite oxidation observed at pH values above 7 (Goldhaber, 1983; Brown and Jurinak, 1989a) (Figure 6.2).

Summarizing Reactions 6.1 through 6.7 gives

$$FeS_2 + 6Fe(H_2O)_6^{3+} + 3H_2O \rightarrow Fe^{2+} + S_2O_3^{2-} + 6Fe(H_2O)_6^{2+} + 6H^+ \qquad (6.8)$$

Therefore, the transfer of six electrons from S_B to six Fe^{3+} produces one $S_2O_3^{2-}$ and six H^+. In the presence of excess Fe^{3+}, $S_2O_3^{2-}$ is rapidly transformed to SO_4^{2-} according to Reaction 6.9.

$$5H_2O + S_2O_3^{2-} + 8Fe^{3+} \rightarrow 8Fe^{2+} + 10H^+ + 2SO_4^{2-} \qquad (6.9)$$

Summation of Reactions 6.8 and 6.9 produces Reaction 6.10 (see Chapter 4).

$$8H_2O + FeS_2 + 14Fe^{3+} \rightarrow 15Fe^{2+} + 16H^+ + 2SO_4^{2-} \quad (6.10)$$

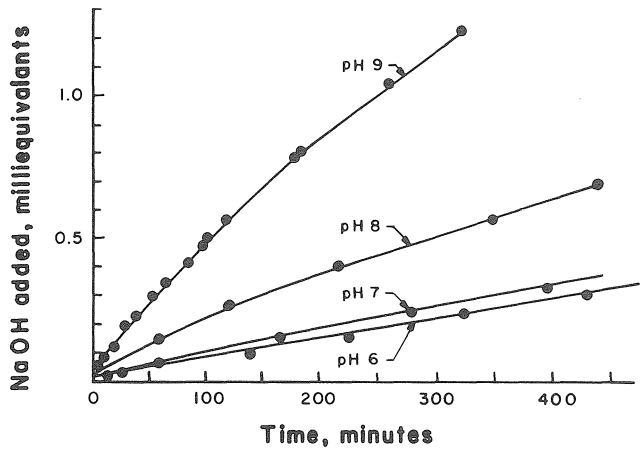

Figure 6.2. Kinetics of pyrite oxidation as influenced by pH. (From Goldhaber, 1983. With permission.)

Data in the literature substantiate that $S_2O_3^{2-}$ in the presence of a strong oxidizer, e.g., Fe^{3+} or H_2O_2, rapidly oxidizes to sulfate (SO_4) (Luther, 1990). In fact, Luther (1990) pointed out that the oxidation of $S_2O_3^{2-}$ and/or sulfite (SO_3^{2-}) by Fe^{3+} or H_2O_2 is rapid enough that such products would not be detected in solution. Moses et al. (1987) carried out pyrite oxidation experiments and specifically focussed on evaluating the production of SO_3^{2-}, $S_2O_3^{2-}$ and $S_nO_6^{2-}$. The results of their study revealed that none of the above sulfoxy anions were detected when the oxidant was Fe^{3+}. However, when the oxidant was dissolved oxygen, significant quantities of sulfoxy anions (SO_3^{2-}, $S_2O_3^{2-}$ and $S_nO_6^{2-}$) were produced at pH greater than 3.9. Similar observations were made by Taylor et al. (1984a,b). Their investigations involved laboratory and field studies and the authors reported that no sulfoxy anion species were detected.

The limiting step in the oxidation of pyrite is oxidation of Fe^{2+} by dissolved O_2.

$$Fe(H_2O)_6^{2+} + 1/4O_2 + H^+ \rightarrow Fe(H_2O)_6^{3+} + 1/2H_2O \quad (6.11)$$

According to Moses et al. (1987) and Moses and Herman (1991), Fe^{3+} is an effective and direct pyrite oxidant at low pH as well as at circumneutral pH and the role played by dissolved O_2 is to sustain the reaction by regenerating Fe^{3+}. It is well known that the rate of Fe^{2+} oxidation increases as pH

increases (Singer and Stumm, 1970; Millero and Izaguirre, 1989). The role of OH^- in oxidizing Fe^{2+} has been postulated by Luther et al. (1992) to be due to the potential increase in frontier molecular orbital electron density of Fe^{2+} upon binding to oxygen by coordinating OH^-. Such coordination increases Fe^{2+} basicity and stabilizes the Fe^{3+} formed. Luther et al. (1992) demonstrated that this increase in electron density also increases the potential of Fe^{2+} to oxidize rapidly to Fe^{3+} when the former (Fe^{2+}) is in the form of a complex with a ligand containing oxygen as the ligating atom. The above, according to Luther et al. (1992), also explain the observed increase in pyrite oxidation as pH increases or as soluble Fe^{3+}-organic complexes increase, especially if the latter is positively charged and less stable than the Fe^{2+}-organic complex.

6.3.1 Other mechamisms of pyrite oxidation

McKibben and Barnes (1986) proposed as a potential pyrite oxidation mechanism by dissolved oxygen, the adsorption of oxygen on the surface of pyrite and the reduction of O_2 by water to H_2O_2; it oxidizes pyrite by acting as electron sink. The reactions are as follows:

$$H_2O + 1/2O_2 \rightarrow H_2O_2 \qquad (6.12)$$

and

$$FeS_2 + H_2O_2 \rightarrow Fe\text{-}S\text{-}S\text{-}O: + H_2O \qquad (6.13)$$

Reaction 6.13 shows the transfer of two electrons from peroxide to pyrite leading to the production of water and the unstable intermediate FeS-S-O:. This unstable intermediate reacts with H_2O_2 as follows:

$$Fe\text{-}S\text{-}S\text{-}O: + 2.5H_2O_2 \rightarrow Fe^{3+} + S_2O_3^{2-} + OH^- + 2H_2O \qquad (6.14)$$

Reaction 6.14 reveals that the unstable intermediate Fe-S-S-O: reacts with peroxide to form Fe^{3+} and thiosulfate ($S_2O_3^{2-}$). Similar reactions employing as oxidizer bimolecular oxygen (O_2) can be written as follows:

$$FeS_2 + 0.5O_2 + H_2O \rightarrow Fe\text{-}S\text{-}S\text{-}O: + H_2O \qquad (6.15)$$

$$Fe\text{-}S\text{-}S\text{-}O: + 1.25O_2 + 2.5H_2O \rightarrow Fe^{3+} + S_2O_3^{2-} + OH^- + 2H_2O \qquad (6.16)$$

and

$$Fe^{3+} + 3H_2O \rightarrow Fe(OH)_3 + 3H^+ \qquad (6.17)$$

Reactions 6.13 and 6.14 and Reactions 6.15 and 6.16 appear similar. Both produce one Fe^{3+} which upon hydrolysis produces three H^+ for a net of two (note, one H^+ is consumed by the OH^- in Reaction 6.14 or 6.16). Two

additional H^+ and two sulfates (SO_4^{2-}) are produced by the oxidation of $S_2O_3^{2-}$ as shown below:

$$S_2O_3^{2-} + 4H_2O_2 \rightarrow 2SO_4^{2-} + 2H^+ + 3H_2O \quad (6.18)$$

or

$$S_2O_3^{2-} + 2H_2O_2 \rightarrow 2HSO_3^- + H_2O \quad (6.19)$$

and

$$2HSO_3^- + 2H_2O_2 \rightarrow 2SO_4^{2-} + 2H_2O + 2H^+ \quad (6.20)$$

In the presence of O_2 the above reactions are as follows:

$$S_2O_3^{2-} + H_2O + 2O_2 \rightarrow 2SO_4^{2-} + 2H^+ \quad (6.21)$$

or

$$S_2O_3^{2-} + H_2O + O_2 \rightarrow 2HSO_3^- \quad (6.22)$$

and

$$2HSO_3^- + O_2 \rightarrow 2SO_4^{2-} + 2H^+ \quad (6.23)$$

There are however, some major differences between pyrite oxidation by H_2O_2 and pyrite oxidation by O_2. Kinetics of pyrite oxidation by O_2 is extremely slow. Because O_2 is not able to share the S_B unshared pair of electrons it does not react strongly with the pyrite surface. Single electron transfers from the disulfide to the O_2 may take place through an outer sphere complex leading to O_2^- formation. According to Luther (1990) and Moses et al. (1987), this process is slow. On the other hand, direct transfer of the S_B unshared electron pair to H_2O_2 or halides, X_2 (e.g., Cl_2, Br_2, F_2) may take place in an inner sphere mode, breaking the covalent H_2O_2 or X_2 bond as shown in Reaction 6.24

$$\text{Fe(II)} - \underline{S_A} - \underline{S_B} \mid + X_2 \rightarrow$$

$$[\text{Fe(II)} - \underline{S_A} - \underline{S_B}]^{2+} + 2X^- \quad (6.24)$$

and forming the metastable S_2O by reacting with H_2O.

$$[\text{Fe(II)} - \underline{S_A} - \underline{S_B}]^{2+} + H_2O \rightarrow$$

$$\text{Fe(II)} - \underline{S_A} - \underline{S_B} - \underline{O} \mid + 2H^+ \quad (6.25)$$

From Reaction 6.25, thiosulfate is produced by

$$\overline{\overline{\overline{Fe(II) - S_A - S_B - O}}} + 2.5X_2 + 2H_2O \rightarrow Fe^{3+} + S_2O_3^{2-} + 5X^- + 4H^+ \quad (6.26)$$

The chemistry of $S_2O_3^{2-}$ is rather complex and its fate is dependent on pH, type of oxidant and presence or absence of pyrite as well as presence or absence of $Fe(OH)_3$ (Moses et al., 1987 and references therein; Goldhaber, 1983 and references therein; Luther, 1987). The general relationship of the various aqueous sulfur species as a function of pH, produced during short term pyrite oxidation experiments are shown in Figure 6.3.

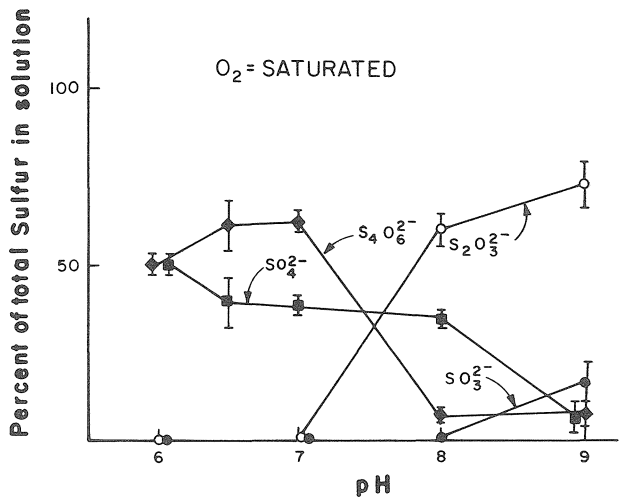

Figure 6.3. Relative amounts of aqueous sulfur species produced during short term pyrite oxidation experiments as a function of pH. (From Goldhaber, 1983. With permission.)

These data clearly demonstrate that at high pH, $S_2O_3^{2-}$ accumulates; decomposes to SO_4^{2-} and/or tetrathionate ($S_4O_6^{2-}$) as pH decreases from pH 8 to pH 7.

$$2S_2O_3^{2-} + 2H^+ \; 1/2O_2 \rightarrow S_4O_6^{2-} + H_2O \quad (6.27)$$

Production of polythionates ($S_nO_6^{2-}$) can also take place through a binuclear nucleophilic (S_n) displacement mechanism as follows (Moses et al., 1987 and references therein):

$$S_nO_6^{2-} + S_2O_3^{2-} \leftrightarrow S_{n+1}O_6^{2-} + SO_3^{2-} \quad (6.28)$$

Brown and Jurinak (1989) postulated that the increase in pH they observed, starting at pH 6, during $S_2O_3^{2-}$ oxidation in the presence of pyrite was due to the limited solubility of $Fe(OH)_3$ at that pH.

$$2S_2O_3^{2-} + 2Fe(OH)_3 \rightarrow S_4O_6^{2-} + 2Fe(OH)_2 + 2OH^- \qquad (6.29)$$

Under mild oxidizing conditions but strongly acid, $S_2O_3^{2-}$ may disproportionate to elemental sulfur (S_8) and sulfite (Goldhaber, 1983 and references therein).

$$S_2O_3^{2-} + H^+ \rightarrow HSO_3^- + S^o \qquad (6.30)$$

However, as pointed out previously, $S_2O_3^{2-}$ in the presence of a strong oxidizer, e.g., Fe^{3+} or H_2O_2, rapidly oxidizes to sulfate (SO_4^{2-}) via HSO_3^- (see Reactions 6.18-6.20) (Luther, 1990 and references therein). In fact, Luther (1990) pointed out that oxidation of $S_2O_3^{2-}$ and/or bisulfite (HSO_3^{2-}) by Fe^{3+} or H_2O_2 is rapid enough that such products would not be detected in solution. Moses et al. (1987) reported that none of the above sulfoxy anions (SO_3^{2-}, $S_2O_3^{2-}$ and $S_nO_6^{2-}$) were detected when the oxidant was Fe^{3+}. When the oxidant was dissolved oxygen, significant quantities of sulfoxy anions were produced at pH greater than 3.9.

The above discussion strongly suggests that when evaluating or quantifying pyrite oxidation experiments, all sulfur species should be quantified, especially when pH is near or above neutral, e.g., limestone treated mine "waste".

6.3.2 Electrochemical mechanisms of pyrite oxidation

According to Lowson (1982), the overall electrochemical oxidation process of pyrite is the sum of the cathodic and anodic reactions occurring at the surface. The anodic process is a complex collection of oxidation reactions in which the pyrite reacts mainly with water to produce Fe^{3+}, sulfates, and protons as shown by Reaction 6.31

$$FeS_2(s) + 8H_2O \rightarrow Fe^{3+} + 2SO_4^{2-} + 16H^+ + 15e^- \qquad (6.31)$$

or to produce Fe^{2+} and S^o when the acid strength increases (Bailey and Peters, 1976) as shown by Reaction 6.32

$$FeS_2(s) \rightarrow Fe^{2+} + 2S^o + 2e^- \qquad (6.32)$$

The electrons released are then transferred to a cathodic site (at the mineral surface) where the principal reaction is an oxygen reduction process as shown by Reaction 6.33

$$1/2O_2(aq) + 2H^+ + 2e^- \rightarrow H_2O. \quad (6.33)$$

It should be noted that, dissolved O_2 is used only as an electron acceptor in a separate cathodic reaction as shown by Reaction 6.33; the oxygen in the SO_4^{2-} is derived from water in an anodic reaction as shown by Reaction 6.31.

6.4. Pyrite Surface Functional Groups

Pyrite/surface exposed S_B (Reaction 6.1) provides a slightly negative charged pyrite surface due to an unshared pair of electrons which attract ions willing to share them, e.g., Fe^{2+}. However, the relatively low negative pyrite/surface charge can not fully compensate for the positive charge of Fe^{2+}; for this reason, Evangelou and Huang (1994) postulated that pyrite/surface adsorbed Fe^{2+} reacts with CO_3^{2-} to form a pyrite/surface Fe(II)-CO_3 complex of certain configuration, e.g., bidentate, unidentate, electrostatic as shown below, respectively.

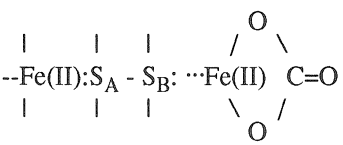

(6.34)

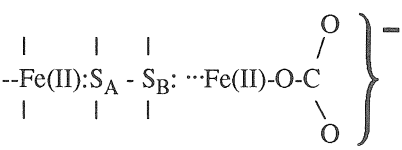

(6.35)

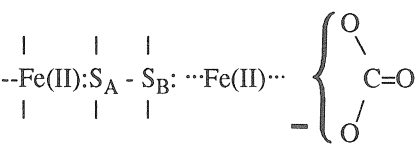

(6.36)

Evangelou and Huang (1994) carried out a detailed FT-IR pyrite/surface chemistry characterization study employing diffuse reflectance, a highly sensitive spectroscopic surface technique (Baes and Bloom, 1989; Evangelou and Wang, 1993). The FT-IR spectra in Figure 6.4 show that both coal and mineral pyrites exhibit a strong infrared absorption band around 440 cm^{-1}. This vibrational band is assignable to the disulfide (S-S) in the pyrite lattice (Hood, 1991; Bellamy, 1975), but does not seem to occur at the same exact wavenumber on all samples; it may suggest structural differences between pyrites. Pyrite samples 1 and 2 represent well crystallized massive

pyrites while the coal pyrite sample represents framboidal and most likely poorly crystallized pyrite (Evangelou and Huang, 1994).

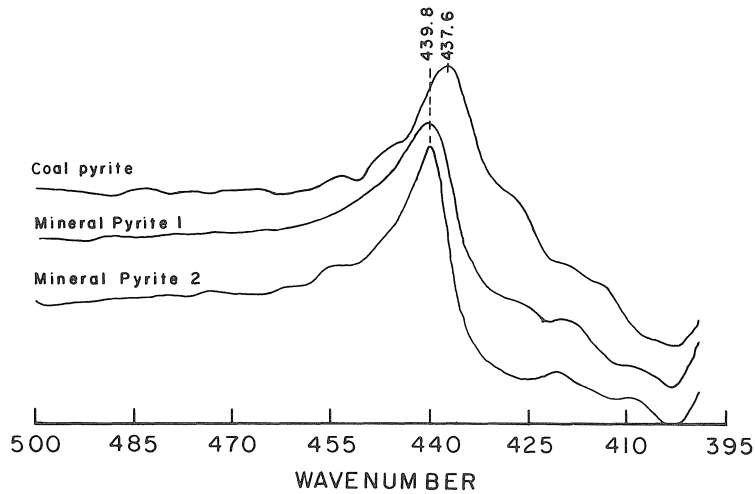

Figure 6.4. Diffuse reflectance FT-IR spectra for disulfide in the lattice of pyrites after washing with strong hydrofluoric solution. (From Evangelou and Huang, 1994. With permission.)

Pyrite is known to be extremely sensitive to exposure to atmospheric air. This may explain the spectra behavior of pyrite below the 1200 cm^{-1} range after hydrofluoric acid (HF) wash to remove any surface impurities, and evacuation at 97°C. For example, the spectrum of coal pyrite in Figure 6.5a exhibits strong absorption at 611 cm^{-1}.

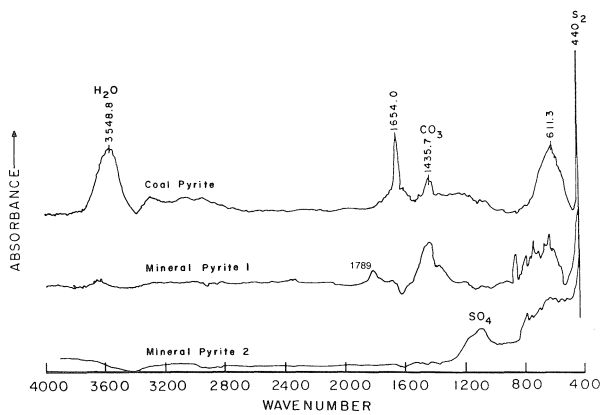

Figure 6.5a. Diffuse reflectance FT-IR spectra of coal pyrite and mineral pyrites after washing with strong hydrofluoric solution. (From Evangelou and Huang, 1994. With permission.)

This might result from SO_4^{2-} associated with Fe^{2+} (Miller and Wilkins, 1952). The broadness of the 611 cm^{-1} band and/or in the case of mineral pyrite 1 its apparent splitting into several bands may suggest differences in amounts and types of sulfoxy anions (e.g., SO_3^{2-}, $S_2O_3^{2-}$ and $S_nO_6^{2-}$) produced under mild oxidizing conditions (Moses et al., 1987). These chemical species absorb infrared in the 600 cm^{-1} range (Nakamoto, 1963, 1986; Miller and Wilkins, 1952). The broad absorption band from 1200 to 900 cm^{-1} on the spectrum of mineral pyrite 2 suggests the presence of some rapidly forming sulfate associated with Fe^{3+} on the surface of pyrite (Donato et al., 1991, 1993).

The spectra in Figure 6.5b represent mineral pyrite exposed to atmospheric air at 100% relative humidity in a chamber for 14 days. The emergence of absorption bands at 1183.3, 1137, 1097, 980.6, and 608.9 cm^{-1} clearly indicate the presence of SO_4 on the pyrite surface.

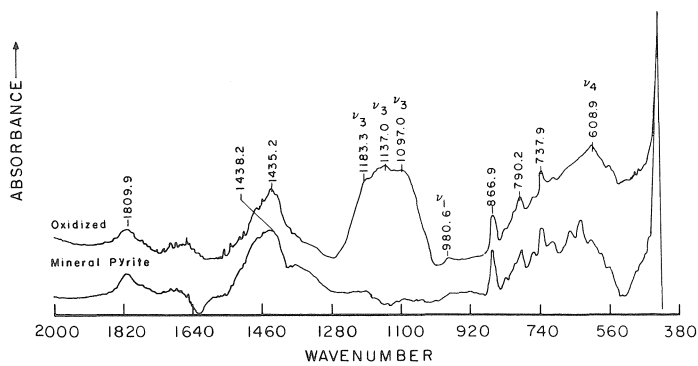

Figure 6.5b. Diffuse reflectance FT-IR spectra of mineral pyrite 1 (Peru pyrite) after oxidation by O_2 at 100% relative humidity. (From Evangelou and Huang, 1994. With permission.)

The sulfate anion species (SO_4^{2-}) is highly symmetrical and of four common fundamental vibrations only v_3 (1200 cm^{-1}) and v_4 (600 cm^{-1}) are infrared active (Nakamoto, 1963, 1986). When the symmetry of sulfate is perturbed due to coordination with cations, the degenerate vibrations (v_3) split into a number of distinct vibrations, depending on strength of the complex, and v_1 vibration is activated. The apparent splitting of v_3 (1183, 1137, 1097) and presence of v_1 (980.6 cm^{-1}) on the spectrum of oxidized mineral pyrite (Figure 6.5b) suggest that sulfate may be bonded to Fe^{3+} in a bindentate fashion (Nakamoto, 1963, 1986; Donato et al., 1993). The spectra in Figure

6.5b also exhibits carbonate absorption bands at 1435 and 867 cm^{-1} which are assigned to CO_3 v_3 and v_2 vibrations, respectively.

The spectra in Figure 6.5a point out the relative ease with which pyrites oxidize when exposed to air and that different pyrites oxidize at different rates. Note that the infrared spectra shown in Figure 6.5a are representative of pyrite samples exposed to air no more than one hour prior to spectroscopic evaluation. Coal pyrite exhibits a 611 cm^{-1} band which most likely represents SO_4^{2-} associated with Fe^{2+}. The same pyrite sample exhibits a CO_3^{2-} band (1430 cm^{-1}) and a carboxylate (COO^-) band (1560 cm^{-1}). In the case of mineral pyrite 1, a broad $SO_4^{2-}/S_2O_3^{2-}$ band is observed below 800 cm^{-1}, as well as a CO_3^{2-} band (1430 cm^{-1}) and most likely a carbonyl (C=O) band near the 1800 cm^{-1} range.

The difference in the infrared spectra between coal pyrite and mineral pyrite 1 (Figure 6.5a) is most likely due to differences in the pK_{bs} of the adsorbed carbonate (assuming the same surface pH) or due to differences in surface pH (assuming differences in oxidation rates). Assuming that the pyrite/surface pH of the two pyrites is the same, but their pK_{bs} differ, then the spectra differences with respect to carboxylate (COO^-) and carbonyl (C=O) bands suggest that one surface is deprotonated (coal pyrite) while the other surface (mineral pyrite 1) is protonated. The spectrum of mineral pyrite 2, on the other hand, does not display a CO_3^{2-} band (note absence of 1430 cm^{-1} band), but it does display a SO_4^{2-} band in the 1200 cm^{-1} range. This band, most likely reflects SO_4^{2-} associated with Fe^{3+} (Donato et al., 1991, 1993). It appears that the low surface pH, due to Fe^{3+}, inhibits formation of surface adsorbed carbonate.

An alternate explanation for the 1430 and 1654 bands of coal pyrite is the direct reaction of CO_2 with S_B (Reaction 6.1) as follows:

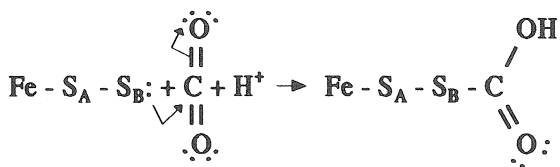

(6.37)

The above reaction product could exhibit infrared absorption bands similar to those of CO_3^{2-} coordinated by pyrite/surface adsorbed Fe^{2+}. In other words, one would be able to observe C-O symmetric vibrations at around 1430 cm^{-1}, carbonyl (C=O) vibrations at about 1750 cm^{-1}, and/or carboxylate vibrations at about 1560 cm^{-1}. The exact wavenumbers of these vibrations would depend on the nature of the disulfide-carbon chemical interactions. Some support for the above postulated pyrite/surface-CO_2 interactions comes from the pyrite-CO_3 infrared spectroscopic observations reported by Donato et al. (1991, 1993). The importance of the above pyrite infrared spectroscopic

observations with respect to pyrite oxidation reactions is discussed in section 6.4.1.

One would assume that the strong acid environment on the surface of pyrite, created by the oxidation of the disulfide, is expected to prevent formation of Fe(II)-CO_x complexes. However, persistence of the carbonate absorption band (1430 cm^{-1}), as shown in Figure 6.5b, demonstrates that the acid produced could be removed due to its reaction with pyrite as follows (Evangelou and Huang, 1984):

$$FeS_2 + H_2SO_4 = FeSO_4 + H_2S + S^o \qquad (6.38)$$

In Reaction 6.38, it is suggested that protons are removed during H_2S volatilization after placing the pyrite sample under vacuum on any other O_2 consuming conditions. Therefore, after oxidation, the surface of pyrite is most likely covered with a layer of ferrous sulfate and most active anodic sites (S_B) are saturated with Fe^{2+} (Goldhaber, 1983; Moses and Herman, 1991).

The infrared absorption band near 1621 cm^{-1} shown in Figure 6.6 can be assigned to the H_2O deformation band. The band at 1650 cm^{-1} suggested the presence of an additional pyrite/surface chemical species.

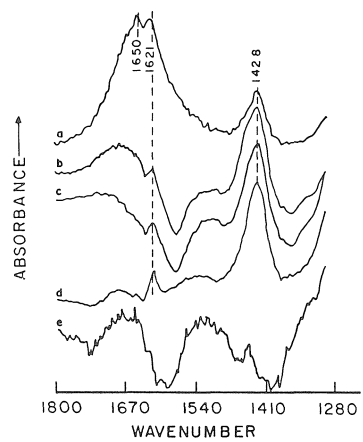

Figure 6.6. Diffuse reflectance FT-IR spectra of oxidized mineral pyrite 2 (South Dakota pyrite) after the following treatments: a) oxidation; b) drying in desiccator; c) heating at 160°C for 3 hr; d) heating at 160°C for 8 hr; e) washing with 4 mol L^{-1} HCl. (From Evangelou and Huang, 1994. With permission.)

When the oxidized mineral pyrite was exposed to desiccation at room temperature or heated to 160°C for 4 hr and 8 hr under a nitrogen gas atmosphere the absorption band at 1650 cm^{-1} decreased in intensity, while the 1621 cm^{-1} band as well as the 1430 cm^{-1} (due to CO_3^{2-} or C-O

symmetric vibrations) appeared intact. This suggested that the 1650 cm^{-1} absorption band was most likely due to carboxylate (COO^-). When the pyrite sample was heated, adsorbed water decreased and, therefore, surface acidity increased leading to carboxylate protonation (Mortland, 1968; Mortland and Raman, 1968; Harter and Ahlrichs, 1968); consequently, the 1650 cm^{-1} band was eliminated. The continuing presence of the 1620 cm^{-1} band may be due to the rapid rehydration of the pyrite surface prior to scanning or due to strongly adsorbed water. Furthermore, after washing the oxidized pyrite sample with HCl, its spectrum did not exhibit the 1430 cm^{-1} band, suggesting that the pyrite/surface CO_x (CO_x = CO_3^{2-} or carboxylic species) was removed by the acid. Additionally, the absence of the 1620 cm^{-1} band, indicative of water loss/absence, could be due to production of elemental sulfur (Lowson, 1982), a hydrophobic substance.

According to Nakamoto (1963, 1983), the extent of splitting (No. of distinguishable bands) of the 1430 cm^{-1} band, representing the free CO_3 ion, could be directly related to the bond strength between CO_3^{2-} and Fe^{II}. Nonsplitting of the CO_3 band in Figure 6.6 indicates that pyrite/surface Fe(II)-CO_3 complexes are most likely weak electrostatic complexes (see Reaction 6.36) or that the 1430 cm^{-1} band represents symmetric C-O vibrations of a carboxylic group (see Reaction 6.37). When the spectrum of bulk $FeCO_3$ is compared to that of oxidized pyrite (Figure 6.7a), it is shown that in the case of bulk $FeCO_3$ the 1430 cm^{-1} band splits into two clearly distinguishable bands, signifying a unidentate complex (see also Figure 6.7b) (see Reaction 6.35) (Nakamoto, 1963, 1983) while in the case of coal pyrite only a single 1430 cm^{-1} band is observed (see also Figure 6.7c).

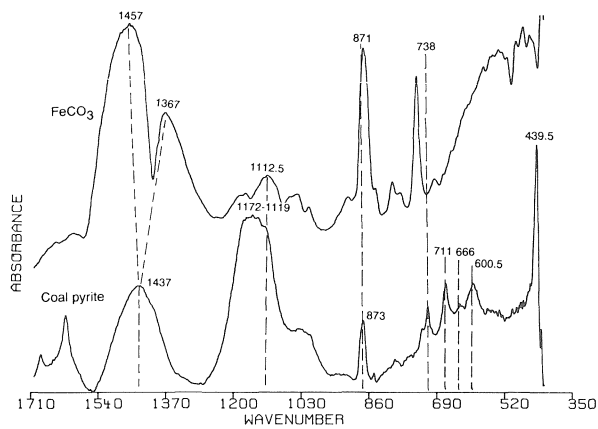

Figure 6.7a. Diffuse reflectance FT-IR spectra of $FeCO_3$ and coal pyrite after a several-month exposure to atmospheric air in room temperature. (From Evangelou and Huang, 1994. With permission.)

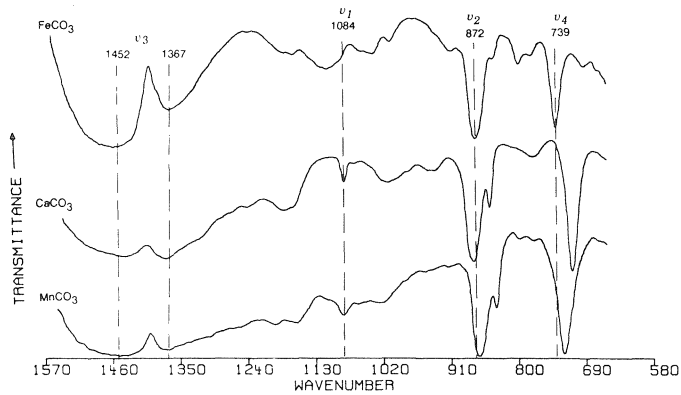

Figure 6.7b. Diffuse reflectance FT-IR spectra of various carbonates.

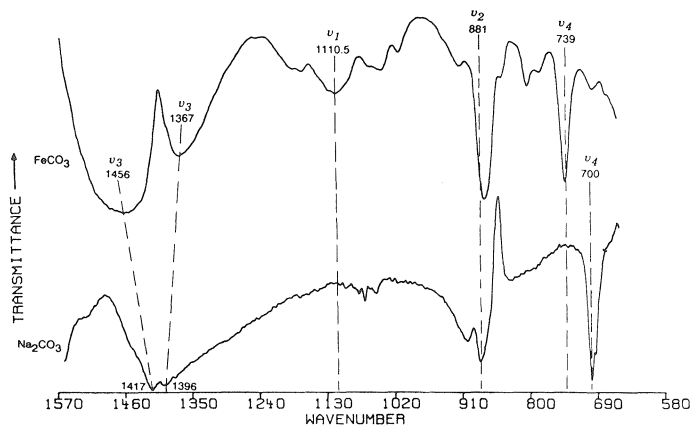

Figure 6.7c. Diffuse reflectance FT-IR spectra of $FeCO_3$ and Na_2CO_3.

The above infrared spectra observations are summarized in Figure 6.8. It shows the symmetric vibrations of CO_3^{2-}/COO^- (1430 cm^{-1} band); presence of pyrite/surface adsorbed water (1620 cm^{-1}), as well as the vibrations of carbonyl (C=O, 1789 cm^{-1} band) and carboxylate (COO^-, 1681 cm^{-1} band).

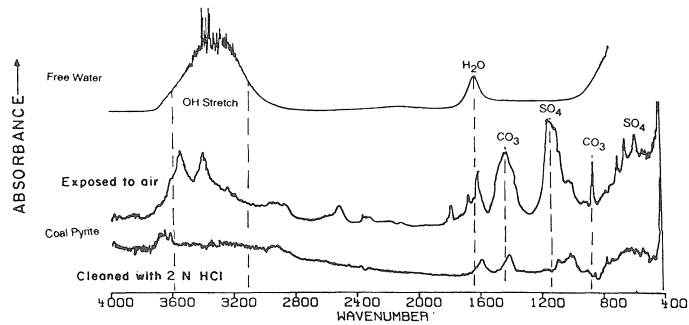

Figure 6.8. Diffuse reflectance FT-IR spectra of coal pyrite and mineral pyrite 1 (Peru pyrite) after a several-month exposure to atmospheric air in room temperature.

Absorption bands in the 3300 to 3600 cm^{-1} range are also shown; they represent OH^- associated with Fe^{III} and OH^- associated with pyrite/surface adsorbed water. The infrared evaluation presented above clearly supports the potential adsorption of CO_2 by the surface of pyrite either as CO_3^{2-} (weakly adsorbed by pyrite/surface Fe^{II} (Moses and Herman, 1991; Goldhaber, 1983)) and/or by directly sharing the disulfide unshared electron pair, thus, forming a pyrite surface carboxylic group.

Pyrite/surface-CO_x complexes may act as promoters to pyrite oxidation (Hood, 1991) or as precursors to pyrite iron-oxide coatings formation (Nicholson et al., 1988, 1990). Conditions necessary for forming Fe(II)-CO_3 complexes or -COO^- on the surface of pyrite in the absence of carbonate rich solutions appear to be 1) low availability of water, and 2) presence of O_2 and CO_2 gasses. However, further wet chemistry experiments are needed in order to demonstrate the mechanism of promoting pyrite oxidation by Fe(II)-CO_3 pyrite/surface complexes or -COO^-, and quantify the conditions leading to formation of iron-oxide coatings which may inhibit pyrite oxidation in nature.

6.4.1 Pyrite oxidation effects by iron-carbonate complexes

Rates of pyrite oxidation in neutral and alkaline environments, e.g., limestone buffered sulfide rich mine wastes, are commonly lower than that in acidic environment due to lower solubility of Fe^{3+} and limited bacteria activity. Studies by Nicholson et al. (1988, 1990) indicated that in neutral to alkaline environments formation of iron-oxide coating on the pyrite surface can act as pyrite/surface barrier to O_2 and/or Fe^{3+}, thereby diminishing pyrite oxidation. Nicholson et al. (1988, 1990) investigating pyrite oxidation kinetics in a bicarbonate buffered system at pH values between 7.5 and 8.5 observed that the oxidation rate initially increased, reached a maximum at about 400 hours, and then decreased to a final relatively constant lower value (Figure 6.9).

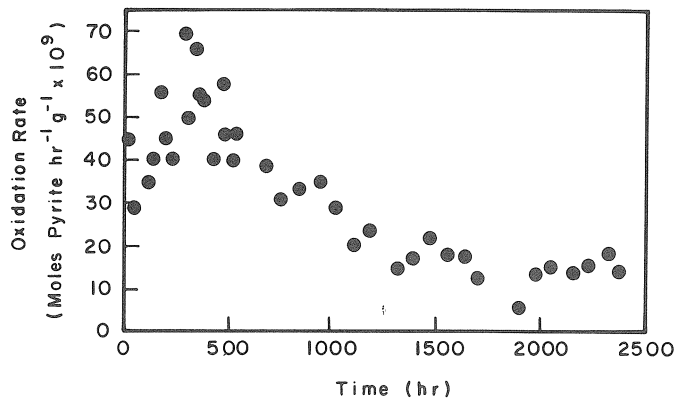

Figure 6.9. Variation in rate of pyrite oxidation in alkaline solutions with time. (From Nicholson et al., 1990. With permission.)

By using X-ray photoelectron spectroscopy and auger electron spectroscopy, Nicholson et al. (1988, 1990) found that pyrite particles (215 μm) when oxidized under alkaline conditions were coated with a ferric oxide coating of approximately 0.6 microns thickness. They concluded that oxide accumulation on the pyrite surface resulted in a significant reduction in oxidation rate over time. Nicholson et al. (1988, 1990), however, did not investigate the mechanisms by which ferric iron could be stabilized on the surface of pyrite.

Hood (1991) studied kinetics of pyrite oxidation in alkaline suspensions at a constant pH by maintaining a constant HCO_3^-/CO_3^{2-} ratio and increasing concentration of the two species. Carbonate single-ion activity

was varied from 0.002 mmol L^{-1} to approximately 0.05 mmol L^{-1} to avoid precipitation of ferrous carbonate in the bulk solution. Hood (1991) observed that the rate of pyrite oxidation increased with increasing carbonate concentration (Figure 6.10). The same phenomenon may explain the large increase in pyrite oxidation rate in the presence of $NaHCO_3$ at pH 9 as observed by Brown and Jurinak (1989a). Hood (1991) concluded that the cause for the observed increase in pyrite oxidation was formation of a pyrite/surface Fe(II)-CO_3 complex which facilitated electron transfer to O_2 and consequently rapid oxidation of ferrous iron. Furthermore, Hood (1991) employed her experimental observations to explain the results (involving pyrite oxidation in alkaline solutions) published by Nicholson et al. (1990).

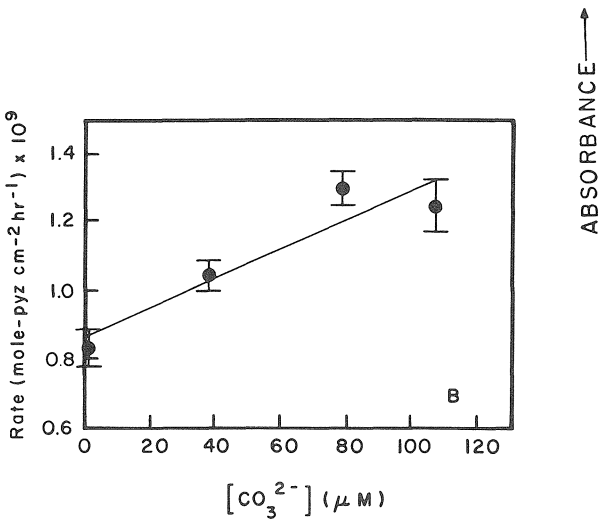

Figure 6.10. Kinetics of pyrite oxidation as influenced by carbonate. (From Hood, 1991. With permission.)

She concluded that the initial increase in the oxidation rate observed by Nicholson et al. (1990) (Figure 6.9) was due to pyrite/surface $FeCO_3^o$ complex formation. Hood (1991) further predicted that upon oxidation of Fe^{II} of $FeCO_3^o$ complexes, they form either $Fe(OH)_3(s)$ or FeOOH(s) on the pyrite surface. These iron oxyhydroxide solids accumulate and become a diffusion barrier for the movement of O_2 to the pyrite surface and oxidation products away from the surface. Due to this barrier, the oxidation rate decreases, eventually reaching the lower value set by the rate of diffusion of reactants and products through the iron oxyhydroxide barrier.

Hood (1991) however, did not provide direct molecular evidence for the ferrous carbonate complex formed on the pyrite surface. Evangelou and Huang (1994) using FT-IR spectroscopy demonstrated that pyrite exposure to

atmospheric air leads to formation of weak pyrite surface Fe(II)-CO_3 complexes and/or a pyrite/surface carboxylic group (see section 6.4) which may promote pyrite oxidation by promoting electron transfer, or may act as precursors to pyrite iron-oxide coating formation. Evangelou and Huang (1994) also suggested that in the absence of carbonate rich-solution, the conditions necessary for forming Fe(II)-CO_3 complexes on the pyrite surface are low availability of water, and presence of O_2 and CO_2. FT-IR evidence of CO_3 on the surface of pyrite were also reported by Donato et al. (1991 and 1993). But the carbonate's potential importance to pyrite oxidation was overlooked by these researchers.

Based on, 1) experimental observations that at constant pH but at increasing solution CO_3^{2-} concentration abiotic pyrite oxidation rate increases (Hood, 1991; Brown and Jurinak, 1989a), and 2) FT-IR data supporting the presence of pyrite/surface-CO_3 complexes and/or pyrite/surface carboxylic group formation (Evangelou and Huang, 1994; Evangelou, 1994a,b), the following model was proposed by Evangelou and Zhang (1994) to complement the model proposed by Moses and Herman (1991) by accounting for the observed abiotic pyrite oxidation enhancement effect observed in environments enriched with CO_2/CO_3 and O_2 at pH near or above neutral.

$$-Fe(H_2O)_5OH^+ + CO_2 \rightarrow Fe(H_2O)_5HCO_3^+ \qquad (6.39)$$

and

$$Fe(H_2O)_5HCO_3^+ + H_2O + O_2 \rightarrow -Fe(H_2O)_4(OH)_2^+ + CO_2 \qquad (6.40)$$

According to Millero and Izaguirre (1989), Fe^{II} oxidation is promoted when in the presence of HCO_3^-/CO_3^{2-} due to Fe^{II}-carbonate complex formation. Luther et al. (1992) postulated and then demonstrated that Fe^{II} complexation by any ligands containing oxygen as the ligating atom promotes Fe^{II} oxidation due to the potential increase in frontier molecular orbital electron density. The latter increases Fe^{II} basicity and consequently, the latter acts as a stronger electron donor. Similar conclusions were reached by Hood (1991). Based on the above, the surface adsorbed -$Fe(H_2O)_4(OH)_2^+$ (Reaction 6.40) forms a persulfido bridge and pyrite oxidation proceeds according to Reactions 6.4-6.7. According to Reaction 6.37, an alternate approach, however, to the CO_2 involvement in pyrite oxidation is through formation of a pyrite/surface carboxylic group

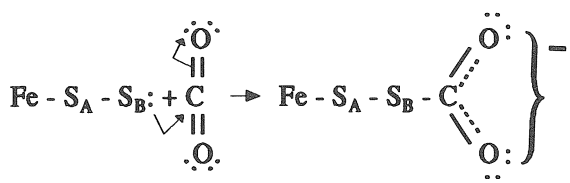

(6.41)

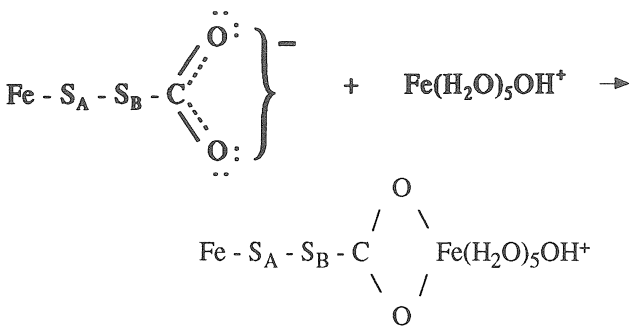

$$Fe - S_A - S_B - C(=O)(-O^-) + Fe(H_2O)_5OH^+ \rightarrow Fe - S_A - S_B - C(=O)(-O) - Fe(H_2O)_5OH^+ \quad (6.42)$$

The Fe - S_A - S_B - COO-Fe(H_2O)OH complex promotes Fe^{II} oxidation due to the fact that the carboxylate ligand contains oxygen as the ligating atom (Luther et al., 1992). Oxidation of Fe^{II} to Fe^{III}, however, is expected to produce a metastable pyrite/surface carboxylate-Fe^{III} complex, leading to pyrite/surface decarboxylation and formation of a persulfido bridge. The latter facilitates electron transfer from S_B to Fe^{III} (see section 6.3).

The pyrite oxidation model proposed by Moses and Herman (1991) was deduced from macroscopic pyrite oxidation data and no direct molecular evidence on most of the intermediates were presented. However, their pyrite oxidation model is consistent with frontier molecular orbital theory (Luther, 1990 and references therein) and classical redox reaction theory. In the case of the proposed complementary pyrite oxidation model proposed by Evangelou and Zhang (1994) (involving CO_2) it is consistent with the model proposed by Moses and Herman (1991) and the CO_3^{2-} pyrite/Fe^{II} oxidation rate enhancement effect reported by Hood (1991), Millero and Izaguirre (1989) and Luther et al. (1992).

6.5 Kinetics of Pyrite Oxidation

Based on classical thermodynamics, negative ΔG^o denotes that a reaction under unit activity of reactants and products will move spontaneously from left to right (Adamson, 1990). Pyrite exposed to atmospheric air exhibits a ΔG^o of -1.21 MJ $mole^{-1}$ (Brown, 1985). However, this negative ΔG^o does not reveal the rate at which the reaction will proceed. Reaction rates are characterized by the number of successful collisions between reactants (pyrite/surface and oxidants) per unit time. The number of successful collisions between reactants is represented by the product of the total number of collisions of the reactants, the number of collisions that have sufficient energy to cause a reaction event (energy factor), and the fraction of collisions that have the proper orientation (probability factor). The theoretical rate constant (k) for any chemical reaction is given by

$$k = PZe^{-E_{a/RT}} \quad (6.43)$$

where

P = probability factor,

Z = collision frequency,
E_a = activation energy,
T = temperature and

$e^{-E_{a/RT}}$ = fraction of collisions with energy sufficiently large to cause a reaction event.

The product PZ is related to the pre-exponential factor (A) of the Arrhenius Reaction and the entropy (S) of the reaction by the relationship.

$$PZ = Ae^{S/R} \tag{6.44}$$

Based on Reactions 6.43 and 6.44, the rate constant of a chemical reaction is inversely dependent on the activation energy of the reaction (an experimentally determined parameter) (Daniels and Alberty, 1975) and directly dependent on the entropy of activation of the reaction. Activation energies (E_a) obtained for pyrite oxidation at room temperature by both ferric iron and molecular oxygen ranged from about 50 to 92 kJ per mole. These high activation energy values suggest that electron transfer reactions occurring at the pyrite surface are the rate limiting step for pyrite oxidation (Lasaga, 1981) and entropy may play an insignificant role. These high activation energies also suggest that the reaction mechanism for pyrite oxidation is surface controlled.

Observations made on the makeup of pyrite surface by scanning electron microscopy have recently been characterized by using surface FT-IR techniques (Donato et al., 1991 and 1993; Evangelou and Huang, 1994; Evangelou and Zhang, 1994), electrochemical techniques (Palencia et al., 1991; Fornasiero et al., 1992), and X-ray photoelectron spectroscopy techniques (XPS) (Donato et al., 1993; Nicholson et al., 1990). The results of these studies can be summarized as follows: 1) The nature of the pyrite/surface products, observed by spectroscopy, resulting from natural oxidation are dependent on the origin of pyrite (e.g., coal pyrite, mineral pyrite) and shape of pyrite (e.g., fresh fracture, polished sample, powdered mineral); 2) the mechanisms at the early stages of oxidation involve adsorption of dissolved bimolecular oxygen and water on the pyrite surface and formation of various intermediates such as ferrous, ferric, sulfite and sulfate ions, sulfur and ferric hydroxide; 3) oxide and/or hydroxide films in the form of goethite, magnetite or hematite on the oxidized pyrite surface have also been identified on various occasions; 4) pyrite mineral surface species during oxidation by *T. ferrooxidans* are ferric and ferrous sulfate.

The presence of hydrophobic elemental sulfur or other sulfur species such as polysulphide on the surface of pyrite is still open to debate. Pyrite/surface intermediates or products formed during oxidation may change the hydrophobic or hydrophilic character of the mineral surface which may

affect the oxidation process with respect to reaction rate and nature of the pyrite/surface intermediates formed.

6.5.1 Empirical pyrite oxidation rate laws

Pyrite oxidation by O_2 can be described as follows (Singer and Stumm, 1970):

$$FeS_2 + 7/2O_2 + H_2O \rightarrow Fe^{II} + 2SO_4 + 2H^+ \quad (6.45)$$

or

$$FeS_2 + 14Fe^{III} + 8H_2O \rightarrow 15Fe^{II} + 2SO_4^{2-} + 16H^+ \quad (6.46)$$

In this book, the Fe exponents (valence) or the exponents of any other cation, are noted in Roman symbols or Arabic symbols and are used alternatively, but without any significant difference. Reactions 6.45 and 6.46, both oxidize pyrite and take place simultaneously as long as there is a reaction that converts Fe^{II} to Fe^{III}. This reaction is

$$Fe^{II} + H^+ + 0.25O_2 \rightarrow Fe^{III} + 1/2H_2O \quad (6.47)$$

Based on Reactions 6.45 and 6.46, the rate of pyrite oxidation can be expressed as follows:

$$-d[FeS_2]/dt = [(k_1(O_2)^{v1} + k_2(Fe^{III})^{v2}](S) \quad (6.48)$$

The parameters O_2 and Fe^{III} refer to partial pressure and concentration of O_2 and Fe^{III}, respectively, k_i refers to rate constants and S denotes surface area. The exponents v_i are experimentally determined (Daniels and Alberty, 1975). Considering that under a given set of pyrite oxidizing conditions (e.g., a constant supply of O_2 in a abiotic suspension system with pH less than 3.5) such that, the rate of Fe^{III} production is slower than the rate of Fe^{III} consumption, then the rate of Fe^{III} production would be the pyrite oxidation rate controlling factor. This was demonstrated by Singer and Stumm (1970) and Moses et al. (1987) who concluded that pyrite oxidation by bimolecular oxygen (first term on the right side of the equal sign of Reaction 6.48) is not significant).

According to Reaction 6.47 the rate of production of Fe^{III}, due to Fe^{II} oxidation, can be expressed as

$$-[Fe^{II}]/dt = k(H^+)^{v1}(Fe^{II})^{v2}(O_2)^{v3} \quad (6.49)$$

Singer and Stumm (1970) demonstrated that the rate of Fe^{II} consumption at pH less than 3.5 is of the form

$$-[Fe^{II}]/dt = k'(Fe^{II})(O_2) \tag{6.50}$$

where k' denotes apparent rate constant. Equation 6.50 reveals that the rate of Fe^{II} oxidation at pH less than 3.5 is independent of pH and first order with respect to Fe^{II} and O_2 (Figure 6.11). Thus, under the conditions stated above, the rate of Fe^{III} production is directly related to Fe^{II} concentration, and partial pressure of bimolecular oxygen. However, at pH values greater than 3.5 the empirical rate expression for Fe^{II} oxidation, according to Singer and Stumm (1970), is of the form

$$-[Fe^{II}]/dt = k(Fe^{II})(O_2)(OH)^2 \tag{6.51}$$

Equation 6.51 reveals that Fe^{II} oxidation is first order with respect to Fe^{II} and O_2 and second order with respect to OH^- (Figure 6.11).

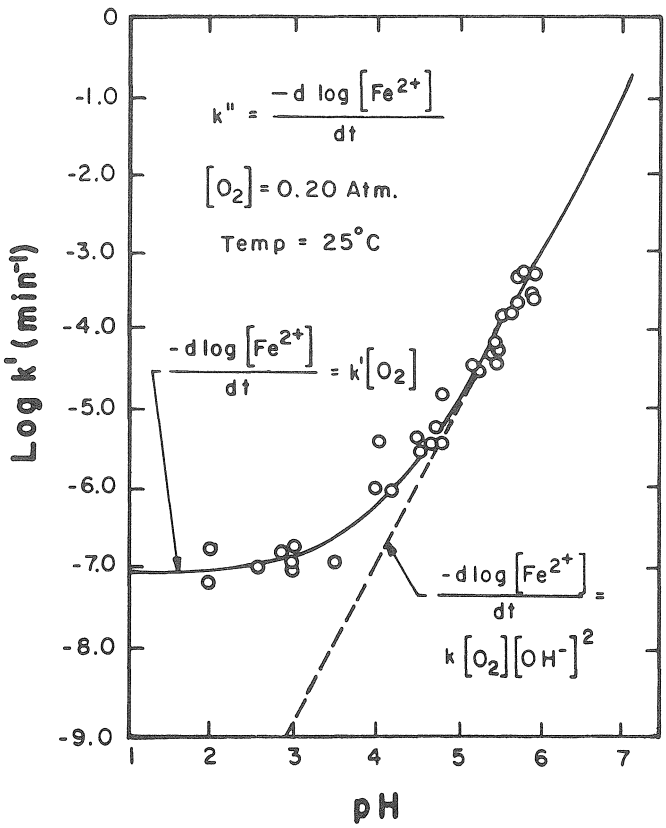

Figure 6.11. Oxidation rates of Fe^{II} as a function of pH. (From Singer and Stumm, 1970. With permission.)

In the case where pH is greater than 3.5 and all other pyrite oxidizing conditions as stated above, then the quantity of Fe^{III} in solution would be controlled by the solubility of amorphous $Fe(OH)_3$.

$$Fe^{II} + H^+ + 0.25O_2 \rightarrow Fe^{III} + 1/2H_2O \quad (6.52)$$

and

$$Fe^{III} + 3H_2O \rightarrow Fe(OH)_3 + 3H^+ \quad (6.53)$$

Summarizing Reactions 6.52 and 6.53 gives

$$Fe^{II} + 2.5H_2O + 0.25O_2 \rightarrow Fe(OH)_3 + 2H^+ \quad (6.54)$$

However, considering that at increasing pH values (pH above 3.5) the half-life of Reaction 6.53 is smaller than the half-life of Fe^{II} oxidation, it would appear that under such abiotic conditions the rate of pyrite oxidation would be controlled by the solubility of $Fe(OH)_3$. The solubility of $Fe(OH)_3$ is described by the reaction

$$Fe(OH)_3 = Fe^{III} + 3OH^- \quad (6.55)$$

and

$$Fe^{III} = K_{sp}/(OH^-)^3 \quad (6.56)$$

where K_{sp} is the solubility product constant of $Fe(OH)_3$. Introducing Equation 6.56 into Equation 6.48, produces

$$-d[FeS_2]/dt = [k_1(O_2)^{\nu 1} + k_2(K_{sp}/(OH^-)^3)^{\nu 2}](S) \quad (6.57)$$

Equation 6.57 reveals that pyrite oxidation in a abiotic system and in the presence of $Fe(OH)_3$ is controlled by pH. As pH decreases (OH^- decreases), free Fe^{III} in solution increases; consequently pyrite oxidation increases. However, under increasing pH it would appear that oxidation of pyrite would be limited due to the low solubility of $Fe(OH)_3$. Based on that, application of limestone to pyrite should be an effective way to control pyrite oxidation. However, this has not been the case in field-scale experiments. In fact, Stiller et al. (1985) noticed that in the presence of limestone pyrite oxidation appeared to accelerate. It may be possible that at the microscopic scale pyrite oxidation in the presence of alkaline material is controlled by the turnover rate of Fe^{III} near the surface of pyrite and not by the solubility of $Fe(OH)_3$ in pure solutions. A similar conclusion was drawn by Moses et al. (1987). Luther (1990) pointed out that the solubility of amorphous $Fe(OH)_3$ may control pyrite oxidation as long as there is physical contact between pyrite and amorphous $Fe(OH)_3$. However, if instead of $Fe(OH)_3$ precipitate one considers FeOOH precipitate then pyrite oxidation would proceed

approximately 50 times slower due to the greater stability of FeOOH in acid solutions.

Pyrite oxidation by H_2O_2 can be described as follows:

$$FeS_2 + 7H_2O_2 \rightarrow Fe^{II} + 2SO_4^{2-} + H^+ + 6H_2O \quad (6.58)$$

$$Fe^{II} + H^+ + 0.5H_2O_2 \rightarrow Fe^{III} + H_2O \quad (6.59)$$

$$FeS_2 + 14Fe^{III} + 8H_2O \rightarrow 15Fe^{II} + 2SO_4^{2-} + 16H^+ \quad (6.60)$$

where Fe^{III} and Fe^{II} denote free iron in the system. According to Reactions 6.58, 6.59 and 6.60, pyrite oxidation is an autocatalytic process as one of the oxidation products, Fe^{III}, can also oxidize pyrite (Moses et al., 1987). Assuming that oxidation of Fe^{II} to Fe^{III} (e.g., Reaction 6.59) is much faster than Reaction 6.58 or 6.60 (Singer and Stumm, 1970; Stumm and Morgan, 1981 and references therein; Luther, 1990 and references therein), the theoretical rate law corresponding to the oxidation of FeS_2 can be written as (Moore, 1972)

$$-d[FeS_2]/dt = [k_1(H_2O_2)^{v1} + k_2(Fe^{III})^{v2}](S) \quad (6.61)$$

where FeS_2 represents the number of moles of unreacted pyrite in the system at any time t. The parameters $[H_2O_2]$ and $[Fe^{III}]$ refer to concentrations of H_2O_2 and Fe^{III}; k_1 and k_2 refer to the rate constants of H_2O_2 and Fe^{III}, respectively, and S stands for the surface of pyrite available to react. The exponents v_i, as previously stated, are experimentally determined (Daniels and Alberty, 1975). For additional information see section *6.5.2*. Experimental data are presented by McKibben and Barnes (1986).

6.5.2 Application of pyrite oxidation kinetics

Assuming that during oxidation the newly exposed pyrite surface (S) remains proportional to the number of moles of unreacted FeS_2 in the system, such that (Turner, 1959; Turner and Skinner, 1959)

$$[S] = K[FeS_2] \quad (6.62)$$

where K is a constant, and considering that the equilibrium coefficients of the pyrite/surface (S) complexes, e.g., $(H_2O_2)(S)$ and $(Fe^{III}(S)$, and concentrations of H_2O_2 and Fe^{III} in solution are held constant, by substituting Reaction 6.62 into Reaction 6.61 it can then be assumed that

$$Kk_1[oxidant]^{v1} = Kk_1' \quad (6.63)$$

and

$$Kk_2[Fe^{III}]^{v_2} = Kk_2' \quad (6.64)$$

According to the Eyring theory (Daniels and Alberty, 1975; Moore, 1972) surface activation complexes are the driving force of reactions and their formation is controlled by the activity of the chemical species involved (Sposito, 1984 and references therein). However, in kinetic processes, e.g., pyrite oxidation by H_2O_2 or O_2, experimental identification and quantification of the various chemical species involved is very difficult because of the chemical complexity of these species, their extremely short half life, and their large number (Luther, 1990). Because of these reasons, in many studies no distinction is made between concentration and activity of reactants and products.

Based on the above, Equation 6.61 can be expressed as the sum of two consecutive pseudo-first-order reactions. Theoretical and experimental basis of pseudo-first-order reactions involving dissolution of solids is given by Turner (Turner, 1959; Turner and Skinner, 1959). By substituting Equations 6.62, 6.63 and 6.64 into Reaction 6.61 and integrating using the appropriate boundary conditions (t = 0, M = Mo; t = t, M = M) (Daniels and Alberty, 1975) yields the relationship of a pseudo-first-order reaction

$$\ln [M] = -K[k_1' + k_2'](t) + \ln [Mo] \quad (6.65)$$

or

$$\log [M/Mo] = -K[k_1' + k_2'/2.3](t) \quad (6.66)$$

where M and Mo denote unreacted and original quantities of pyrite, respectively.

According to Equation 6.66, if kinetic data of pyrite oxidation (e.g., SO_4 release) obtained by employing a constant concentration of H_2O_2 were plotted as a first-order reaction, log M/Mo versus t, will give a linear function as long as a) concentration of Fe^{III} in solution remained constant, b) apparent Fe^{III} control on pyrite oxidation remained unaffected with time, and c) the relationship between surface and mass of unreacted pyrite remained constant (Turner, 1959; Turner and Skinner, 1959). However, in leaching oxidation experiments, the concentration of Fe^{III} in the pore solution is expected to decrease with time, thus, due to this factor alone, a plot of log M/Mo versus t is expected to decrease in slope with increasing time. This is demonstrated in Figure 6.12. These pyrite oxidation data (Figure 6.12) demonstrate that curve A exhibits curvilinearity because both terms in Reaction 6.62 participate in the process. On the other hand, curve B appears linear. This curve represents pyrite oxidation in the presence of EDTA. The latter forms strong Fe^{III} complexes and for this reason pyrite oxidation is controlled only by H_2O_2.

Pyrite oxidation involves various intermediate sulfoxy anions such as sulfite, SO_3^{2-}, thiosulfate, $S_2O_3^{2-}$, and polythionates, $S_nO_6^{2-}$, n = 4, 5, and 6. However, during kinetic studies experimental identification and

quantification of the various chemical species involved is very difficult, if not impossible, because of the chemical complexity of these species, their extremely short half life, and their large number (McKibben and Barnes, 1986 and references therein; Wiersma and Rimstidt, 1984; Taylor et al., 1984a,b; Moses et al 1987; Luther, 1990 and references therein). Because of these reasons, commonly, no distinction is made between concentration and activity of reactants and products involved (Sposito, 1984a and references therein).

Based on the above, pyrite oxidation rate laws can only be determined experimentally under a given set of well controlled experimental conditions.

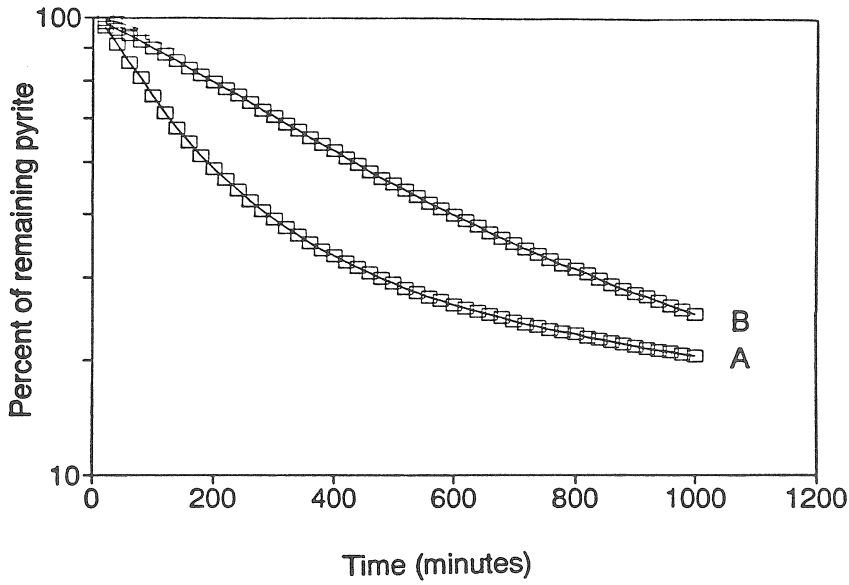

Figure 6.12. Kinetics of pyrite oxidation by H_2O_2 in the absence of A) EDTA, and B) presence of EDTA. (From Huang and Evangelou, 1994. With permission.)

For example, Brown and Jurinak (1989a) determined that the rate law of pyrite oxidation in suspensions was zero order (independent of time) in alkaline to acid environments (Figure 6.13). Similar results were obtained by Hood (1991 and references therein). Further investigations by Hood (1991 and references therein) on the dependency of pyrite oxidation on O_2 showed that the reaction was greater than zero order but smaller than first order. The author's data on pyrite oxidation with respect to peroxide using a miscible displacement technique was shown to be 0.68 order. Further characterization of pyrite oxidation kinetics is in Chapter 8.

The rate of pyrite oxidation as a "dual site" process (one site involving O_2, whereas as a second site involving Fe^{III}) has been proposed by Smith and Shumate (1970, 1971; see also Brown, 1985 and references therein) after studying pyrite oxidation kinetics under various pH values, oxygen pressures, temperatures, and Fe^{III} concentrations. The reactions proposed can be expressed as follows:

$$-d(FeS_2)/dt = k_oC_o/[1+(K_oC_o)^{1/2}+K_NC_N]^2 + k_{Fe(III)}/(Fe^{III})^{-1/2}+K_1^{1/2} \quad (6.67)$$

where k_o and $k_{Fe(III)}$ are rate constants of pyrite oxidation by O_2 and Fe^{III}, respectively, C_o and Fe^{III} are O_2 and iron III concentration, respectively, C_N is the concentration of an inert gas, e.g., nitrogen, competing for reaction sites with O_2, and K_N, K_o, and K_1 are adsorption equilibrium constants for inert gas, O_2 and Fe^{III}, respectively.

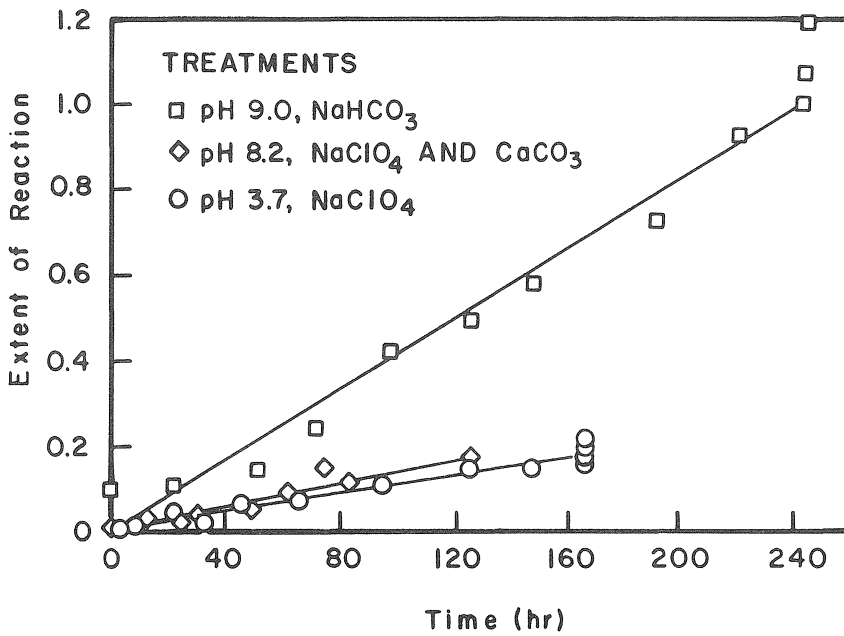

Figure 6.13. Kinetics of pyrite oxidation as influenced by pH. (From Brown and Jurinak, 1989a. With permission.)

For the above model, it is assumed that Fe^{II} concentration is fixed or negligible. For some detailed information on the concepts employed in developing Equation 6.67, see Chapter 8.

Ideally, understanding the fundamental properties of a particular mineral should allow the development of a model for describing rates of chemical reactions. In the case of pyrite, however, no single model is expected to describe kinetics of oxidation due to the large number of variables controlling such process. These variables include crystallinity, particle size, mass to surface ratio, impurities, types of impurities, nature of impurities (physically or chemically involved with the pyrite crystal), crystal imperfections, presence/absence of other minerals/organics, ionic strength, pH, Fe^{3+}/Fe^{2+} ratio, type of oxidant, presence/absence of potentially determining ions, nature of reaction products formed, etc.

6.5.3 Shrinking core model kinetics

Wen (1986) developed a model, called shrinking core model, which combined surface reaction with accumulation of product layer on the surface. In this model it is assumed that the reaction rate is first-order with respect to the principal gas reactant and the surface area (mole numbers) of remaining solids, and that the reaction rate is also controlled by the steady-state diffusion of the reactant gas through the accumulated layer of product on the unreacted core (Nicholson et al., 1990).

According to Wen's model (Nicholson et al., 1990), the time required for a specified quantity (X) of pyrite to oxidize can be expressed as a function of the surface rate constant (K_s), the effective diffusion coefficient for H_2O_2 or O_2 through any surface coating (D_s), and the bulk solution concentration (C) of H_2O_2 or O_2 as follows:

$$t = [1/(D_s'C)][(1-3(1-X)^{2/3} + 2(1-X)] + [1/(K_s'C)\,[1-(1-X)^{1/3}] \qquad (6.68)$$

where D_s' and K_s' refer to the apparent diffusion coefficient and the apparent surface rate constant, respectively. The first term of Reaction 6.67 accounts for the effect of increased thickness of surface coating on the reaction rate, while the second term accounts for the effect of the decreased amount of pyrite on the reaction rate. During oxidation of pyrite by H_2O_2 or O_2 alone, the first term of Equation 6.68 is omitted and it turns to

$$t = [1/(K_s'C)]\,[1-(1-X)^{1/3}] \qquad (6.69)$$

Thus, Equation 6.69 describes first-order kinetics with respect to FeS_2. Therefore, as expected, plots of t versus $[1-(1-X)^{1/3}]$ should display a straight line. In order to test Equation 6.69, Evangelou (1994) and Huang and Evangelou (1994) oxidized pyrite by H_2O_2 in the presence of Ethylene-

diaminetetraacetic acid (EDTA), a strong Fe^{III} chelator and thus a Fe^{III} catalytic inhibitor. These data are presented in Figure 6.14. Deviation of the data from straight line is believed to be due to failure of constant proportionality between surface area and remaining pyrite when more than 50% of pyrite had been oxidized (Turner, 1959).

It is argued that phosphate could act as a pyrite oxidation inhibitor due to its potential to form an iron phosphate coating. To test this hypotheses Huang and Evangelou (1993), oxidized pyrite in the presence of 10^{-3} mol L^{-1} KH_2PO_4 and plotted the data as of $[(1-3(1-X)^{2/3} + 2(1-X)]$ versus $t-[1/(K_s'C][1-(1-X)^{1/3}]$ (the values of $1/(CK_s')$ were obtained from the slope of the plot shown in Figure 6.14.

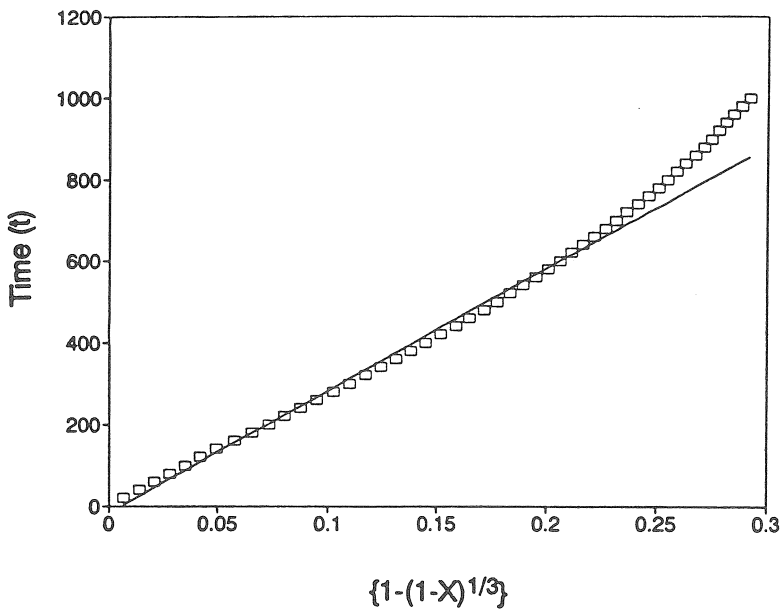

Figure 6.14. A model plot of t vs. $\{1-(1-X)^{1/3}\}$ for the data of pyrite oxidation during leaching with the solution containing 0.147 mol L^{-1} H_2O_2 and 0.013 mol L^{-1} EDTA.

Figure 6.15 showed that the plot followed a straight line, thus, pyrite oxidation behavior was consistent with the shrinking core model. Differences in oxidation rate between data obtained in the presence of EDTA and data

obtained in the presence of phosphate was thus completely due to formation of coatings on the surface of pyrite. The values of $t-[1/(K_s'C)][1-(1-X)^{1/3}]$ represent the extra time required for H_2O_2 to oxidize a given fraction of pyrite due to iron phosphate coatings. As shown in Figure 6.15, the plot followed a straight line after 100 minutes of leaching. The shrinking model requires that all the iron phosphate formed precipitate as a coating on pyritic surfaces. The deviation from linearity before 100 minutes indicates that some iron phosphate did not precipitate as coating. Part of the reason is that the concentration of acid produced by pyrite oxidation was relatively high during the initial stages of leaching. The acid can increase the solubility of $FePO_4$ and thus inhibit formation of iron phosphate coatings on the surface of pyrite.

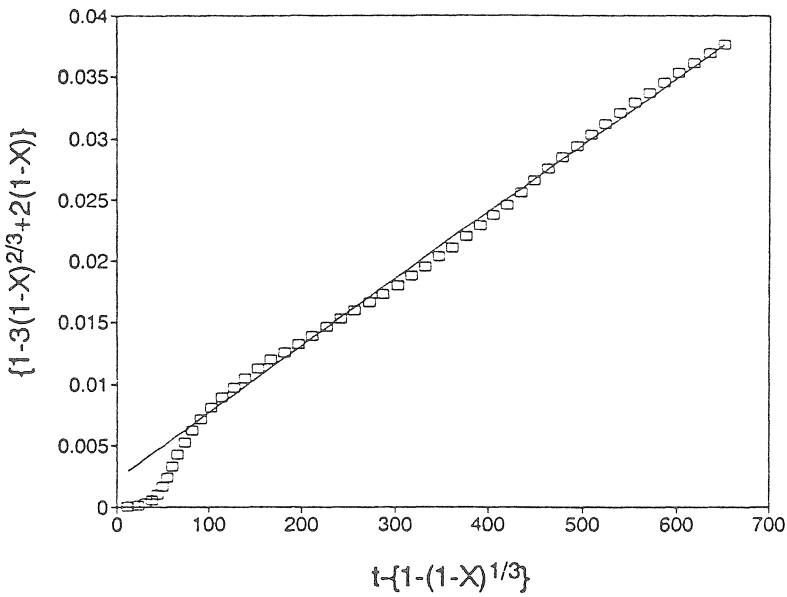

Figure 6.15. A model plot of $\{1-3(1-X)^{2/3}+2(1-X)\}$ vs. $t-\{1-(1-X)^{1/3}\}$ for the data of pyrite oxidation during leaching with the solution containing 0.147 mol L^{-1} H_2O_2 and 0.01 mol L^{-1} KH_2PO_4.

6.6 Effect of Anions on Oxidation of Fe^{2+}

Abiotic oxidation of Fe^{2+} is affected differently by various anions often present in natural water, e.g., OH^-, HCO_3^-, Br^-, NO_3^-, ClO_4^-, Cl^-, SO_4^{2-} and $B(OH)_4^-$. Millero (1985) discussed that the second-order pyrite oxidation dependence on $[OH^-]$ (see Equation 6.51) can be attributed to the following reaction rate determining step

$$Fe(II)(H_2O)_5(OH)_2 + O_2 \rightarrow Fe(III)(H_2O)_5(OH)^{2+} + O^{2-} \qquad (6.70)$$

The O^{2-} radical formed as shown in Reaction 6.70 quickly reacts with Fe^{2+} or $Fe(II)(H_2O)_5(OH)^+$. Goto et al. (1970) proposed a reaction scheme in which $Fe(II)(H_2O)_5(OH)^+$ reacted with hydrolyzed bimolecular oxygen (O_2OH^-) and formed a transition complex with only one Fe(III) as shown below in Reaction 6.71.

$$Fe(II)(H_2O)_5OH^+ + O_2OH^- \rightarrow Fe(III)(H_2O)_5(OH)O_2 + O^{2-} + H_2O \quad (6.71)$$

Millero and Izaquirre (1989) also suggested that the second-order Fe^{II} oxidation dependence on $[OH^-]$ apparently was due to the greater reactivity of $Fe(II)(H_2O)_5(OH)^+$. However, Reactions 6.70 and 6.71 are unlikely to take place because superoxide (O^{2-}) may not be an oxygen reduction intermediate in Fe^{II} oxidation. Millero and Izaquirre (1989) investigated oxidation of aqueous Fe^{II} at circumneutral pH and in the absence of ligands (other than H_2O, OH^-, and Cl^-) and in the absence of catalysts (e.g., microbes or solid surface). Their kinetic evidence suggested that Fe^{II} and dissolved oxygen reacted and produced hydrogen peroxide which oxidized Fe^{II}.

Millero and Izaguirre (1989) examined the effect various other anions have on the abiotic oxidation rate of Fe^{II} at constant ionic strength (I=1.0) and found that this effect was in the order of $HCO_3^- > Br^- > NO_3^- > ClO_4^- > Cl^- > SO_4^{2-} > B(OH)_4^-$. Strong decrease in the rate of Fe^{II} oxidation due to the addition of SO_4^{2-} and $B(OH)_4^-$ was attributed to formation of $FeSO_4^o$ and $Fe[B(OH)_4]^+$ pairs which they assumed were difficult to oxidize. They also reported that the oxidation of Fe^{2+} is first-order with respect to HCO_3^-. This HCO_3^- dependence of Fe^{2+} oxidation could be related to the formation of $FeHCO_3^+$ pair which has a faster rate of oxidation than $Fe(OH)_2^o$ pair. The change in the rate of oxidation of Fe^{II} due to various anions has important implications in the kinetics of pyrite oxidation in neutral to alkaline conditions.

Taylor & Francis
Taylor & Francis Group
http://taylorandfrancis.com

Chapter 7
PYRITE REDOX CHEMISTRY

7.1 General Information on Research Approach

According to the literature, a number of approaches can be used to study pyrite oxidation. They include a) inorganic/biochemical reaction approaches, b) electrochemical reaction approaches and b) reaction kinetics approaches. Each of these approaches may reveal some information with respect to pyrite oxidation, but all approaches are to some degree interrelated on interdependent. For example, under kinetic approaches one is interested in finding out, under certain controlled conditions, the rate at which certain chemical species are produced (biotically or abiotically). These controlled conditions, however, are described by the redox-state and the chemical state of the oxidizing system. If during kinetic oxidation experiments electron poor ions are produced, e.g., Fe(III) or Mn(III) or Mn(IV), then the complexity of the oxidizing system will be changing (see Chapter 6). Also, as oxidation proceeds and products accumulate in the reaction environment, the chemical-oxidation status of the system will be changing due to chemical complexation taking place between the chemical species produced (see Chapter 1). Thus, the study of pyrite oxidation is a rather complex process because one can not separate kinetic processes from electric processes and/or from chemical processes, inorganic or biological in nature.

In Chapter 1 of this book, some detailed information is given on the complexities and quantification of solution chemistry with respect to chemical complexation and/or solution-ion pairing, and how such processes alter the chemical behavior (dissolution/precipitation) of minerals. In addition, in Chapter 1, the relationship between chemical equilibria and kinetics of reversible reactions is demonstrated. In Chapters 6 and 8, kinetics of pyrite oxidation are derived and demonstrated and the various oxidation mechanisms are discussed. Based on what is said above, understanding the processes controlling pyrite oxidation requires understanding of the basic principles of redox chemistry and the parameters affecting/quantifying redox, e.g., Eh, pe, pH.

The terms oxidation or reduction with respect to chemical considerations refer to potential processes. Under the process of oxidation, any chemical element or molecular species donates electrons (e^-), while under the process of reduction, a chemical element or molecular species accepts/receives electrons. These processes by themselves are meaningless to a nontrained chemist and for this reason some additional explanations will be given on the practical importance of electron transfer processes.

Classical chemistry tells us that an atom, of any given element, is made-up of neutrons, protons and electrons. The positive charge of the nucleus is balanced by electrons (e^-) which swarm about the nucleus in orbitals. Only two electrons may occupy a particular orbital. The potential of

an atom, of any given element, to react depends on the affinity of its nucleus for electrons and the strong tendency of the atom to gain maximum stability by filling its outer electron shells.

The potential of any atom to react is described/predicted by the Frontier-molecular-orbital theory (Luther, 1990). Generally, when the outer shell of an atom contains a complete set of paired electrons and the total number of electrons of all the orbiting shells exceeds the number of the positively charged protons in the nucleus, then the atom is referred to as a negatively charged ion (anion). The magnitude of the difference between electrons and protons is commonly referred to as anion charge (e.g., 1^-, 2^-, 3^- etc.). On the other hand, when the number of protons exceeds the sum of all the orbiting electrons and the latter are complete sets of pairs, then the atom is referred to as a positively charged ion (cation). The magnitude of the difference between protons and electrons is commonly referred to as cation charge (e.g., 1^+, 2^+, 3^+, etc.). Attraction between two opposite charged ions forms what is known as an ionic bond. Ionic bonding is characteristic of salts such as NaCl, KCl, $NaNO_3$ etc., and it is generally known to be a weak bond, which explains the high solubility of most such salts.

When atoms possess an incomplete outer shell (e.g., non-paired electrons), yet their net charge is zero, attraction between such atoms takes place because of their strong tendency to complete their outer electron orbital shell by sharing electrons. This gives rise to a strong covalent bond. An example of such covalent bond is that of a bimolecular gas, e.g., O_2. Covalent bonds may also arise between two atoms when one of the atoms shares its outer shell pair of electrons (Lewis base) with the second atom which has an empty outer shell (Lewis acid) (Luther, 1990). Such bonds are known as coordinated covalent bonds. They are commonly weaker than the covalent bond of two atoms with incomplete outer shells, e.g., O_2. Coordinated covalent bonds often involve organometallic complexes.

Based on what is said above, reactions and types of reactions occur because of outer shell electron deficiencies or excesses. There are a number of elements/atoms listed in the *Periodic Table* with varying degrees of outer shell electron deficiencies or excesses. An example of such an element is Fe. Iron may exist as Fe^{II} or Fe^{III} and reacts differently, depending on its charge. The reason for this difference in reactivity is that each form (II versus III) completes its outer-shell electron requirement differently. For example, Fe^{II} reacts strongly with disulfide, S_2^{2-} to form a relatively strong covalent bond, hence, pyrite. However, when S_2^{2-} reacts with Fe^{III}, the latter's outer-shell electron configuration cannot be satisfied by the S_2^{2-} and an electron is transferred from S_2^{2-} to Fe^{III}. This electron transfer weakens the covalent character of the disulfide ($S\text{-}S^{2-}$) (Luther, 1987, 1990, 1992; Luther et al., 1992), hence, electron transfer continues until a stable configuration is attained by the sulfur atoms. Under strong pyrite oxidizing conditions, a

stable electron configuration by the disulfide's sulfur atoms appears to favor formation of SO_4^{2-}.

The above clearly demonstrate that oxidation/reduction processes are important in nature because they control the stability of substances. During oxidation/reduction, reactants are altered and new products are formed. These products, depending on makeup and chemistry, may be environmental pollutants.

7.2 Pyrite Stability Diagrams

Commonly, redox processes in nature are quantified through the use of stability diagrams which are bounded by the upper and lower stability limits of water. For example, for the upper stability limit of water the reaction is

$$2H_2O = O_2(g) + 4H^+ + 4e^- \tag{7.1}$$

and the redox potential (Eh) is described by the equation

$$Eh = E^o + [0.059/4]\log [(pO_2)(H)^4/(H_2O)^2] \tag{7.2}$$

where E^o is the standard half cell potential, pO_2 is the partial pressure of O_2, and $[H^+]$ and $[H_2O]$ represent activities. By setting pO_2 and $[H_2O]$ equal 1, and considering that the ratio of H^+ to e^- also equals 1, Eh can be expressed as

$$Eh = E^o + 0.059 \log (H^+) \tag{7.3}$$

and by substituting –pH for (H^+)

$$Eh = E^o - 0.059\ pH \tag{7.4}$$

Quantification of E^o can be carried out by considering that

$$E^o = -\Delta F_r^o/nF \tag{7.5}$$

where ΔF_r^o is the standard free energy of Reaction 7.1, n is the number of electrons transferred, and F is Faraday's constant (23.06 kcal per volt-gram equivalent). From the classical thermodynamic relationship

$$\Delta F_r^o = \Delta F^o_{products} - \Delta F^o_{reactants} \tag{7.6}$$

and by substituting ΔF^o values (taken from Garrels Christ, 1965) for the products and reactants in Equation 7.1,

$$0 + [4 \times 0] - [2 \times (-56.69)] = 113.4 \text{ kcal} \quad (7.7)$$

Substituting the answer of Equation 7.7 into Equation 7.5

$$E^o = 113.4/(4 \times 23.06) = 1.23 \text{ volts} \quad (7.8)$$

and by introducing the magnitude of E^o into Equation 7.4

$$Eh = 1.23 - 0.059\ pH \quad (7.9)$$

which describes the upper stability limit of H_2O (Figure 7.1).

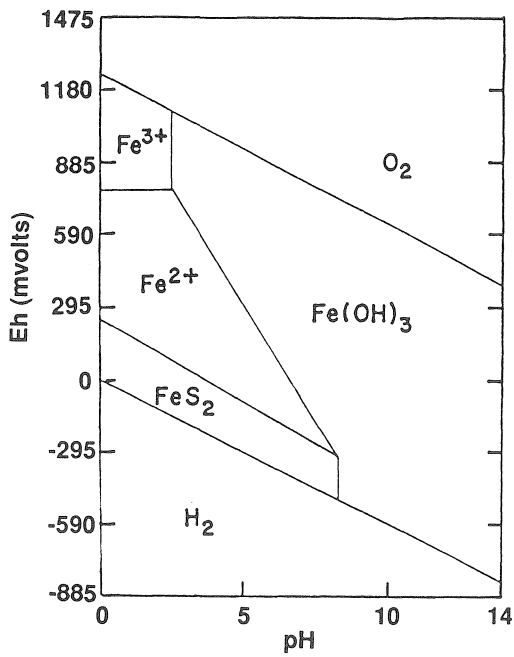

Figure 7.1. Stability relations of pyrite and $Fe(OH)_3$ in water at 25°C and 1 atmosphere total pressure. Activity of $SO_4^{2-}=10^{-3}$ *M*; activity of $Fe^{2+}=10^{-4}$ *M*. (After Brown, 1985. With permission.)

Similarly, for the lower stability limit of water described by the reaction

$$2H_2O = 2H_2(g) + O_2 \quad (7.10)$$

the equation is (Garrels and Christ, 1965)

$$Eh = (-0.059/2)\ \log pH_2 - 0.059\ pH \tag{7.11}$$

where pH_2 denotes the partial pressure of H_2 gas (Figure 7.1).

In a manner similar to the above, one may also derive equations describing the stability diagram of metals such as Fe. In this case, stability lines can be drawn using the equations describing upper and lower limits of H_2O, Fe^{2+}, Fe^{3+}, and $Fe(OH)_3$. The equations describing the system would be:

$$Fe^{2+} = Fe^{3+} + e^- \tag{7.12}$$

and

$$Fe^{2+} + 3H_2O = Fe(OH)_3 + e^- + 3H^+ \tag{7.13}$$

Similarly, one can add any number of additional solids such as, for example, pyrite,

$$FeS_2 + 8H_2O = 15e^- + 16H^+ + Fe^{3+} + 2SO_4^{2-} \tag{7.14}$$

and

$$Fe^{3+} + 3H_2O = Fe(OH)_3 + 3H^+ \tag{7.15}$$

The above Equations (7.12 - 7.15) can be solved simultaneously by trial and error or by any chemical equilibria computer simulation program, e.g., Geochem by Sposito and Mattigod (1979). The numbers generated from the simultaneous solution of the above equations can be plotted as an Eh-pH or pe-pH diagram (recall pe=Eh/0.059). An excellent discussion on generating boundary lines between phases for such diagrams is given by Garrels and Christ (1965). For the purpose of this book, some generalizations will be discussed to shed light on construction and utility of Eh-pH or pe-pH diagrams.

Reaction 7.12 shows the oxidation of Fe^{II} to Fe^{III} through loss of an e^-. Such a reaction can be expressed as

$$pe = p(Fe^{3+}/Fe^{2+}) \tag{7.16}$$

The above equation demonstrates that pe (or Eh) is related to the ratio of Fe^{3+} to Fe^{2+}. Therefore, for a constant $p(Fe^{3+}/Fe^{2+})$, pe or Eh would be represented by a horizontal line on the pe-pH or Eh-pH stability diagram (Figure 7.1). In the case of a redox reaction involving one H^+ per electron transfer as well as any solids and/or solution species with activity ratio of products and reactants equals 1, the reaction can be expressed as

$$pe + pH = pK^o \tag{7.17}$$

where pK^o is the negative logarithm of the equilibrium constant. The equilibrium constant can be obtained from the ΔF^o of the products/reactants involved, utilizing the following two classical thermodynamic relationships, i) $\Delta F_r^o = \Delta F^o_{products} - \Delta F^o_{reactants}$ (Equation 7.6) (note that e^- and H^+ do not contribute to the ΔF_r^o because their ΔF^o are set to zero by convention (Garrels and Christ, 1965)), and ii) under standard pressure and temperature (one atmosphere pressure at 25°C)

$$\Delta F_r^o = -1.364 \log K^o \qquad (7.18)$$

For additional information on these relationships see Garrels and Christ (1965), Lindsay (1979, 1981), Bartlett (1981), Blanchar and Marshall (1981), and Lowson (1982). Equation 7.17 reveals that a plot of Eh versus pH would produce a straight line with slope 59. This line, for example, could represent the boundary between two solid phases. Eh-pH values above or below the boundary line would suggest the potential transformation of one solid to the other.

Finally, in the case of Reaction 7.15, where electron transfer is not involved, classical K_{sp} relationships allow one to estimate Fe^{3+} at any given pH (see also Chapter 1). This relationship on an Eh or pe versus pH diagram is commonly shown as a vertical line (Figure 7.1) (Garrels and Christ, 1965).

In general, Eh-pH diagrams, such as the one shown in Figure 7.1, may be used to demonstrate if a particular geologic site is under pyrite oxidizing conditions or pyrite stabilizing conditions. The data in Figure 7.2 and 7.3 demonstrate examples of such conditions. Commonly, Eh-pH values falling within the boundaries of $Fe(OH)_3$ (see for example the data in Figure 7.2) represent acid mine drainage producing conditions (Ainsworth, 1979). A particular geologic material represented by such Eh-pH values would be under strong oxidative conditions or pyrite decomposing conditions, and all iron released, most likely, would precipitate as $Fe(OH)_3$. The experimental data in Figure 7.3, on the other hand, falling within the boundaries of Fe^{2+} or $Fe(OH)_3$ suggest that pyrite would decompose and the iron may be released as dissoved ferrous sulfate, or may precipitate as $Fe(OH)_3$. Finally, in the case where Eh-pH data fall within the boundaries of FeS_2 (Figure 7.3) pyrite would be considered under stabilizing conditions.

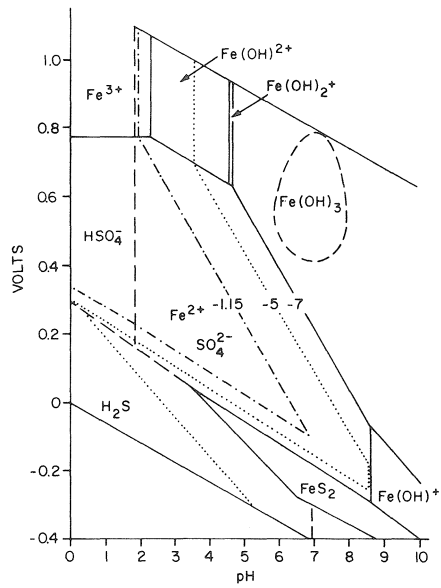

Figure 7.2. Iron and sulfur stability diagram with Eh and pH measurements taken at the 20 cm depth at some sites in Missouri. Stability fields taken from Loomis and Hood (1984); data, represented by broken line, are taken from Ainsworth (1979).

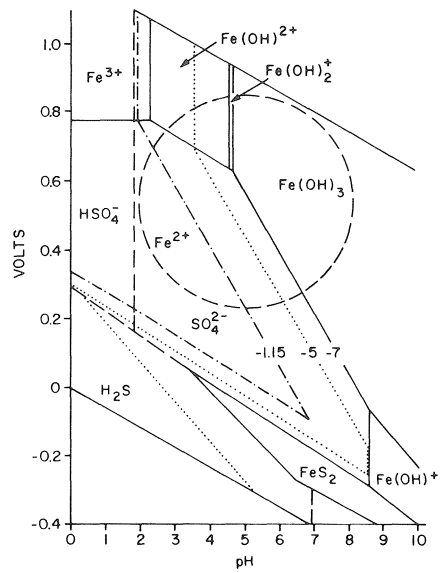

Figure 7.3. Iron and sulfur stability diagram with Eh and pH measurements taken at the 40 cm depth at some sites in Missouri. Stability fields taken from Loomis and Hood (1984); data, represented by broken line, are taken from Ainsworth (1979).

Commonly, stability diagrams rely on classical thermodynamic constants obtained from studies on pure minerals. Because of this, the use of stability diagrams in explaining potential field data behavior requires acceptance of some assumptions. For example, the solubility of a pure mineral can be related to the solubility of a similar mineral present in mine 'waste' as follows

$$K_{sp(\text{waste mineral})} = (\text{Fractional purity})(\text{Activity coefficient})(K_{sp(\text{pure mineral})}) \quad (7.19)$$

where fractional purity reflects presence of additional elements (impurities) in the mineral structure, and activity coefficient reflects degree to which the mineral is affected chemically by its impurities. As an example, assuming that one is interested is predicting the solubility of $CaCO_3$ in nature through a stability diagram, such a diagram could be constructed by assuming that the mineral is pure, permitting use of the classical thermodynamic K_{sp} to generate solubility data (see Chapter 1). Direct use of such a diagram to explain field data would be based on the assumption that fractional purity of field limestone equals 1 (for example, no other cation (M) has substituted for Ca^{2+} to form $CaM(CO_3)_2$) and solid phase activity coefficient also equals 1. However, since impurities would most likely be present (especially on the surface of waste-limestone particles), fractional purity would be less than 1 and the solid phase activity coefficient would be less or greater than 1, depending on the nature of metal substitution and how it has affected bonding strength between Ca^{2+} and CO_3^{2-}. This would need to be determined experimentally. In essence, mineral impurity may diminish the practical utility of the pure phase stability diagram since the K_{sp} of the mineral present in 'waste' would differ from the K_{sp} of the pure mineral. Additional limitations of theoretical stability diagrams include chemical coatings on minerals and chemical kinetics.

7.3 Eh Measurements

Eh measurements are commonly made with a platinum electrode and a calomel reference electrode connected to a volt meter. In general, most electronic pH meters are capable of measuring Eh. Although Eh measurements are believed to be based on sound scientific theory, the accuracy of field measurements is often questionable because a) the electrodes may react with gasses, e.g., O_2 or H_2S, introducing coatings of oxides or sulfides, b) measurements may represent complex values (mixed potentials) due to the heterogeneity of the solid material (e.g., waste, soils, etc.), c) moisture may influence Eh measurements, and d) Eh spatial variability is inherently large.

In addition to the general limitations of field Eh measurements pointed out above, Luther (1990) pointed out that platinum is an ideal

electron transfer medium whereas redox reactions in nature are affected because of specific localized electron transfer effects, steric effects, specific electron repulsion effects, and in general electron transfer 'bottle-necks'.

Based on the above limitations, one may find it difficult to assign absolute meaning to a given Eh measurement. However, field Eh measurements provide an excellent tool for detecting relative redox changes in the environment as a function of changing conditions, natural or human made, e.g., disturbed versus undisturbed environments.

Taylor & Francis
Taylor & Francis Group
http://taylorandfrancis.com

PART III

ROLE OF BACTERIA ON PYRITE OXIDATION

Taylor & Francis
Taylor & Francis Group
http://taylorandfrancis.com

Chapter 8
ROLE OF BACTERIA ON PYRITE OXIDATION

8.1 Mechanisms of Bacterial Pyrite Oxidation

Pyrite is an extremely insoluble mineral but it is well known that it is able to undergo dismutation. Dismutation is the process by which pyrite at low pH undergoes oxidation/reduction with one of its sulfur atoms acting as electron donor and the other sulfur atom acting as electron acceptor. The reaction is as follows:

$$FeS_2 + H^+ \text{---> } Fe^{2+} + HS^- + S^o \qquad (8.1)$$

The solubility product of Reaction 8.1 (see also Chapter 1) is 2×10^{-19} for $[Fe^{2+}][HS^-]$ at pH 2.3 (Morse et al., 1987). Lizama and Suzuki (1989) evaluated the kinetics of Reaction 1 and reported that the reaction was first-order with respect to pyrite with a slope of 3.5 mmoles L^{-1} Fe^{2+} per min per FeS_2 %PD (%PD = [g of pyrite per ml solution] x 100) (Table 8.1). Furthermore, the same researchers observed that in the presence of dead microbial cells the dismutation reaction approached a slope of zero. When the rate of dismutation without cells was compared to the rate of pyrite oxidation by *T. ferrooxidans*, it was determined that dismutation rate was only 0 to 5% of the bacterial rate (Lizama and Suzuki, 1989). The above imply that the dismutation reaction most likely contributes little to pyrite dissolution in nature.

Mechanisms of bacterial pyrite oxidation have mainly been derived from investigations of metal bioleaching. The most widely studied pyrite-oxidizing bacterium is *T. ferrooxidans*. *T. ferrooxidans* is an obligate chemoautotrophic and acidophilic and it is now well established that it is able to oxidize Fe^{2+}, S^o, and metal sulfides, as well as other reduced inorganic sulfur compounds. *T. Thiooxidans* has also been isolated from acid mine wastes and has been studied extensively with respect to its pyrite oxidation potential. It has been determined that *T. thiooxidans* can oxidize both elemental sulfur and sulfide to sulfuric acid ($S^o + 1.5O_2 + H_2O \text{ -> } H_2SO_4$ and $S^{2-} + 2O_2 + 2H^+ \text{ -> } H_2SO_4$) (Brierley, 1982; Lundgren and Silver, 1980). But unlike *T. ferrooxidans*, *T. thiooxidans* cannot oxidize Fe^{2+} (Harrison, 1984).

The mechanisms of bacterial pyrite oxidation have been studied extensively (Gormely et al., 1975; Chang and Myerson, 1982; Konishi et al., 1990; Mustin et al., 1992; Wakao et al., 1982, 1983, 1984) and the results have been discussed and summarized in a number of articles (Ehrlich, 1964; Lundgren et al., 1972; Nordstrom, 1982a). Generally, the mechanisms of pyrite oxidation by bacteria are classified into a) direct metabolic reactions and b) indirect metabolic reactions. Direct metabolic reactions require physical contact between bacteria and pyrite particles, while indirect

Table 8.1. Summary of various reaction rates[a]. After Lizama and Suzuki (1989), with permission

	Reaction no. and type	Rate equation	Constants
(1)	Spontaneous	$v = k[FeS_2]$	$k = 3.5$ mM Fe^{2+}/min per FeS_2 % PD
(2)	Indirect leaching	$v = \frac{k_p[Fe^{3+}][FeS_2]}{K_m + [FeS_2]}$	$k_p = 10$ mM Fe^{2+}/min per mM Fe^{3+} $K_m = 1.9\%$ PD FeS_2
(3)	*T. ferrooxidans* washed FeS_2	$v = \frac{k_p[cell][FeS_2]}{K_m[FeS_2]}$	$k = 90$ mM O_2/min per mg of cells per ml $K_m = 2.5\%$ PD FeS_2
(4)	*T. ferrooxidans* unwashed FeS_2	$v = \frac{k_p[cell][FeS_2]}{K_m(1 + [cell]/K_i) + [FeS_2]}$	$k_p = 250$ mM O_2/min per mg of cells per ml $K_m = 2.75\%$ PD FeS_2 $K_i = K_{eq}' = 0.13$ mg of cells/ml
(5)	*T. ferrooxidans* Fe^{2+} oxidation	$v = \frac{k_p'[cell][Fe^{2+}]}{K_m(1 + [cell]/K_i + [Fe^{2+}]}$	$k_p' = 125$ mM O_2/min per mg of cells per ml $K_m = 110$ mM Fe^{2+} $K_i = K_{eq}' = 0.33$ mg of cells/ml

[a] $[FeS_2]$, Pyrite concentration in % PD; $[Fe^{3+}]$, Fe^{3+} concentration (millimolar); [cell], cell concentration in milligrams of wet cells per milliliter; $[Fe^{2+}]$, Fe^{2+} concentration (micromolar).
FeS_2 %PD (%PD = [g of pyrite per ml solution] x 100).

metabolic reactions do not require physical contact. Under indirect metabolic reactions, bacteria oxidize Fe^{2+} to Fe^{3+}, thereby regenerating the Fe^{3+} required for the chemical oxidation of pyrite (Singer and Stumm, 1970). More details on direct and indirect metabolic pyrite oxidation are given in the reactions below without considering complete mass or charge balance.

8.1.1 Direct metabolic oxidation

According to Torma (1988) and references therein, direct metabolic pyrite oxidation can be given by

$$FeS_2 + O_2 \xrightarrow{\text{Bacteria}} Fe^{2+} + 2SO_4^{2-} + H^+ \quad (8.2)$$

Reaction 8.2 consists of dissolution of iron disulfide (FeS_2) as shown in Reaction 8.3 below

$$FeS_2 \rightarrow Fe^{2+} + S_2^{2-} \quad (8.3)$$

and the released disulfide anion is immediately bound by bacterial enzymes and is oxidized to sulfate as shown by Reaction 8.4 (Torma, 1988; Silver, 1978).

$$S_2^{2-} + 4O_2 \xrightarrow{\text{Bacteria}} 2SO_4^{2-} \quad (8.4)$$

Theoretically, the process described by Reactions 8.3 and 8.4 can be continued until all disulfide is converted to sulfate. Konishi et al. (1990), suggested that direct microbial pyritic sulfur oxidation to sulfate was due to multiplication of *T. ferrooxidans* on pyrite surface using pyritic sulfur as nutrient. Konishi et al. (1990) however, did not mention if dissolution of the disulfide mineral occurred prior to microbial oxidation of the disulfide anion. Palencia et al. (1991) suggested that pyrite is directly attacked by oxidizing bacteria according to Reaction 8.5 shown below

$$4FeS_2 + 15O_2 + 2H_2O \rightarrow 2Fe_2(SO_4)_3 + 2H_2SO_4 \quad (8.5)$$

Reaction 8.5 is the sum of the bacteria-catalyzed oxidation of sulfur and iron by O_2.

Attachment of *T. ferrooxidans* to the pyrite/surface and consequent oxidative corrosion have been investigated by many workers (Wakao et al., 1982, 1983, 1984; Chang and Myerson, 1982; Konishi et al., 1990; Mustin et al., 1992; Bennett and Tributsch, 1978). Bennett and Tributsch (1978) confirmed that the chemical processes taking place on the pyrite surface due to oxidizing bacteria occur mainly in the region of contact between bacteria and pyrite. The same authors also suggested that bacterial distribution on the pyrite surface are critically dependent on crystal structure and on diversity in

the crystal orders (fracture lines, dislocations) of the pyrite. Konishi et al., (1990) indicated that *T. ferrooxidans* may multiply on the pyrite surface as well as in the liquid phase. Their data on dissolution kinetics of pyrite by *T. ferrooxidans* in a batch reactor indicated that the concentration of bacteria in the liquid phase could be related to the concentration of bacteria adsorbed on to the pyrite surface. Observations by scanning electron microscopy of pyrite particles inoculated with *T. ferrooxidans* revealed appearance of corrosion, cracks, and small pits on pyrite surfaces. Mustin et al. (1992) indicated that the specific surface areas of pyrite before and after bioleaching were 1.1 m^2 g^{-1} and 1.6 m^2 g^{-1}, respectively. Thus, bacterial oxidation increased porosity and specific surface in pyrite grains.

8.1.2 Indirect metabolic oxidation

In the case of indirect metabolic oxidation (Torma, 1988 and references therein), pyrite is chemically oxidized by Fe^{3+} according to Reactions 8.6 and 8.7 shown below

$$FeS_2 + Fe_2(SO_4)_3 \rightarrow 3FeSO_4 + 2S^o \quad (8.6)$$

and

$$2S^o + 6Fe_2(SO_4)_3 + 8H_2O \rightarrow 12FeSO_4 + 8H_2SO_4 \quad (8.7)$$

Ferrous iron and elemental sulfur, S^o, produced by these chemical reactions are oxidized by *T. ferrooxidans*, thus regenerating Fe^{3+} and acid. These oxidation reactions may take place on the pyrite surface or in the interstitial solution and are as follows:

$$4FeSO_4 + 2O_2 + 2H_2SO_4 \rightarrow 2Fe_2(SO_4)_3 + 2H_2O \quad (8.8)$$

and

$$2S^o + 3O_2 + 8H_2O \rightarrow 2H_2SO_4 \quad (8.9)$$

The role of bacteria in oxidizing pyrite can, therefore, be seen as indirect in which their function is to regenerate Fe^{3+}, the major pyrite oxidant. Reactions 8.5 and 8.6 have been found to occur in sterile environments; inoculated environments and anaerobic environments. Note that the sum of Reactions 8.6 and 8.7 (which is Reaction 4.4, see Chapter 4) is the common way to describe oxidation of pyrite by Fe^{3+}, through pyrite dissolution mainly by Reaction 8.6, oxidation of part of S^o by Fe^{3+} through Reaction 8.7, reoxidation of Fe^{2+} by Reaction 8.8 and oxidation of the remaining S^o by Reaction 8.9 (LeRoux et al., 1980; Silverman, 1967).

Relative contributions by each of the mechanisms of direct and indirect metabolic pathways to pyrite oxidation remain disputed. Silverman (1967) reported that the two mechanisms of pyrite oxidation may operate concurrently. On the other hand, Carranza (1983) reported that the direct metabolic contact mechanism is the main operative mechanism for oxidation

of pyrite in the presence of *T. ferrooxidans*. Wakao et al. (1982, 1983, and 1984) indicated that concentration of *T. ferrooxidans* in an aqueous phase, rather than on the surface of pyrite particles, plays a major role in enhancing pyrite oxidation through the indirect metabolic pathway. They based their conclusion on their own observation that cells of *T. ferrooxidans* adsorbed onto pyrite surface did not proliferate and their oxidizing activity was strongly inhibited.

8.2 Kinetics of Bacterially Mediated Oxidation of Fe^{2+}

Pesic et al. (1989) using an electrochemical method to measure the oxidation rate of Fe^{2+} to Fe^{3+} by O_2 in the presence of *T. ferrooxidans* determined that the rate is directly proportional to the concentration of bacteria, Fe^{2+}, O_2 and H^+. They also reported that above pH 2.2 oxidation of Fe^{2+} was governed by the following rate expression:

$$-d[Fe^{2+}]/dt = [1.62][10^{11}][C_{bact}][H^+][Fe^{2+}][^{P}O_2]e^{-(58.77/RT)} \qquad (8.10)$$

where C_{bact} denotes bacteria concentration, T is absolute temperature, and R is the universal gas constant. Below pH 2.2, the rate expression is the same as the one above pH 2.2 except that it is independent of pH.

The half-time, the time required to achieve 50% conversion of initial reactant, can be used to demonstrate the importance of pH and *T. ferrooxidans* during oxidation of Fe^{2+} with O_2. The halftime of 0.001 mol L^{-1} Fe^{2+} in an abiotic system, was found to be 2.86 days at pH 5.5, 286 days at pH 4.5, and 3740 days at pH 1.45. This indicated that abiotic oxidation of Fe^{2+} with O_2 was extremely pH sensitive. The reaction was rapid above pH 5, and became extremely slow in very acidic solution. But, in the presence of *T. ferrooxidans* the halftime was much shorter, even under acidic conditions. It took only 31 min and 7.8 min to react 50% of 0.001 M Fe^{2+} in the presence of 1.5 mg and 6.0 mg (dry weight) of *T. ferrooxidans*, respectively (Pesic et al., 1989 and references therein).

It is generally accepted that the Michaelis-Menten equation can be used to explain the rate of biological Fe^{2+} oxidation (see section 8.3). This was demonstrated by Suzuki et al. (1989) who studied the oxidation of Fe^{2+} to Fe^{3+} with O_2 by various strains and cell concentrations of *T. ferrooxidans*. They found that the Michaelis-Menten constant (K_m) values remained the same at different cell concentrations of laboratory strains but increased with increasing cell concentrations of mine isolates. They suggested that competitive inhibition of the Fe^{2+}-binding site of a cell by other cells in the reaction mixture explained the behavior of the mine isolates. In the case of the Michaelis-Menten data by Suzuki et al. (1989), K_m refers to the concentration of the substrate, Fe^{2+}, at which the rate (v) of the oxidation reaction equals one half of maximum v ($1/2V_{max}$). Therefore, the higher the K_m, the lower the affinity of the bacteria for the Fe^{2+}. Suzuki et al. (1989)

reported Fe^{2+} K_m values for *T. ferrooxidans* in the range of 0.1 to 0.8 mmol L^{-1}. Commonly, such K_m values reported in the literature vary from 0.43 mmol L^{-1} to 9.4 mmol L^{-1} of Fe^{2+} (Suzuki et al., 1989 and references therein).

As pointed out above, bacteria appear to play a very important role in pyrite oxidation through oxidation of Fe^{2+} to Fe^{3+}. The latter is a strong pyrite oxidant. For this reason, pyrite oxidation kinetics are strongly linked to Fe^{2+} oxidation (Jaynes et al., 1984) and bacterial activity. Jaynes et al. (1984) reviewed and summarized the conditions under which *T. ferrooxidans* activity is optimized. The data in Figure 8.1 show that optimum temperature for *T. ferrooxidans* is around 30°C.

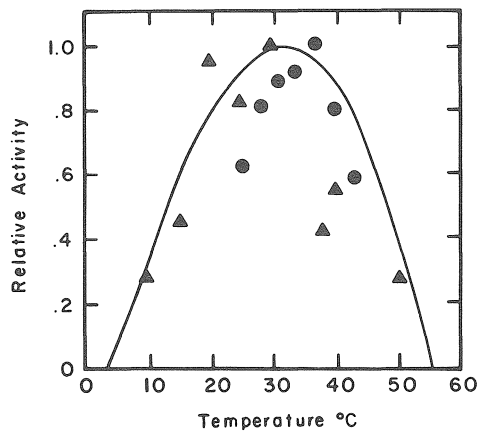

Figure 8.1. Influence of temperature on relative activity of *T. ferrooxidans*. (From Jaynes et al., 1984. With permission.)

Bacteria activity diminishes greatly above and below that temperature, reaching a minimum at approximately 5°C and 55°C.

The data in Figure 8.2 show that *T. ferrooxidans* (obligate aerobes) activity ceases when O_2 is depleted. However, bacterial activity resumes even under extremely small increases in O_2 content and reaches maximum at approximately 0.01 mole fraction of O_2 or 1%. Influence of pH on *T. ferrooxidans* is shown in Figure 8.3. Maximum activity is reached around pH 3.2 whereas minimum activity is reached at approximately pH 1.5 and pH 5. Jaynes et al. (1984) linked the above behavior to pH due to the fact that at pH below 2.5, physiological limitations of bacteria diminish their potential to oxidize Fe^{2+} whereas above pH 3.5 pyrite oxidation rate is limited by the decreasing solubility of $Fe(OH)_3$.

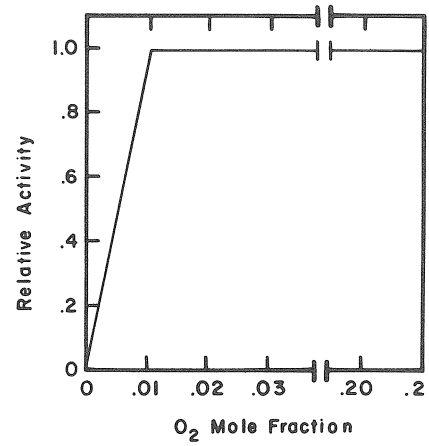

Figure 8.2. Influence of O_2 concentration on relative activity of *T. ferrooxidans*. (From Jaynes et al., 1984. With permission.)

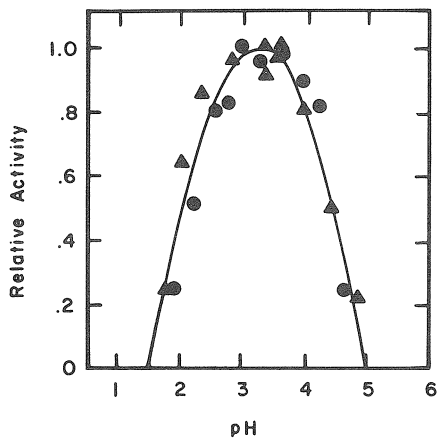

Figure 8.3. Influence of pH on relative activity of *T. ferrooxidans*. (From Jaynes et al., 1984. With permission.)

The influence of pH and temperature on pyrite oxidation as reported by Jaynes et al. (1984) is demonstrated in Figures 8.4 and 8.5. The data in Figure 8.4 show pyrite oxidation progress in mine waste at 21°C and pH 3 (pH of maximum bacterial activity) in the presence and absence of bacteria. It is clearly shown that bacteria catalyze the oxidation of pyrite. The data in Figure 8.5 show pyrite oxidation progress in mine waste at 6°C and pH 3.

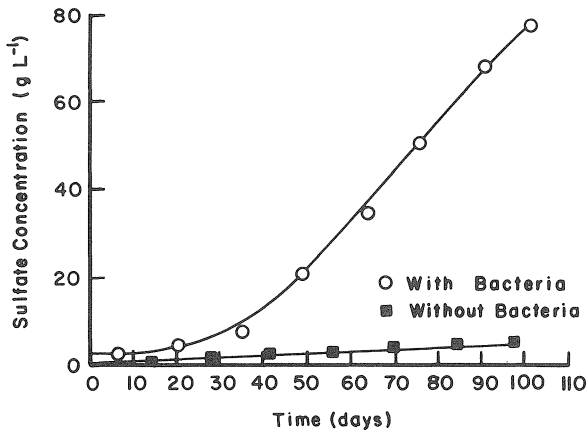

Figure 8.4. Pyrite oxidation kinetics in mine waste at 21°C and pH 3 in the presence and absence of bacteria. (From Scharer et al., 1991).

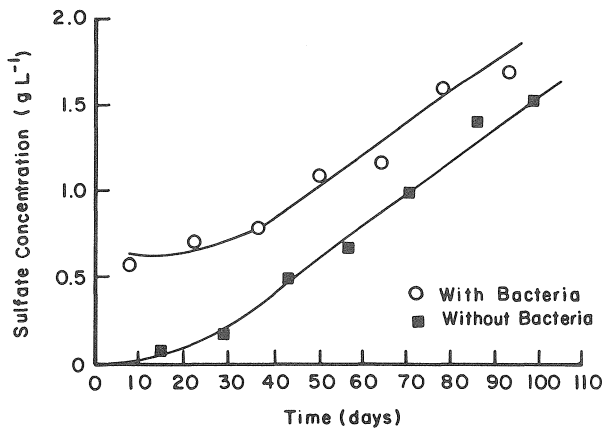

Figure 8.5. Pyrite oxidation kinetics in mine waste at 6°C and pH 3 in the presence and absence of bacteria. (From Scharer et al., 1991).

These data reveal that after 40 days the rate of pyrite oxidation was the same in the presence or absence of bacteria. These observations demonstrate that bacterial activity is indeed temperature dependent and bacterial activity is involved in pyrite oxidation. Note that under optimum conditions for bacterial activity pyrite oxidation rate (Figure 8.4) is much greater than that under limiting conditions of bacterial activity (Figure 8.5).

Based on the above, pyrite oxidation is greatly reduced at pH above 4.5. For this reason, limestone application in the field for controlling pyrite oxidation is recommended. However, there is evidence to show that pyrite oxidation accelerates at pH values near neutral to alkaline (see Chapter 6).

8.3 Michaelis-Menten Kinetics

The Michaelis-Menten mathematical expression provides the potential to describe/predict rates of enzymatic reactions. An advantage of the Michaelis-Menten expression over other expressions is that the former is consistent with molecular reaction processes. Commonly, the reactants/participants involve an enzyme and a substrate. The enzyme can also be equated to a surface with reaction-catalyzing potential. Michaelis-Menten kinetics are based on the consideration that the concentration of enzyme reactive centers is constant and small compared with the concentration of reactants with which they may combine. The enzyme/surface reacts with the substrate to form a complex (described by the Langmuir adsorption isotherm, Epstein, 1972) leading to the generation and detachment of the product from the enzyme/surface; the enzyme/surface is then regenerated (Epstein and Hagen, 1952 and references therein).

The Michaelis-Menten equation allows estimation of the so called adjustable parameters through graphical representation of appropriate experimental data (Segel, 1976). The adjustable parameters include 1) the K_m (in units of concentration) which denotes affinity of the substrate by the enzyme/surface, 2) V_{max} (in units of product quantity per unit surface per unit time, or quantity of product per unit time) which denotes maximum rate of product formation, and 3) K_i or K_{eq} which denotes inhibitor constant describing solution-enzyme/surface equilibrium between the substrate and any other solution component that may compete with the substrate for enzyme/surface sites.

Kinetics of pyrite oxidation is most certainly a surface controlled reaction (see Chapter 6). Michaelis-Menten equations describing pyrite oxidation may be developed in accordance with a) attachment of bacteria to the pyrite surface (direct metabolic approach; see section 8.1.1), and b) bacterial pyrite oxidation through oxidation of Fe^{2+} to Fe^{3+} (indirect metabolic approach; see section 8.1.2). In the first approach (direct metabolic), pyrite serves as the substrate and the microbes serve as the enzyme/surface. In the second approach (indirect metabolic), Fe^{3+} (regenerated by microbes) serves as the substrate whereas pyrite itself serves as the catalyzing surface for reducing Fe^{3+} to Fe^{2+}. In the first approach K_m represents pyrite concentration in suspension, while in the second approach, K_m represents Fe^{3+} concentration in suspension. Note that pyrite can not be considered a true catalyst since during Fe^{3+} reduction pyrite undergoes oxidation. Therefore, characterization of pyrite/surface as catalyst is strictly an assumption applying only for relatively short oxidation periods or for

relatively small quantities of pyrite consumed in relationship to the original amount of pyrite introduced in the reaction vessel.

In accordance with Michaelis-Menten theory, pyrite oxidation can be described as a three-step process. The first step involves the displacement of an inert (nonelectron-accepting) species from the pyrite/surface by an oxidant. The inert species could be any divalent metal, e.g., Fe^{2+}, or any natural or anthropogenic polar organic compound. The oxidant could be any surface competing species with electron accepting potential, e.g., Fe^{3+}. It is assumed that the pyrite/surface $-S_2^-$ is the site of competition between the two species (inert versus oxidant) for the unshared $-S_2^-$ electron pair (see Chapter 6). The second step involves formation of an activated pyrite/surface complex (Daniels and Alberty, 1975; Moore, 1972). Formation of this complex allows the transfer of the $-S_2^-$ unshared pair of electrons to the oxidant, e.g., Fe^{3+}, leading to formation of thiosulfate and Fe^{2+} (thiosulfate is then oxidized to sulfate, SO_4^{2-}). The third step involves detachment of thiosulfate from the pyrite/surface. If thiosulfate detachment is slower than formation of the surface activated complex plus electron transfer, then the former would be the rate controlling step in the pyrite oxidation process. On the other hand, if thiosulfate detachment is faster than formation of the activated complex plus electron transfer, then the latter would be the rate controlling step. Commonly, in Michaelis-Menten type reactions formation of the activated complex plus electron transfer are considered to be the rate controlling processes (Lizama and Suzuki, 1989).

Below, derivation of a binary competitive interaction is demonstrated using the pyrite-surface to quantify formation dynamics of the pyrite/surface activated complex. A binary competitive interaction can be expressed as follows:

$$Fe^{II}{:}S_1\text{-}S_2{:}A + B^{b+} \underset{k_{-1}}{\overset{k_1}{=}} Fe^{II}{:}S_1\text{-}S_2{:}B + A^{a+} \qquad (8.11)$$

where:

$Fe^{II}:S_1\text{-}S_2:$ = adsorbing pyrite surface,
A^{a+}, B^{b+} = surface competing cations,
$Fe^{II}:S_1\text{-}S_2:A$, $Fe^{II}:S_1\text{-}S_2:B$ = surface complexes,
k_1 = rate constant for the forward reaction and,
k_{-1} = rate constant for the backward reaction.

In the case of pyrite oxidation, A^{a+} and B^{b+} can be assigned to Fe^{2+} and Fe^{3+}, respectively (Garrels and Thompson, 1960). Note also, however, that reference to cations A^{a+} and B^{b+} does not imply that pyrite may react only with cations. The pyrite surface is a soft Lewis base and would react with any soft Lewis acid that is willing to accept or share electrons (Luther, 1990). Reaction 8.11 is composed of two reactions: A forward one,

$$Fe^{II}{:}S_1\text{-}S_2{:}A + B^{b+} \xrightarrow{k_1} Fe^{II}{:}S_1\text{-}S_2{:}B + A^{a+} \quad (8.12)$$

and a backward one,

$$Fe^{II}{:}S_1\text{-}S_2{:}B + A^{a+} \xrightarrow{k_{-1}} Fe^{II}{:}S_1\text{-}S_2{:}A + B^{b+} \quad (8.13)$$

When the rate of the forward reaction equals the rate of the backward reaction a chemical equilibrium state is met, and

$$K_{eq} = (k_1/k_{-1}) = \frac{[Fe^{II}{:}S_1\text{-}S_2{:}B][A^{a+}]}{[Fe^{II}{:}S_1\text{-}S_2{:}A][B^{b+}]} \quad (8.14)$$

where K_{eq} is the selectivity coefficient. Assuming that A^{a+} is an inhibitor and $Fe^{II}{:}S_1\text{-}S_2{:}B$ is the activated complex, the latter can be predicted by rearranging Equation 8.14 (Evangelou and Phillips, 1987, 1988) such that

$$Fe^{II}{:}S_1\text{-}S_2{:}B = \frac{[Fe^{II}{:}S_1\text{-}S_2{:}_{max}][B^{b+}/A^{a+}]}{[1/K_{eq} + B^{b+}/A^{a+}]} \quad (8.15)$$

where $Fe^{II}{:}S_1\text{-}S_2{:}_{max}$ denotes maximum pyrite/surface reactive sites. When K_{eq} equals 1, the pyrite surface would show no preference for either A^{a+} or B^{b+}, whereas when K_{eq} is less than 1, the surface prefers B^{b+}, and when K_{eq} is greater than 1, the surface prefers A^{a+} (Evangelou and Phillips, 1987, 1988; Evangelou et al., 1994). Moses and Herman (1991) postulated that the pyrite/surface should prefer Fe^{2+} instead of Fe^{3+}. The reason is that the pyrite/surface is a soft Lewis base (willing to share its unpaired electrons) and would react stronger with a soft Lewis acid. Reduced iron (Fe^{2+}) is a relatively softer Lewis acid than Fe^{3+}. In any case, the $Fe^{3+} - Fe^{2+}$ exchange K_{eq} on pyrite/surface needs to be quantified in order to demonstrate that the proportionality of these two cations in the solution phase reflects the proportionality of the two cations on the pyrite/surface (Garrels and Thompson, 1960). Recall that the Fe^{3+}/Fe^{2+} ratio on the pyrite/surface is representative of the activation complex. Fornasiero et al. (1992) studied pyrite/surface-Fe^{3+} stability constants using electrophoretic mobility. He pointed out that as Fe^{3+} hydroxylates, it is preferred by the pyrite surface, perhaps because of entropy effects (better physical fit). However, Fornasiero et al. (1992) did not investigate $Fe^{3+}(H_2O)_{6-n}OH_n^{3-n} - Fe^{2+}$ exchange equilibrium constants (K_{eq}).

Equation 8.15 reveals that the magnitude of the activation complex depends on magnitude of $Fe^{II}\text{-}S_1\text{-}S_2{:}_{max}$, K_{eq}, and ratio between substrate and inhibitor. The above imply that under equilibrium considerations activation

complex magnitude is predictable. In the case where equilibria is not met, one may employ the steady-state approach to make activation complex predictions. Moreover, in order to put the activation complex to practical use, it is important that it is linked mathematically to product formation. This is carried out below.

8.3.1 Michaelis-Menten steady-state

Generally speaking, interpretation of equations describing chemical processes is dependent on the assumptions made in deriving such equations. In the case of kinetics of exchange reactions, two different equations can be derived on the basis of a) *steady-state* assumption, attained under non-equilibrium conditions, and b) *rapid equilibrium* assumption, attained under rapid surface (enzyme)-substrate equilibrium conditions.

In the case of a *steady-state* assumption, attained under non-equilibrium conditions, for a binary cation exchange reaction describing formation of the activated complex, the kinetic expression describing formation of product B_p can be written as follows:

$$Fe^{II}{:}S_1\text{-}S_2{:}A + B^{b+} \underset{k_{-1}}{\overset{k_1}{=}} A^{a+} + Fe^{II}{:}S_1\text{-}S_2{:}B \xrightarrow{k_p} B_p \qquad (8.16)$$

where k_p = rate constant of product B_p formation. In the case of biotic pyrite oxidation, B_p can be experimentally determined by considering it to represent O_2 or Fe^{3+} consumption, or Fe^{2+} and/or solution sulfur species production (see also Chapter 6). Assuming that reaction B_p ---> $Fe^{II}{:}S_1\text{-}S_2{:}B$ is limited by the rapid removal of product B_p, the reaction rate can be expressed by

$$d[Fe^{II}{:}S_1\text{-}S_2{:}B]/dt = k_1\,[Fe^{II}{:}S_1\text{-}S_2{:}A][B^{b+}] - k_{-1}[Fe^{II}{:}S_1S_2{:}B][A^{a+}] - k_p[Fe^{II}{:}S_1\text{-}S_2{:}B] \qquad (8.17)$$

Under steady state considerations

$$d[Fe^{II}{:}S_1\text{-}S_2{:}B]/dt = k_1[Fe^{II}{:}S_1\text{-}S_2{:}A][B^{b+}] - k_{-1}[Fe^{II}{:}S_1\text{-}S_2{:}B][A^{a+}] - k_p[Fe^{II}{:}S_1\text{-}S_2{:}B] = 0 \qquad (8.18)$$

By rearranging Equation 8.18 as shown below

$$k_1[Fe^{II}{:}S_1\text{-}S_2{:}A][B^{b+}] = Fe^{II}{:}S_1\text{-}S_2{:}B[k_{-1} + k_p] \qquad (8.19)$$

collecting terms and rearranging again,

$$k_1/[k_{-1} + k_p] = [Fe^{II}{:}S_1\text{-}S_2{:}B]/[Fe^{II}{:}S_1\text{-}S_2{:}A][B^{b+}] \qquad (8.20)$$

where

$$k_1/[k_{-1} + k_p] = 1/k_d. \qquad (8.21)$$

and

$$K_m = k_d = [k_{-1} + k_p]/k_1 \tag{8.22}$$

Note that A^{a+} is omitted from Equation 8.19 recognizing that this omission makes the experimental constants conditional. Considering that

$$Fe^{II}{:}S_1\text{-}S_2{:}_{max} = [Fe^{II}{:}S_1\text{-}S_2{:}A] + [Fe^{II}{:}S_1\text{-}S_2{:}B] \tag{8.23}$$

where $Fe^{II}{:}S_1\text{-}S_2{:}_{max}$ = maximum number of adsorption sites capable of forming $Fe^{II}{:}S_1\text{-}S_2{:}B$; substituting $Fe^{II}{:}S_1\text{-}S_2{:}A$ of Equation 8.23 by the expression

$$[Fe^{II}{:}S_1\text{-}S_2{:}A] = [Fe^{II}{:}S_1\text{-}S_2{:}B][k_d]/[B^{b+}] \tag{8.24}$$

(obtained from Equations 8.20 and 8.21) and rearranging gives

$$[Fe^{II}{:}S_1\text{-}S_2{:}B] = [Fe^{II}{:}S_1\text{-}S_2{:}_{max}][B^{b+}]/(k_d + [B^{b+}]) \tag{8.25}$$

The rate function describing generation of product B_p with respect to time is given by

$$d[B_p]/dt = V_{Bp} = k_p[Fe^{II}{:}S_1\text{-}S_2{:}B] \tag{8.26}$$

By substituting Equation 8.25 into Equation 8.26 and rearranging, rate of B_p production (V_{Bp}) is given by

$$V_{Bp} = \frac{k_p[Fe^{II}{:}S_1\text{-}S_2{:}_{max}][B^{b+}]}{(k_d + [B^{b+}])} \tag{8.27}$$

In the case of biotic pyrite oxidation, rate of B_p production (V_{Bp}) is considered to be at maximum (V_{Bpmax}) when $B^{b+} >>> k_d$. Thus,

$$V_{Bpmax} = k_p[Fe^{II}{:}S_1\text{-}S_2{:}_{max}] \tag{8.28}$$

and Equation 8.27 takes the form of

$$V_{Bp} = V_{Bpmax}[B^{b+}]/(k_d + [B^{b+}]) \tag{8.29}$$

A plot of V_{Bp} versus B^{b+} produces a curvilinear line asymptotically approaching V_{Bpmax} (Evangelou and Phillips, 1987). In the case of microbial pyrite oxidation one may substitute V_{Bpmax} by $[k_p]$[No. of bacterial cells] (Lizama and Suzuki, 1989).

8.3.2 Michaelis-Menten rapid equilibrium

When Equation 8.11 approaches rapid equilibrium, the expression describing formation of product B_p takes the form

$$Fe^{II}{:}S_1\text{-}S_2{:}A + B^{b+} \underset{k_{-1}}{\overset{k_1}{=}} A^{a+} + Fe^{II}{:}S_1\text{-}S_2{:}B \xrightarrow{k_p} B_p \qquad (8.30)$$

Assuming that the formation rate of $Fe^{II}{:}S_1\text{-}S_2{:}B$ is much greater than the formation rate of B_p, the rate expression for $Fe^{II}{:}S_1\text{-}S_2{:}B$ formation can be given by

$$d[Fe^{II}{:}S_1\text{-}S_2{:}B]/dt = k_1[Fe^{II}{:}S_1\text{-}S_2{:}A][B^{b+}] - k_{-1}[Fe^{II}{:}S_1\text{-}S_2{:}B][A^{a+}] \qquad (8.31)$$

Under the condition

$$d[Fe^{II}{:}S_1\text{-}S_2{:}B]/dt = 0 \qquad (8.32)$$

Equation 8.31 can be rearranged to

$$k_1/k_{-1} = [Fe^{II}{:}S_1\text{-}S_2{:}B][A^{a+}]/[Fe^{II}{:}S_1\text{-}S_2{:}A][B^{b+}] \qquad (8.33)$$

where

$$k_1/k_{-1} = K_{eq} \qquad (8.34)$$

Considering that

$$Fe^{II}{:}S_1\text{-}S_2{:}_{max} = [Fe^{II}{:}S_1\text{-}S_2{:}A] + [Fe^{II}{:}S_1\text{-}S_2{:}B] \qquad (8.35)$$

by substituting component $Fe^{II}{:}S_1\text{-}S_2{:}A$ of Equation 8.35 by the expression derived from Equations 8.33 and 8.34, gives

$$Fe^{II}{:}S_1\text{-}S_2{:}A = \frac{[Fe^{II}{:}S_1\text{-}S_2{:}_B][A^{a+}]}{(K_{eq}\,[B^{b+}])} \qquad (8.36)$$

and upon rearranging Equation 8.36 to solve for $Fe^{II}{:}S_1\text{-}S_2{:}B$

$$Fe^{II}{:}S_1\text{-}S_2{:}B = Fe^{II}{:}S_1\text{-}S_2{:}_{max}/\{1+(1/K_{eq})([A^{a+}]/[B^{b+}])\} \qquad (8.37)$$

Considering that the concentration of $Fe^{II}{:}S_1\text{-}S_2{:}B$ controls the formation rate of B_p

$$d[B_p]/dt = V_{Bp} = k_p[Fe^{II}{:}S_1\text{-}S_2{:}B] \qquad (8.38)$$

and by substituting Equation 8.37 into Equation 8.38, produces

$$V_{Bp} = \{k_p\, Fe^{II}{:}S_1\text{-}S_2{:}_{max}([B^{b+}]/[A^{a+}])\}/\{(1/K_{eq}) + ([B^{b+}]/[A^{a+}])\} \qquad (8.39)$$

In the case of biotic pyrite oxidation, rate of B_p production (V_{Bp}) is considered to be at maximum (V_{Bpmax}) when B^{b+} is much larger than A^{a+} and $([B^{b+}]/[A^{a+}])>>>1/K_{eq}$. Thus,

$$V_{Bp} = k_p[Fe^{II}{:}S_1\text{-}S_2{:}_{max}] = V_{Bpmax} \tag{8.40}$$

and by substituting Equation 8.40 into Equation 8.39

$$V_{Bp} = \{V_{Bpmax}([B^{b+}]/[A^{a+}])\}/\{(1/K_{eq}) + ([B^{b+}]/[A^{a+}])\} \tag{8.41}$$

or

$$V_{Bp} = \{V_{Bpmax}([B^{b+}]/[A^{b+}])\}/\{[B^{b+}] + ([A^{a+}]/[K_{eq}])\} \tag{8.42}$$

Note also that,

$$1/K_{eq} = k_{-1}/k_1 = K_m' = k_d' \tag{8.43}$$

and

$$K_m = k_d = k_{-1}/k_1 + k_p/k_1 \tag{8.44}$$

or

$$K_m = k_d = 1/K_{eq} + k_p/k_1 \tag{8.45}$$

Therefore, a rapid equilibrium steady-state K_m' or k_d' differs from that of a non-equilibrium steady-state K_m by the term k_p/k_1 (see Equation 8.45). Note also that K_m is related to K_{eq} inversely. When K_m increases, affinity of the surface (enzyme) for the substrate decreases, whereas when K_{eq} increases, affinity of the surface (enzyme) for the substrate also increases.

Equations 8.29 and 8.42, however, have identical solutions. When they are plotted in the form of V_{Bp} versus B^{b+} they produce curvilinear plots asymptotically approaching V_{Bpmax}. These equations can be linearized by taking their inverse (see section *8.4.4*). Thus, Equation 8.29 transforms to

$$\frac{1}{V_{Bp}} = \frac{1}{V_{Bpmax}} + \frac{k_d}{V_{Bpmax}} \cdot \frac{1}{[B^{b+}]} \tag{8.46}$$

and Equation 8.42 transforms to

$$\frac{1}{V_{Bp}} = \frac{1}{V_{Bpmax}} + \frac{[A^{a+}]}{K_{eq}V_{Bpmax}} \cdot \frac{1}{[B^{b+}]} \tag{8.47}$$

The double reciprocal plots of Equations 8.46 and 8.47 ($1/V_{Bp}$ versus $1/B^{b+}$) produce linear plots differing only by the terms describing slope (k_d/V_{Bpmax} versus $1/K_{eq}V_{Bpmax}$), assuming constant or negligible A^{a+}. Therefore, strictly on the basis of double reciprocal plots one may not be able to

distinguish a rapid equilibrium steady-steady from non-equilibrium steady state.

8.4 Surface Catalyzed Oxidation

In Chapter 6, discussion was carried out on the potential of pyrite to share the unshared electron pair of the pyrite/surface-S_2^-. For the purpose of continuity, designation of solution species A^{a+} and B^{b+} as in section 8.3 will be continued. Moreover, a third species will be introduced, C^{c+}. Species A^{a+}, B^{b+} and C^{c+} are designated as pyrite/surface competing species but only species C^{c+} is capable of fully accepting electrons, thus, acting as oxidizer. Also, species B^{b+} is able to react with species C^{c+} on the pyrite surface, forming a pyrite/surface-C·B complex and diminishing the capacity of C^{c+} to act as an oxidizing agent. An example of such a system would be an Fe^{2+}-Al^{3+}-Fe^{3+} system where A^{a+} denotes Fe^{2+}, B^{b+} denotes Al^{3+} and C^{c+} denotes Fe^{III}. Based on the above, a pyrite/surface-C·B complex may be hypothesized as a pyrite/surface-Fe-O-O-Al co-precipitate. To this author's knowledge such a pyrite oxidizing system has not been studied. Lizama and Suzuki (1989) postulated that competitive inhibition could also take place by coordination of bacterial cells by Fe^{3+}.

8.4.1 Competitive inhibition

The case of a competitive inhibition can be described as follows:

$$\begin{array}{l} Fe^{II}{:}S_1\text{-}S_2{:}A + C^{c+} \overset{K_{eq}}{=} Fe^{II}{:}S_1\text{-}S_2{:}C \overset{k_d}{\dashrightarrow} B_p \\ \quad + \\ \quad B^{b+} \\ \quad \| \; K_{eq}' \\ Fe^{II}{:}S_1\text{-}S_2{:}B \end{array} \qquad (8.48)$$

Species A^{a+} is omitted after its displacement from the pyrite/surface by assuming that its quantity in the solution phase is maintained constant. This makes the experimentally determined constants conditional but simplifies the equations shown below. The total pyrite/surface reactive groups are given by

$$[Fe^{II}{:}S_1\text{-}S_2{:}_{max}] = [Fe^{II}{:}S_1\text{-}S_2{:}A] + [Fe^{II}{:}S_1\text{-}S_2{:}C] + [Fe^{II}{:}S_1\text{-}S_2{:}B] \qquad (8.49)$$

Assuming a rapid equilibrium steady-state is established, for the Reaction(s) 8.48 in reverse

$$K_{eq} = \frac{[Fe^{II}{:}S_1\text{-}S_2{:}A][C^{c+}]^{1/c}}{[Fe^{II}{:}S_1\text{-}S_2{:}C]} \qquad (8.50)$$

and

$$K_{eq}' = \frac{[Fe^{II}:S_1\text{-}S_2:A][B^{b+}]^{1/b}}{[Fe^{II}:S_1\text{-}S_2:B]} \tag{8.51}$$

Letting V_{Bp} be the velocity of B_p production, then

$$V_{Bp} = k_d[Fe^{II}:S_1\text{-}S_2:C] \tag{8.52}$$

and

$$V_{Bpmax} = k_d[Fe^{II}:S_1\text{-}S_2:_{max}] \tag{8.53}$$

Dividing Equation 8.52 by Equation 8.49 and incorporating the quotient into Equation 8.53 gives

$$\frac{V_{Bp}}{V_{Bpmax}} = \frac{[Fe^{II}:S_1\text{-}S_2:C]}{[Fe^{II}:S_1\text{-}S_2:A] + [Fe^{II}:S_1\text{-}S_2:C] + [Fe^{II}:S_1\text{-}S_2:B]} \tag{8.54}$$

By incorporating Equations 8.50 and 8.51 into Equation 8.54 one obtains

$$\frac{V_{Bp}}{V_{Bpmax}} = \frac{[C^{c+}]^{1/c}}{K_{eq}\left(1 + \dfrac{[B^{b+}]^{1/b}}{K_{eq}'}\right) + [C^{c+}]^{1/c}} \tag{8.55}$$

and by inverting Equation 8.55

$$\frac{V_{Bpmax}}{V_{Bp}} = 1 + K_{eq}\left(1 + \frac{[B^{b+}]^{1/b}}{K_{eq}'}\right)\frac{1}{[C^{c+}]^{1/c}} \tag{8.56}$$

Equation 8.56 can be linearized by taking its inverse with respect to reaction velocity and concentration of C^{c+}, giving

$$\frac{1}{V_{Bp}} = \frac{1}{V_{Bpmax}} + \frac{K_{eq}}{V_{Bpmax}}\left(1 + \frac{[B^{b+}]^{1/b}}{K_{eq}'}\right)\frac{1}{[C^{c+}]^{1/c}} \tag{8.57}$$

Equation 8.57 when plotted as $1/V_{Bp}$ versus $1/[C^{c+}]^{1/c}$ for various quantities of inhibitor B^{b+} would produce a straight line for each quantity of B^{b+} with a common y-intercept but different slope. The slope would differ from that of a system without inhibitor B^{b+} by the factor

$$(1 + \frac{[B^{b+}]^{1/b}}{K_{eq}'}) \tag{8.58}$$

For additional information on competitive inhibition, see section 8.4.4.

8.4.2 Uncompetitive inhibition

An uncompetitive inhibition is shown below

$$Fe^{II}{:}S_1\text{-}S_2{:}A + C^{c+} \overset{K_{eq}}{=} Fe^{II}{:}S_1\text{-}S_2{:}C \overset{k_d}{\longrightarrow} B_p \tag{8.59}$$

$$Fe^{II}{:}S_1\text{-}S_2{:}C + B^{b+} \overset{\| K_{eq}'}{=} Fe^{II}{:}S_1\text{-}S_2{:}C{\cdot}B$$

where $Fe^{II}{:}S_1\text{-}S_2{:}C{\cdot}B$ denotes specific adsorption complex. In uncompetitive inhibition, C^{c+} competes for pyrite/surface sites on $Fe^{II}{:}S_1\text{-}S_2$: occupied by A^{a+}. Species B^{b+} reacts specifically with $Fe^{II}{:}S_1\text{-}S_2{:}C$ to form $Fe^{II}{:}S_1\text{-}S_2{:}C{\cdot}B$. However, specific reaction of B^{b+} with $Fe^{II}{:}S_1\text{-}S_2{:}C$ alters the potential of C^{c+} to accept unshared electrons from the pyrite surface. Examples of uncompetitive inhibition may include $Fe^{III}Cl_x$ complexes or co-precipitation of Fe^{3+} and Al^{3+} as oxyhydroxides on the pyrite surface. Mathematical justification for uncompetitive inhibition is given below. The total pyrite/surface reactive groups are given by

$$[Fe^{II}{:}S_1\text{-}S_2{:}_{max}] = [Fe^{II}{:}S_1\text{-}S_2{:}A] + [Fe^{II}{:}S_1\text{-}S_2{:}C] + [Fe^{II}{:}S_1\text{-}S_2{:}C{\cdot}B] \tag{8.60}$$

Assuming a rapid equilibrium steady-state is established, for the Reaction(s) 8.59 in reverse

$$K_{eq} = \frac{[Fe^{II}{:}S_1\text{-}S_2{:}A][C^{c+}]^{1/c}}{[Fe^{II}{:}S_1\text{-}S_2{:}C]} \tag{8.61}$$

and

$$K_{eq}' = \frac{[Fe^{II}{:}S_1\text{-}S_2{:}C][B^{b+}]^{1/b}}{[Fe^{II}{:}S_1\text{-}S_2{:}C{\cdot}B]} \tag{8.62}$$

Letting V_{Bp} be the velocity of B_p production, then

$$V_{Bp} = k_d[Fe^{II}{:}S_1\text{-}S_2{:}C] \tag{8.63}$$

and

$$V_{Bpmax} = k_d[Fe^{II}:S_1\text{-}S_2{:}_{max}] \tag{8.64}$$

An expression relating V_{Bp}, V_{Bpmax}, $[C^{c+}]$, K_{eq}, K_{eq}' and $[B^{b+}]$ can be derived as in case of competitive inhibition (see section 8.4.1)

$$\frac{V_{Bp}}{[Fe^{II}:S_1\text{-}S_2:A]_T} = \frac{k_d[Fe^{II}:S_1\text{-}S_2:C]}{[Fe^{II}:S_1\text{-}S_2:A] + [Fe^{II}:S_1\text{-}S_2:C] + [Fe^{II}:S_1\text{-}S_2:C\cdot B]} \tag{8.65}$$

where for simplicity $[Fe^{II}:S_1\text{-}S_2:A]_T = [Fe^{II}:S_1\text{-}S_2{:}_{max}]$;

upon rearranging

$$\frac{V_{Bp}}{V_{Bpmax}} = \frac{[C^{c+}]^{1/c}}{K_{eq} + \left(1 + \dfrac{[B^{b+}]^{1/b}}{K_{eq}'}\right)[C^{c+}]^{1/c}} \tag{8.66}$$

Equation 8.66 can be linearized by taking its inverse with respect to reaction velocity and concentration of C^{c+}, giving

$$\frac{1}{V_{Bp}} = \frac{1}{V_{Bpmax}}\left(1 + \frac{[B^{b+}]^{1/b}}{K_{eq}'}\right) + \frac{K_{eq}}{V_{Bpmax}[C^{c+}]^{1/c}} \tag{8.67}$$

Equation 8.67 when plotted as $1/V_{Bp}$ versus $1/[C^{c+}]^{1/c}$ for various quantities of inhibitor B^{b+} would produce a straight line for each quantity of B^{b+} with a different y-intercept for each chosen B^{b+} but the same slope (Segel, 1976). The y-intercept would differ from that of a system without inhibitor B^{b+} by the factor

$$\left(1 + \frac{[B^{b+}]^{1/b}}{K_{eq}'}\right) \tag{8.68}$$

For additional information on uncompetitive inhibition, see section 8.4.4.

8.4.3 Competitive/uncompetitive inhibition

A competitive/uncompetitive inhibition is shown below:

$$\begin{array}{lcl} & K_{eq} & k_d \\ Fe^{II}{:}S_1\text{-}S_2{:}A + C^{c+} & = & Fe^{II}{:}S_1\text{-}S_2{:}C \ \text{---}> B_p \\ + & & + \\ B^{b+} & & B^{b+} \\ \| \ K_{eq'} & K_{eq} & \| \ K_{eq'} \\ Fe^{II}{:}S_1\text{-}S_2{:}B + C^{c+} & = & Fe^{II}{:}S_1\text{-}S_2{:}C\cdot B \end{array} \qquad (8.69)$$

In this case, species B^{b+} undergoes two types of surface reactions. In the first type of reaction, species B^{b+} may react specifically with the pyrite/surface to produce the $Fe^{II}{:}S_1\text{-}S_2{:}C\cdot B$ complex, inhibiting oxidation. In the second type of reaction, species B^{b+} competes with C^{c+} for sites on $Fe^{II}{:}S_1\text{-}S_2$: occupied by A^{a+}. In this case, the total number of reactive sites on the pyrite surface is given by

$$\begin{aligned} [Fe^{II}{:}S_1\text{-}S_2{:}_{max}] = {} & [Fe^{II}{:}S_1\text{-}S_2{:}A] + [Fe^{II}{:}S_1\text{-}S_2{:}C] \\ & + [Fe^{II}{:}S_1\text{-}S_2{:}B] + [Fe^{II}{:}S_1\text{-}S_2{:}C\cdot B] \end{aligned} \qquad (8.70)$$

Under a rapid equilibrium steady-state, for the Reaction(s) 8.69 in reverse

$$K_{eq} = \frac{[Fe^{II}{:}S_1\text{-}S_2{:}A][C^{c+}]^{1/c}}{[Fe^{II}{:}S_1\text{-}S_2{:}C]} = \frac{[Fe^{II}{:}S_1\text{-}S_2{:}B][C^{c+}]^{1/c}}{[Fe^{II}{:}S_1\text{-}S_2{:}C\cdot B]} \qquad (8.71)$$

$$K_{eq}' = \frac{[Fe^{II}{:}S_1\text{-}S_2{:}A][B^{b+}]^{1/b}}{[Fe^{II}{:}S_1\text{-}S_2{:}B]} = \frac{[Fe^{II}{:}S_1\text{-}S_2{:}C][B^{b+}]^{1/b}}{[Fe^{II}{:}S_1\text{-}S_2{:}C\cdot B]} \qquad (8.72)$$

Letting V_{Bp} be the velocity of B_p production, then

$$V_{Bp} = k_d[Fe^{II}{:}S_1\text{-}S_2{:}C] \qquad (8.73)$$

and

$$V_{Bpmax} = k_d[Fe^{II}{:}S_1\text{-}S_2{:}_{max}] \qquad (8.74)$$

An expression relating V_{Bp}, V_{Bpmax}, $[C^{c+}]$, K_{eq}, K_{eq}' and $[B^{b+}]$ can be derived as in the case of competitive inhibition (section 8.4.1), producing

$$\frac{V_{Bp}}{[Fe^{II}{:}S_1\text{-}S_2{:}A]_T} = \frac{k_d[Fe^{II}{:}S_1\text{-}S_2{:}C]}{[Fe^{II}{:}S_1\text{-}S_2{:}A] + [Fe^{II}{:}S_1\text{-}S_2{:}C] + [Fe^{II}{:}S_1\text{-}S_2{:}B] + [Fe^{II}{:}S_1\text{-}S_2{:}C\cdot B]} \qquad (8.75)$$

where for simplicity $[Fe^{II}{:}S_1\text{-}S_2{:}A]_T = [Fe^{II}{:}S_1\text{-}S_2{:}_{max}]$; upon rearranging

$$\frac{V_{Bp}}{V_{Bpmax}} = \frac{[C^{c+}]^{1/c}}{K_{eq} + [C^{c+}]^{1/c} + \left(\frac{K_{eq}}{K_{eq}'}\right)[B^{b+}]^{1/b} + \frac{[B^{b+}]^{1/b}}{K_{eq}'}[C^{c+}]^{1/c}} \quad (8.76)$$

Equation 8.76 can be linearized by taking its inverse with respect to reaction velocity and concentration of C^{c+}, giving

$$\frac{1}{V_{Bp}} = \frac{1}{V_{Bpmax}}\left(1+\frac{[B^{b+}]^{1/b}}{K_{eq}'}\right) + \frac{K_{eq}}{V_{Bpmax}}\left(1+\frac{[B^{b+}]^{1/b}}{K_{eq}'}\right)\frac{1}{[C^{c+}]^{1/c}} \quad (8.77)$$

A plot of $1/V_{Bp}$ versus $1/[C^{c+}]^{1/c}$ for the competitive/uncompetitive system would differ from a similar plot in the absence of inhibitor B^{b+} in the slope and y-intercept by

$$\left(1 + \frac{[B^{b+}]^{1/b}}{K_{eq}'}\right) \quad (8.78)$$

See also Segel (1976). For additional information on competitive/uncompetitive inhibition, see section 8.4.4.

8.4.4 Experimental data

Lizama and Suzuki (1989) and Suzuki et al. (1989) presented detailed studies on Fe^{2+} and pyrite oxidation by *T. ferrooxidans* employing Michaelis-Menten kinetics (see Table 8.1). Their findings point out that different types of kinetics were observed depending on bacteria types/source (laboratory strains, ATCC 13661 and ATCC 19859; mine isolates, SM-4 and SM-5) and pre-conditioning of pyrite surface. Pre-conditioning refers to washing the pyrite surfaces with the HP medium (0.1 g of K_2HPO_4, 0.4 g of $(NH_4)_2SO_4$), and 0.4 g of $MgSO_4 \cdot 7H_2O$ L^{-1}, adjusted to pH 2.3 with H_2SO_4).

The data in Figure 8.6 shows an example of HP washed pyrite oxidation kinetics employing Fe^{3+}. These data show that iron II release (pyrite oxidation) was linear (first-order) with respect to Fe^{3+} concentration. Note that for the concentrations of Fe^{3+} tested no apparent V_{max} was attained, suggesting potential competitive interactions between Fe^{2+} and Fe^{3+} for pyrite/surface reactive sites (Garrels and Thompson, 1960). The data in the insert of Figure 8.7 shows an example of HP washed pyrite saturation oxidation kinetics employing Fe^{3+}. The two Fe^{3+} concentrations display (as expected) different V_{max}. Furthermore, the double reciprocal data in Figure 8.7 revealed that a decreasing Fe^{3+} concentration or most likely an increasing Fe^{2+}/Fe^{3+} ratio on the pyrite surface acted (as expected) as a pyrite oxidation

inhibitor. The common x-intercept signified the same K_m; difference in slope and y-intercept (due to changes in Fe^{3+} concentration) suggested competitive/uncompetitive inhibition (see section 8.4.3). In essence, the data suggested that Fe^{2+} was a a strong competitor with respect to Fe^{3+} for pyrite/surface reactive sites (Moses and Herman, 1991).

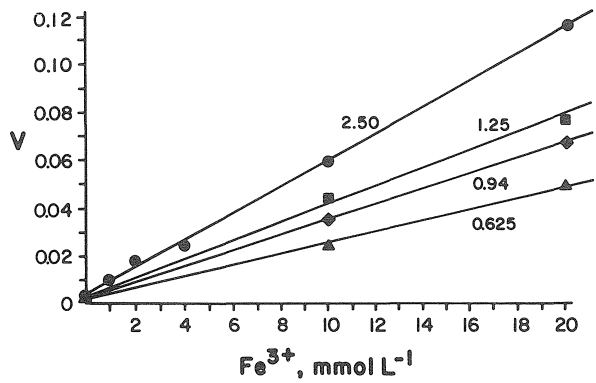

Figure 8.6. Effect of Fe^{3+} concentration on the indirect leaching of HP washed pyrite. The rate of Fe^{2+} dissolution was determined at various Fe^{3+} concentrations and fixed pyrite concentrations (0.625, 0.94, 1.25, and 2.5% PD), as indicated. The rate (v) was expressed as micromolar Fe^{2+} per minute at 30°C. FeS_2 % PD (PD = [g of pyrite per ml solution] x 100). HP = 0.1 g of K_2HPO_4, 0.4 g of $(NH_4)_2SO_4$), and 0.4 g of $MgSO_4 \cdot 7H_2O$ L^{-1}, adjusted to pH 2.3 with H_2SO_4. (From Lizama and Suzuki, 1989. With permission.)

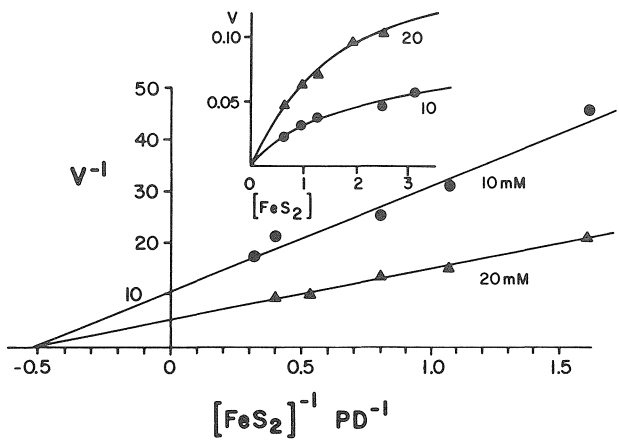

Figure 8.7. Effect of HP washed pyrite concentration on the indirect leaching of pyrite at two fixed Fe^{3+} concentrations (10 and 20 mM). FeS_2 % PD (PD = [g of pyrite per ml solution] x 100). HP = 0.1 g of K_2HPO_4, 0.4 g of $(NH_4)_2SO_4$), and 0.4 g of $MgSO_4 \cdot 7H_2O$ L^{-1}, adjusted to pH 2.3 with H_2SO_4. (From Lizama and Suzuki, 1989. With permission.)

Oxidation of surface pretreated pyrite (pyrite washed with HP medium) by SM-4 cells (mine isolates) appeared to follow competitive/uncompetitive inhibition (Figure 8.8, slope and y-intercept changed).

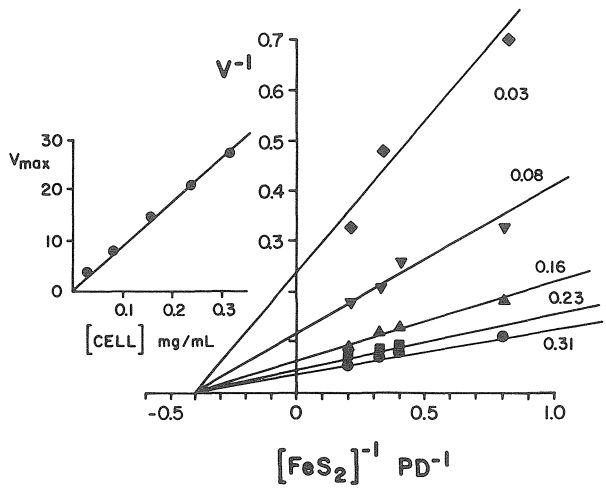

Figure 8.8. Effect of HP washed pyrite concentration on the rate of oxygen consumption by *T. ferrooxidans* SM-4 cells. The rate (v) was determined as micromolar O_2 per minute at 30°C by using various amounts of washed pyrite and fixed concentrations of cells (0.03, 0.08, 0.16, 0.23, and 0.31 mg of wet cells per ml), as indicated. FeS_2 % PD (PD = [g of pyrite ml^{-1} solution] x 100). HP = (0.1 g of K_2HPO_4, 0.4 g of $(NH_4)_2SO_4$), and 0.4 g of $MgSO_4 \cdot 7H_2O$ L^{-1}, adjusted to pH 2.3 with H_2SO_4. (From Lizama and Suzuki, 1989. With permission.)

In this case, oxidation inhibition reflected fewer bacterial cells. These results were expected since fewer cells implied less enzyme (see insert in Figure 8.8). Thus, the data, as expected, exhibited the same K_m but different V_{max}. This suggested that bacterial cells besides being involved in metabolic pyrite oxidation, also reacted with the pyrite surface in a manner which appeared to alter the potential of pyrite to oxidize. This was perhaps due to the potential of bacterial cells to eliminate the competitive effect of Fe^{2+} with respect to Fe^{3+} for pyrite surface reactive sites due to the former's rapid turnover in the presence of *T. ferrooxidans*. This observation was analogous to oxidizing HP washed pyrite by Fe^{3+} only. Iron II (Fe^{2+}) oxidation data by laboratory strains (ATCC 13661 and ATCC 19859) demonstrated competitive/uncompetitive inhibition (single K_m by changing cell population, but different V_{max}).

In the case of unwashed pyrite, the double reciprocal plot appeared to be more of the uncompetitive form (Figure 8.9) (nearly the same slope but different x-intercept, hence, different K_m).

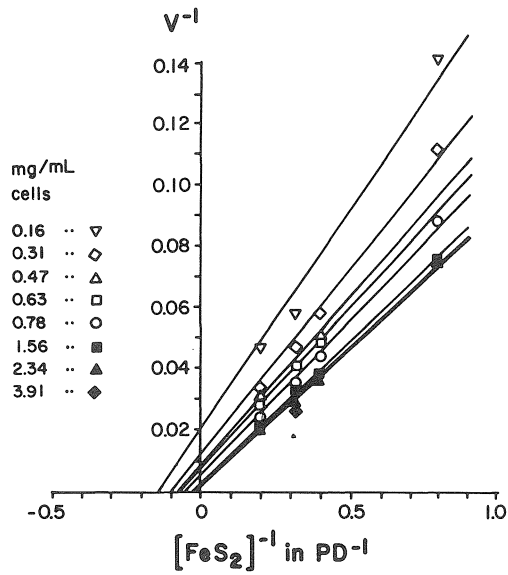

Figure 8.9. Effect of unwashed pyrite concentrations on the rate of oxygen consumption by *T. ferrooxidans* SM-4 cells. FeS_2 % PD (PD = [g of pyrite per ml solution] x 100). HP = 0.1 g of K_2HPO_4, 0.4 g of $(NH_4)_2SO_4$), and 0.4 g of $MgSO_4 \cdot 7H_2O$ L^{-1}, adjusted to pH 2.3 with H_2SO_4. (From Lizama and Suzuki, 1989. With permission.)

Suzuki et al. (1989) obtained similar results when SM-5 cells were used to oxidize Fe^{2+} shown in Figure 8.10. Note, same slope but different y-intercept. This implied that as the quantity of bacterial cells changed, K_m changed, which signified change in enzymatic affinity for Fe^{2+}. Based on this, Lizama and Suzuki (1989) postulated that the uncompetitive nature of the pyrite oxidation reaction was due to the competition of cells for the same pyrite/surface Fe^{2+} reactive sites. They came to this conclusion by replotting the data of Figures 8.9 and 8.10 as the reciprocal of specific reaction rate, V_{sp}^{-1} (calculated by dividing rate (v) by the number of cells) versus reciprocal of substrate. These data (Figure 8.11) revealed that the nature of the plot was clearly competitive (single K_m and single V_{max}; see also insert). Similar results were obtained from the pyrite oxidation experiment with mine isolates (Lizama and Suzuki, 1989). It appeared that the difference between HP washed and unwashed pyrite was that the former after washing contained

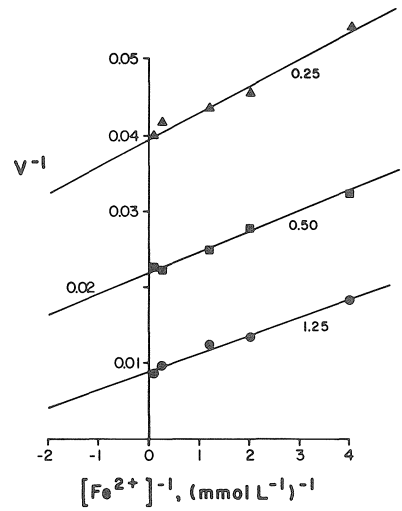

Figure 8.10. Effect of Fe^{2+} concentrations on the Fe^{2+}-oxidizing activity of SM-5 cells at concentrations 0.25, 0.50, and 0.25 mg ml^{-1}. (From Suzuki et al., 1989. With permission.)

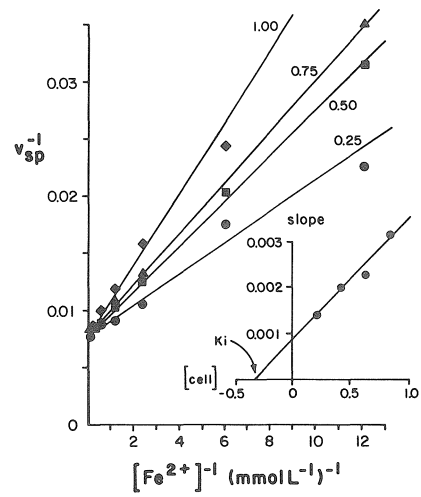

Figure 8.11. Competitive inhibition of Fe^{2+} oxidizing activity of SM-4 cells at concentrations of 0.25, 0.50, 0.75, and 1.0 mg per ml. The specific V_{sp}^{-1} was calculated by dividing rate V in Figure 8.10 by cell concentration. The insert is a plot of the slope versus cell concentration to obtain the inhibition constant K_i or K_{eq}' in mg of cells ml^{-1}. (From Suzuki et al., 1989. With permission.)

mostly Fe^{2+} on its surface, while the latter (unwashed) contained a significant quantity of Fe^{3+}. The latter could be responsible for the uncompetitive nature of pyrite oxidation by basically inducing the bacterial cells to form clusters through coordination by cell wall Fe^{3+} (Suzuki et al., 1989).

The above results suggested that laboratory bacterial strains differed from the mine isolates. Some support for the above observations/conclusions could come from the data in Figure 8.12 which shows that the release of Fe^{2+} from pyrite is highly dependent on Fe^{3+} and on a synergistic effect between Fe^{3+} and cells.

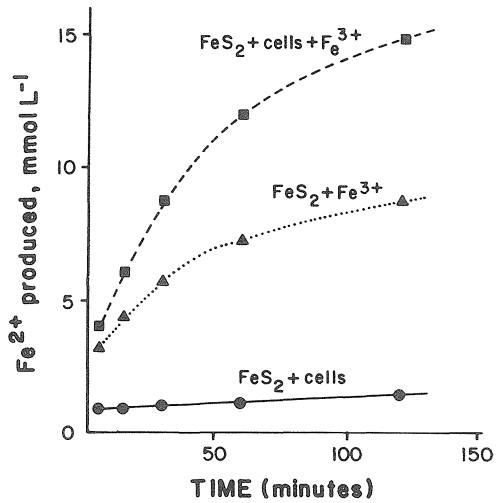

Figure 8.12. Anaerobic Fe^{2+} production in the presence of pyrite and SM-4 cells with and without Fe^{3+}, with and without cells and pyrite plus Fe^{3+} without cells. 3.125% PD (PD = [g of pyrite per ml solution] x 100); HP washed pyrite (HP = 0.1 g of K_2HPO_4, 0.4 g of $(NH_4)_2SO_4$), and 0.4 g of $MgSO_4 \cdot 7H_2O$ L^{-1}, adjusted to pH 2.3 with H_2SO_4), *T ferrooxidans* at 1 mg ml^{-1}; Fe^{3+} 13.5 *mM*. (From Lizama and Suzuki, 1989. With permission.)

The exact causes for this synergistic effect are not obvious. However, Lizama and Suzuki (1989) postulated that this could be due to Fe^{3+}-sulfur (sulfide) oxidoreductase discovered recently in *T. ferrooxidans* (Sugio et al., 1989, 1987) ($S + 4Fe^{3+}\ 3H_2O \rightarrow H_2SO_3 + 4Fe^{2+} + 4H^+$).

Double reciprocal plots have been extensively used in enzyme kinetic studies to quantify the so-called adjustable parameters, maximum rate of the reaction (V_{max}) and the affinity of the enzyme for the substrate (K_m). However, use of double reciprocal plots to estimate the adjustable parameters has been criticized because such plots show excellent correlations but their accuracy in predicting K_m and V_{max} is inherently poor (Dowd and Riggs, 1965; Kinniburgh, 1986; Evangelou and Coale, 1988). Kinniburgh (1986) pointed out that the double reciprocal plot alters the original error distribution in the data leading to erroneous Michaelis-Menten adjustable parameters. He further concluded that the most acceptable linear data transformation is that

which changes the original error distribution in the experimental data the least. Evangelou and Coale (1988) and Dowd and Riggs (1965) concluded that the most acceptable linear transformations are those of V_{Bp} versus $V_{Bp}/[B^{b+}]^{1/b}$ (Hofstee plot) or $[B^{b+}]^{1/b}/V_{Bp}$ versus $[B^{b+}]^{1/b}$ (Hanes-Woolf plot) (see Segel, 1976). Kinniburgh (1986) pointed out that the best approach to estimate the Michaelis-Menten adjustable parameters is through nonlinear regression.

8.5. Other Microbial Processes

This Chapter has focused mainly in the biotic oxidation of pyrite. However, bacteria, depending on availability of oxygen and substrate, are also able to carry other processes such as dissimilatory sulfate reduction, a process which renders wetlands capable of removing sulfur and metals from solution. Dissimilatory sulfate-reduction has been summarized eloquently by Hammack and Hedin (1986) and for the purpose of this book some of the information will be presented here.

Dissimilatory sulfate-reducing bacteria reduce inorganic sulfate or other oxidized sulfur forms to sulfide which is not incorporated into the organism but is released as "free" H_2S. The two best known genera of dissimilatory sulfate-reducing bacteria are *Desulfovibrio* and *Desulfotomaculum*. Others include *Desulfobulbus*, *Desulfococcus*, *Desulfosarcina*, *Desulfobacter*, and *Desulfonema*, although the latter three genera are restricted to marine environments (Postgate, 1984). Dissimilatory sulfate-reducing bacteria are anaerobes and are severely inhibited by even small amounts of oxygen. However, they do survive long periods of oxygen exposure and become active when anaerobic conditions are restored.

Dissimilatory sulfate-reducing bacteria require an organic carbon source (heterotrophs). In the case of *Desulfovibrio spp.*, this carbon source can be supplied by simple organic molecules such as lactate, pyruvate, and malate, which are oxidized to acetate and CO_2 by reducing sulfate to sulfide (Ehrlich, 1981). Because the sulfate-reducing bacteria can oxidize simple organic compounds and will only oxidize carbohydrates under rare circumstances (Ehrlich, 1981), they generally rely on fermentative bacteria and fungi to break complex organic compounds into simple molecules.

In the natural environment, dissimilatory sulfate-reducing bacteria grow at temperatures between 0 and 70°C. *Desulfovibrio spp.* grow between 0 and 44°C with optimum growth occurring between 25 and 30°C. *Desulfotomaculum spp.* prefer higher temperatures (30-70°C) with optimum growth occurring between 35 and 55°C (Ehrlich, 1981). Sulfate reduction is thought to cease when the pH drops below 4 (Wakao et al., 1979). Mixed cultures of sulfate-reducing bacteria and heterotrophic bacteria can become established in solutions with an initial pH as low as 2.7 (Wakao et al., 1979), but sulfate reduction does not commence until the pH rises above 4.

The overall bacterial sulfate reduction process can be represented by the following schematic reaction:

$$\text{Fermentative end products} + SO_4^{2-} \text{ --> acetate} + HS^- + HCO_3^- \quad (8.79)$$

Reaction 8.79 shows that the end products of biomass fermentation and sulfate are converted to acetate, bisulfide or hydrogen sulfide, and bicarbonate. Hammack and Hadin (1986) pointed out that application of this process to acid mine effluents or otherwise known as AMD may improve water quality as follows:

1. The process consumes sulfate which is undesirable in high concentrations,
2. sulfide generated will react quickly with many metals to form insoluble metal-sulfide precipitates,
3. alkalinity of the bicarbonate and acetate form will help neutralize acidity and raise pH,
4. aluminum will precipitate as hydroxide in response to the pH increase, and
5. manganese may precipitate as a carbonate, depending on pH and/or pCO_2.

Based on the above, in order to treat AMD by dissimilatory sulfate-reducing bacteria an organic-rich, anaerobic environment must be engineered and an active population of sulfate-reducing bacteria and fermentative organisms established. These engineered environments may take the form of tanks such as anaerobic digesters used for the treatment of municipal wastewaters, or constructed wetlands with thick organic substrates. AMD should be introduced with minimal dissolved oxygen in order to maximize sulfate-reducing bacteria activity.

PART IV

ADVANCES IN PYRITE MICROENCAPSULATING TECHNOLOGIES

Taylor & Francis
Taylor & Francis Group
http://taylorandfrancis.com

Chapter 9
PHOSPHATE INFLUENCE ON PYRITE OXIDATION

9.1 A Review

Upon exposing iron sulfide minerals, e.g., pyrite (FeS_2), pyrrhotite ($Fe_{1-x}S$), etc.), to the atmosphere they oxidize and produce AMD, a severe environmental pollution problem. Acid mine drainage is extremely acidic (pH as low as 2) and enriched with iron, aluminum, sulfate, and heavy metals such as Pb, Hg, Cd, and in some cases Th and U nuclides.

As pointed out previously, the need to prevent AMD formation has triggered numerous investigations into the mechanisms of pyrite oxidation and its prevention (Mckibben and Barnes, 1986; Luther, 1990; Brown, 1985; Moses et al., 1987; Lowson, 1982 and references therein; Singer and Stumm, 1970; Silverman, 1967; Nordstrom, 1982a and references therein; Kleinmann, 1981; Skousen et al, 1987; Renton et al., 1988). Recall that pyrite in mining 'waste' is initially oxidized by the atmospheric O_2, producing H^+, SO_4^{2-}, and Fe^{II}. The Fe^{II} produced can be further oxidized by O_2 into Fe^{III}, which in turn hydrolyzes into iron hydroxide and releases additional amounts of acid into the environment.

Oxidation of pyrite in mining 'waste' is initially a relatively slow process and most iron released ends up as iron hydroxide due to the relatively high pH on pyrite surfaces (Ivanov, 1962; Fornasiero et al., 1992). As acid production continues and pH in the vicinity of pyrite surfaces drops below 3.5, formation of iron hydroxide is hindered and activity of free Fe^{III} in solution increases. At low pH, oxidation of pyrite by Fe^{III} is the main mechanism for acid production in mining waste, since Fe^{III} can oxidize pyrite approximately one order of magnitude faster than O_2 (Singer and Stumm, 1970). The role of Fe^{III} in the oxidation of pyrite is demonstrated below:

$$FeS_2 + 14Fe^{III} + 8H_2O = 15Fe^{II} + 2SO_4^{2-} + 16H^+$$

(O_2; Iron-oxidizing bacteria)

At low pH, an acidophilic, chemoautotrophic, iron-oxidizing bacterium--*T. ferrooxidans* catalyzes and accelerates the oxidation of Fe^{II} into Fe^{III} by a factor larger than 10^6 (Singer and Stumm, 1970).

Based on the above, pyrite oxidation can be significantly reduced by complexing Fe^{III}, depriving the system of oxygen (O_2), and using alkaline material to neutralize any acid products. A list of these technologies are reported in Skousen et al. (1987). An extensive review on these technologies, with respect to their effectiveness and their limitations, is given in Chapter 5. At this point a brief discussion is presented.

9.2 Functional Prediction Technologies

A common approach for predicting outcome of complex processes in nature, e.g., pyrite oxidation in mine 'waste', is through computer modelling. Pyrite oxidation models can be classified into two groups 1) *deterministic functional models*, and 2) *mechanistic models*. *Deterministic models* include functional and mechanistic approaches to make pyrite oxidation predictions. According to Addiscott and Wagenet (1985), in general, *functional models* are "models that employ simplified treatments to make outcome predictions" for a given process, e.g., pyrite oxidation, and "make no claim to fundamentality", whereas *mechanistic* models employ "the most fundamental mechanisms of the process". Currently, there are a number of models for predicting pyrite oxidation which have been published in the literature (Jaynes et al., 1984; Renton et al. 1988; Batarseh et al. 1989; Caruccio and Geidel, 1980, 1981, 1985; Scharer et al. 1991). For the most part these models are *functional models* or *macroscopic models*.

Macroscopic models are excellent tools for understanding extreme situations. For example, the models by Renton et al. (1988), Batarseh et al. (1989), Caruccio and Geidel (1980, 1981, 1985) and Scharer et al. (1991), in general, they could predict if a geologic pyritic stratum under oxidative conditions would produce acid drainage. These models, however, could not predict pH and/or heavy metal concentration in the leachate as a function of time simply because they do not include chemical processes, molecular or otherwise, that would allow such predictions. *Macroscopic models* are designed to provide an overview on the outcome of complex reaction processes.

Conceptual macroscopic characterization of natural processes provides an excellent tool for understanding complex problems and allow us to make decisions leading to potential problem solutions. Such conceptual macroscopic characterization can be carried out on pyrite oxidation described by the following schematic reaction

$$FeS_2 + O_2 + H_2O \text{ ------> } Fe^{II} + H^+ + SO_4^{2-} \qquad (9.1)$$

Equation 9.1 demonstrates that under mild oxidizing conditions, FeS_2 undergoes congruent oxidative dissolution. In other words, upon introducing O_2 to a water insoluble compound such as FeS_2 (Lindsay, 1979) it breaks down and forms water soluble Fe(II) compounds, e.g., $FeSO_4$ or $Fe(HSO_4)_2$, classified as water pollutants.

Under mild oxidative conditions and in the presence of pyrite, limestone and water, the potential reaction products are shown schematically below

$$FeS_2 + CaCO_3 + O_2 + H_2O \begin{cases} \text{-------> } CaSO_4 \cdot 2H_2O \\ \text{------> } FeCO_3 + Fe(OH)_2 \\ \text{-------> } FeSO_4 \end{cases} \quad (9.2)$$

Equation 9.2 reveals that under mild oxidizing conditions FeS_2 undergoes congruent oxidative dissolution with respect to $CaSO_4 \cdot 2H_2O$, $FeSO_4$, $FeCO_3$ and $Fe(OH)_2$. In other words, upon introducing O_2 and $CaCO_3$ to FeS_2, the latter breaks down and forms various compounds classified as pollutants. Calcium sulfate or gypsum ($CaSO_4 \cdot 2H_2O$) is fairly water soluble (2,200 mg L^{-1}; Evangelou et al., 1987; Evangelou and Wagner, 1987; for details also see Chapter 1); $FeSO_4$ is highly water soluble, but the solubility of $FeCO_3$ or $Fe(OH)_2$ is highly dependent on pH which is controlled by pCO_2 (Stumm and Morgan, 1970, 1981; Lindsay, 1979). The latter (pCO_2) in geologic systems could be high enough to reduce pH below 7, even in the presence of $CaCO_3$ (see Chapter 1).

Production of $FeSO_4$ is highly dependent on apparent $CaCO_3$ neutralization effectiveness. Under maximum $CaCO_3$ neutralization effectiveness and strong oxidative conditions no $FeSO_4$ is produced. Also, under mild oxidative conditions and pH equal to/or greater than 7, incongruent production of $FeCO_3$ could take place because the solubility of $CaCO_3$ is approximately one order of magnitude greater than the solubility of $FeCO_3$ (Stumm and Morgan, 1981).

Incongruent production of $Fe(OH)_2$ as shown in Equation 9.2 could not take place much below pH 8 (Lindsay, 1979). However, even if the pH of mine 'waste' material could be maintained above 8, high pCO_2 would transform $Fe(OH)_2$ incongruently to $FeCO_3$. This is demonstrated by the FT-IR spectrum in Figure 9.1. It reveals the spontaneous transformation of $Ca(OH)_2$ to $CaCO_3$ when the former is exposed to atmospheric CO_2. Note the broad absorption band in the 1400 cm^{-1} range. This broad band signifies that coordination of CO_3^{2-} by the surface of $Ca(OH)_2$ takes place immediately after exposing reagent grade $Ca(OH)_2$ to atmospheric CO_2 (Evangelou and Huang, 1994). The 1400 cm^{-1} band, however, is not apparent on the spectrum of the $CaCl_2$ salt, signifying the importance of OH^- to the carbonation process of a divalent metal behaving as a relatively weak Lewis acid.

Under strong oxidative conditions and in the presence of pyrite, limestone, water and Fe^{III}, the potential reaction products are shown schematically below

$$FeS_2 + CaCO_3 + O_2 + Fe^{III} + H_2O \begin{cases} \text{-------> } CaSO_4 \cdot 2H_2O \\ \text{-------> } FeOOH \end{cases} \quad (9.3)$$

Equation 9.3 reveals that FeS_2 undergoes congruent oxidative dissolution with respect to $CaSO_4 \cdot 2H_2O$, and incongruent oxidative dissolution with respect to iron oxyhydroxide (FeOOH). In other words, upon introducing O_2 and $CaCO_3$ to FeS_2, the latter breaks down and forms $CaSO_4 \cdot 2H_2O$ which is fairly water soluble (2,200 mg L^{-1}; Evangelou et al., 1987; Evangelou and Wagner, 1987; for details also see Chapter 1), and FeOOH which under oxidative conditions is highly stable (Garrels and Christ, 1965).

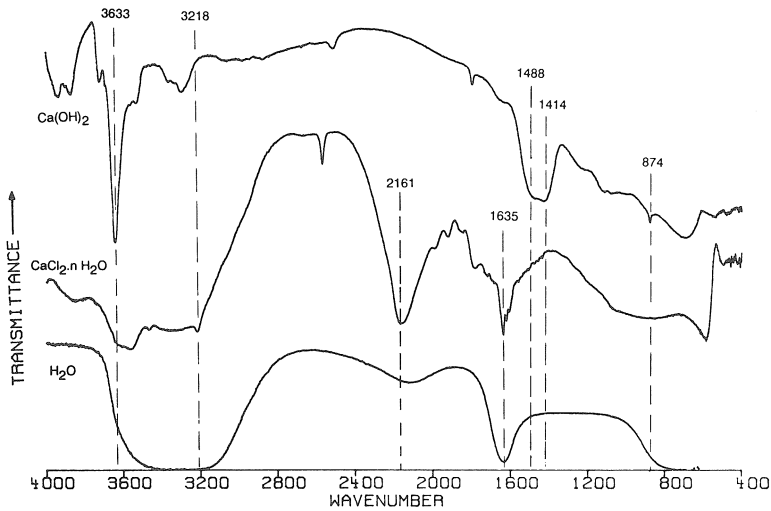

Figure 9.1. FT-IR spectra of $Ca(OH)_2$ and $CaCl_2 \cdot 2H_2O$ after exposure to atmospheric CO_2.

Equations 9.1, 9.2 and 9.3 point out that pyrite oxidation is a spontaneous process and can not be stopped, but reaction rates may vary (see Chapter 6). One may regulate the adverse environmental effects of pyrite oxidation by regulating the end-products of the process. The above conceptual macroscopic analysis clearly points out that the most ideal conditions for minimizing adverse environmental pyrite oxidation effects are through pyrite oxidation under strong oxidative/alkaline conditions.

Nicholson et al. (1988, 1990) reported that reduction in the rate of pyrite oxidation could be attained under strong oxidative/alkaline conditions. The mechanism for this reduction in the oxidation rate appears to be coating of pyrite with iron oxyhydroxide, thus, limiting O_2 diffusion to the pyrite surface. This type of pyrite oxidation control should be viewed as strictly

passive. Evidence also suggest, however, that pyrite oxidation may accelerate in the presence of amorphous $Fe(OH)_3$. Aller and Rude (1988) demonstrated that application of goethite to pyritic sediments increased SO_4^{2-} production in comparison to the control. On the other hand, addition of hematite (a well crystalized iron oxide mineral) showed no influence on pyrite oxidation (Figure 9.2).

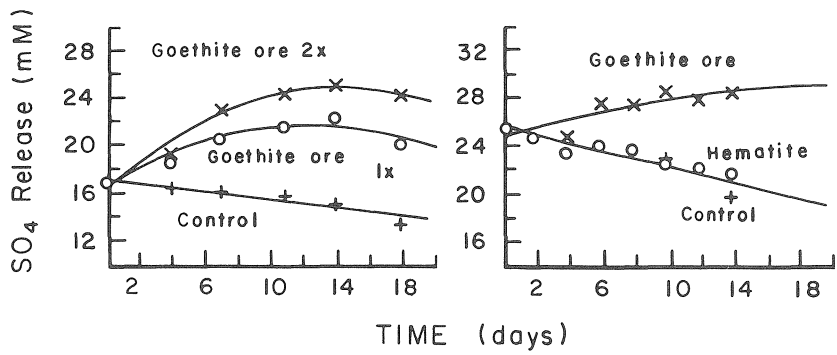

Figure 9.2. Influence of iron oxides on pyrite oxidation. (From Aller and Rude, 1988. With permission.)

9.3 Abatement Technologies

Acid mine drainage abatement technologies involve physical barriers to prohibit transfer of water and oxygen to the sulfidic minerals. The physical barriers include plastic liners, clay liners, and even asphalt. None of these techniques appear to be effective due to the tendency of the liners to break (Caruccio and Geidel, 1983; Skousen et al., 1987). Additionally, use of such liners is costly and often technically unfeasible.

Another technology for controlling acid drainage generation is use of alkaline materials such as limestone, rock phosphates, and, at times, sewage sludge (Stiller et al., 1985; Stiller et al., 1986; Loomis and Hood, 1984). Evidence shows, however, that limestone may, in fact, enhance pyrite oxidation (Evangelou et al., 1985; Stiller et al., 1985). Alkaline earth materials are believed to control acid drainage production through neutralization of pyrite oxidation products and through precipitation of Fe^{III}. However, a low pH could exist near pyrite surfaces even when alkaline earth materials are present. The relatively high pH near alkaline material surfaces promotes inorganic oxidation of Fe^{II} to Fe^{III} and consequently the large quantity of Fe^{III} available near pyrite surfaces due to diffusion, promotes S_2^{2-} oxidation. This is demonstrated in Figure 9.3.

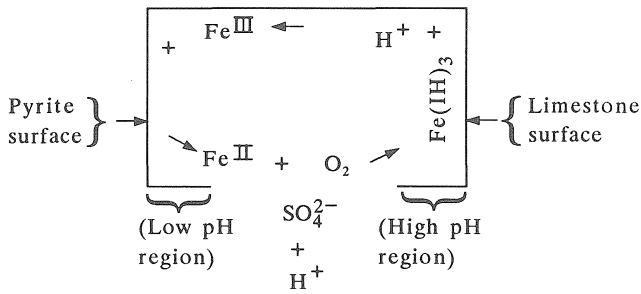

Figure 9.3. Diagram demonstrating the role of limestone in enhancing pyrite oxidation through turnover of Fe^{II} to Fe^{III}.

At least in theory, pyrite oxidation could be controlled by removal of Fe^{III} from solution. This could be accomplished by thoroughly mixing pulverized limestone with the pyrite such that direct contact between pyrite and limestone is made. However, even under such ideal conditions, oxidation of pyrite would not stop since dissolved oxygen would carry on the reaction (see section 6.3) (Moses et al., 1987; Moses and Herman, 1991).

Based on the above, pyrite oxidation control by the introduction of alkaline earth carbonates (e.g., limestone) may not be effective under long-term conditions. In fact, Stiller et al (1984) noticed that in the presence of limestone pyrite oxidation in mine 'waste' (placed in large barrels and allowed to oxidize in the natural environment) was enhanced. Similar inferences were made by Evangelou et al (1984) by observing the oxidation of pyrite in mine 'waste' suspensions having received large quantities of reagent grade $CaCO_3$. Moses et al (1987) postulated, based on experimental observations, that pyrite oxidation under alkaline conditions may not be controlled by the solubility of $Fe(OH)_3$ but rather by the turnover rate of Fe (Fe^{II} to Fe^{III}) through O_2. This turnover rate of Fe, at pH greater than 6, exhibits a half life of only a few minutes (Stumm and Morgan, 1981). The diagram in Figure 9.3 shows how this Fe turnover may be facilitated through an electrochemical gradient between the pyrite and limestone surfaces.

Nicholson et al. (1988, 1990) in controlled laboratory studies were able to demonstrate diminishing rates of pyrite oxidation by oxidizing pyrite suspension reactors through which a carbonate-buffered solution and air (20% O_2) flawed continuously. However, they attributed this diminishing rate of pyrite oxidation on iron-oxide coatings forming on the surface of pyrite. Note that in the case of the studies by Nicholson et al. (1988, 1990), direct contact between limestone and the surface of pyrite was not an issue since the researchers employed 0.005 mol L^{-1} $NaHCO_3$ solution. Their data suggested that even under such ideal conditions pyrite oxidation by O_2 was significant.

The role of reaction product surface deposition on the oxidation of pyrite has also been observed by Goldhaber (1983).

Another form of acid drainage control is through application of bactericides which have a suppressing effect on the activity of *T. ferrooxidans* bacteria which convert Fe^{II} to Fe^{III} (Kleinmann, 1980). Slow release pellets of such bactericides are commercially available (Rastogi et al., 1986). The major disadvantage of this technology is that acid mine drainage production is suppressed for relatively short periods since abiotic iron sulfide oxidation remains unaffected.

Organic waste may also inhibit pyrite oxidation via various mechanisms including 1) consumption of O_2 because of bacterial growth, 2) removal of Fe^{III} from solution through complexation, and 3) formation of pyrite-Fe^{II}-humate complexes. Organic waste, however, may also promote pyrite oxidation by solubilization of $Fe(OH)_3$ through formation of Fe^{III}-organic acid complexes. Such complexes, especially if positively charged, they could adsorb onto the pyrite surface and act as electron acceptors in an outer sphere mode (Luther et al., 1992). These electron transfer reactions could also be favored in some cases when Fe^{II}-organic acid complexes would be more stable than Fe^{III}-organic acid complexes (Luther et al., 1992). To avoid such potential pyrite oxidation problems, well decomposed organic waste (Loomis and Hood, 1984) (composted, heat treated so that simple carboxylic acids are destroyed) should be applied to pyritic waste prior to formation of $Fe(OH)_3$ precipitates so that a) pyrite-Fe^{II}-humate complexes would be the only complexes, b) Fe^{III}-humate complexes formed should be preferably neutral or negatively charged (note, pyrite surface is also negatively charged), and c) any Fe^{III}-humate complexes formed should be preferably water insoluble.

9.4 Microencapsulation

Recently, in the author's laboratory the discovery was made that pyrite particles could be protected against oxidation by a surface coating of ferric phosphate or iron oxide. Coating was generated by leaching coal 'waste' with a solution with or without phosphate buffered at pH 5 to 7 with sodium acetate (NaAC) in the presence of low concentrations of H_2O_2. The coatings shut off electron transfer between pyrite and oxidizers. There are many advantages to using such a technology. The inactivation of pyrite could be long lasting and highly cost effective since only the surface of pyrite would need to be inactivated. Currently, no other available technology for treating pyrite meets these conditions.

The mechanism of ferric-phosphate coating deposition on pyrite is demonstrated in Figure 9.4.

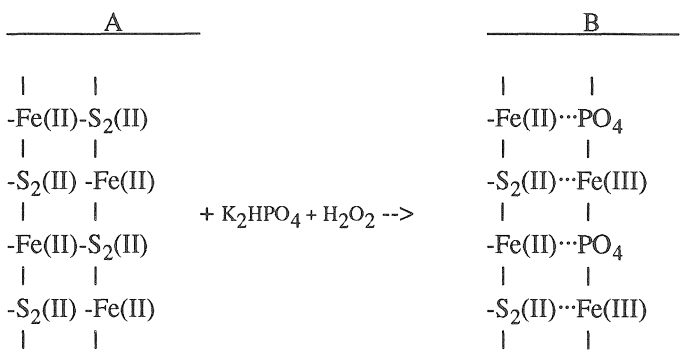

Figure 9.4. Schematic demonstrating proposed microencapsulation technology.

The above schematic diagram shows that upon introducing pyrite in a solution mixture of K_2HPO_4 and H_2O_2, surface Fe^{II} reacts with peroxide to convert to Fe^{III} which in turn precipitates as ferric phosphate coating on the surface of pyrite. The source of surface iron can be either a) the pyrite mineral structure and/or b) pyrite surface adsorbed Fe^{II}. In the first case, H_2O_2 attacks the pyrite structure itself and the coating forming process also oxidizes the disulfide (S_2^{2-}), producing SO_4^{2-}. In the second case, H_2O_2 may oxidize structural iron as well as pyrite surface adsorbed iron. The latter iron is adsorbed to the pyrite surface due to the negative charge associated with the frontier-molecular-orbital configuration of pyrite (see Chapter 6). In either case, surface ferric phosphate precipitation results. The precipitation of ferric phosphate on the surface of pyrite is necessary for long-term control of pyrite oxidation. Thus, at the cost of a small percentage of pyrite, the surfaces of pyrite particles in coal waste could be passivated due to ferric phosphate or iron oxide coatings; as a result, production of acid drainage could be prevented.

The technology of coating pyrite as described above should not be confused with application of rock phosphate (Flynn, 1969; Renton et al., 1988). Rock phosphate complexes Fe^{II} and thus reduces potential production of Fe^{III}; consequently, pyrite oxidation potential is also reduced (Stumm and Morgan, 1970). Rock phosphate does not coat pyrite, rather, it complexes Fe^{II} released from the oxidizing pyrite (Evangelou et al., 1992; see also Chapter 5). This surface coating of rock phosphate renders it inactive. Therefore, effectiveness of rock phosphate in controlling pyrite oxidation in nature is short lived. These results appear to have some support from field observations (Meek, 1991). The ferric phosphate coating technology controls pyrite oxidation via two mechanisms 1) converts Fe^{II} to Fe^{III} and the latter is strongly complexed by phosphate, and 2) ferric phosphate precipitate forms a

stable coating on the surface of pyrite and renders it inactive for as long as O_2 and H_2O do not diffuse through the coating.

9.5 Mechanisms

Pyrite oxidation by H_2O_2 in the absence of phosphate can be described schematically

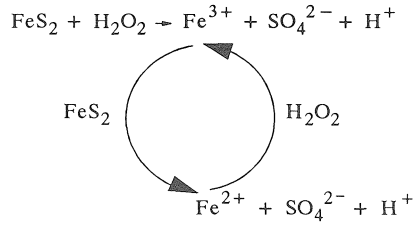

(9.4)

and pyrite oxidation by H_2O_2 in the presence of phosphate can be described by

$$FeS_2 + 7.5H_2O_2 + H_2PO_4 \rightarrow FePO_4 + 2SO4^{2-} + 3H^+ + 7H_2O \quad (9.5)$$

The iron phosphate formed as shown in Equation 9.5 can precipitate either as a discrete phase or as coating on pyrite surfaces, depending on degree of supersaturation of the solution on pyrite surfaces with respect to iron phosphate (Lindsay, 1979). If the degree of supersaturation is relatively low, the iron phosphate might not precipitate instantly and thereby exist as a discrete phase. In this case, the term $Sk_2[Fe^{III}]^{\nu_2}$ (Equation (6.48)) would approach zero and pyrite oxidation would be described by

$$\log M/Mo = -K[k_1'/2.3](t) \quad (9.6)$$

where M and Mo denote unreacted and original quantities of pyrite respectively. Equation 9.6 implies that when Fe(III) is precipitated as a discrete $FePO_4$ phase, pyrite oxidation would be characterized by a linear pseudo-first- order plot of log M/Mo versus t at constant H_2O_2. However, if the degree of supersaturation with respect to $FePO_4$ is high, iron phosphate could precipitate as a coating on pyrite surfaces and the rate of pyrite oxidation would be smaller than that predicted by Equation (9.6) when $FePO_4$ was assumed to precipitate as a discrete phase (see section 9.6).

9.6 Microencapsulation

Pyrite used in the microencapsulation studies was separated from a pyritic shale. The sample particle size varied from 5 μm to 20 μm. Kinetics of pyrite oxidation were studied employing a bed-reactor technique similar to that described by Bashour and Carlson (1984), Frantz and Carlson (1987) and Lumbanraja (1991). Briefly, the porous bed reactor system consisted of a 12

cm long and 1 cm inside diameter chromatographic column equipped with a water jacket for temperature control. For details in these experimental studies see Huang and Evangelou (1994). The purpose of these studies was to simply demonstrate if pyrite microencapsulation could be a controlled process. Further studies would be required to demonstrate the application of such a process in the field.

The following solutions were used in the leaching process for the purpose of inducing pyrite microencapsulation and for evaluating the mechanisms of microencapsulation: The first type of solution was H_2O_2 at various concentrations with 0.2 mol L^{-1} NaCl serving as background electrolyte. The second type of solution was H_2O_2 at various concentrations in 0.2 mol L^{-1} NaCl plus 0.013 mol L^{-1} EDTA. The third type of solution was H_2O_2 at various concentrations in 0.2 mol L^{-1} NaCl plus 10^{-3} mol L^{-1} KH_2PO_4. All oxidizing solutions, except those employed to evaluate pH dependence of pyrite oxidation, were adjusted to pH 4 with 0.1 mol L^{-1} HCl or 0.1 mol L^{-1} NaOH. At pH 4, it was expected that the Fe^{III} produced during pyrite oxidation was either completely complexed in the presence of EDTA or precipitated by phosphate as $FePO_4$ in the absence of EDTA (Lindsay, 1979).

9.6.1 H_2O_2

During leaching experiments with 0.147 mol L^{-1} H_2O_2, Huang and Evangelou (1992, 1994) noted that pyrite oxidized rapidly and by the end of leaching approximately 70% of the pyrite in the column was consumed. The first order plot for these data shown in Figure 9.5 is curvilinear.

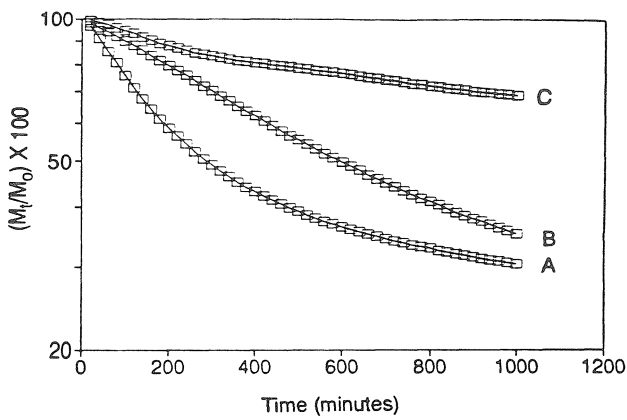

Figure 9.5. Plot of log (M_t/M_o x 100) vs. time of the oxidation data of pure pyrite leached at 40°C with the following three pH 4 solutions: A. 0.147 mol L^{-1} H_2O_2; B) 0.147 mol L^{-1} H_2O_2 and 0.013 mol L^{-1} EDTA; C) 0.147 mol L^{-1} H_2O_2 and 0.01 mol L^{-1} KH_2PO_4 (M_o = original amount of pyrite; M_t = amount of pyrite remaining at any time t). (From Huang and Evangelou, 1994. With permission.)

They considered that the curvature of the first order plot was most likely due to pyrite oxidation by the Fe^{III} released from pyrite, as indicated by Equation 6.61. In the first 200 minutes of leaching, most of the iron released from pyrite stayed in the solution (Figure 9.6).

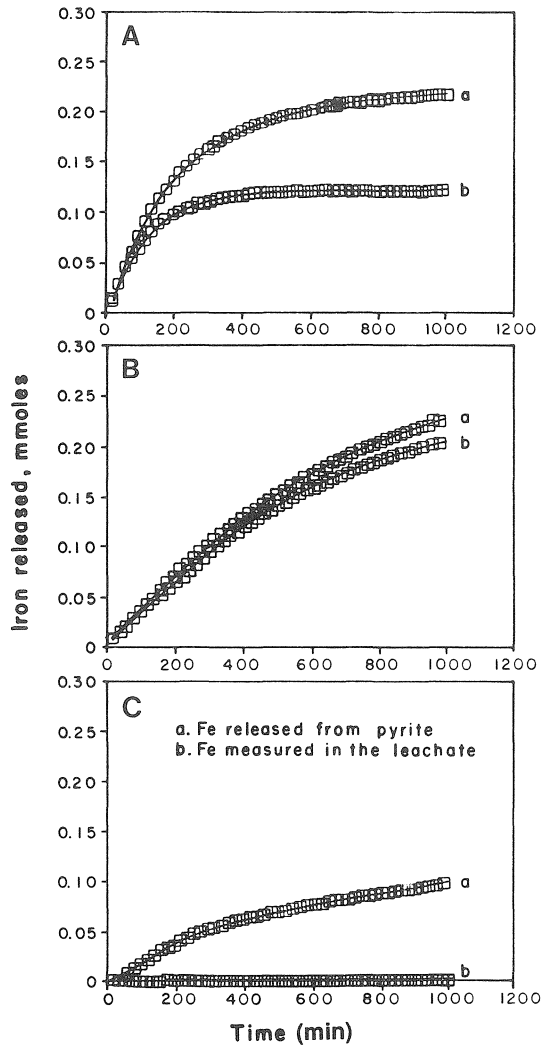

Figure 9.6. Amount of iron released during oxidation of 50 mg pyrite with the following solutions: A. 0.147 mol L^{-1} H_2O_2; B) 0.147 mol L^{-1} H_2O_2 and 0.013 mol L^{-1} EDTA; C) 0.147 mol L^{-1} H_2O_2 and 0.01 mol L^{-1} KH_2PO_4 (Mo = original amount of pyrite; M_t = amount of pyrite remaining during any time t) as calculated according to the expected pyrite Fe to S stoichiometry and measured analytically.

This is consistent with the high initial oxidation rate in the first 200 minutes of leaching with 0.147 mol L^{-1} H_2O_2 (Figure 9.5). However, after 200 minutes of leaching, apparently almost all iron released from pyrite had precipitated (Figure 9.6). Also from Figure 9.5, it seems clear that precipitation of iron within the column significantly reduced the rate of pyrite oxidation after 300 minutes. Apparently, much of the iron may have precipitated as a coating on the pyrite surfaces.

9.6.2 Phosphate

When phosphate is introduced into the leaching-oxidation system, there are two possibilities. The first possibility is that the leaching oxidation solution is undersaturated with respect to $FePO_4$ in the region adjacent to the surface of pyrite, but supersaturated with respect to $FePO_4$ in the bulk solution. It is possible that pH at the surface of pyrite is lower than the pH in the bulk solution. This is known to be true for surfaces that exhibit a negative surface potential (Mortland, 1968; Mortland and Raman, 1968). Pyrite is reported to exhibit a negative surface potential at bulk water pH above 2 (Ahmed, 1991; Fornasiero et al., 1992). Under these conditions, $FePO_4$ is very likely to precipitate as a discrete phase in the bulk solution. Under these conditions, the effect of phosphate on the kinetics of pyrite oxidation is expected to be the same as that of EDTA.

In the second possibility, the solution is supersaturated with respect to $FePO_4$ in the region adjacent to the surface of pyrite and $FePO_4$ will be deposited directly onto the surface of pyrite, forming a protective coating. Pyrite oxidation will gradually come to a stop with the latter possibility. Results in Figure 9.6C show that when pyrite was oxidized by 0.147 mol L^{-1} H_2O_2 and in the presence of 0.001 mol L^{-1} KH_2PO_4, almost 90% of Fe released from pyrite remained in the column. The results in Figure 9.6C clearly show that pyrite oxidation gradually came to a stop after an initial rapid reaction rate. By comparing the data in Figure 9.5B (pyrite oxidized with H_2O_2 in the presence of EDTA) with the data in Figure 9.5C (pyrite oxidized with H_2O_2 in the presence of phosphate) it can be concluded that phosphate controls pyrite oxidation via a mechanism other than precipitation of $FePO_4$ in the column as a discrete phase. This mechanism is most likely a $FePO_4$ coating on the surface of pyrite.

Additional support for the $FePO_4$ coating mechanism in controlling pyrite oxidation is given by the data in Figure 9.7. The rate of iron oxidation in the presence of an oxidizer is pH controlled. However, under strong acid conditions no ferric phosphate is expected to form. Therefore, when the pH of the influent leaching solution is decreased much below 3, the degree of saturation with respect to $FePO_4$ adjacent to the surface of pyrite is also decreased. Under such conditions, deposition of $FePO_4$ precipitates onto pyrite surfaces is expected to be diminished. Thus, coating control on the rate of pyrite oxidation will gradually disappear as pH is decreased. In this case,

pyrite oxidation is supposed to follow pseudo-first-order kinetics as shown by Equation 9.6.

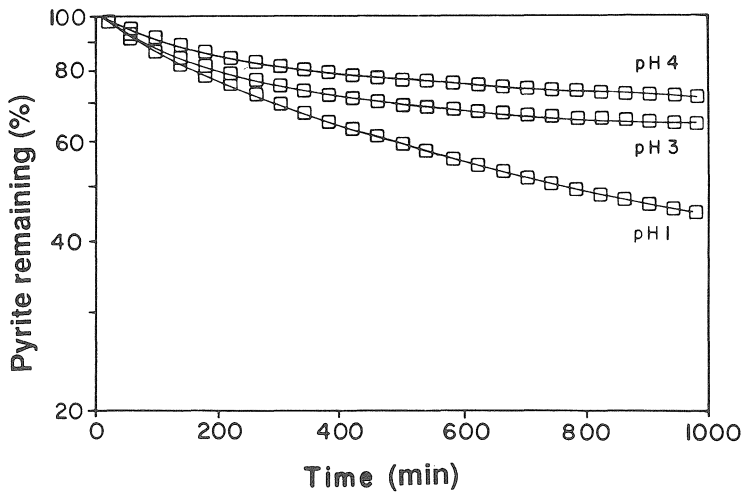

Figure 9.7. The influence of pH on pyrite oxidation by 0.147 mol L^{-1} H_2O_2 in the presence of 0.001 mol L^{-1} KH_2PO_4.

Results in Figure 9.7 lent support to such a trend. At pH 3 and 4, rate of pyrite oxidation gradually decreased; when pH was decreased to 1, the first-order plots of pyrite became nearly a straight line, suggesting that no coatings were formed. However, note also in Figure 9.7 that after 1000 minutes of leaching with 0.147 mol L^{-1} H_2O_2 and 10^{-3} mol L^{-1} phosphate approximately 40% of the pyrite remained unreacted as opposed to 30% when oxidation was carried out at pH 4 with 0.147 mol L^{-1} H_2O_2 but in the absence of phosphate (Figure 9.5A). This suggests that in the absence of phosphate, iron oxides may also form as coatings but their effectiveness in controlling pyrite oxidation may be less than that of $FePO_4$ coatings.

9.6.3 EDTA

Oxidation of S_2^{2-} by Fe^{III} could also be inhibited by employing a strong Fe^{III} complexing agent. Huang and Evangelou, (1993a, b) used EDTA to complex Fe^{III} by forming Fe-EDTA complexes (Lindsay, 1979), thereby preventing oxidation of pyrite by Fe^{III} and also formation of $Fe(OH)_3$, which might also coat pyrite particles. Luther et al. (1992) indicated that the standard redox potential of Fe^{III}/Fe^{II} could be lowered from 0.77 volts to approximately 0 volts by EDTA. Brown and Jurinak (1989a) used DTPA, another strong Fe^{III} complexing agent, to evaluate the role of O_2 on pyrite oxidation. Thus, assuming that the concentration of EDTA used had insignificant influence on the potential of H_2O_2 to oxidize pyrite, e.g., standard reference potential remained unaffected, or EDTA did not adsorb on to the surface of pyrite, then the presence of EDTA would represent a situation where the observed rate of pyrite oxidation was solely due to the direct oxidation of S_2^{2-} by H_2O_2. The kinetic oxidation data from this treatment were expected to give a log M/M_o versus t plot (Equation 9.6) with a single slope.

Data on the standard reference potential (SRP) (Kokholm, 1977) employing a platinum electrode and a calomel reference electrode showed that the EDTA, at the concentration level used in this study, did not affect the SRP. Standard reference potential values in the absence and presence of 0.147 mol L^{-1} H_2O_2 differed less that 5% in the pH range 4 to 9 (Figure 9.8).

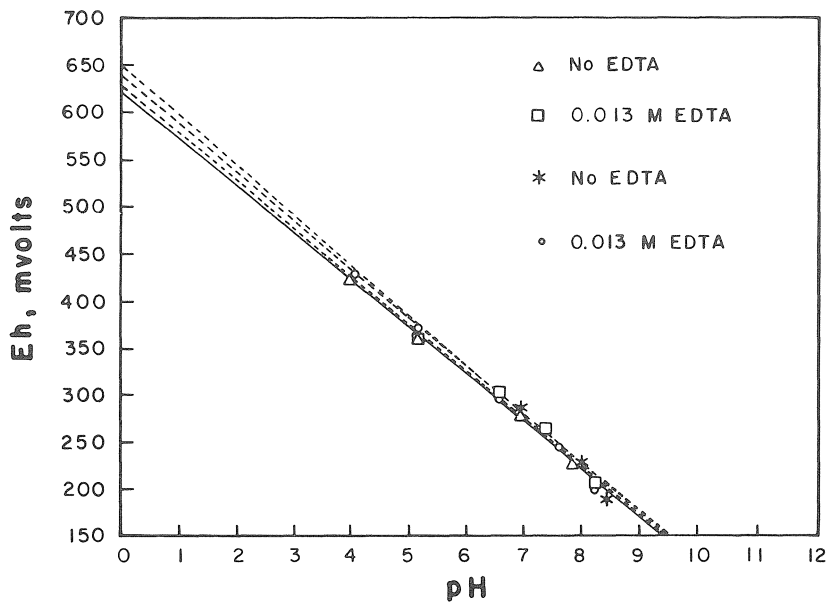

Figure 9.8. Dependence of the standard redox-electrode reference potential (SERP) on pH in the presence and absence of 0.013 mol L^{-1} EDTA after an equilibration time of 10 min or 4 hours.

However, EDTA could still affect the rate of pyrite oxidation by perhaps forming pyrite/surface-EDTA complexes, thus, affecting the electrical potential difference between pyrite surface and bulk solution. This is, however, highly unlikely since Fe^{III}-EDTA complexes are negatively charged and the pyrite surface is also negatively charged (Luther et al., 1992). Furthermore, mechanistic inferences as pointed out by Evangelou (1994) do not lent support to the hypothesis that EDTA may have direct influence on pyrite oxidation because 1) pseudo-first order plots of pyrite oxidation under varying H_2O_2 concentrations exhibit single slope which infers a single mechanism of pyrite oxidation (Turner, 1959; Turner and Skinner, 1959), 2) in the presence of EDTA all iron released from pyrite oxidation was kept in solution and flushed out of the pyrite oxidizing column (Figure 9.6B), and 3) as expected, initial rate of pyrite oxidation in the presence of EDTA was smaller than in the absence of EDTA (Figure 9.5). Based on the above, one would conclude that the observed rate of pyrite oxidation in the presence of EDTA was solely due to the direct oxidation of pyrite by H_2O_2.

According to the data in Figure 9.5B, the linearity of the plots (when pyrite was oxidized in the presence of EDTA) infer that pyrite oxidation at constant H_2O_2 concentration obeyed pseudo-first-order kinetics. This can be justified by considering that in the presence of EDTA the second term of Equation (6.61) approaches zero. However, plot linearity does not infer that the oxidation process is a true first-order reaction with respect to H_2O_2. In order to test this, the slopes of the pseudo-first-order plots, obtained under various H_2O_2 concentrations, were plotted against the concentration of H_2O_2. The relationship is

$$\text{Slope} = K[k_1/2.3][H_2O_2]^{v_1} \tag{9.7}$$

Taking logarithms on both sides of Equation 9.7 transforms to

$$\log \text{Slope} = \log K[k_1/2.3] + v_1 \log [H_2O_2] \tag{9.8}$$

A plot of log slope vs. log $[H_2O_2]$ would produce a straight line with v_1 as the slope, signifying order of reaction, and log $K[k_1/2.3]$ as the y-intercept. The plot for these data is shown in Figure 9.9. These data suggest that pyrite oxidation is not a true first order reaction with respect to H_2O_2 (slope=0.68). Similar results were obtained when using O_2 (Hood, 1991 and references therein).

9.6.4 Michaelis-Menten kinetics/application

The theory of Michaelis-Menten-kinetics is described in Chapter 8. In this section, the inorganic oxidation of pyrite will be treated as a Michaelis-Menten process (which is analogous to a Langmuir surface process) to evaluate the role of the pyrite surface on oxidation. The data in

Figure 9.10 represent three pyrite oxidation treatments 1) H_2O_2 alone, 2) H_2O_2 plus EDTA as an oxidation inhibitor, and 3) H_2O_2 plus PO_4 also as an oxidation inhibitor. The data in Figure 9.10 show that in general all three lines appear to point towards a common Y-intercept.

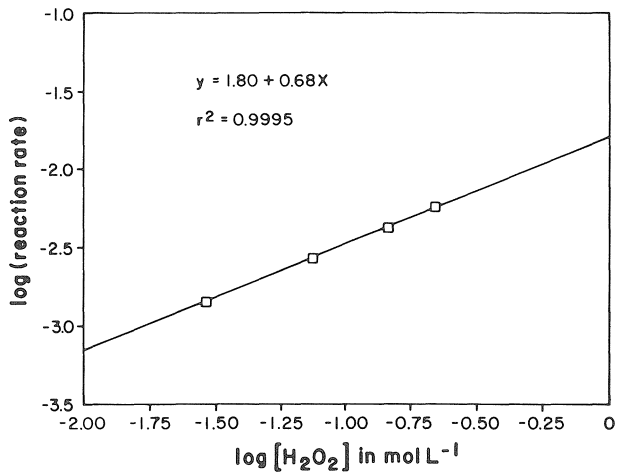

Figure 9.9. Relationship between log[slope] of pseudo-first-order plots of pyrite oxidation and log[H_2O_2] concentration in the presence of 0.013 mol L^{-1} EDTA.

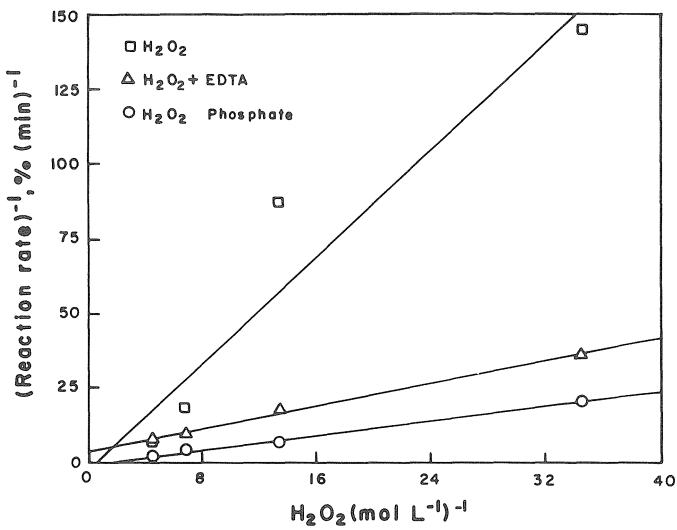

Figure 9.10. Double reciprocal plots of pyrite oxidation by H_2O_2 using EDTA and phosphate as inhibitors.

This suggested that neither of the inhibitors, as expected, reacted with the surface of pyrite to alter its oxidation potential. Another way to put it is that the Y-intercepts do not clearly suggest any specific pyrite surface/inhibitor interaction. However, the slopes of these three lines, representing the three treatments, are clearly distinct. This suggests that the interaction between H_2O_2 and inhibitor(s) is most likely competitive.

In the case of H_2O_2 alone, the shape of the plot was not affected by the concentration of H_2O_2. This suggested perhaps a high affinity of the H_2O_2 by the pyrite surface (Luther, 1990). In the case of H_2O_2 plus EDTA, the slope of the plot is greater than that of H_2O_2 alone suggesting that in the the case of H_2O_2 alone Fe^{III} is contributing significantly to pyrite oxidation, as expected.

In the case of H_2O_2 plus phosphate, the slope of the plot increased dramatically. This suggested that phosphate acted as a competitive inhibitor. The mechanism by which phosphate acted as a competitive inhibitor during the initial stages of oxidation (prior to any coating formation on the surface of pyrite) was that perhaps the adsorbed Fe^{III} appeared to form Fe-phosphate complexes on the surface of pyrite, thus diminishing the capacity of Fe^{III} to act as an electron sink. A similar role have been demonstrated by Cl^- in the oxidation of Fe^{II} (Millero and Izaguirre, 1989). In this case, the relatively strong $FeCl^+$ complexes diminish the capacity of Fe^{II} to donate electrons. Thus, the Fe-phosphate complexes forming on the surface of pyrite may inhibit electron transfer to Fe^{III} as well as to H_2O_2. Inhibition of pyrite oxidation by phosphate has also been demonstrated by Hood (1991).

9.6.5 Surface analysis

Field emission scanning electron microscope photos shown in Figure 9.11 reveal that after leaching pyrite with 0.147 M H_2O_2, the residual pyrite particles were coated with a layer of iron hydroxide (Figure 9.11A). As expected, the residual pyrite particles of the system leached with the solution containing 0.147 mol L^{-1} H_2O_2 and 0.013 mol L^{-1} EDTA (Figure 9.11B) were free of any coatings and most pyrite particles displayed a typical framboidal morphology. However, after leaching the pyrite with the solution containing 0.147 mol L^{-1} H_2O_2 and 0.01 mol L^{-1} KH_2PO_4, residual pyrite particles were heavily coated with $FePO_4$ (Figure 9.11C).

Huang and Evangelou, (1994) used the element specific x-ray energy-dispersive analysis from the (EDAX) SEM to locate the distribution of Fe, S, and P on the surfaces of pyrite pre-leached with H_2O_2/KH_2PO_4 solution. These data/evidence are presented in Figure 9.12. As shown in Figure 9.12, the distribution of Fe and S was similar to the of P, but the intensity of iron was much higher than those of S and P. This strongly suggested the presence of iron phosphate on pyrite surfaces. The higher intensity of Fe was apparently due to its presence in both minerals FeS_2 and $FePO_4$.

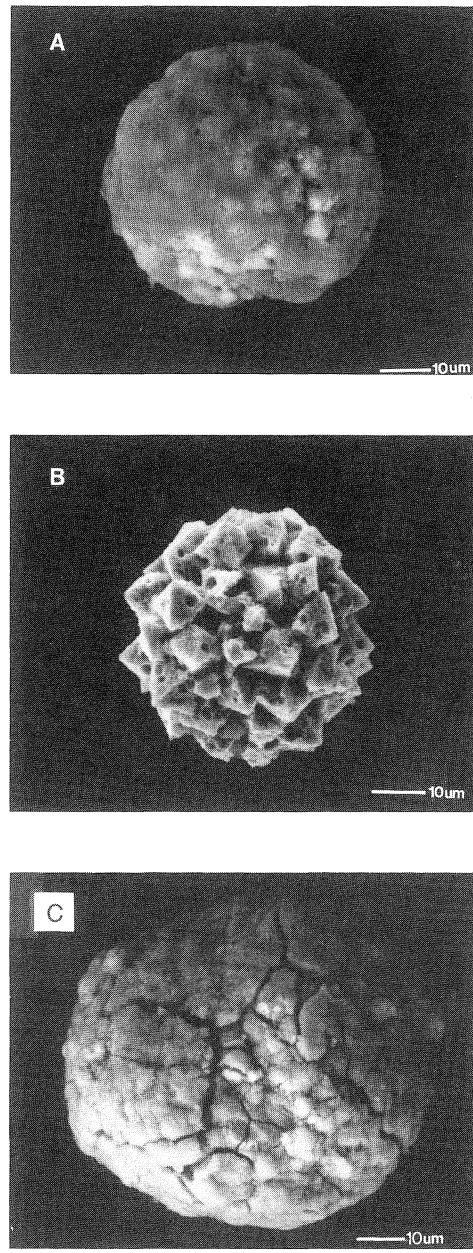

Figure 9.11. Scanning electron microscope photos showing the surface status of single particles after leaching with the following solutions: A. 0.147 mol L^{-1} H_2O_2; B. 0.147 mol L^{-1} H_2O_2 and 0.013 mol L^{-1} EDTA; C. 0.147 mol L^{-1} H_2O_2 and 0.01 mol L^{-1} KH_2PO_4.

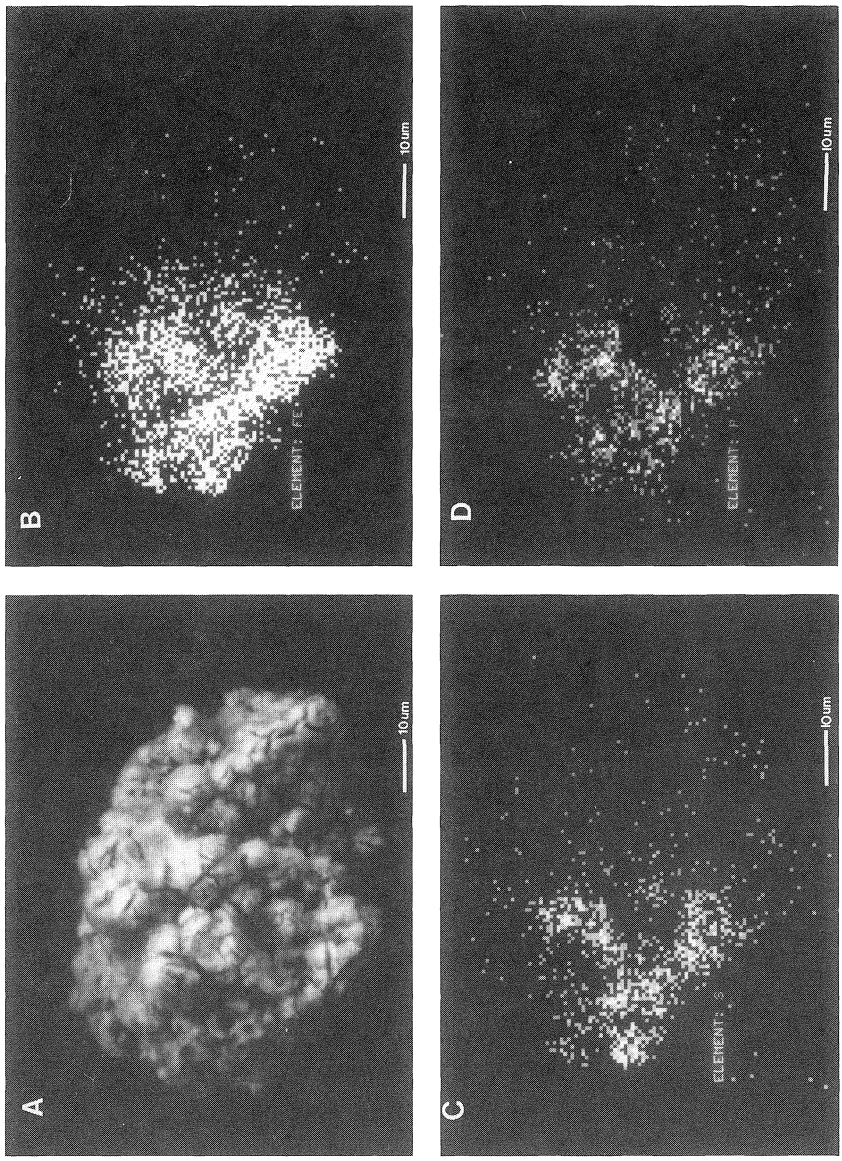

Figure 9.12. EDAX dot mapping of a pyrite particle after it was leached with a solution containing 0.147 mol L^{-1} H_2O_2 and 0.01 mol L^{-1} KH_2PO_4, showing distribution of iron, phosphorus, and sulfur on its surface. A. morphology of the particle examined; B. distribution of iron; C. distribution of sulfur; D. distribution of phosphorus. (From Huang and Evangelou, 1994. With permission.)

The fact that S appeared also on the $FePO_4$ coated sample suggested that the coating was very thin and or S may be a SO_4 impurity on the $FePO_4$ coatings.

Acid dissolution and analyses of the $FePO_4$ coatings revealed that the mole ratio of iron to phosphate was 1.0, suggesting that the coating was $FePO_4$ and that no significant hydroxyl quantity entered the structure of iron phosphate (Huang and Evangelou, 1994). Coated pyrite was also examined using diffuse reflectance infrared spectroscopy (FT-IR) (Griffiths and Fuller, 1981; Nakamoto, 1963, 1986). As shown in Figure 9.13, after leaching with the solution containing 0.147 mol L^{-1} H_2O_2 and 0.01 mol L^{-1} KH_2PO_4, the intensity of the IR absorption band at 439.7 cm^{-1} on the spectrum of the pyrite dramatically decreased.

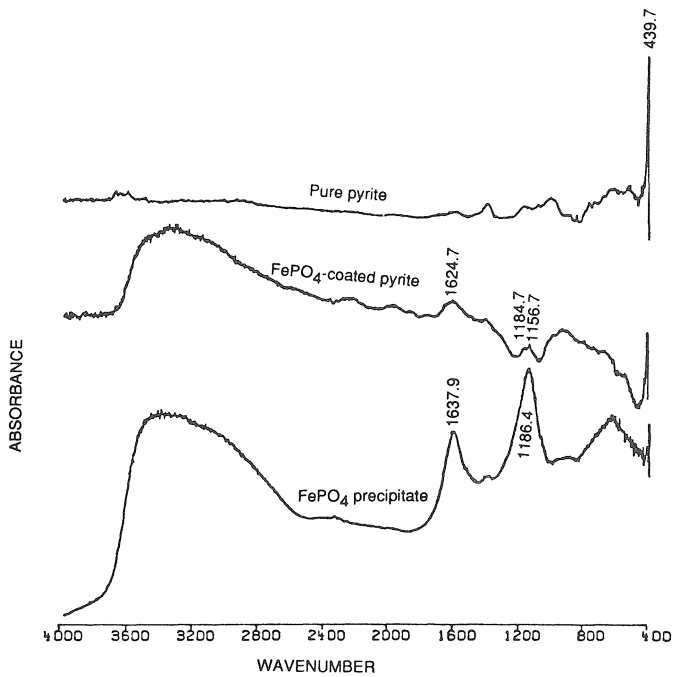

Figure 9.13. Diffuse reflectance infrared spectra of pyrite before and after leaching with a solution containing 0.147 mol L^{-1} H_2O_2 and 0.01 mol L^{-1} KH_2PO_4.

This absorption band was due to the vibration of the disulfide (S-S) in the lattice of pyrite; the decrease in intensity of this band supported the presence of the coating on pyritic surfaces. Two additional bands at 1637.9 and 1186.4 cm^{-1} and a broad band ranging from 3700 to 2800 cm^{-1} were also observed on the spectrum of the $FePO_4$-coated pyrite. The absorption band at 1837.9 cm^{-1} and the absorption hump around 3000 cm^{-1} were attributed to the bending vibration and rotation of water molecules either adsorbed on iron

phosphate or present within the structure of iron phosphate. The adsorption band at 1186.4 cm^{-1} was due to the P-O internal stretching vibration of PO_4 group (Nanzyo, 1986). Comparison of the spectra of $FePO_4$-coated pyrite with the spectra of freshly precipitated $FePO_4$ in H_2O at pH 4 suggested that the coating of the surface of pyrite was most likely $FePO_4\,nH_2O$.

9.6.6 Effectiveness

Feasibility of this coating approach in preventing pyrite oxidation was tested on pulverized coal refuse pyritic shale. Huang and Evangelou (1994) leached the shale sample (500 mg) with 500 mL of the solution containing 0.053 mol L^{-1} H_2O_2 and 10^{-3} mol L^{-1} KH_2PO_4. This coating process consumed approximately ten percent of the total amount of pyrite in the pyritic shale. The pyritic shale was then subjected to leaching with 0.088 mol L^{-1} H_2O_2 to test the effectiveness of the coating in preventing pyrite oxidation. As shown in Figure 9.14, the data strongly suggest the presence of $FePO_4$-coated pyrite.

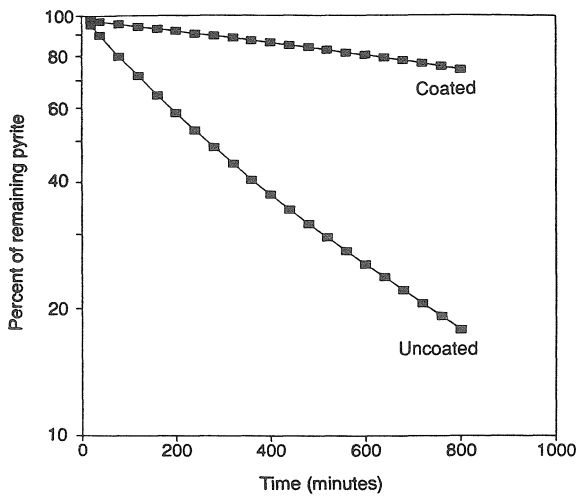

Figure 9.14. Relationship between percent pyrite oxidized vs. time: Pyrite first treated with 0.001 mol L^{-1} KH_2PO_4 and 0.073 mol L^{-1} H_2O_2 at 40°C; and then sample in one column was leached with 2 mol L^{-1} HCl, while other sample was not leached with HCl. Then, both samples were leached with H_2O_2 as shown.

The data presented in this paper represent a summary of the data of all the experiments we have carried out on this pyrite microencapsulation approach. For more information on this see the formal report of the project to the U.S. Bureau of Mines, Department of Interior (Huang and Evangelou, 1992).

Taylor & Francis
Taylor & Francis Group
http://taylorandfrancis.com

Chapter 10
PRELIMINARY DATA ON PYRITE MICROENCAPSULATION IN MINE WASTE

A pyrite microencapsulation (coating) approach was described in Chapter 9. It involved leaching pyrite or pyritic shale with a weak phosphate solution containing hydrogen peroxide (H_2O_2). The latter oxidized a surface portion of pyrite, released Fe^{III} and formed an iron phosphate ($FePO_4$) coating on pyrite. Hydrogen peroxide oxidation tests on coated and uncoated pyrite demonstrated that this coating could control pyrite oxidation.

In this chapter the optimal conditions for generating stable, oxidation-proof ferric phosphate or iron oxide coatings on the surface of pyrite will be discussed based on results from leaching columns of coal refuse pyritic shale. The sample was first pulverized, then passed through a 60 mesh sieve. Pyrite content of the shale was 6.5% (Huang and Evangelou, 1992; Huang and Evangelou, 1994; Evangelou, 1994). Coating and leaching-oxidation tests were carried out using 0.5 g of the pyritic shale sample mixed with approximately 1 g of sand and using a miscible displacement technique (for more details see Evangelou, 1994; Huang and Evangelou, 1994).

10.1 pH

The data in Figure 10.1 show the effect of pH on the effectiveness of the H_2O_2/KH_2PO_4 solution in preventing oxidation. Leaching the pyritic shale with the coating solution adjusted to pH 2 did not lead to any significant suppression of pyrite oxidation (curve C) (approximately 50% of the pyrite present in the shale was oxidized during the coating process (Table 10.1)). However, leaching the pyritic shale with the coating solution (H_2O_2/KH_2PO_4) adjusted to pH above 4, oxidation of pyrite was substantially suppressed.

The percent of pyrite oxidized during leaching with the coating solutions of H_2O_2/KH_2PO_4, adjusted to pH 4 and 6 is nearly the same (approximately 20% (Table 10.1)). However, there was a slight difference in the suppression of pyrite oxidation between these two systems (pH 4 and pH 6.) (Figure 10.1). The pyritic shale sample precoated with pH 6 coating solution displayed a faster oxidation rate than that of the pyritic shale precoated with pH 4 H_2O_2/KH_2PO_4 solution. This was probably due to the decomposition of iron phosphate coatings. At pH 6 and 0.001 mol L^{-1} phosphate, iron phosphate and iron hydroxide both are likely to form (Figure 10.2). Thus, hydroxyl may enter the structure of the coatings and decrease their stability. This inference needs further investigation.

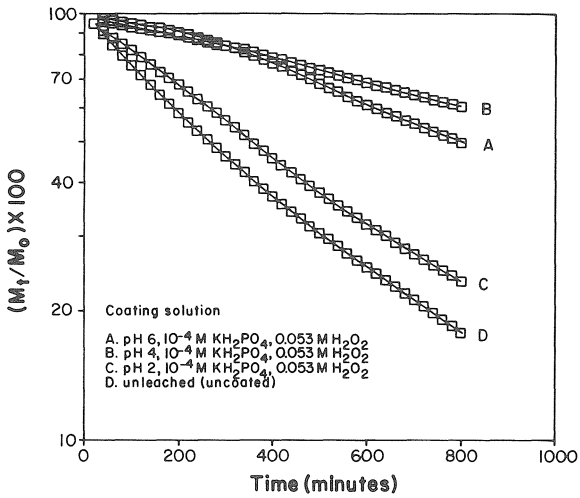

Figure 10.1. Effect of pH on the effectiveness of the leaching solution in coating pyrite in shale and preventing its oxidation. (First, the samples were treated with the coating solution; coating effectiveness was then tested by leaching the iron phosphate coated pyritic shale (Table 1) with 0.088 mol L^{-1} H_2O_2 at 40°C).

Table 10.1
Chemical composition of the coating solutions and percent of pyrite oxidized during leaching of the pyritic shale columns with 0.088 mol L^{-1} H_2O_2.

H_2O_2 mol L^{-1}	KH_2PO_4 mol L^{-1}	pH	Temperature °C	Percent pyrite oxidized
0.053	10^{-3}	4	40	20.0
0.027	10^{-3}	4	40	11.4
0.000	10^{-3}	4	40	0.0
0.053	10^{-4}	4	40	24.0
0.053	10^{-3}	4	40	20.0
0.053	10^{-2}	4	40	23.0
0.053	10^{-3}	2	40	49.6
0.053	10^{-3}	4	40	20.0
0.053	10^{-3}	6	40	19.6
0.053	10^{-3}	4	25	13.4
0.053	10^{-3}	4	40	20.0
0.053	10^{-3}	4	60	80.0

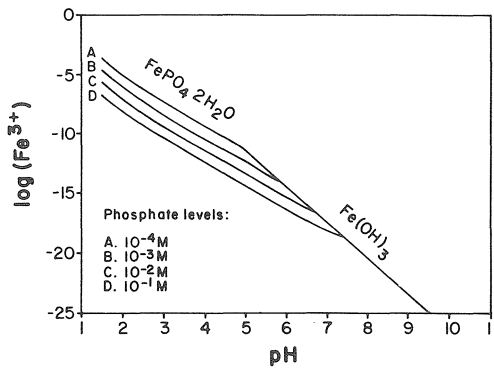

Figure 10.2. Stability diagram of iron phosphate and iron hydroxide. Equilibria constants for determining stability lines were obtained from Lindsay (1979).

10.2 Temperature

Temperature might influence coating formation in two ways. First, precipitation and crystallization of iron phosphate is influenced by temperature, and effectiveness of coatings in preventing pyrite oxidation depends on degree of crystallinity of iron phosphate. Second, rate of pyrite oxidation is dependent on temperature; so are activity of Fe^{III} and H^+ on pyrite surfaces during leaching with coating solutions. Increase in free Fe^{III} concentration (activity) could lead to a thicker coating on pyrite, while increase in acidity could inhibit formation of iron phosphate coating.

As shown in Figure 10.3, leaching the pyritic shale with the H_2O_2/KH_2PO_4 solution at both 25°C and 40°C resulted in a significant suppression of pyrite oxidation. However, leaching at 40°C resulted in more pyrite oxidation suppression than at 25°C. This suggests thicker coating was created at 40°C than at 25°C.

As expected, percent of pyrite oxidized during the coating process increased from 13.4% at 25°C to 20% at 40°C (Table 10.1). Part of the increase in the percent of pyrite oxidized during coating as temperature was increased, could be due to the increased amount of acid produced. When the temperature was raised to 60°C, leaching with the coating solution led to 80% of the pyrite to be oxidized (Table 10.1), indicating that no iron phosphate coating was formed. This suggested that at this temperature, the acid produced from pyrite oxidation completely prevented formation of iron phosphate coatings.

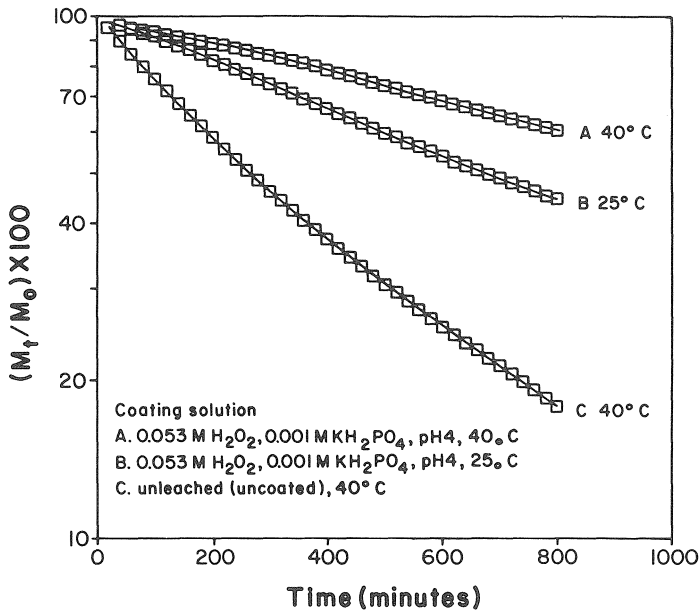

Figure 10.3. Effect of temperature on the effectiveness of the leaching solution in coating pyrite and preventing its oxidation. (First, the samples were treated with the coating solution; coating effectiveness was then tested by leaching the iron phosphate coated pyritic shale (Table 1) with 0.088 mol L^{-1} H_2O_2 at 40°C).

10.3 H_2O_2

Figure 10.4 shows the effect of H_2O_2 concentration in the coating solution on coating pyrite and preventing pyrite oxidation. Attempting to coat pyrite with a phosphate solution but in the absence of H_2O_2 did not lead to any suppression of pyrite oxidation during leaching with 0.088 mol L^{-1} H_2O_2. This indicated that application of solution phosphate alone to pyritic materials did not introduce an iron phosphate coating on pyrite surfaces. However, after leaching pyrite with 0.001 mol L^{-1} phosphate solution containing 0.027 mol L^{-1} or 0.053 mol L^{-1} H_2O_2, pyrite oxidation was substantially suppressed compared to the control (curve A, B, and D).

At the end of leaching of all the pyritic shale columns with 0.088 mol L^{-1} H_2O_2, only 25%-35% of the pyrite present in the system was oxidized in the coated columns as opposed to more than 75% in the uncoated columns. This indicated that H_2O_2 in the concentration ranging from 0.027

mol L^{-1} H_2O_2 to 0.053 mol L^{-1} generated enough Fe^{III} near the pyrite surfaces to form $FePO_4$ coatings.

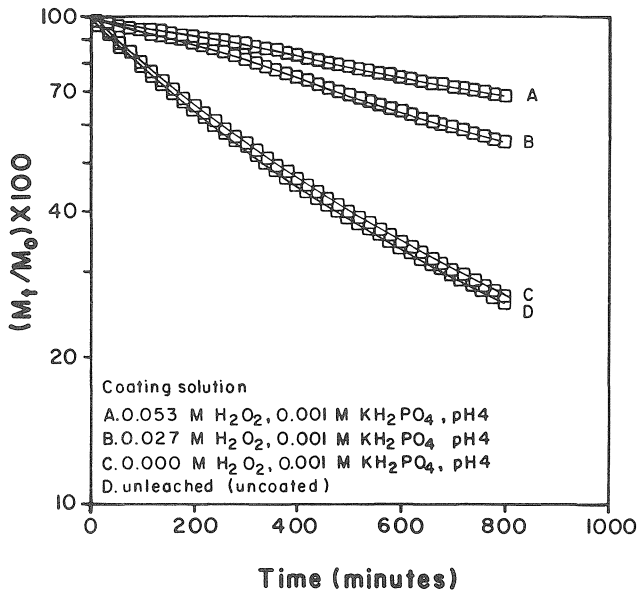

Figure 10.4. Influence of H_2O_2 concentration on the effectiveness of the leaching solution in coating and preventing oxidation of a pyritic shale sample. (First, the samples were treated with the coating solution; coating effectiveness was then tested by leaching the iron phosphate coated pyritic shale (Table 1) with 0.088 mol L^{-1} H_2O_2 at 40°C).

Percent of pyrite oxidized during the pyrite coating process increased almost proportionally to the increase in H_2O_2 concentration. When H_2O_2 concentration was increased from 0.027 mol L^{-1} to 0.053 mol L^{-1}, the percent of pyrite oxidized increased from 11.4% to 20% (Table 10.1). However, the resultant suppression of pyrite oxidation due to coating did not correspond proportionally to the amount of pyrite consumed during coating. In the first 200 minutes of leaching with 0.088 mol L^{-1} H_2O_2, the rate of pyrite oxidation in the pyritic shale precoated with 0.027 mol L^{-1} H_2O_2 was nearly similar to that in the shale precoated with 0.053 mol L^{-1} H_2O_2 (Figure 10.4). This indicated that the use of higher concentration of H_2O_2 did not necessarily mean that a thicker coating would be created on pyrite surfaces, even through pyrite would be oxidized. The reason for this is that as H_2O_2

concentration increases, Fe^{III} concentration and H^+ concentration on pyrite surfaces increases. The low pH near the pyrite surfaces can effectively hinder precipitation of iron phosphate as coating. Meanwhile, once Fe^{III} exceeds a certain level of activity (formation of iron phosphate requires a very low Fe^{III} activity, see Figure 10.2), it can no longer promote formation of iron phosphate coatings. Thus, H_2O_2 concentration should be chosen on the basis of coating pyrite by consuming the least amount of pyrite.

The rate of pyrite oxidation in the shale precoated with 0.027 mol L^{-1} H_2O_2 and 0.001 mol L^{-1} phosphate (Figure 10.4B) was faster than that precoated with 0.053 mol L^{-1} KH_2PO_4 (Figure 10.4A) after 200 minutes of leaching with 0.088 mol L^{-1} H_2O_2. This suggested that the thickness or the structure of iron phosphate coatings is indeed influenced by the concentration of H_2O_2 in the coating solution as long as pH is maintained constant in both systems.

10.4 Phosphate

The data in Figure 10.5 show the effect of phosphate concentration on the effectiveness of the coating solution in preventing pyrite oxidation.

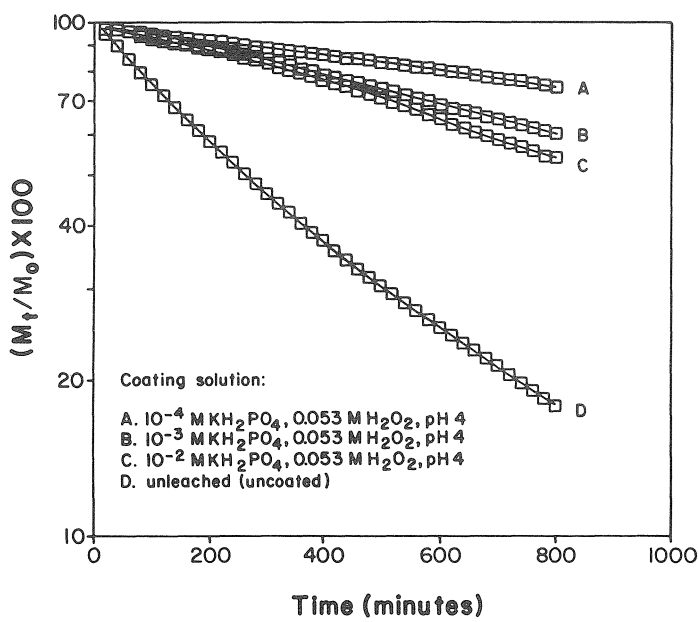

Figure 10.5. Influence of phosphate concentration on the effectiveness of the leaching solution in coating pyrite and preventing its oxidation. (First, the samples were treated with the coating solution; coating effectiveness was then tested by leaching the iron phosphate coated pyritic shale (Table 1) with 0.088 mol L^{-1} H_2O_2 at 40°C).

When phosphate concentration was increased from 0.0001 mol L^{-1} to 0.01 mol L^{-1}, percent of pyrite oxidized during the coating process was the same (about 20%, Table 10.1). In addition, after precoating pyritic shale under various solution phosphate levels, pyrite oxidation rates with 0.88 mol L^{-1} H_2O_2 were similar. This indicated that formation of iron phosphate coating was somewhat independent of phosphate concentration. This was mainly due to the extremely low solubility of iron phosphate.

According to the solubility product of strengite ($FePO_4 \cdot 2H_2O$) at pH 4 and 0.0001 mol L^{-1} phosphate, the minimum approximate concentration of free Fe^{III} required for formation of $FePO_4$ is 10^{-9} mol L^{-1}. The approximate concentration of free Fe^{III} in the leachate (calculated from the SO_4 experimental data according to the Fe/S pyrite stoichiometry) when pyrite was leached with 0.053 mol L^{-1} H_2O_2 ranged from 0.0001 to 0.001 mol L^{-1}. This concentration was well above the Fe^{III} concentration required for formation of iron phosphate coating (Figure 10.2). Thus, variation in phosphate concentration would not cause any decrease in the efficiency of the H_2O_2/KH_2PO_4 solution in forming pyrite coating.

Based on the above results, one may conclude that iron phosphate coating on pyrite surfaces can be established at a wide range of H_2O_2/KH_2PO_4 solution conditions: 1) H_2O_2 concentration can range from 0.027 mol L^{-1} to 0.053 mol L^{-1}; 2) phosphate concentration can vary from 0.0001 to 0.01 mol L^{-1}; 3) pH of the coating solution should always be above 4; 4) leaching pyritic shale with the coating solution at both room temperature and 40°C can effectively introduce an iron phosphate pyrite coating.

Concerns were raised, however, about the potential instability of hydrogen peroxide in the presence of organics. For this reason, a series of experiments were carried out employing a sample composed mostly of bituminous coal with 11% pyrite. The sample was first ground and then passed through two consecutive sieves, a 1 mm sieve and a 60 mesh sieve. The sample that passed through the 60 mesh sieve was used in column experiments. Detail on these studies are given in Huang and Evangelou, (1992).

Small column experiments as previously discussed, were intended to determine optimal conditions for coating pyrite in the presence of coal and to examine the necessity of sodium acetate (NaAC) to be used as a pH buffer. Previously, the necessity of adjusting the pH somewhere near 5 for effective pyrite microencapsulation to occur was demonstrated. In this part of the study, columns were prepared by loading a mixture of 0.5 g fine fraction coal waste and 1.0 g of 100 mesh sand into the chromatographic column, forming a coal waste column height of 1 cm (Huang and Evangelou, 1992). All the columns were first leached with 50 mL of 2 *M* HCl to expose pyrite surfaces. The columns were then leached with various NaAC containing coating solutions at 40°C temperature. To test the effectiveness of

H_2O_2/KH_2PO_4/NaAC solutions in inhibiting pyrite oxidation, some of the columns served as control. All columns were leached with a 0.053 mol L^{-1} H_2O_2 and 0.05 mol L^{-1} NaAC at pH 5 in the absence of phosphate at 40°C.

10.5 Effect of Na-Acetate on Kinetics of Pyrite Oxidation

The data in Figure 10.6 show the first order kinetics (log M_t/M_o x 100 vs. t) of pyrite oxidation when columns were leached with three NaAC-containing solutions at 40°C.

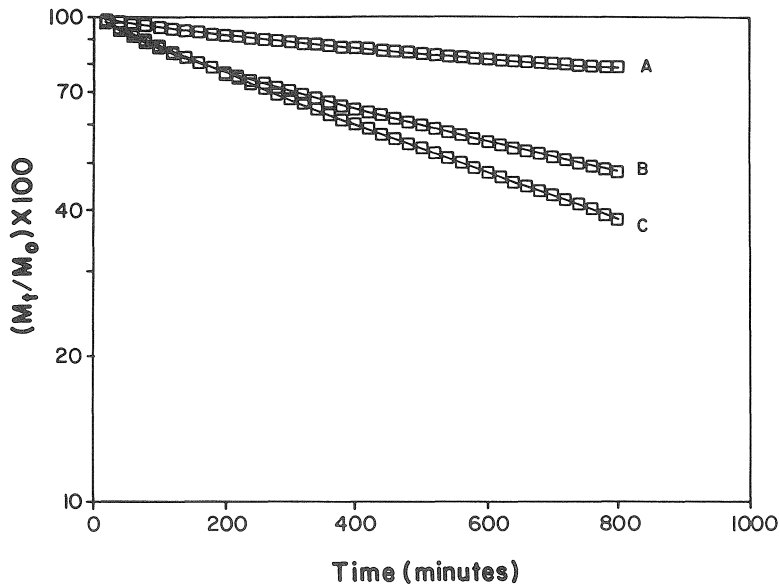

Figure 10.6. Plot of log (M_t/M_o x 100) vs. time for the data of oxidation of pyrite present in 0.5 g coal waste leached with the following three solutions at 40°C: A. solution containing 0.053 mol L^{-1} H_2O_2, 0.001 mol L^{-1} KH_2PO_4, and 0.1 mol L^{-1} NaAC pH 5; B. solution containing 0.053 mol L^{-1} H_2O_2 and 0.1 mol L^{-1} NaAC pH 5; C. solution containing 0.053 mol L^{-1} H_2O_2, 0.013 mol L^{-1} EDTA, and 0.1 mol L^{-1} NaAC pH 5 (Mo = original amount of pyrite present; M_t = amount of pyrite remaining at time t).

As expected, the rate of pyrite oxidation was much lower when coal waste was leached with solution containing 0.053 mol L^{-1} H_2O_2, 0.001 mol L^{-1} KH_2PO_4 plus 0.1 mol L^{-1} NaAC (curve A) than when coal waste was leached with a solution containing 0.053 mol L^{-1} H_2O_2, 0.013 mol L^{-1} EDTA plus 0.1 mol L^{-1} NaAC (curve C). This strongly suggested that leaching coal waste with the coating solution containing NaAC can effectively introduce

iron phosphate coatings on pyrite surfaces. This is consistent with the results obtained in the absence of NaAC. Furthermore, the rate of pyrite oxidation when he coal waste was leached with 0.053 mol L^{-1} H_2O_2 plus 0.1 mol L^{-1} NaAC (curve B) was similar to that of pyrite leached with 0.053 mol L^{-1} H_2O_2 containing 0.013 mol L^{-1} EDTA during the first 200 minutes, and decreased after 200 minutes. This suggested that iron released from pyrite in the presence of NaAC hydrolyzed forming iron hydroxide and perhaps some of this iron hydroxide may even precipitated as a coating on pyrite surfaces.

The results shown in Figure 10.7 demonstrate that during leaching coal waste with the coating solution (10^{-3} mol L^{-1} KH_2PO_4 and 0.053 mol L^{-1} H_2O_2) in the absence of NaAC, pyrite oxidized rapidly and at the end of leaching nearly 40% of it was consumed.

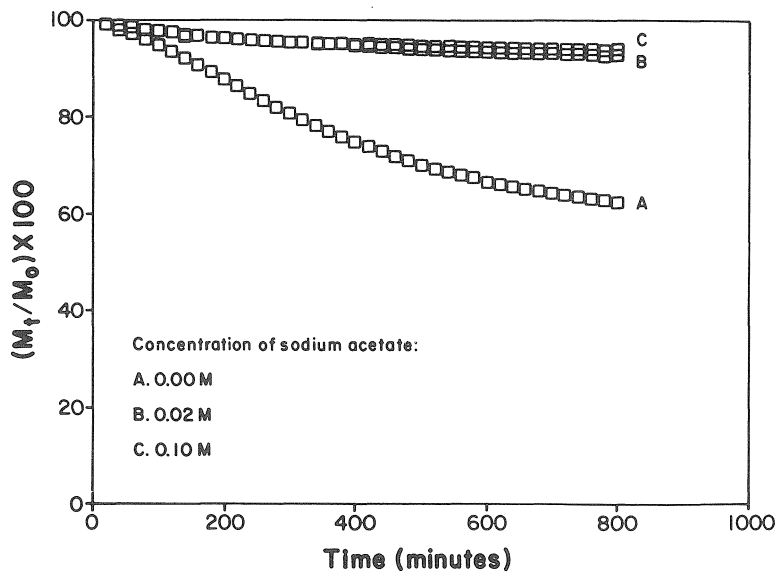

Figure 10.7. Effect of concentration of NaAC on the rate of oxidation of pyrite present in 0.5 g coal waste, leached at room temperature with pH 6 solutions containing 0.053 mol L^{-1} H_2O_2, 0.001 mol L^{-1} KH_2PO_4, and a varying concentration of NaAC.

This indicates that the H^+ produced during pyrite oxidation, had inhibited formation of iron phosphate coatings. When coal waste was leached with H_2O_2/KH_2PO_4 in the presence of 0.01 mol L^{-1} NaAC, pyrite oxidation was greatly suppressed and the end of leaching less than 10% of the pyrite was oxidized. Therefore, by maintaining pH of the coating solution near 5, NaAC promoted effectively precipitation of iron phosphate as a coating. When the sodium acetate concentration was set above 0.02 mol L^{-1}, further suppression

of pyrite oxidation during leaching was not observed (Figure 10.7). This suggested that the effect of H^+ on formation of iron phosphate coatings can be effectively prevented in the presence of a low concentration sodium acetate as long as NaAC maintains constant pH.

10.6 pH, Phosphate and H_2O_2

The data in Figure 10.8 show the effect of pH on pyrite oxidation during leaching with the NaAC-containing coating solution (0.001 mol L^{-1} KH_2PO_4 and 0.053 mol L^{-1} H_2O_2).

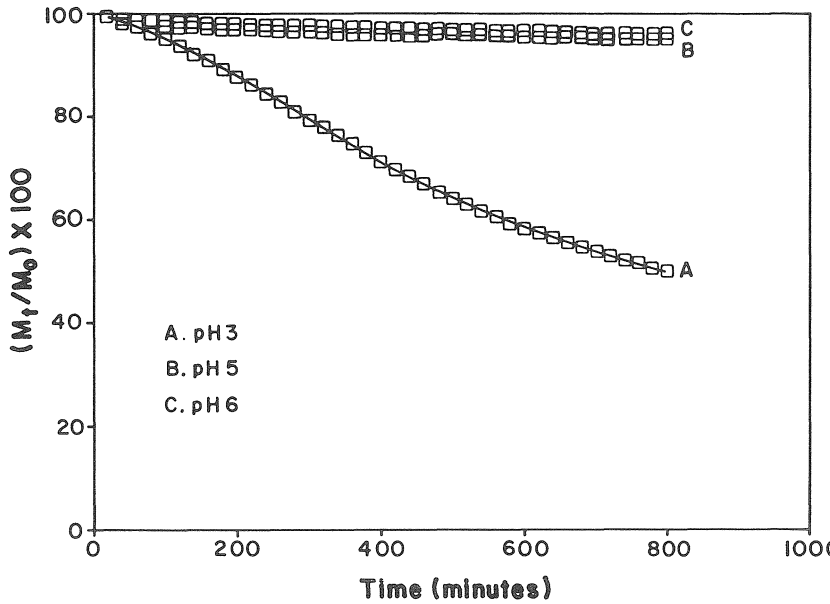

Figure 10.8. Effect of pH on the rate of oxidation of pyrite present in 0.5 g coal waste, leached at room temperature with solution containing 0.053 mol L^{-1} H_2O_2, 0.001 mol L^{-1} KH_2PO_4, and 0.1 mol L^{-1} NaAC but varying in pH from 3 to 6.

When the coal waste was leached with a pH 3 coating solution, pyrite oxidized rapidly and at the end of leaching more than 50% of the pyrite present was oxidized. This suggested that no iron phosphate coatings were formed during leaching with the pH 3 coating solution. When coal waste was leached with the pH 5 coating solution, the rate of pyrite oxidation substantially decreased and at the end of leaching, only approximately 6% of the pyrite present was oxidized. Above pH 5, pH seemed to have no increasing significant influence on inhibiting pyrite oxidation during leaching with the coating solution (Figure 10.8).

Figure 10.9 shows the effect of phosphate concentration on pyrite oxidation during leaching with the H_2O_2/KH_2PO_4 coating solution containing NaAC. It indicated that formation of iron phosphate coatings was not sensitive to the variation in phosphate concentration.

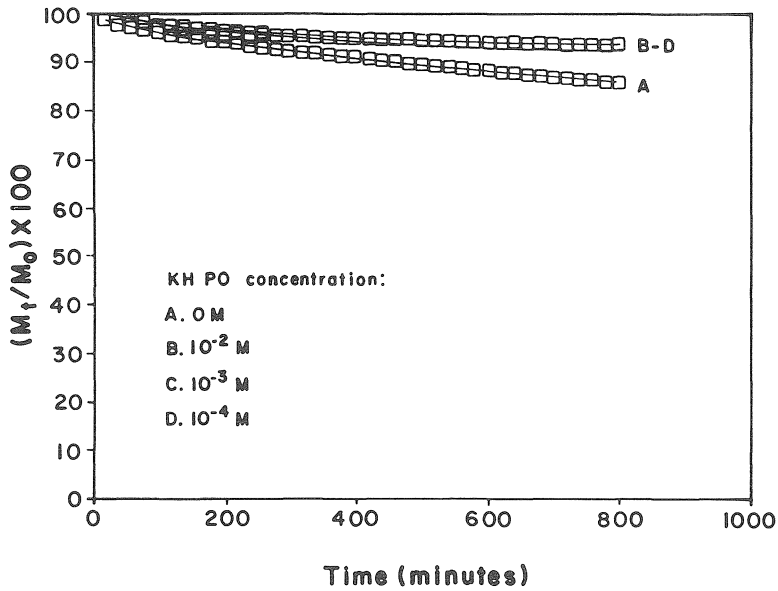

Figure 10.9. Effect of phosphate concentration on the rate of oxidation of pyrite present in 0.5 g coal waste, leached at room temperature with the solutions (pH 6) containing 0.053 mol L^{-1} H_2O_2, 0.1 mol L^{-1} NaAC, and a varying concentration of phosphate.

The rate of pyrite oxidation was almost the same when coal waste was leached with coating solutions varying in phosphate solution concentration from 0.0001 mol L^{-1} to 0.01 mol L^{-1}. This result indicated that any decrease in phosphate concentration as the coating solution moves through the coal waste will not decrease the efficiency of the coating solution in forming pyrite coatings.

The data in Figure 10.10 show the effect of H_2O_2 concentration on the coating process. As H_2O_2 concentration was increased from 0.0173 to 0.173 mol L^{-1}, percent of pyrite oxidized at the end of leaching increased nearly proportionally from 5% to 16.0%. However, the magnitude of the increase was much smaller than that during leaching with the coating solution without NaAC. This suggested that the negative influence of H^+ on formation of iron phosphate coating was largely eliminated by NaAC.

Precoated columns were also leached with a oxidizing solution containing 0.053 mol L^{-1} H_2O_2 and 0.05 mol L^{-1} NaAC pH 5 at 40°C. As shown in Figure 10.11, the iron phosphate coatings created by using different concentrations of H_2O_2 displayed only slightly different effectiveness in preventing pyrite oxidation.

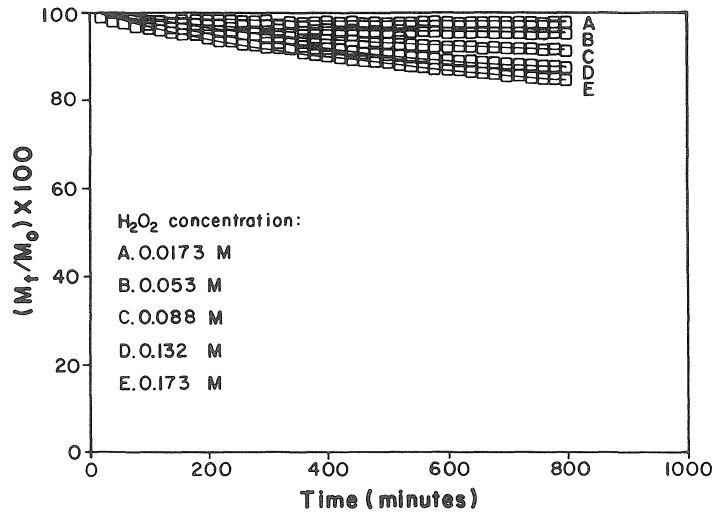

Figure 10.10. Effect of H_2O_2 concentrations on the rate of oxidation of pyrite present in 0.5 g coal waste, leached at room temperature with pH 6 solutions containing 0.001 mol L^{-1} KH_2PO_4, 0.1 mol L^{-1} NaAC, and a varying concentration of H_2O_2.

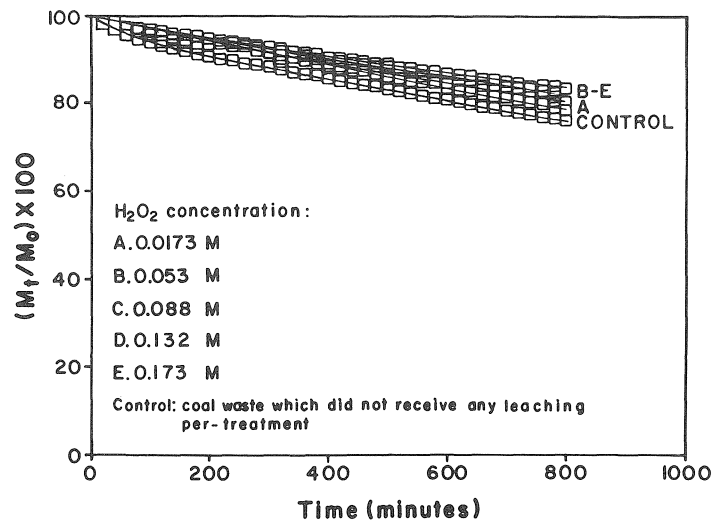

Figure 10.11. Kinetics of pyrite oxidation in coal waste preleached (coated) with iron phosphate with the solutions described in Figure 6.5, subjected to leaching with a solution containing 0.053 mol L^{-1} H_2O_2 and 0.05 mol L^{-1} pH 6 NaAC at 40°C.

This could have two implications. One is that the thickness of the iron phosphate coating did not increase significantly with H_2O_2 concentration. The other is that iron phosphate coatings are an effective H_2O_2 diffusion-inhibitor and the coating thickness has little influence on effectiveness in preventing pyrite oxidation. Rate of pyrite oxidation when the uncoated coal waste was leached with the oxidizing solution in the presence of NaAC was surprisingly low. This resulted mainly from formation of iron hydroxide coatings. Thus, it appeared necessary to use an oxidizing solution in the absence of NaAC to test further the effectiveness of the iron phosphate coatings created in the presence of sodium acetate.

Additional experiments were run to test the effectiveness of the iron phosphate coating in inhibiting pyrite oxidation using H_2O_2 without NaAC. Two columns containing a mixture of 0.5 g coal waste and 100 mesh sand were leached with 50 mL of 2 mol L^{-1} HCl and 10 mL of nitrogen gas-purged distilled water to remove any natural coating on pyrite surfaces. Both columns were then leached with 500 mL of a pH 6 coating solution containing 0.001 mol L^{-1} KH_2PO_4, 0.053 mol L^{-1} H_2O_2, and 0.02 mol L^{-1} NaAC. One of the columns was then leached with 50 mL of 2 mol L^{-1} HCl to remove iron phosphate coatings. Finally, both uncoated and coated columns were subjected to leaching with a oxidizing solution containing 0.053 mol L^{-1} H_2O_2 to test the effectiveness of iron phosphate coating in inhibiting pyrite oxidation. As shown in Figure 10.12, when only 5% of the total pyrite present in the coal waste was consumed during leaching with the coating solution, the pyrite in the coated coal waste displayed a much slower oxidation rate than the pyrite in the uncoated coal waste. This result clearly demonstrated the feasibility of creating iron phosphate coating with the H_2O_2/KH_2PO_4 solution in the presence of NaAC.

All the coating studies discussed above were carried out using microcolumns, (Huang and Evangelou, 1994) and testing of coating effectiveness was carried out by leaching the microcolumns with H_2O_2. It is essential however, to study formation of iron phosphate coatings in relatively large columns and to test the effectiveness of iron phosphate coatings using pyrite oxidizing bacteria.

10.7 Coating Evaluation in Large Columns

The pyritic sample used in this study was a coal waste product with approximately 13% pyrite. Leaching columns with 40 g coarse coal 'waste' were prepared as shown in Figure 10.13. The columns were first leached with 100 ml of 0.1 mol L^{-1} HCl to remove free iron sulfate because it can precipitate phosphate in the coating solution which may complicate data interpretation. The columns were then leached with 2500 mL of the coating solutions containing 0.1 mol L^{-1} NaAC pH 5 and 0.001 mol L^{-1} KH_2PO_4 but

varying in H_2O_2 concentration. After leaching with the above solutions was completed the coal waste was subjected to leaching with a 0.088 mol L^{-1} H_2O_2 to test the effectiveness of the coating solutions.

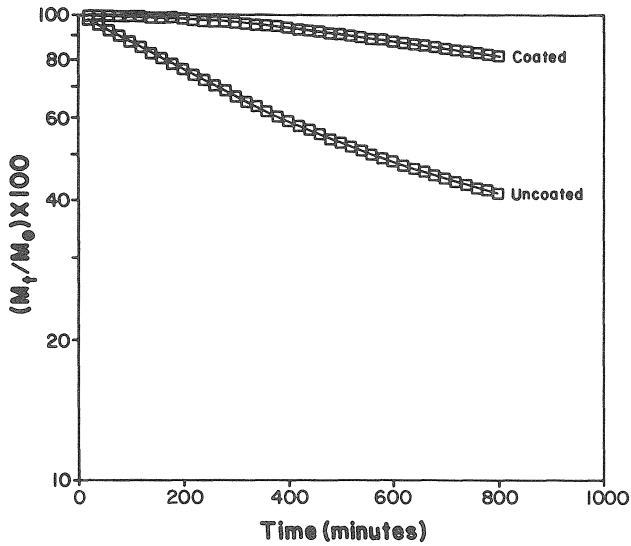

Figure 10.12. Effectiveness of iron phosphate coatings, created by a NaAC-containing coating solution, in preventing oxidation of pyrite in coal waste. Coatings were established by leaching 0.5 g coal waste with the coating solution (pH 6) containing 0.001 mol L^{-1} KH_2PO_4, 0.053 mol L^{-1} H_2O_2, and 0.02 mol L^{-1} NaAC. The coating process consumed 5% of the available pyrite. Coating effectiveness was tested by leaching with 0.053 mol L^{-1} H_2O_2 at room temperature.

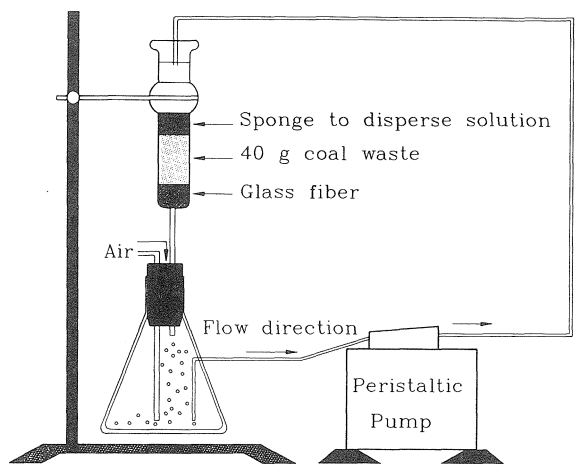

Figure 10.13. Schematic of the leaching apparatus for testing the effectiveness of the iron phosphate coating technology in preventing acid production in coal waste.

The data in Figure 10.14 show that SO_4^{2-} release was directly related to solution volume and concentration of H_2O_2. The treatment which released the least amount of SO_4^{2-}, as expected was the one without H_2O_2 (Figure 10.15A).

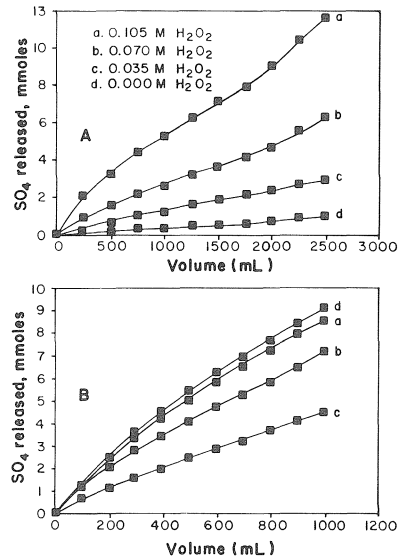

Figure 10.14. A. Release of SO_4^{2-} as a function of the volume of the leaching solution when 40 g of coal waste was leached with solutions containing 0.01 mol L^{-1} KH_2PO_4, 0.1 mol L^{-1} NaAC, and a varying concentration of H_2O_2. B. Release of SO_4^{2-} as a function of the volume of the leaching solution when iron phosphate coated coal waste with the above coating solutions were exposed to an oxidizing solution containing 0.088 mol L^{-1} H_2O_2 and 0.1 mol L^{-1} NaAC adjusted to pH 5.

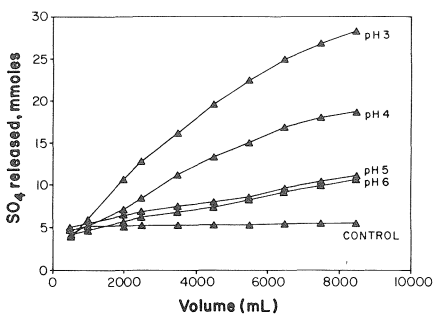

Figure 10.15. Release of SO_4^{2-} as a function of the volume of leaching solution when 40 g of coal waste was leached with the coating solutions containing 0.01 mol L^{-1} KH_2PO_4, 0.035 mol L^{-1} H_2O_2, and 0.1 mol L^{-1} NaAC but varying in pH from 3 to 6. Control refers to leaching with pH 6 solution containing 0.01 mol L^{-1} KH_2PO_4 and 0.1 mol L^{-1} NaAC.

However, when this sample was leached with the oxidizing solution (0.088 mol L^{-1} H_2O_2) it released the most SO_4^{2-} (Figure 10.15B). The coating solution containing 0.035 mol L^{-1} H_2O_2 (Figure 10.15B) showed the highest effectiveness in suppressing pyrite oxidation, compared to the effectiveness of the coatings formed with coating solution without H_2O_2 or with H_2O_2 concentration higher than 0.035 mol L^{-1}. This demonstrated that leaching coal waste with phosphate solution alone cannot prevent pyrite oxidation and H_2O_2 was essential to induce iron phosphate coatings on pyrite surface in order to prevent pyrite oxidation.

The results in Figure 10.14 also indicate that higher H_2O_2 concentration does not necessarily mean thicker iron phosphate coating. There are two reasons for this. First, with increased H_2O_2 concentration the quantity of H^+ produced from pyrite oxidation increased as well. When H^+ concentration reached a point where 0.1 mol L^{-1} NaAC could not maintain pH above 5, efficiency of the coating solution significantly decreased. Average pH of leachate was found to be 4.9, 4.8 and 4.7 when coal 'waste' were leached with the coating solutions containing 0.035, 0.070, and 0.105 mol L^{-1} H_2O_2, respectively.

Another factor which might influence formation of iron phosphate coatings is the molar ratio of phosphate to Fe(III). Preliminary experiments on synthesis of iron phosphate indicate that precipitation of iron phosphate is determined by degree of supersaturation of solution with respect to iron phosphate and the molar ratio of phosphate to Fe(III). High P/Fe mole ratio favors formation of iron phosphate. According to the stoichiometry between H_2O_2 and Fe(III), 0.035 moles of H_2O_2 can produce 0.0047 moles of Fe(III). Thus, if coal waste were leached with a solution containing 0.01 mol L^{-1} KH_2PO_4, the P/Fe ratio will be approximately 2:1, a value optimal for precipitation of iron phosphate. On the other hand, if H_2O_2 concentrations were higher than 0.035 M, the mole number of Fe(III) produced would be equal to or larger than that of available phosphate. In this case, iron phosphate would be more difficult to precipitate as coatings. These explanations are speculative and need further verification. Based on the above results, one might conclude that for a coating solution containing 10^{-2} mol L^{-1} KH_2PO_4 and 0.1 mol L^{-1} NaAC, H_2O_2 concentration should be less than 0.04 mol L^{-1} in order to effectively coat pyrite.

In order to determine the optimal pH for coatings formation, columns with 40 g of coal waste were leached with solutions containing 0.1 mol L^{-1} NaAC, 0.001 mol L^{-1} KH_2PO_4, and 0.035 mol L^{-1} H_2O_2 and varying pH from 3 to 6. As shown in Figure 10.15, in order to effectively induce formation of iron phosphate coatings on pyrite surfaces and avoid excessive oxidation of pyrite, the pH of the coating solution should be always above 5. At pH above 5, pH seems to have little additional influence on the formation of iron phosphate coatings. This is consistent with the conclusion drawn based on the small column experiments.

Pyrite oxidation in the field is actually an autocatalytic process, since Fe^{III} released from pyrite can effectively oxidize pyrite as well (see Chapter 6). In addition, the iron-oxidizing bacteria also contribute greatly to pyrite oxidation. In order to simulate these field conditions coated columns were leached by circulating 500 ml of solution inoculated with iron-oxidizing bacteria (Figure 10.13). The data in Figure 10.16 show release of SO_4^{2-} during leaching 40 g of coal waste with two solutions: A) 0.01 mol L^{-1} KH_2PO_4, 0.1 mol L^{-1} NaAC, and 0.035 mol L^{-1} H_2O_2; B) 0.01 mol L^{-1} KH_2PO_4 and 0.1 mol L^{-1} NaAC.

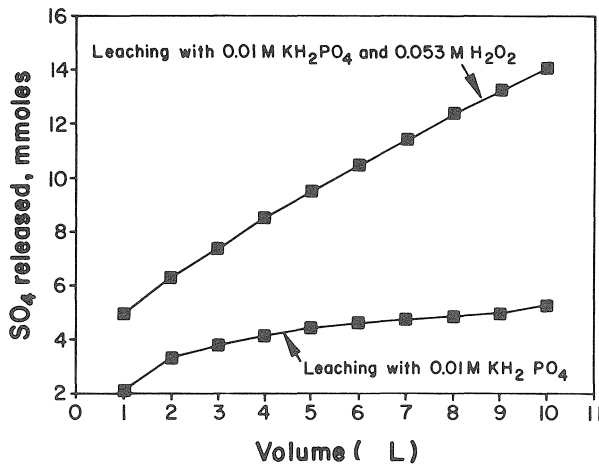

Figure 10.16. Release of SO_4^{2-} as a function of the volume of leaching solution during leaching 40 g of coal waste with a pH 6 solution containing 0.01 mol L^{-1} KH_2PO_4, 0.035 mol L^{-1} H_2O_2, and 0.1 mol L^{-1} NaAC.

After leaching with 10 liters of the coating solution(s), 14 mmoles of SO_4 were released by solution A, compared to 5 mmoles of SO_4^{2-} released by solution B. This indicated that 4.5 mmoles of pyrite (calculated according to the pyrite Fe/S_2 stoichiometry) were oxidized during the coating process and accounted for approximately 10% of the total pyrite present in 40 g of coal waste. No trace of iron was found in the leachate and pH of the leachate was always maintained around 6. This result indicated that leaching coal waste with the coating solution (H_2O_2/KH_2PO_4) will not cause any increase in iron concentration in the drainage or a decrease in pH of the drainage.

Figure 10.17 shows the potential (due to pyrite oxidizing bacteria) changes with time in pH of the solution circulating through columns with different preleaching treatments.

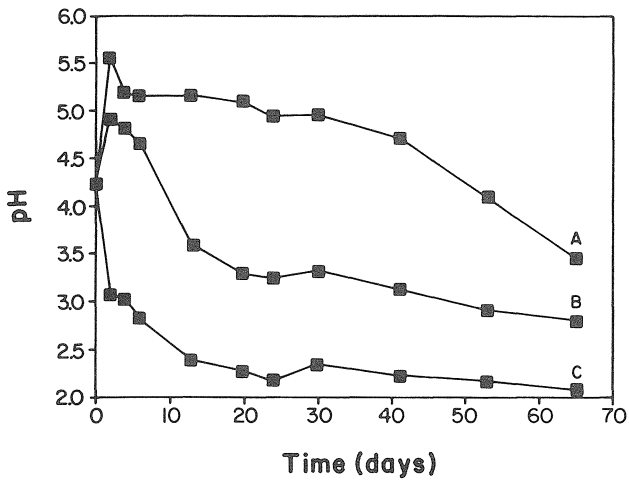

Figure 10.17. Changes in pH of the solution circulating through coal waste columns having received different pre-treatments. A. column preleached (coated with iron phosphate) with a pH 6 coating solution containing 0.01 mol L^{-1} KH_2PO_4, 0.035 mol L^{-1} H_2O_2, and 0.1 mol L^{-1} NaAC; B. column preleached (coated) with the pH 6 solution containing 0.01 mol L^{-1} KH_2PO_4 and 0.1 mol L^{-1} NaAC; C. columns did not receive any preleaching (coating) treatment.

The pH of the circulating solution through the precoated column was maintained around 5 for at least 40 days, whereas pH of the solution circulating through pretreated (0.01 mol L^{-1} KH_2PO_4) column B dropped to 3.5 within 15 days. The pH of the solution circulating through the column which did not receive any pretreatment fell near 2 in 15 days. These results strongly demonstrated that leaching (coating) coal 'waste' with phosphate solution without H_2O_2 can probably slow down but cannot prevent acid production. The coating technology (H_2O_2 plus phosphate) on the other hand, may prevent acid production. Failure of the circulating solution through the precoated column to maintain pH around 5 after 40 days probably resulted from the disintegration of clay-pyrite aggregates in coal 'waste' during circulation-leaching.

Pyrite particles buried in aggregates cannot be coated with iron phosphate and can produce acid once the aggregates disintegrate. Thus, in order to completely prevent acid production in coal waste, it appears essential to stabilize these aggregates from disintegrating. Otherwise, it would be necessary to repeat the coating process.

Figure 10.18 shows release of SO_4^{2-} during leaching of large coal waste columns by circulating 500 ml of distilled water. Without any preleaching treatments, the coal waste released approximately 30 mmoles of SO_4^{2-} in 53 days (curve C).

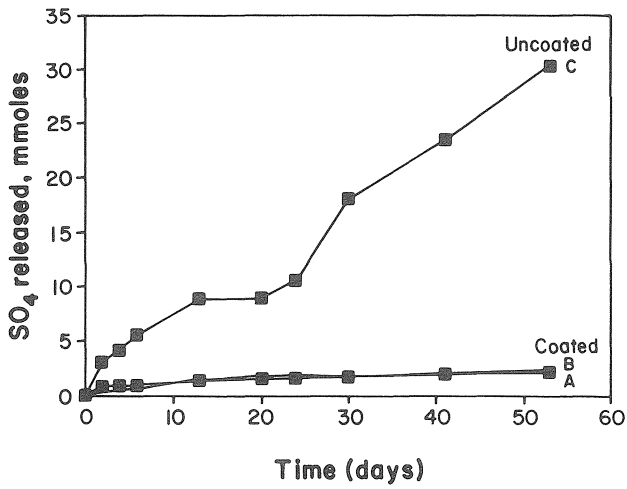

Figure 10.18. Release of SO_4^{2-} as a function of time during pretreated-column leaching by circulating 500 mL of solution. A. column preleached (coated with iron phosphate) with a pH 6 coating solution containing 0.01 mol L^{-1} KH_2PO_4, 0.035 mol L^{-1} H_2O_2, and 0.1 mol L^{-1} NaAC; B. column preleached (coated) with a pH 6 solution containing 0.01 mol L^{-1} KH_2PO_4 and 0.1 mol L^{-1} NaAC; C. columns which did not receive any preleaching (coating) treatment.

Forty grams of preleached coal 'waste' contained approximately 6.5 mmoles of free SO_4^{2-}. Thus, approximately 23.5 mmoles of SO_4^{2-} released were due to pyrite oxidation during the circulation-leaching process. This value was significantly larger than the amount of SO_4^{2-} released from the columns which had been leached with 0.01 mol L^{-1} KH_2PO_4 or the coating H_2O_2/KH_2PO_4 solution (curve B and C). This indicated that removal of free iron from coal 'waste' by using phosphate can effectively suppress pyrite

oxidation, but it cannot completely prevent pyrite oxidation and acid production. The amount of SO_4^{2-} released from precoated coal waste was surprisingly higher than that released from the columns preleached with 0.01 mol L^{-1} KH_2PO_4. This is mainly because part of the SO_4^{2-} released from the precoated column was due to pyrite oxidation during the coating process. Portion of this sulfate was most likely absorbed by iron oxides in the coal waste. This can be confirmed by the fact that release of SO_4^{2-} from the coated column during circulation/leaching was not accompanied by a drop in pH. Conversely, all SO_4^{2-} released from the column preleached with 0.01 mol L^{-1} KH_2PO_4 was expected to be completely due to pyrite oxidation during the circulation-leaching process, since preleaching with 10 liters of 0.01 mol L^{-1} KH_2PO_4 had completely removed free or adsorbed SO_4^{2-} from coal wastes (Figure 10.17).

Generally, the difference in the rate of pyrite oxidation in coal wastes preleached with 0.01 mol L^{-1} KH_2PO_4 and precoated with H_2O_2/KH_2PO_4 was supposed to be much larger than that shown in Figure 10.18. This speculation can be confirmed by the trend in ferrous (Fe^{II}) concentration in the circulating solution (Figure 10.19).

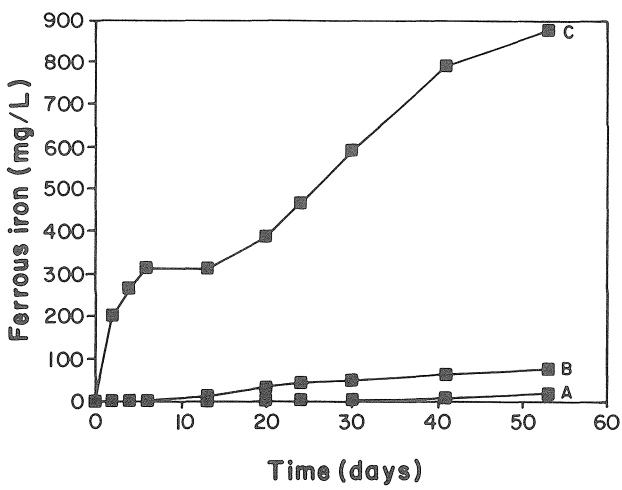

Figure 10.19. Changes in iron concentration as a function of time during pretreated-column leaching by circulating 500 ml of solution. A. column preleached with a pH 6 coating solution containing 0.01 mol L^{-1} KH_2PO_4, 0.035 mol L^{-1} H_2O_2, and 0.1 mol L^{-1} NaAC; B. column preleached (coated) with a pH 6 solution containing 0.01 mol L^{-1} KH_2PO_4 and 0.1 mol L^{-1} NaAC; C. columns did not receive any preleaching (coating) treatment.

As shown in Figure 10.19, Fe^{II} concentration in the solution circulating through the column preleached with 0.01 M KH_2PO_4 increased from 0 to 75 mg L^{-1} in 53 days, compared to 18 mg L^{-1} in the circulating solution of the precoated column. In addition, ferrous concentration in the latter circulating solution was always less than 4 mg L^{-1} up to the 30th day, a value much smaller than that in the former circulating solution. This result further confirms that the iron phosphate coating technology is more effective in preventing pyrite oxidation than application of solution phosphate alone.

Based on the results of this study, the following conclusions can be drawn. 1) Sodium acetate is an essential component of the coating solution in order to effectively precipitate Fe^{III} as iron phosphate coatings; 2) both, application of solution phosphate without H_2O_2 and solution phosphate with H_2O_2 can greatly suppress pyrite oxidation in coal 'waste'. However, solution phosphate with H_2O_2 (coating technology) appears to be more effective in preventing acid production in coal waste.

The above results simply demonstrate that when conditions are such that ferric phosphate precipitation on the pyrite surfaces is promoted, pyrite oxidation potential is significantly reduced. These data however, are not conclusive enough to suggest that such a technology could easily be applied in the field. The technology should be scaled-up to larger columns for further testing.

10.8 Conclusions

Based on the overall results of this study, one may conclude that an iron phosphate coating can be established on pyrite surfaces by leaching coal waste with a solution containing KH_2PO_4, H_2O_2, and NaAC and that the iron phosphate coating on pyrite surfaces can prevent pyrite oxidation in coal waste. The mechanism underlying this technology is that Fe^{III} released from pyrite by H_2O_2 will be precipitated by phosphate as a coating on pyrite surfaces while the protons produced from pyrite oxidation by H_2O_2 are consumed by a buffer such as NaAC. The iron phosphate coatings on pyrite surfaces can be established under a wide range of conditions: 1) H_2O_2 concentration can range from 0.017 to 0.173 mol L^{-1}; 2) phosphate concentration can vary from 10^{-4} to 10^{-2} mol L^{-1}; 3) pH of the coating solution has to be above 5 in order for phosphate to effectively precipitate Fe^{III} as coating; 4) NaAC concentration can be as low as 0.02 mol L^{-1}; 5) temperature can range from room temperature to 40°C.

The conclusions drawn in this study are based on small-column experiments. To determine the coating conditions workable in the field, large-scale leaching experiments involving several hundred kilograms of coal wastes are needed.

The results obtained from this study have definitely thrown new light on the production and control of acid mine drainage. The advantages of this coating technology over other approaches are obvious. First, due to the

potential permanence of the iron phosphate coatings on pyrite surfaces, pyrite particles in mining wastes could no longer be oxidized and release acid; thus, prevention of acid drainage production will be long-lasting. Second, the coating process does not require physical mixing of coal 'waste' with ameliorates and thus can greatly simplify the operation. Third, the coating approach involves low concentrations of phosphate and hydrogen peroxide and can possibly decrease the cost in controlling production of acid mine drainage. However, field application of this coating technology probably could not be carried out without limestone. The latter may always be required to maintain appropriate pH and levels of alkalinity to protect the $FePO_4$ from dissolution. In any case, extensive field testing of the coating technology is needed to determine its potential effective use.

PART V

SUMMARY

Taylor & Francis
Taylor & Francis Group
http://taylorandfrancis.com

SUMMARY

Pyrite in mining 'waste' is initially oxidized by atmospheric O_2, producing H^+, SO_4^{2-}, and Fe^{2+} (Singer and Stumm, 1970)

$$FeS_2 + 7/2O_2 + H_2O \rightarrow Fe^{2+} + 2SO_4^{2-} + 2H^+ \quad (E.1)$$

The Fe^{2+} produced can be further oxidized by O_2 into Fe^{3+}, which in turn hydrolyzes into iron hydroxide and releases additional amounts of acid into the environment (Nordstrom, 1982a)

$$Fe^{2+} + 1/4O_2 + H^+ \rightarrow Fe^{3+} + 1/2H_2O \quad (E.2)$$

and

$$Fe^{3+} + 3H_2O \rightarrow Fe(OH)_3 + 3H^+ \quad (E.3)$$

Most iron released during the initial stages of pyrite oxidation ends up as iron hydroxide due to the relatively high pH on pyrite surfaces (Ivanov, 1962; Fornasiero et al., 1992). However, when pH in the vicinity of pyrite surfaces drops below 3.5 (due to acid production) activity of free Fe^{3+} in solution increases and oxidation of pyrite by Fe^{3+} becomes the main mechanism for acid production. Singer and Stumm (1970) reported that Fe^{3+} can oxidize pyrite at a much higher rate than O_2.

The role of Fe^{3+} in the oxidation of pyrite is demonstrated below:

$$FeS_2 + 14Fe^{3+} + 8H_2O = 15Fe^{2+} + 2SO_4^{2-} + 16H^+ \quad (E.4)$$

O_2

Iron-oxidizing bacteria

At low pH, an acidophilic, chemoautotrophic, iron-oxidizing bacterium, *T. ferrooxidans* catalyzes and accelerates the oxidation of Fe^{2+} by a factor larger than 10^6 (Singer and Stumm, 1970). Thus, the processes of reduction of Fe^{3+} to Fe^{2+} by pyrite and oxidation of Fe^{2+} to Fe^{3+} by atmospheric O_2, catalyzed by *T. ferrooxidans*, constitute an effective continuous pyrite oxidation cycle. For this reason, *T. ferrooxidans* is considered to be primarily responsible for the rapid oxidation of pyrite in mine waste at low pH (Nordstrom, 1982a). Based on the above, pyrite oxidation can be significantly reduced by complexing/precipitating Fe^{3+}, inhibiting Fe^{3+} production and/or depriving the system of oxygen (O_2) (Jaynes et al., 1984; Scharer et al., 1991; Erickson et al., 1985).

It is commonly believed that pyrite oxidation can be controlled by adding alkaline material to pyrite, a widely used field practice. This is due to the fact that at high pH, *T. ferrooxidans* activity diminishes and Fe^{3+} becomes insoluble (Jaynes et al, 1984 and references therein). However, recent

findings (Moses and Herman, 1991) showed that nonmicrobial pyrite oxidation rate increased as pH increased. At high pH, nonmicrobial pyrite oxidation appeared to be carried out by a surface-catalyzed mechanism involving Fe^{2+}, O_2, and Fe^{3+}; the latter's low water solubility at high pH (pH > 3.5) did not appear to be a rate limiting factor. Data by Brown and Jurinak (1989a) and Hood (1991) also supported these findings. An accepted mechanism justifying enhancement of nonmicrobial pyrite oxidation in high pH environments is OH^- involvement in an inner-sphere electron transfer process (Luther, 1990; Brown and Jurinak, 1989). In this process an OH^- and an electron are exchanged simultaneously between the pyrite/surface-$Fe(III)(OH)_n^{3-n}$ and the pyrite/surface disulfide.

According to Luther (1990) and references therein, pyrite/surface exposed disulfide provides a slightly negatively charged pyrite surface due to an unshared pair of electrons which attract ions willing to share them, e.g. Fe^{2+}. Moses and Herman (1991) concluded that because of this unshared pair of electrons, the pyrite/surface behaved as a soft base (Sposito, 1984 and references therein) showing higher preference for Fe^{2+} than for Fe^{3+} since the former is a relatively softer Lewis acid. However, pyrite/surface adsorbed Fe^{2+} in the presence of O_2 rapidly oxidizes to Fe^{3+}, depending on surface pH. Fornasiero et al. (1992) demonstrated formation of $Fe(OH)_n^{3-n}$ complexes on the surface of pyrite upon exposure to O_2. Hood (1991) concluded that the cause for the increase in the rate of pyrite oxidation under alkaline conditions was the formation of a pyrite/surface-CO_3 complex which facilitated electron transfer and rapid turnover of Fe(II) to Fe(III) (Millero and Izaguirre, 1989).

Evangelou and Huang (1994) and Evangelou and Zhang (1994) using FT-IR spectroscopy demonstrated that pyrite exposed to humidified CO_2 plus O_2 formed pyrite/surface-CO_x complexes. Two potential mechanisms were proposed to account for these complexes. One mechanism involved formation of a weak pyrite/surface-Fe(II)-CO_3 complex, whereas a second mechanism involved formation of a pyrite/surface-carboxylic group complex (-Fe(II)-S_A-S_B-COO^-). Based on the above results, it was postulated by Evangelou and Zhang (1994) that CO_2 (owing to its potential to react with surface -OH) tended to form weak pyrite/surface-Fe(II)-CO_3 complexes which could promote nonmicrobial pyrite oxidation by accelerating Fe(II) oxidation. The latter has been validated in previous published studies employing ferrous-carbonate solution systems (Millero and Izaguirre, 1989). In the case of -Fe(II)-S_A-S_B-COO^-, Evangelou and Zhang (1994) postulated that Fe^{2+} oxidation is promoted when the latter interacts with the pyrite/surface carboxylate in the presence of bimolecular oxygen (Luther et al., 1992).

Currently, acid metallic drainages produced by Fe-sulfide oxidation are controlled by several approaches: i) application of limestone/rock phosphate, or sewage sludge, ii) application of bactericides, iii) creation of fully anoxic environments by using clay liners, plastic liners, asphalt etc., and

iv) establishment of wetlands. The first two acid drainage remediation technologies slow down the production of acidic drainages, but do not stop it, and have a short life span due to the coating potential (armoring) of limestone/rock phosphate by iron oxides (Stiller et al., 1985; Stiller et al., 1986; Loomis and Hood, 1984). This limestone/rock phosphate coating problem is commonly observed in the field and extensive investigations on the factors causing it have been reported (Evangelou et al., 1992 and references therein). All ameliorates listed above have one major limitation. They are difficult to apply in actual sites where acid mine drainage is produced and due to their relatively low solubility they require physical mixing with the sulfide rich strata.

Organic waste may also inhibit pyrite oxidation via various mechanisms including 1) consumption of O_2 because of bacterial growth, 2) removal of Fe^{III} from solution through complexation, and 3) formation of pyrite-Fe^{II}-humate complexes. Organic waste, however, may also promote pyrite oxidation by solubilization of $Fe(OH)_3$ through formation of Fe^{III}-organic acid complexes. Such complexes, especially if positively charged, they could adsorb onto the pyrite surface and act as electron acceptors in an outer-sphere mode (Luther et al., 1992). These electron transfer reactions could also be favored in some cases when Fe^{II}-organic acid complexes are more stable than Fe^{III}-organic acid complexes (Luther et al., 1992). To avoid such potential pyrite oxidation problems, well-decomposed organic waste (composted or heat treated so that simple organic acids are destroyed) should be applied to pyritic 'waste' prior to formation of $Fe(OH)_3$ precipitates so that a) pyrite-Fe^{II}-humate complexes would be the only complexes, b) Fe^{III}-humate complexes formed should be preferably neutral or negatively charged (note, pyrite surface is also negatively charged), and c) any Fe^{III}-humate complexes formed should be preferably water insoluble.

Application of bactericides also has a suppressing effect on the activity of *T. ferrooxidans*. Kleinmann (1980) was one of the first to introduce bactericidal control on acid drainage. Slow release pellets of such bactericides are currently available in the market (Rastogi et al., 1986). The major disadvantages of this approach are: i) acid mine drainage is suppressed for relatively short periods, and chemical oxidation of pyrite by O_2 is not inhibited by bactericides; ii) in the case of acid drainage produced at lower depths of a geologic stratum, mixing of the pellets with the geologic material could be a difficult task, and iii) bactericides do not have much of an effect on acid metallic drainages already present.

A more recent approach in controlling acid mine drainage production is the use of alkaline recharge trenches (e.g., NaOH) (Caruccio et al., 1985). However, effectiveness may last only as long as someone supplies neutralizers. This can be costly and at times not very practical.

Wetland technologies are effective in treating the symptoms of pyrite oxidation when low levels of acidity are involved. However,

"constructed wetlands" (Erickson et al., 1987; Kleinmann, 1985; Girts and Kleinmann, 1986) as an acid mine drainage amelioration technology has limitations when availability of H_2O is highly variable and when high levels of acidity are involved. Also, many question the long term effectiveness of such systems in the absence of any management. More importantly however, "constructed wetlands" treat the symptoms of pyrite oxidation and not the problem itself which is pyrite oxidation.

Novel microencapsulation (coating) technologies to prevent pyrite oxidation and acid production in pyritic wastes are currently under development in our laboratory. The first coating technology involves leaching coal waste with a solution composed of low but critical concentrations of H_2O_2, KH_2PO_4, and a pH-buffer. During the leaching process, H_2O_2 oxidizes pyrite and produces Fe^{3+} so that iron phosphate precipitates as a coating on pyrite surfaces. The second coating technology involves leaching pyritic waste with a solution composed of low but critical concentrations of H_2O_2 and a pH-buffer. During the leaching process, H_2O_2 oxidizes pyrite and produces an iron oxide coating on the surface of pyrite. Successful application of these pyrite coating technologies in the field could mean long-term solution to certain types of AMD problems.

REFERENCES

Abd-Alfattah, A. and Wada, K., Adsorption of lead, copper, zinc, cobalt, and cadmium by soils that differ in cation exchange materials, *J. Soil Sci.*, 32, p. 271, 1981.

Adams, F., Ionic concentrations and activities in soil solutions, *Soil Sci. Soc. Amer. Proc.*, 35, p. 420, 1971.

Adams, F. and Evans, C. E., A rapid method for measuring lime requirements of red-yellow podzolic soils, *Soil Sci. Am. Proc.*, 26, p. 355, 1962.

Adamson, A. W., *Physical Chemistry of Surfaces,* 5th ed., John Wiley & Sons Inc., NY, 1990.

Addiscott, T. M. and Wagenet, R. J., Concepts of solute leaching in soils: a review of modeling approaches, *J. Soil Sci.*, 36, p. 411, 1985.

Ahmed, S. M., Electrochemical and surface chemical methods for prevention of the atmospheric oxidation of sulfide tailings, In *The Second International Conference on the Abatement of Acidic Drainage,* Vol. 2, Sept. 16-18, Montreal, Canada, 1991, p. 305.

Ainsworth, C. C., Pyrite Forms and Oxidation Rates in Missouri Shales, M.S. thesis, Agronomy Dept., University of Missouri, Columbia, 1979, p. 144.

Ainsworth, C. C., Blanchar R.W., and King E.J., Morphology of pyrite from Pennsylvania-age shales in Missouri, *Soil Sci.*, 134, p. 244, 1982.

Aller, R. C. and Rude, P. D., Complete oxidation of solid phase sulfides by manganese and bacteria in anoxic marine sediments, *Geochim. Cosmochim. Acta,* 52, p. 751, 1988.

Amacher, M. C., Determination of ionic activities in soil solutions and suspensions; principal limitations, *Soil Sci. Soc. of Am. J.*, 48, p. 519, 1984.

Arai, S. and Kumada, K., An interpretation of the conductometric titration curve of humic acid, *Geoderma*, 21, p. 21, 1977.

Arora, H. S., Dixon J. B., and Hossner, L. R., Pyrite morphology in lignitic coal and associated strata of east Texas, *Soil Sci.*, 125, p. 151, 1978.

Asghar, M. and Kanehiron, Y., The fate of applied iron and manganese in an oxisol and an ultisol from Hawaii, *Soil Sci.*, 131, p. 53, 1981.

Aspiras, R. B., Keeney, D. R., and Chesters, G., Determination of reduced inorganic surfur forms as suphide by zinc-hydrochloric acid distillation, *Anal. Lett.*, 5, p. 425, 1972.

Babcock, K. L., Theory of chemical properties of soil and colloidal systems at equilibria, *Hilgardia*, 34, p. 417, 1963.

Baes, A. U. and Bloom, P. R., Diffuse reflectance and transmission fourier transform infrared, *Soil Sci. Am. J.*, 53, p. 695, 1989.

Bailey, L. K. and Peters E., Decomposition of pyrite in acids by pressure leaching and anodization: The case for electrochemical mechanism, *Can. Met. Quart.*, 15, p. 333, 1976.

Barnhisel, R. I., Powell, J. L., Akin, G. W., and Ebelhar, M. W., Characteristics and reclamation of 'acid sulfate' mine spoils, in *Proceedings of Symposium on Acid Sulfate Weathering*, American Society of Agronomy, Madison, WI, 1982, p. 225.

Barnhisel, R. I. and Massey, H. F., Chemical, mineralogical and physical properties of eastern Kentucky acid-forming coal spoil materials, *Soil Sci.*, 108, p. 367, 1969.

Barriga, F. J. A. S. and Fyfe, W. S., Giant pyritic base-metal deposits: The example of feitais (Aljustrel, Portugal), *Chem. Geol.*, 69, p. 331, 1988.

Bartlett, R. J., Oxidation-reduction status of aerobic soils, in *Chemistry in the Soil Environment,* Baker, D. E. (Ed.) ASA monograph No. 40, Soil Science Society of America, Madison, WI, 1981.

Bashour, I. and Carlson, P. M., Rubidium as a controlling factor in potassium release from micaseous minerals, *Soil Sci. Soc.*, 58, p. 1010, 1984.

Batarseh, K. I., Swaney, G. P., and Stiller, A. H., A mathematecal model for heterogeneous reactions with a moving boundary, *AIChE,* 35, p. 625, 1989.

Bell, A. B., Prevention of acid generation in base metal tailings and waste rock, in *Proceedings of acid mine drainage,* Seminar and Workshop, March 23-26, 1987, Halifax, Nova Scotia, p. 391.

Bellamy, L. J., *Infrared Spectra of Complex Molecules,* Chapman and Hall, London, 433 pp., 1975.

Benjamin, M. M. and Leckie, J. O., Adsorption of metals and oxide interfaces: effect of the concentrations of adsorbate and competing metals, in *Contaminants and Sediments,* Baker, R. A. (Ed.), Ann Arbor Science Publishers, Inc., Ann Arbor, MI, 1980, p. 305.

Bennett, J. C. and Tributsch, H., Bacteria leaching patterns on pyrite crystal surface, *J. Bacteriol.*, 134, p. 310, 1978.

Berner, R. A., Sedimentary pyrite formation: an update, *Geochim. Cosmochim. Acta,* 48, p. 605, 1984.

Berner, R. A., Sedimentary pyrite oxidation, *Amer. J. Sci.*, 268, p. 1, 1970.

Beveridge, A., and Pickering, W. P., Influence of humate-solute interactions on aqueous heavy metal ion levels. *Water, Air, and Soil Pollution,* 14, p. 171, 1980.

Blanchar, R. W. and Marshall, C. E., Eh and pH measurement in Menfro and Mexico soils, in *Chemistry in the Soil Environment,* Baker, D.E. (Ed.), ASA monograph No. 40, Soil Science Society of America, Madison, WI, 1981.

Bloom, P. R., McBride, M. B., and Chadbourne, B., Adsorption of aluminum by a smectite: 1. Surface hydrolysis during Ca^{2+} -Al^{3+} exchange, *Soil Sci. Soc. Am. J,* 41, p. 1068, 1977.

Bohn, H. L., McNeak, B. L., and O'Connor, G. A., *Soil Chemistry*, Wiley-Interscience, NY, 1979.

Boischot, P., Durroux, M., and Sylvestre, G., Etude sur la fixation du fer et du manganese dans les sols calcaires, *Ann. Inst. Natl. Recherche Agron., Ann. Agron. [A]*, 1, p. 307, 1950.

Brierley, C. L., Microbiological mining, *Sci. Am.*, 247, p. 42, 1982.

Brodie, G. A., Britt, C. R., Tomaszewski, T. M., and Taylor, H. N., Use of the passive anoxic limestone drains to enhance performance of acid drainage treatment wetlands, in Oaks, W. and Bowden, J. (Eds.), *Proceedings Reclamation 2000: Technologies for Success,* Durango, CO, 1991, p. 211.

Bronswiijk, J. J. B., and Groenenberg, J. E., SMASS, : A simulation model for acid sulfate soils. I. Basic principles. in Dent, D. and van Mensvoort, M. E. F. (Eds.), *Selected Pap. Saigon Symp. Acid Sulfate Soils, Ho Chi Minh City, Vietnam.* 2-6- Mar. 1992. ILRI Publ. 52. Inst. for Land Reclam. and Improve., Wageningen, the Netherlands, 1993.

Brown, A. D. and Jurinak, J. J., Mechanism of pyrite oxidation in aqueous mixtures, *J. Environ. Qual.*, 18, p. 545, 1989a.

Brown, A. D. and Jurinak, J. J., Mechanisms of nonmicrobial pyritic sulfur oxidation under alkaline conditions, *Arid Soil Res.*, 3, p. 65, 1989b.

Brown, A. D., Chemical Weathering of Pyrite in Soils, Ph.D thesis. Utah State University, Logan, 1985.

Buffle, J. Natural organic matter and metal-organic interactions in aquatic systems, in *Metal Ions in Biological Systems*, Sigel, H. (Ed.), Marcel Dekker, New York, 1984.

Carpenter, P. L., *Microbiology*, W. B. Saunders Company, Philadelphia, PA, p. 218, 1977.

Carranza, F., Ph.D. Thesis, University of Seville, Seville, Spain, 1983.

Caruccio, F. T. and Geidel, G., Estimating the minimum acid load that can be expected from a coal strip mine, in *Proceedings of National Symposium on Surface Mine Hydrology, Sedimentology, and Reclamation.*, Univ. of Kentucky, Lexington, p. 117, 1981.

Caruccio, F. T. and Geidel, G, The predictions of acid mine drainage from coal strip mines, in *Proc. Recl. Aband. Acid Spoils*, Dept. of Nat. Resour. Land Recl. Commis, Columbia, MO, p. 21, 1985.

Caruccio, F. T. and Geidel, G., The assessment of a stratum's capability to produce acidic drainage, in *Proceedings of National Symposium on Surface Mine Hydrology, Sedimentology and Reclamation.*, Univ. of Kentucky, Lexington, p. 437, 1980.

Caruccio, F. T. and Geidel, G., Geochemical factors affecting coal mine drainage quality, in *Reclamation of Drastically Disturbed Lands,* Schaller, F.W. and Sutton, P. (Eds.), American Society of Agronomy, Madison, WI, p. 129, 1978.

Caruccio, F. T., and. Geidel, G., The effect of plastic liner on acid loads/DLM site, WV, in *Proceedings, Fourth West Virginia Surface Mine Drainage Task Force Symposium,* Clarksburg, WV, 1983.

Caruccio, F. T., Geidel, G., and Williams, R., Induced alkaline recharge trenches - An innovative method to bate acid mine drainage, in *Proc. Surf. Min. Wat. Qual. West. Virg. Surf. Mine Drain. Task Force Symp.*, Morgantown, WV, p. 12, 1985.

Caruccio, F. T., Estimating of the acid potential of the coal mine refuse, in Chadwick, M. J. and Goodman, G. T. (Eds.), *The Ecology of Resource Degradation and Renewal*, Blackwell Sci. Publ., London, England, 1975.

Caruccio, F. T., Ferm, J. C., Horne, J., Geidel, G., and Baganz, B., Paleoenvironment of Coal and its Relation to Drainage Quality, EPA-600/7-77-067, 1977.

Cathles, L. M., Acid mine drainage, *Earth and Mineral Sciences,* 51, p. 37, 1982.

Chang, Y. C. and Myerson, A. S., Growth model of the continuous bacteria leaching of the iron pyrite by *Thiobacillus ferrooxidans, Biotechnol. Bioeng.*, 24, p. 889, 1982.

Chapman, H. D., Cation exchange capacity, In Black, C.A. et al. (ed.) Methods of soil analysis. Part II. Agronomy 9:891-901. American Society of Agronomy, Madison, WI, 1965.

Coleman, N. T. and Thomas, G. W., The basic chemistry of soil acidity. in *Soil Acidity and Liming*, Pearson, R. W. and Adams, F. (Eds.), American Society of Agronomy, Madison, WI, 1967, p. 1.

Daniels, F. and Alberty, R. A., *Physical Chemistry*, 4th ed., John Wiley & Sons, NY, 1975.

Davies, C. W., *Ion Association*, Butterworths, London, 1962.

Di Toro, M., Mahony, J. D., Kirchgraber, P. R., O'Byrne, A. L., Pasquale, L. R., and Piccirilli, D. C., Effects of nonreversibility, particle concentration, and ionic strength on heavy metal sorption, *Environ. Sci. Technol.*, 20, p. 55, 1986.

Dixon, J. B., and Weed, S. B. (Eds.), *Minerals in Soil Environments,* Soil Science Society of America, Madison, WI., 1977.

Dollhopf, D. J. and DePuit, E. J., Chemical amendment and irrigation effects on sodium migration and vegetation characteristics in sodic mine soils in the Northern Great Plains, in *Proceedings of the National Symposium on Surface Mine Hydrology, Sedimentology and Reclamation*, University of Kentucky, Lexington, 1981, p. 481.

Donato, P. de, Mustin, C., Benoit, R., and Erre, R., Spatial distribution of iron and sulphur species on the surface of pyrite, *Appl. Surf. Sci.*, 68, p. 81, 1993.

Donato, P. de, Mustin, C., Berthelin, J., and Marion, P., An infrared investigation of pellicular phases observed on pyrite by Scanning Electron Microscopy, during its bacteria oxidation. *C. R. Acad. Sci. Paris, t. 321, Serie II*, p. 241, 1991.

Dowd, J. E. and Riggs, D. S., A comparison of estimates of Michaelis-Menten kinetic constants from various linear transformations, *J. Biol. Chem.*, 240, p. 863, 1965.

Dudley, L. M. and McNeal, B. L., A model for electrostatic interactions among charged sites of water-soluble, organic polyions. 1. Description and sensitivity, *Soil Sci.*, 143, p. 329, 1987.

Dugan, P. R., Prevention of formation of acid drainage from high-sulfur coal refuse by inhibition of iron- and sulfur-xoidizing microorganisms, II., Inhibition in "Run of Mine" refuse under simulated field conditions, *Biotech. and Bioeng.*, 29, p. 49, 1987.

Dzombak, D. A., Fish, W., and Morel, F. M. M., Metal-humate interaction. 1. Discrete ligand and continous distribution models, *Environ. Soil Technol.*, 20, p. 669, 1986.

Eger, P., The use of sulfate reduction to remove metals from acid mine drainage, in Achieving Land Use Potential Through Reclamation, *Proceedings of 9th National Meeting of the American Society for Surface Mining and Reclamation*, June 14-18, 1992, Duluth, MN, p. 563, 1992.

Ehrlich, H. L., Bacterial oxidation of arsenopyrite and enargite, *Econ. Geol.*, 59, p. 1306, 1964.

Ehrlich, H. L., *Geomicrobiology,* Marcel Dekker, Inc., New York, 1981.

Ephraim, J. H., Boren, H., Petterson, C., Arsenie, I., and Allard, B, A novel description of acid-base properties of an aquatic fulvic acid, *Environ. Sci. Technol.*, 23, p. 356, 1989.

Epstein, E., *Mineral Nutrition of Plants: Principles and Perspectives,* John Wiley and Sons, Inc., New York, 1972.

Epstein, E. and Hagen, C. E., A kinetic study of adsorption of alkali cations by barley roots, *Plant Physiol.*, 27, p. 457, 1952.

Erickson, P. M., Girts, M. A., and Kleinmann, R.L.P., Use of constructed wetlands to treat coal mine drainage, *Proc. National Western Mining Conference*, Denver, CO, Feb. 11-13, 1987.

Erickson, P. M., Ladwig, K. J., and Kleinmann, R. L. P., Acid mine drainage from inactive eastern coal operations, *Environ. Geochem. & Health,* 7, p. 16, 1985.

Erickson, P. M. and Ladwig, K. J., Control of acid formation by inhibition of bacteria and by coating pyritic surfaces, Final Report to the West Virginia Department of Energy, Division of Reclamation, Charleston, WV., 1985.

Evangelou, V. P., The influence of anions on potassium quantity-intensity relationships, *Soil Sci. Soc. of Am. J,* 50, p. 1128, 1986.

Evangelou, V. P. and Sobek, A. A., *Water quality evaluation and control,* 22, 24, in *Reclamation of Disturbed Lands,* Vol. II, Hossner, L. R., Ed., CRC Press, Boca Raton, FL, 1988, p.17.

Evangelou, V. P. and Wagner, G. J., Effects of ion activity and sugar polyalcohol osmotica on ion uptake, *J. Exp. Botany,* 38, p. 1637, 1987.

Evangelou, V. P., Influence of water chemistry on suspended solids in coal mine sedimentation ponds, *J. Env. Qual.*, 19, p. 428, 1989.

Evangelou, V. P. and Karathanasis, A. D., Influence of sodium on the kinetics of settling of suspended solids in coal mine sedimentation pond environments, *J. Env. Qual.*, 20, p. 783, 1991.

Evangelou, V. P. and Huang, X., Hydrogen Peroxide Induced Oxidation Proof Phosphate Surface Coating on Iron Sulfides, U. S. Patent Application Document, Reference No. 434-136, 1993.

Evangelou, V. P. and Huang, X., Infrared spectroscopic evidence of an Iron(II)-carbonate complex on the surface of pyrite, *Spectrochimica Acta,* 50A, p. 1333, 1994.

Evangelou, V. P. and Phillips, R. E, Ionic composition of pyritic coal spoil leachate - Interactions and effect on saturated hydraulic conductivity, *In Recl. Reveg. Res.*, 3, p. 65, 1984.

Evangelou, V. P. and Wang J., Differences between infrared spectra of aatrazine obtained under transmittance and diffuse reflectance modes, *Spectrochimica Acta,* 49A, p. 291, 1993.

Evangelou, V. P., Potential microencapsulation of pyrite by artificial inducement of $FePO_4$ coatings, *J. Environ. Qual.*, (In Press), 1994.

Evangelou, V. P., Barnhisel, R. I and Barfield, B. J, *Modeling release of chemical constituents in surface mine runoff and in coal mine sediment ponds*, Trans. ASAE, 30, p. 82, 1987.

Evangelou, V. P., Grove, J. H., and Rawlings, F. D., Rates of iron sulfide oxidation in coal spoil suspension, *J. Environ. Qual.*, 14, p. 91, 1985.

Evangelou, V. P., Grove, J. H., and Phillips, R. E., Factors controlling water movement in acid spoils, in *Proc. Nat. Symp. on Surface Mine Hydrology, Sedimentology, and Reclamation*, Univ. of Kentucky, Lexington, KY, p. 5, 1982a.

Evangelou, V. P., Mancos Shale as a Source of Salts in the Upper Colorado River Basin, Ph.D. Dissertation. Dept. of Land, Water and Air Resources, University of California, Davis, p. 197, 1981.

Evangelou, V. P., Phillips, R. E., and Shepard, J. S., Salt generation in pyritic coal spoils and its effect on saturated hydraulic conductivity, *Soil Sci. Soc. Am. J.*, 46, p. 457, 1982b.

Evangelou, V. P., Pyritic coal spoils: Their chemistry and water interactions, in *Leaching and Diffusion.*, Augustithis, S., (Ed.), International Committee for the Studies of Bausites, Alumina and Aluminum, Theophrastus Publications, Athens, Greece, p. 175, 1983.

Evangelou, V. P. and Phillips, R. E., Ionic composition of pyritic coal spoil leachate-Interactions and effect on saturated hydraulic conductivity, *Reclam. Reveg. Res.*, 3, p. 65, 1984.

Evangelou, V. P., Sainju, U. M., and Huang, X., Evaluation and quantification of calcite, dolomite and rock phosphate by manganese, in *Proc. Int. Symp. on Land Reclamation: Advances in Research and Technology*, Younos, T., Diplas, P., and Mostaghimi, S., (Eds.), Nashville, TN, p. 304, 1992.

Evangelou, V. P. and Coale, F. J., An investigation on the dependence of the Gapon coefficient on exchangeable sodium by three linear transformations, *Can. J. Soil Sci.*, 68, p. 813, 1988.

Evangelou, V. P. and Phillips, R. E., Comparison between the Vanselow and Gapon exchange selectivity coefficients, *Soil Sci. Soc. Am. J.*, 52, p. 379, 1988.

Evangelou, V. P. and Phillips, R. E., Sensitivity analysis on the comparison between the Gapon and Vanselow exchange coefficients, *Soil Sci. Soc. Am. J.*, 51, p. 1473, 1987.

Evangelou, V. P., Remediation of Acid Drainage Through Surface Coating of iron Sulfides, U. S. Geological Survey, Water Resources Research Act Grant Program (7846), 85 p., 1994.

Evangelou, V. P., Whittig, L. D., Tanji, K. K., An automated manometric method for differentiation and quantitative determination of calcite and dolomite, *Soil Sci. Soc. Am. J.*, 48, p. 1236, 1984

Evangelou, V. P. and Zhang, Y. L., A review: pyrite oxidation mechanisms and acid mine drainage prevention, *Crit. Rev. Environ. Sci. Tech.*, (In Press), 1994.

Evans, L. J., Chemistry of metal retention by soils, *Environ. Sci. Technol.*, 23, p. 1046, 1989.

Fisher, S. and Kunin, R., Effect of cross linking on the properties of carboxylic polymers: Apparent dissociation constants of acrylic and methacrylic acid polymers, *J. Phys. Chem.*, 60, p. 1030, 1956.

Flynn, J. P, Treatment of Earth Surface and Subsurface for Prevention of Acidic Drainage from the Soil, U.S. Patent 3,443,882, May 13, 1969.

Foreman, J. W., Evaluation of mine sealing in Butler County, Pennsylvania, *4th Symp. Coal Mine Drainage Res.*, Louisville, KY, p. 83, 1972.

Fornasiero, D., Eijt, V., and Ralston, J., An electrokinetic study of pyrite oxidation, *Colloids and Surfaces*, 62, p. 63, 1992.

Frantz, G., and Carlson, P. M., Effects of rubidium, cesium, and thallium on interlayer potassium release from Transvaal vermiculite, *Soil Sci. Soc. Am. J.*, 51, p. 305, 1987.

Gamble, D. S., Schnitzer, M., and Hoffmen, I., Cu^{2+}-fulvic acid chelation equilibrium in 0.1 M KCl at 25°C, *Can. J. Chem.*, 48, p. 3197, 1970.

Gamble, D. S., Schnitzer, M., Kerndorff, H., and Longford, C. H., Multiple metal ion exchange equilibria with humic acid, *Geochim. Cosmochim. Acta*, 47, p. 1311, 1983.

Garrels , R. M., and Thompson, M. E., Oxidation of pyrite by iron sulfate solution, *Am. J. Sci.*, 258A, p. 57, 1960.

Garrels, R. M. and Christ, C. L., *Solutions, Minerals and Equilibria*, Freeman, Cooper & Company, San Francisco, CA., 1965.

Gast, R. G., Surface and colloid chemistry, in *Minerals in Soil Environments.*, Dixon, J.B. and Weed, S.B. (Eds.), American Society of Agronomy, Madison, WI, p. 27, 1977.

Giblin, A. E., Pyrite formation in marshes during early diagnoses, *Biotecnol. Bioeng.*, 9, p. 471, 1988.

Girts, M. A. and Kleinmann, R. L. P., Constructed wetlands for treatment of acid mine drainage: a preliminary review, *National Symposium on Mining, Hydrology, Sedimentology, and Reclamation*, University of Kentucky, Lexington, KY, 1986.

Goldhaber, M. B., Experimental study of metastable sulfur oxyanion formation during pyrite oxidation at pH 6-9 and 30° C, *Am. J. Sci.*, 283, p. 193, 1983.

Goldhaber, M. B. and Kalan, I. R., The sulfur cycle, in *The Sea,* Vol. 5, *Marine Chemistry*, Goldberg, E. D. (Ed.), Wiley-Interscience, NY, p. 527, 1974.

Gormely, L. S., Duncan, D. W., Branion, R. M. R., and Pinder, K. L., Continues culture of *Thiobacillus ferrooxidans* on a zinc sulfide concentrate, *Biotechnol. Bioeng.*, 17, p. 31, 1975.

Grady, W. C., Microscopic varieties of pyrite in West Virginia coals, *Trans. Soc. Min. Eng. AIME*, 262, p. 268, 1977.

Greenland, D. J., Interaction between humic and fulvic acids and clays, *Soil Sci.*, 111, p. 34, 1971.

Greer, R. T., Coal microstructure and the significance of pyrite inclusions, *Scanning Electron Microsc.*, 10, p. 79, 1977.

Griffiths, P. R. and Fuller, P. M., Mid-infrared spectroscopy of powdered samples, in *Advances in Infrared and Raman Spectroscopy,* Vol. 9, Heyden, London, p. 63, 1981.

Guy, R. D. and Chakrabarti, C. L., Studies of metal-organic interactions in model systems pertaining to natural waters, *Can. J. Chem.,* 54, p. 2600, 1976.

Hajek, B. F., Adams, F., and Cope, J. T. Jr., Rapid determination of exchangeable bases, acidity, and base saturation for soil characterization, in *Soil Sci. Soc. Amer. Proc.*, 36, p. 436, 1972.

Hamilton, I. C. and Woods, R., An investigation of surface oxidation of pyrite and pyrrhotite by linear potential sweep voltammetry, *J. Electroanal. Chem.*, 118, p. 327, 1981.

Hammack, R. W. and Edenborn, H. M., The removal of nickel from mine waters using bacteria sulfate reduction, in *Proceeding of the 1991 National Meeting of the American Society of Surface Mining and Reclamation*, Oaks, W. and Bowden, J. (Eds.), Princeton, WV, 1, p. 97, 1991.

Hammack, R. W. and Watzlaf, G. R., The effect of oxygen on pyrite oxidation, *In Proceedings of the Mining and Reclamation Conference*, Charleston, WV, April 23-26, p. 257, 1990.

Hammack, R. W. and Hedin, R. S., Microbial sulfate reduction for the treatment of acid mine drainage: a laboratory study, *Proceedings of the Ninth Annual Virginia Surface Mine Drainage Task Force,* Morgantown , WV, 1989.

Handershot, W. H. and Duquette, M., A simple barium chloride method for determining cation exchange capacity and exchangeable cations, *Soil Sci. Soc. Am. J.*, 50, p. 605, 1986.

Hargrove, W. L. and Thomas, G. W., Effect of organic matter on exchangeable alumunum and plant growth in acid soils, *In* Chemistry in the Soil Environment, Baker, D.E. (Ed.), ASA monograph No. 40, *Soil Science Society of America*, Madison, WI, 1981.

Harrison, A. P., The acidophilic thiobacilli and other acidophilic bacteria that share their habitat, *Annu. Rev. Microbio.*, 38, p. 265, 1984.

Hart, W. and Stiller, A., Application of phosphate refuse to coal mine refuse for melioration of acid mine drainage, In *The Second International Conference on the Abatement of Acidic Drainage,* Vol. 2 Sept. 16, 17, 18, Montreal, Canada, p. 173, 1991.

Harter, R. D. and Ahlrichs, J. L., Determination of clay surface acidity by infrared spectroscopy, *Soil Sci. Soc. Amer. Proc.*, 31, p. 30, 1967.

Harter, R. D., Effect of soil pH on adsorption of lead, copper, zinc, and nickel, *Soil Sci. Soc. Am. J.*, 47, p. 47, 1983.

Hatcher, P. G., Schnitzer, M., Dennis, L. W., and Maciel, G. E., Aromaticity of humic substances in soils, *Soil Sci. Soc. Am. J.*, 45, p. 1089, 1981.

Hatton, D. and Pickering, W. P., The effect of pH on the retention of Cu, Pb, Zn, and Cd by clay-humic acid mixture, *Water, Air, and Soil Pollution*, 14, p. 13, 1980.

Hider, R. C., Siderophore mediated absorption of iron, *Struct. Bonding (Berlin)*, 58, p. 26, 1984.

Hiller, R. M., Relative effectiveness of some coal mine refuse revegetation techniques: Leachate quality, in *Proc. of National Symposium on Surface Mine Hydrology, Sedimentology and Reclamation* , Univ. of Kentucky, Lexington, KY, 1981, p. 377.

Hiskey, J. B. and Schlitt, W. J., Aqueous oxidation of pyrite , in *Interfacing Technologies in Solution Mining*, (Eds.) Schlitt, W. J. and Hiskey, J. B., *Proc.2nd SME-SPE Intl Soln Mining Symp.*, Denver, p. 55, 1982.

Hoffmann, M. R., Faust, B. C., Panda, F. A., Koo, H. H., and Tsuchiya, H. M., Kinetics of the removal of iron pyrite from coal by microbial catalysis, *Appl. Environ. Microbiol.*, 42, p. 259, 1981.

Hood, W. C. and Oertal, A. O., A leaching column method for predicting effluent quality from surface mines, in *Proc. Symp. Surf. Min. Hydr. Sedim. Recl.*, University of Kentucky, Lexington, KY, p. 271, 1984.

Hood, T. A., The Kinetics of Pyrite Oxidation in Marine Systems, Ph.D. Thesis, University of Miami, FL, 1991.

Howarth, R. W. and Teal, J. M., Sulfur reduction in New England salt marsh, *Limnol. Oceanogr.*, 24, p. 999, 1979.

Huang, X. and Evangelou, V. P., Abatement of Acid Mine Drainage by Encapsulation of Acid Producing Geologic Materials, U. S. Department of the Interior, Bureau of Mines, Contract No. J0309013., 60 pp., 1992.

Huang, X. and Evangelou, V. P., Suppression of pyrite oxidation rate by phosphate addition, in *The Environmental Geochemistry of Sulfide Oxidation*, Alpers, C. N. and Blowes, D. W., (Eds.), American Chemical Society, Washington, DC, p. 562, 1994.

Infarger, M. and Hood, W. C., Positioning acid-producing overburden for minimal pollution, in *Proc. of Nat. Symp. on Surface Mine Hydrology, Sedimentology and Reclamation*, Univ. of Kentucky, Lexington, KY, 1980, p. 325.

Inskeep, W. P. and Baham, J., Competitive complexation of Cd(II) and Cu(II) by water soluble organic ligands and Na-montmorillonite. *Soil Sci. Soc. Am. J.* 47, p. 1109, 1983a.

Ivanov, V. I., Effect of some factors on iron oxidation by cultures of *Thiobacillus Ferrooxidans*, *Microbiology*, (Engl. Transl.), 31, p. 645, 1962.

Iwasaki, K., Sakurai, K. and Takahashi, E., Copper binding by the root cell walls of Italian ryegrass and red clover. *Soil Sci. Plant Nutr.*, 36, p. 431, 1990.

Jackson, J. L., Soluble salts analysis for soils and waters, in *Soil Chemical Analysis*, Prentice-Hall; Englewood Cliff, NJ, Chap. 10, 1958.

Jackson, M. L., Soil Chemical Analysis-Advanced Course, University of Wisconsin, Madison, Published by the author, 1975.

Jackson, M. L., Stewart, B.R., and Daniels, W.L., Influence of flyash, topsoil, lime and rock-P on acid mine drainage from coal refuse, in *Proceedings of 1993 National Meeting of the American Society for Surface Mining and Reclamation*, Spokane, Washington, May 16-19, p. 266, 1993.

Jardine, P. M., Weber, N. L., and McCarthy, J. F., Mechanisms of dissolved organic carbon adsorption on soil, *Soil Sci. Soc. Am. J.*, 53, p. 1378, 1989.

Jaynes, D. B., Modeling acid mine drainage from reclaimed coal stripmines, In *The Second International Conference on the Abatement of Acidic Drainage,* Vol. 2, Sept. 16-18, Montreal, Canada, 1991, p. 191.

Jaynes, D. B., Rogowski, A. S. and Pionke H. B., Acid mine drainage from reclaimed coal strip mines. 1. Model description, *Water Resources Research*, 20, p. 233, 1984.

Jurinak, J. J., Amrhein, C., and Wagenet, R. l., The effect of salinity and SAR on the sodic hazard of overburden materials, in *Proc. of Nat. Symp. on Surface Mine Hydrology, Sedimentology and Reclamation*, Univ. of Kentucky, Lexington, KY, 1981, p. 31.

Jurinak, J. J. and Bauer, N, Thermodynamics of zinc adsorption on calcite, dolomite and magnesite-type minerals, *Soil Sci. Soc. Am. Proc.*, 20, p. 466, 1956.

Khan, S. U., Interaction between the humic acid fraction of soils and certain metallic cations, *Soil Sci. Soc Am. Proc.*, 33, p. 851, 1969.

Kinniburgh, D. G., General purpose adsorption isotherms, *Environ. Sci. Technol.*, 20, p. 895, 1986.

Kleinmann, R. L. P., Bactericidal control of acid problems in surface mines and coal refuse, in *Proc. of Nat. Symp. on Surface Mine Hydrology, Sedimentology and Reclamation*, Univ. of Kentucky, Lexington, KY, 1980, p. 333.

Kleinmann, R. L. P., The US Bureau of Mines acid mine drainage research program, in *Proceedings, Second West Virginia Surface Mine Drainage Task Force Symposium,* Clarksburg, WV, 1981.

Kleinmann, R. L. P., Acid mine drainage: U.S. Bureau of mines researches and develops control methods for both coal and metal mines, *E&MJ.* July 1989. p. 16I, 1989.

Kleinmann, R. L. P., Crerar, D. A., and Pacelli, R. P., *Mining Engineering,* 3, p. 300, 1981.

Kleinmann, R. L. P., Treatment of acid mine water by wetlands, In Control of Acid Mine Drainage, Bureau of Mines IC 9027, p. 61, 1985.

Kleinmann, R. L. P. and Crerar, D. A., *Thiobacillus Ferrooxidans* and the formation of acidity in simulated coal mine environments, *Geomicrobiology J.*, 1, p. 373, 1979.

Kokholm, G., Redox Measurements: Their Theory and Technique, Radiometer A/S Emdrupvej 72 DK-2400 Copenhagen NV Denmark, 1977.

Konishi, Y., Asai, S., and Sakai, H. K., Bacteria dissolution of pyrite by *Thiobacillus ferrooxidans, Bioprocess Engineering*, 5, p. 231, 1990.

Kuo, S. and Baker, A. S., Sorption of copper,zinc, and cadmium by some acid soils, *Soil Sci. Soc. Am. J.*, 44, p. 969, 1980.

Ladwig, K. J., Erickson, P. M., and Kleinmann, R. L. P., Alkaline injection: an overview of recent work, In Control of Acid Mine Drainage, Bur. of Mines IC 9027. USDA, Bureau of Mines, p. 35, 1985.

Lasaga, A. C., Rate laws of chemical reactions, in Lasaga, A. C. and Kirkpatrick, R. J. (Eds.). *Kinetics of Geochemical Processes, Reviews in Mineralogy*, 8, p. 1, 1981.

Lekhakul, S., The Effect of Lime on Chemical Composition of Surface Mined Coal Spoils, and the Leachate from Spoils, Ph.D. Dissertation, Agronomy Dept., Univ. of Kentucky, Lexington, KY, p. 134, 1981.

LeRoux, N. W., Dacey, P. W., and Temple, K. L., The microbial role in pyrite oxidation at alkaline pH in coal mine spoil, in *Biogeochemistry of Ancient and Modern Environments*, Truidnger, P. A., Walter, M. R., and Ralph, B. J. (Eds.), Springer-Verlag, Berlin, p. 515, 1980.

Lindsay, W. L., *Chemical equilibria in soils*, John Wiley & Sons, New York, 1979.

Lindsay, W. L., Solid phase-solution equilibria in soils, in *Chemistry in the Soil Environment*, Baker, D. E. (Ed.) ASA monograph No. 40, Soil Science Society of America, Madison, WI, 1981.

Lizama, H. M. and Suzuki, I., Rate equation and kinetic parameters of the reactions involved in pyrite oxidation by *Thiobacillus ferrooxidans, Appl. Environ. Microbiol.*, 55, p. 2918, 1989.

Loomis, E. C. and Hood, W. C., The effects of anaerobically digested sludge on the oxidation of pyrite and the formation of acid mine drainage, in *Proc. of Nat. Symp. on Surface Mine Hydrology, Sedimentology and Reclamation*, Univ. of Kentucky, Lexington, KY, 1984, p. 1.

Lorenz, W. C. and Tarpley, E. C., Oxidation of Coal Mine Pyrites, *U.S. Bureau of Mines*, RI 6247, 1963.

Lowe, L. E., Distribution and properties of organic fraction in selected Alberta soils, *Can. J. Soil Sci.*, 49, p. 129, 1969.

Lowson, R. T., Aqueous oxidation of pyrite by molecular oxygen, *Chemical Rev.*, 82, p. 461, 1982.

Lumbanraja, J., Binary and Ternary K-NH_4-Ca Exchange Equilibria, Kinetics and Spectroscopic Evidence Of Cation-soil Mineral Surface Interactions, Ph.D Thesis, University of Kentucky, Lexington, KY, 1991.

Lumbanraja, J., and Evangelou, V. P., Influence of acidification and liming on surface charge behavior of three Kentucky subsoils, *Soil Sci. Soc. Am. J.*, 54, p. 26, 1991.

Lundgren, D. G. and Silver, M., Ore leaching by bacteria, *Annu. Rev. Microbio.*, 34, p. 263, 1980.

Lundgren, D. G., Vestal, J. R. and Tabita, F. R., *Water Polltion Microbiology*, Wiley-Interscience, New York, NY, 1972.

Luther, G. W. III, The frontier-molecular-orbital theory approach in geotechnical processes, in *Aquatic Chemical Kinetics*, Stumm, W. (Ed.), John Wiley & Sons, Inc., New York, NY, 1990, p. 173.

Luther, G. W. III, Kostka, J. E., Church, T. M., Sulzberger, B., and Stumm, W., Seasonal iron cycling in the salt-marsh sedimentary environment: the importance of ligand complexes with Fe(II) and Fe(III) in the dissolution of Fe(III) minerals and pyrite, respectively, *Marine Chemistry*, 40, p. 81, 1992.

Luther, G. W. III, Pyrite and oxidized iron mineral phases from pyrite oxidation in salt marsh and estuarine sediments, *Geochim. et Cosmochim. Acta*, 46, p. 2665, 1982.

Luther, G. W. III, Pyrite oxidation and reduction: Molecular orbital theory consideration, *Geochem. et Cosmochem. Acta*, 51, p. 3193, 1987.

Magdoff, F. R, and Bartlett, R. J., Soil pH buffering revisited. *Soil Sci. Soc. Am. J.* 49, p. 145 1985.

Marsi, M, and Evangelou, V. P., Modeling brackish solution influences on the chemical and physical behavior of temperate region soils, *In Emerging Technologies in Hazardous Waste Management III*, D. W. Tedder and F. G. Pohland, Eds., Chapter 15, American Chemical Society, Washington, DC, 1993.

Martin, J. P. and Haider, K., Influence of mineral colloids on turnover rates of soil organic carbon, p. 283-304, in *Interactions of Soil Minerals With Natural Organics and Microbes*, Huang, P. M. and Schnitzer, M. (Eds.), Soil Sci. Soc. Am. Spec. Publ. No. 17, Madison, WI, 1986.

McBride, M. B., Chemisorption and precipitation of Mn^{2+} at $CaCO_3$ surfaces , *Soil Sci. Soc. Am. J.*, 43, p. 693, 1979.

Mckibben, M. A., Kinetics of aqueous oxidation of pyrite by ferric iron, oxygen and Hydrogen peroxide from pH 1-4 and 20-40ºC, Ph.D. thesis, The Pennsylvania State University, University Park, PA, 1984.

McKibben, M. A. and Barnes, H. L., Oxidation of pyrite in low temperature acidic solutions: Rate laws and surface textures, *Geochim. Cosmochim. Acta,* 50, p. 1509, 1986.

Meek, A. Jr., Assessment of acid-preventive techniques employed at the Island Creek Mining Company, Tenmile Site, in *Proceedings of the Twelfth Annual West Virginia Surface Mine Drainage Task Force Symposium,* Morgantown, WV, 1984.

Meek, F. A., Research into the use of apatite rock for acidic drainage prevention, in *Proceedings, Fifth West Virginia Surface Mine Drainage Task Force Symposium,* Morgantown, WV, 1984.

Mehlich, A., Charge properties in relation to sorption and desorption of selected cations and anions, in *Chemistry in the Soil Environment*, Dowdy, R.H., Ryan, I.A., Volk, V.V., and Baker, D.E. (Eds.), Am. Soc. of Agron., Madison, WI, p. 47, 1981.

Mehta, A. P. and Murr, L. E., Fundamental studies of the contribution of galvanic interaction to acid-bacterial leaching of mixed metal sulfides, *Hydrometallurgy*, 9, p. 235, 1983.

Miller, F. A. and Wilkins, C. H., Analytical Chem., 24, pp 1253-1294, 1952.

Miller, S. D. and Moor, D., Coal mine rehabilitation in Australia - the role of soil and overburden, in *Proceedings of National Symposium on Surface Mine Hydrology, Sedimentology and Reclamation.*, Univ. of Kentucky, Lexington, KY, 1981, p. 1.

Millero, F. J. and Izaquirre, M., The effect of ionic strength and ionic interactions on the oxidation of Fe(II), *J. Solution Chem.,* 18, p. 585, 1989.

Millero, F. J., The effect of ionic interactions on the oxidation of metals in natural waters, *Geochim. Cosmochim. Acta*, 49, p. 547, 1985.

Moore W. J., *Physical Chemistry,* 4th ed., Prentice-Hall, London, 1972.

Morse, J.W., Millero, F. J., Cornwell, J. C., and Rickard, D., The chemistry of the hydrogen sulfide and iron sulfide systems in natural waters, *Earth-Sci. Rev.*, 24, p. 1, 1987.

Mortensen, J. L., Complexing of metals by soil organic matter, *Soil Sci. Soc. Am. Proc.*, 27, p. 179, 1963.

Mortland, M. M., Protonation of compounds on clay mineral surfaces, *9th Int. Congr. Soil Sci.*, Vol I, p. 691, 1968.

Mortland, M. M. and Raman, K. V., Surface acidity of smectites in relation to hydration, exchangeable cation and structure, *Clays and Clay Min.*, 16, p. 393, 1968.

Moses, C. O., Nordstrom, D. K, Herman, J. S and Mills, A, Aqueous pyrite oxidation by dissolved oxygen and by ferric iron, *Geochim. Cosmochim. Acta,* 54, p. 395, 1987.

Moses, C. O. and Herman, J. S., Pyrite oxidation at circumneutral pH, *Geochim. Cosmochim. Acta*, 55, p. 471, 1991.

Murthy, A. R. V. and Sharada, K., Determination of sulfide sulfur in minerals, *Analyst,* 85, p. 299, 1960.

Mustin, C., Berthelin, J., Marion, P. and Donato, P. de., Corrosion and Electrochemical oxidation of a pyrite by *Thiobacillus ferrooxidans, Appl. Environ. Microbiol.*, 58, p. 1175, 1992.

Nairn, R. W., Hedin, R. S. and Watzlaf, G. R., A preliminary review of the use of anoxic limestone drains in the passive treatment of acid mine drainage, in *Proceedings of the Twelfth Annual West Virginia Surface Mine Drainage Task Force Symposium*, Morgantown, WV, p. 23, 1991.

Nairn, R. W., Hedin, R.S., and Watzlaf, G.R., Genaration of alkalinity in an anoxic limestone drain, in *Proceedings of the 9th Annual Meeting of the American Society for Surface Mining and Reclamation*, Duluth, MN, June 14-18, 1992.

Nakamoto, K., *Infrared and Raman Spectra of Inorganic and Coordination Compounds,* John Wiley & Sons, New York, 1963, 1986.

Nand, R. and Raman, K. V., Characterization of metal-humic and fulvic acid complexes, *Pedologie*, 23, p. 137, 1983.

Nanzyo, M., Infrared spectra of phosphate sorbed on iron hydroxide gel and the sorption products, *Soil Sci. Plant Nutr.*, 32, p. 51, 1986.

Nicholson, R. V., Gillham, R. W., and Reardon, E. J., Pyrite oxidation in carbonate-buffered solution: 1. Experimental kinetics, *Geochim. Cosmochim. Acta,* 52, p 1077, 1988.

Nicholson, R. V., Gillham, R. W., and Reardon, E. J., Pyrite oxidation in carbonate-buffered solution: 2. Rate control by oxide coatings, *Geochim. Cosmochim. Acta,* 54, p 395, 1990.

Nielson, D. R., Jackson, R. D., Gary, J. W., and Evans, D. D., (eds), Soil Water, American Soc. Agron., Madison, WI, 1972.

Nordstrom, D. K., Aqueous pyrite oxidation and the consequent formation of secondary iron minerals, in *Acid Sulfate Weathering, Pedogeochemistry and Relationship to Manipulation of Soil Minerals*, Hossner, L.R., Kittrick, J.A., and

Fanning, D.F., (Eds.), Soil Science Society of America Press, Madison, WI, p. 46, 1982a.

Nordstrom, D. K., The effect of sulfate on aluminum concentrations in natural waters: some stability relations in the system Al_2O_3-SO_3-H_2O at 298 K , *Geoch. et Cosmoch. Acta*, 46, p. 681, 1982b.

Novak, J. M. and Smeck, N. E., Comparisons of humic substances extracted from contiguous Alfisols and Mollisols of Southwestern Ohio, *Soil Sci. Soc. Am. J.* 55, p. 96, 1991.

O'Shay, T., Hossner, L. R. and Dixon, J. B., A modified hydrogen peroxide oxidation method for determination of potential acidity in pyritic overburden, *J. Environ. Qual.*, 19, p. 778, 1990.

Oster, J. D., Shainberg, I., and Wood J. D., Flocullation value and gel structure of sodium/calcium montmorillonite and illite suspensions, *Soil Sci. Soc. Am. J.*, 44, p. 959, 1980.

Palencia, I. R., Wan, W., and Miller, J. D., The electrochemical behavior of a semiconducting natural pyrite in the presence of bacteria, *Metallurgical Trans. B.*, 22B, p. 765, 1991.

Pavan, M. A. and Bingham, F. T., Toxicity of aluminium to coffee seedlings grown in nutrient solution, *Soil Sci. Soc. of Am. J.*, 46, p. 993, 1982.

Parker, J. C., Zelazny, L. W., Samprath, S., and Harris, W. G., A critical evaluation of the extension of the zero point of charge (zpc) theory to soil soil systems, *Soil Sci. Soc. Am. J.*, 43, p. 668, 1979.

Pesic, B. D., Oliver, J., and Wichlacz, P., An electrochemical method of measuring rate of ferrous to ferric iron with oxygen in the presence of *Thiobacillus ferrooxidans*, *Biotech and Bioengr.*, 33, p. 428, 1989.

Petersen, W. G., and Chesters, G., Quantitative determination of calcite and dolomite in pure carbonates and limestones, *J. Soil Sci.*, 17, p. 317, 1966.

Petersen, W. G., Chesters, G., and Lee, G. B., Quantitaive determination of calcite and dolomite in soils, *J. Soil Sci.*, 17, p. 329, 1966.

Piccolo, A. and Stevenson, F. J., Infrared spectra of Cu^{2+}, Pb^{2+}, and Ca^{2+} complexes of soil humic substances, *Geoderma* 27, p. 195, 1982.

Pionke, H. B., Rogowski, A. S., and Deangelis, R. J., Controlling the rate of acid loss from strip mine spoil, *J. Environ. Qual.*, 9, p. 694, 1980.

Polemio, M. and Rhodes, J. D., Determining Cation Exchange Capacity: a new procedure for calcaceous and gypsiferous soils, *Soil Sci. Soc. Am. J.*, 41, p. 524, 1977.

Posner, A. M., Titration curves of humic acids, *8th Int. Congr., Soil Sci.*, 17, p. 161, 1966.

Posner, A. M., The humic acid extracted by various reagents from soil. Part I. Yield, inorganic components, and titration curves, *J. Soil Sci.*, 17, p. 65, 1966.

Postgate, J. R., *The Sulphate-Reducing Bacteria*, Cambridge University Press, New York, 2nd ed.,208 pp., 1984.

Prutton, C. F. and Maron, S. H., *Principles of Physical Chemistry*, MacMillan, New York, 1956.

Quisenberry, V. L. and Phillips, R. E., Displacement of soil water by simulated rainfall, *Soil Sci. Soc. Am. J.*, 42, p. 675, 1978.

Quisenberry, V. L. and Phillips, R. E., Percolation of simulated rainfall under field conditions, *Soil Sci. Soc. Am. J.*, 40, p. 484, 1976.

Rastogi, V., Krecic, R., and Sobek, A. A., ProMac systems for reclamation and control of acid production in toxic mine waste, in *Proceedings, Seventh West Virginia Surface Mine Drainage Task Force Symposium,* Morgantown, WV, 1986..

Renton, J. J., Stiller A. H., and Thomas, R., The use of phosphate materials as ameliorators for acid mine drainage, in *Mine Drainage and Surface Mine Reclamation, Mine Water and Mine Wastes,* Vol 1, p. 67, 1988.

Renton, J. J., Rymer, T., and Stiller, A. H., A laboratory procedure to evaluate the acid producing potential of coal associated rocks, *Mining Science and Technology,* 7, p. 227, 1988.

Renton, J. J., Stiller, A. H., and Rymer, T., The use of phosphate materials as ameliorates for acid mine drainage, in *Mine Drainage and Surface Mine Reclamation.* Vol. I, *Mine Water and Mine Waste*, p. 67, 1991.

Richard, D. T., Kinetics and mechanism of pyrite formation at low temperatures, *Am. J. Sci.*, 275, p. 636, 1975.

Ritcey, G. M., Deep water disposal of pyritic tailings, in *Proceedings of the second International Conference on the Abatement of Acidic Drainage*, Sept. 16-18. Montreal, Canada, 1991, p. 421.

Ritshema, C. J. and Groennenberg, J. E., Pyrite oxidation, carbonate weathering, and gypsum formation in a drained potential acid sulfate soil, *Soil Sci. Am. J.*, 57, p. 968, 1993.

Roberts, K., Evangelou, V. P., and Szekeres, G. W., A rapid kinetic technique for quantifying polycarbonate species in coal spoils, *Miner. Environ.*, 2, p. 72, 1984.

Robinson, R. A. and Stokes, R. H., *Electrolyte Solutions*, 2nd ed., (Rev.), Butterworths, London, 1968.

Saar, R. A. and Weber, J. H., Fulvic acid: modifier of metal-ion chemistry. *Environ. Sci. Technol.*, 16, p. 510A, 1982.

Saiz-Jemenez, C., Hawkins, B. L., and Maciel, G. E., Cross polarization, magic angle spinning ^{13}C nuclear magnetic resonance spectroscopy of soil humic fractions, *Org. Geochem.*, 9, p. 277, 1986.

Sajwan, K. S. and Evangelou, V. P., Apparent activation energies of acid dissolution of carbonates by an isothermal automanometric apparatus, *Soil Sci.*, 152, p. 243, 1991.

Sajwan, K. S., Evangelou, V. P., and Lumbanraja, J., A new rapid approach for evaluating limestone quality by an automanometric isothermal apparatus, *Soil Sci.*, 151, p. 444, 1991.

Scharer, J. M., Garga, V., Smith, R., and Halbert, B. E., Use of steady state models for assessing acid generation in pyritic mine tailings, in *The Second International*

Conference on the Abatement of Acidic Drainage, Vol. 2 Sept. 16-18, Montreal, Canada, 1991, p. 211.

Schnitzer, M., Binding of humic substances by soil mineral colloids. p. 77-101, in *Interactions of Soil Minerals With Natural Organics and Microbes*, Huang, P. M. and Schnitzer, M. (Eds.), Soil Sci. Soc. Am. Spec. Publ. No. 17, Madison, WI, 1986.

Schnitzer, M., Reaction between fulvic acid, a soil humic compound and inorganic soil constituents. *Soil Sci. Soc. Am. Proc.*, 33, p. 75, 1969.

Schnitzer, M., Soil organic matter - the next 75 years, *Soil Sci.*, 151, p. 41, 1991.

Schnitzer, M.. and Kodama, H., Reaction of minerals with humic substances. p. 741-770, in *Minerals in Soil Environments,* Dixon, J.B. and Weed, S.B. (Eds.), Soil Sci. Soc. Am., Madison, WI., 1977.

Schnitzer, M. and Skinner, S. I. M., Organo-metallic interactions in soils: 4. Carboxyl and hydroxyl groups in organic matter and metal ion retention, *Soil Sci.*, 99, p. 278, 1965.

Schnitzer, M. and Khan, S. U., Humic Substances in the Environment, Marcel Dekker. New York, 327 pp., 1972.

Schofield, R. K. and Samson, H. R., Deflocculation of kaolinite clay, *Clay Min. Bul.*, 2, p. 45, 1953.

Segel, I. H., *Biochemical Calculations*, 2nd ed., John Wiley & Sons, Inc., New York, 1976.

Severson, R. C. and Gough, L. P., Rehabilitation materials from Surfaces coal mines in Western U.S.A. III. Relations between elements in mime soil and uptake by plants, *Reclam. Revegetation Res.*, 3, p. 185, 1985.

Shellhorn, M. and Rastogi, V., Practical control of acid mine drainage using bactericides, in *Proceedings, Sixth West Virginia Surface Mine Drainage Task Force Symposium*, Morgantown, WV, 1985.

Silver, M., The mechanism of iron-oxidizing thiobacilli. in Metallurgical Application of Bacteria Leaching And Related Microbiological Phenomena, Murr, L.E., Torma, A.E., and Brierley, J.A. (Eds.), Academic Press, New York, 1978.

Silverman, M. P., Mechanisms of bacterial pyrite oxidation, *J. Bacteriol.*, 94, p. 1046, 1967.

Singer, P. C. and Stumm, W., Acidic mine drainage: the rate-determining step, *Science*, 167, p. 1121, 1970.

Singh, U. and Uehara, G., Electrochemistry of the double-layer: Principles and applications to soils, in Sparks, D.L. (Ed.), *Soil Physical Chemistry*. CRC Press, Boca Raton, FL, 1986, p. 1-38.

Skinner, S. I. M., Halstead, R. L., and Boydon, J. E., Quantitative manometric determination of calcite and dolomite in soils and limestones, *Can. J. Soil Sci.*, 39, p. 197, 1959.

Skjemstad, J. O., Frost, R. L., and Barron, P. F., Structural units in humic acids from Southestern Queensland soils as determined by ^{13}C NMR spectroscopy, *Aust. J. Soil Res.*, 21, p. 539, 1983.

Skousen, J. G., Sencindiver, J. C., and Smith, R. M., Procedures for Mining and Reclamation in Areas with Acid-producing Materials, The Surface Mine Drainage Task Force and the West Virginia University Energy Research Center, p. 43., 1987.

Smith, E. E. and Shumate, K. S., Sulfide to Sulfate Reaction Mechanism, Water Pollution Control Research Series, US Department of the Interior, 1970.

Smith, E. E. and Shumate, K. S., Rate of pyrite oxidation and acid production rate in the field. in Ahmad, M. (Ed.), *Proc. Acid Mine Drainage workshop*, Ohio Univ., Athens, p. 11-18, 1971.

Smith, R. M. and Sobek, A. A., Physical and chemical properties of overburdens, spoils, wastes, and new soils, in *Reclamation of Drastically Disturbed Lands,* Schaller, F.W. and Sutton, P. (Eds.), American Society of Agronomy, Madison, WI, p. 149, 1978..

Sobek, A. A., Shuller, A. W, Freeman, J. R and. Smith, R. M., Field and Laboratory Methods Applicable to Overburdens and Mine Soils, EPA-600/2-78-054, U.S. EPA, Cincinnati, OHIO, 1978.

Sorenson, D. L., Kneib, W. A., and Porcella, D. B., Determination of sulfide in pyritic soils and minerals with a sulfide ion electrode, *Anal. Chem.*, 51, p. 1870, 1979.

Sparks, D. L., (ed.), *Soil Physical Chemistry*, CRC Press Inc., Boca Raton, FL, 1986.

Sposito, G., Sorption of trace metals by humic materials in soils and natural waters. *CRC Crit. Rev. Environ. Control*, 15, p. 1, 1985.

Sposito, G. and Mattigod, S.V., GEOCHEM: A Computer Program for the Calculation of Chemical Equilibria in Soil Solutions and Other Natural Water Systems, *The Kearney Foundation of Soil Science*, University of California, Riverside, 1979.

Sposito, G., The operational definition of zero point of charge in soils, *Soil Sci. Soc. Am. J.*, 45, p. 292, 1981.

Sposito, G. and Mattigod, S.V., GEOCHEM: A Computer Program for the Calculation of Chemical Equilibria in Soil Solutions and Other Natural Water Systems, *The Kearney Foundation of Soil Science*, University of California, Riverside, 1979.

Sposito, G., Holtzclaw, K., M., and LeVesque-Madore, C. S., Cupric ion complexation by fulvic acid extracted from sewage sludge-soil mixtures, *Soil Sci. Soc. Am. J.*, 43, p. 1148, 1979.

Sposito, G., Holtzclaw, K. M., and LeVesque-Madore, C. S., Calcium ion complexation by fulvic acid extracted from sewage sludge-soil mixtures. *Soil Sci. Soc. Am. J.*, 42, p. 600, 1978.

Sposito, G., Holtzclaw, K. M., and Baham, J., Analytical properties of the soluble, metal complexing fractions in sludge-soil mixtures. II. Comperative structural chemistry of the fulvic acid, *Soil Sci. Soc. Am. J.*, 40, p. 691, 1976.

Sposito, G., The future of an illusion: ion activities in soil solutions , *Soil Sci. Soc. Am J.,* 48, p. 531, 1984a.

Sposito, G., *The Surface Chemistry of Soils,* Oxford University Press, New York, 1984b.

Spotts, E. and Dollhopf, D. J., Evaluation of phosphate materials for control of acid production in pyritic mine overburden, *J. Environ. Qual.*, 21, p. 627, 1992.

Staub, M. W. and Cohen, R. R. H., A passive mine drainage treatment system as a bioreactor: Treatment efficiency, pH increase, and sulfate reduction in two parallel reactors, Achieving Land use Potential Throuth the Reclamation, in *Proceedings of the 9th National Meeting of the American Society of Surface Mining and Reclamation*, June 14-18, Duluth, MN, p. 550, 1992.

Stevenson, F. J., Stability constants of Cu^{2+}, Pb^{2+}, and Cd^{2+} complexes with humic acids, *Soil Sci. Soc. Am. J.*, 40, p. 665, 1976.

Stevenson, F. J., Geochemistry of soil humic substances. in *Humic Substances in Soil, Sediment, and Water: Geochemistry, isolation, and characterization,* Aiken, G. R. et al. (Eds.), John Wiley & Sons, New York, 1985, p. 13-52.

Stevenson, F. J., *Humus Chemistry: Genesis, Composition, and Reactions*, John Wiley & Sons, Ltd., New York, 443 pp, 1982.

Stiller, A. H., Renton, J. J., and Rymer, T. E., The use of phosphates for ameliorization, in *Proceedings, Seventh West Virginia Surface Mine Drainage Task Force Symposium*, Clarksburg, WV, 1986.

Stiller, A. H., Renton, J. J, Rymer, T. E., and McConaghy, B. G., The effect of limestone treatment on the production of acid from toxic mine waste in barrel scale weathering experiments, in *Proceedings, Fifth West Virginia Surface Mine Drainage Task Force Symposium,* Morgantown, WV, p. 9, 1985.

Stumm, W. and Morgan, J. J., *Aquatic Chemistry,* John Wiley & Sons, New York, 1981.

Stumm, W. and Morgan, J. J., *Aquatic Chemistry*, John Wiley and Sons, Inc., New York, 1970.

Sturey, C. S., Freeman, J. R., Keeney, T. A., and Sturm, J. W., Overburden analysis by acid-base accounting and simulated weathering studies as a means of determining the probable hydrological consquences of mining and reclamation, in *Proceedings of National Symposium on Surface Mine Hydrology, Sedimentology, and Reclamation.*, Univ. of Kentucky, Lexington, p. 163, 1982.

Sugio, T., Katagiri, T., Inagaki, K., and Tano, T., Actual substrate for elemental sulfur oxidation by sulfur:ferric ion oxidoreductace purified from *Thiobacillus ferrooxidans* on synthetic pyrite, *Biochim. Biophys. Acta*, 973, p. 250, 1989.

Sugio, T., Mizunashi, W., Inagaki, K., and Tano, T., Purification and some properties of sulfur:ferric ion oxidoreductace purified from *Thiobacillus ferrooxidans*, *J. Bacteriol.*, 169, p. 4916, 1987.

Suzuki, I., Lizama, H. M., and Tackaberry, P. D., Competitive inhibition of ferrous iron xoidation by *Thiobacillus ferrooxidans* by increasing concentrations of cells, *Appl. Environ. Microbiol.*, 55, p. 1117, 1989.

Tanji, K. K., Predicting specific conductance from electrolytic properties and ion association in some aqueous solutions, *Soil Sci. Soc. Am. Proc.*, 33, p. 887, 1969a.

Tanji, K. K., Solubility of gypsum in aqueous electrolytes as affected by ion association and ionic strengths up to 0.15 M at 25 C, *Envir. Sci. and Tech.*, 3, p. 656, 1969b.

Tate, K. R. and Theng, B., K. G., Organic matter and its interactions with inorganic soil constituents, in Theng, B. K. G. (Ed.), *Soil with Variable Charge*, N. Z. Soc. Soil. Sci., Lowerr Hutt, New Zealand, p. 225, 1980.

Taylor, S. A., *Physical Edaphology*, W. H. Freeman and Company, San Francisco, 1972.

Taylor, B. E., Wheeler, M. C., and Nordstrom, D. K., Oxygen and sulfur compositions of sulfate in acid mine drainage: Evidence for oxidation mechanisms, *Nature,* 308, p. 538, 1984a.

Taylor, B. E., Wheeler, M. C., and Nordstrom, D. K., Stable isotope geochemistry of acid mine drainage: Experimental oxidation of pyrite, *Geochim. Cosmochim. Acta,* 48, p. 2669, 1984b.

Thomas, G. W., and Hargrove, W. L., The chemistry of soil acidity, In Adams, F. (Ed.), *Soil Acidity and Liming*. 2nd. ed., Am. Soc. of Agron., Madison, WI, 1984.

Thomas, G. W., Exchangeable Cations, in *Methods of Soil Analysis, Part 2, Chemical and Microbiological Properties, Agronomy Monograph No. 9, 2nd ed.*, Page, A.L., Miller, R.H., and Keeney, D.R. Eds., American Society of Agronomy, Soil Science Society of America, Madison, Wis., Chap. 9, 1982.

Thomas, G. W. and Phillips, R. E., Consequences of water movement in macropores, *J. Envir. Qual.*, 8, p. 149, 1979.

Tiller, K. G., Gerth, J., and Brummer, G., The relative affinities of Cd, Ni, and Zn for different soil clay fractions and goethite, *Geoderma*, 34, p. 17, 1984.

Torma, A. E., Osoka, A. S. and Valayapetre, M., Electrochemical method in recovery of metal from sulfide minerals, *Res. Assoc. Miner. Sarda.*, 84, p. 5, 1979.

Torma, A. E., Osoka, A. S., and Valayapetre, M., Electrochemical methods in recovery of metals from sulfide minerals, *Res. Assoc. Miner. Sarda*, 84, p. 5, 1979.

Torma, A. F., Biohydrometallurgy as an emerging technology, in Ehrlich, H. L. and Holmes, D. S. (Eds.), *Workshop on Biotechnology for the mining, metal refining and fossil fuel processing industries*, John Wiley & Sons, Inc., New York., 1986.

Torma, A. E., Leaching of metals, in Rehm, H. J. and Reed, G. (Ed.), *Biotechnology*, Vol. 6B, VCH Verlagsgesellschaft, Weinheim, Germany, 1988, p. 367-399.

Turner, D. and McCoy, D., Anoxic alkaline drain treatment system, a low cost acid mine drainage treatment alternative, in *Proceedings of the 1990 National Symposium on Mining*, Graves, D.H. and De Vore, R.W. (Eds.) Lexington, KY, p.73, 1990.

Turner, R. C., An investigation of the intercept method for determining the proportion of dolomite and calcite in mixtures of the two. I Theoretical aspects of the rate of solution of dolomite when a number of crystals are present, *Can. J. Soil Sci.*, 40, p. 219, 1960.

Turner, R. C. and Skinner, S. I. M., An investigation of the intercept method for determining the proportion of dolomite and calcite in mixtures of the two. II Experimental rate of solution of dolomite and calcite in samples consisting of a number of crystals, *Can. J. Soil Sci.*, 40, p. 232, 1960.

Uehara, G. and Gillman. G. P., Charge characteristics of soils with variable and permanent charge minerals: I. Theory, *Soil Sci. Soc. Am. J.*, 44, p. 250, 1980.

Uehara, G. and Gillman. G. P., *The Mineralogy, Chemistry, and Physics of Tropical Soils with Variable Charge Clays*, Westview Trop. Agric. Series, No. 4, Boulder, Colorado, 1981.

United States Environmental Protection Agency, Design Manual: Neutralization of Acid Mine Drainage, Office of Research and Development, Industrial Environmental Research Laboratory, Washington, DC, 231 pp. 1983.

Van Dijk, H., Cation binding of humic acids, *Geoderma*, 5, p. 53, 1971.

Van Raij, B. and Peech, M., Electrochemical properties of some oxisols and alfisols of the tropics, *Soil Sci. Soc. Am. Proc.*, 36, p. 587, 1972.

Van Ophen, H., *An Introduction to Clay Colloid Chemistry*, John Wiley and Sons, Inc. N. Y., 2nd ed., 1977.

Varadachari, C., Mondal, A. H. and Ghosh, K., Some aspects of clay-humus complexation: Effect of exchangeable cations and lattice charge, *Soil Sci.*. 151, p. 220, 1991.

Wakao, N., Mishina, M., Sakurai, Y., and Shiota, H., Bacteria pyrite oxidation I.The effect of the pure and mixed cultures of *Thiobacillus ferrooxidans* and *Thiobacillus thiooxidans* on release of iron, *J. Gen. Appl. Microbiol.*, 28, p. 331, 1982.

Wakao, N., Mishina, M., Sakurai, Y., and Shiota, H., Bacteria pyrite oxidation II.The effect of varous organic substances on release of iron from pyrite by *Thiobacillus ferrooxidans*, *J. Gen. Appl. Microbiol.*, 29, p. 177, 1983.

Wakao, N., Mishina, M., Sakurai, Y., and Shiota, H., Bacteria pyrite oxidation III. Adsorption of *Thiobacillus ferrooxidans* on solid surfaces and its effect on iron release from pyrite, *J. Gen. Appl. Microbiol.*, 30, p. 63, 1984.

Wakao, N., Takahashi, T., Sakurai, Y., and Shiota H., The Treatment of Acid Mine Water Using Sulfate-reducing Bacteria, *J. Ferment. Technol.*, 57, No. 5, p. 445, 1979.

Wang, J., Evangelou V. P. and Creech, P., Characteristics of Mn-Ca exchange behavior on kaolinite and illite and pH influence, *J. Env. Sci. and Health*, A28(6), p. 1381, 1993.

Wann, S. S. and Uehara, G., Surface charge manipulation of constant surface potential soil colloids: I. Relation to sorbed phosphorus, *Soil Sci. Soc. Am. J.*, 42, p. 565, 1978.

Washburn, E. W., Ed., International Critical Tables, Vol. VI, McGraw-Hill, New York, 1929.

Watzlaf, G. R., and Hedin, R. S., A method for predicting alkalinity generated by anoxic limestone drains, in *Proceedings of the 1993 West Virginia Surface Mine Drainage Task Force Symposium*, Morgantown, West Virginia, April 27-28, 1993.

Watzlaf, G. R., Pyrite oxidation in saturated and unsaturated coal waste, in *Proceedings of 9th national meeting of the American Society for Surface Mining and Reclamation*, Duluth, MN, June 14-18, 1992, p. 191, 1992.

Wen, C. Y., Noncatalytic heterogeneous solid-fluid reaction models, *Ind. Eng. Chem.*, No.60, 9, p. 34, 1986.

Wentzler, T. H. and Aphan, F. F., Kinetics of limestone dissolution by acid waste waters, in *Environmental Control.*, Rampacek, C. (Ed.), San Francisco, CA, p. 513, 1972.

Wiersma, C. L. and Rimstidt, J. D., Rate of reaction of pyrite and marcasite with ferric iron at pH 2, *Geochim. Cosmochim. Acta*, 48, p. 85, 1984.

Wildeman, T. R., Drainage from coal mine: Chemistry and environmental problems, in *Geology in Coal Resource Utilization*, Peters, D. C. (Ed.), Techbooks, Fairfax, VA, p. 499, 1991.

Zhang, Y. L., Blanchar, R. W., and Hammer, R. D., Composition and pyrite morphology of materials separated from coal, in *Proceeding of 10th National Meeting of American Society of Surface Mining and Reclamation*, Spokane, Washington, May 16-19, 2, p. 284, 1993.

Zhang, Y. L., Chemistry of fly ash and scrubber sludge compounds in plant-soil-water systems, Ph.D. Dissertation, University of Missouri-Columbia., 1994.

Taylor & Francis
Taylor & Francis Group
http://taylorandfrancis.com

SUBJECT INDEX

O

P

Q

R

S